DSE Group 07 - AEOLUSIM

Design a wind-driven or ventilator-driven motion-based simulator

T.R.J.W. Follender Grossfeld	1507001	E.J.P. Riegman	4085892
		S.T. Spronk	4016521
G.M. ter Horst	4156749	O.W.M. Thijssens	4154592
A.B. Mahabir	1397184	S.C.F. Vrouwenvelder	4050150
C.P.H. Ramakers	4157982	I.J. Welschen	4148363

Final Report

Design Synthesis Excercise

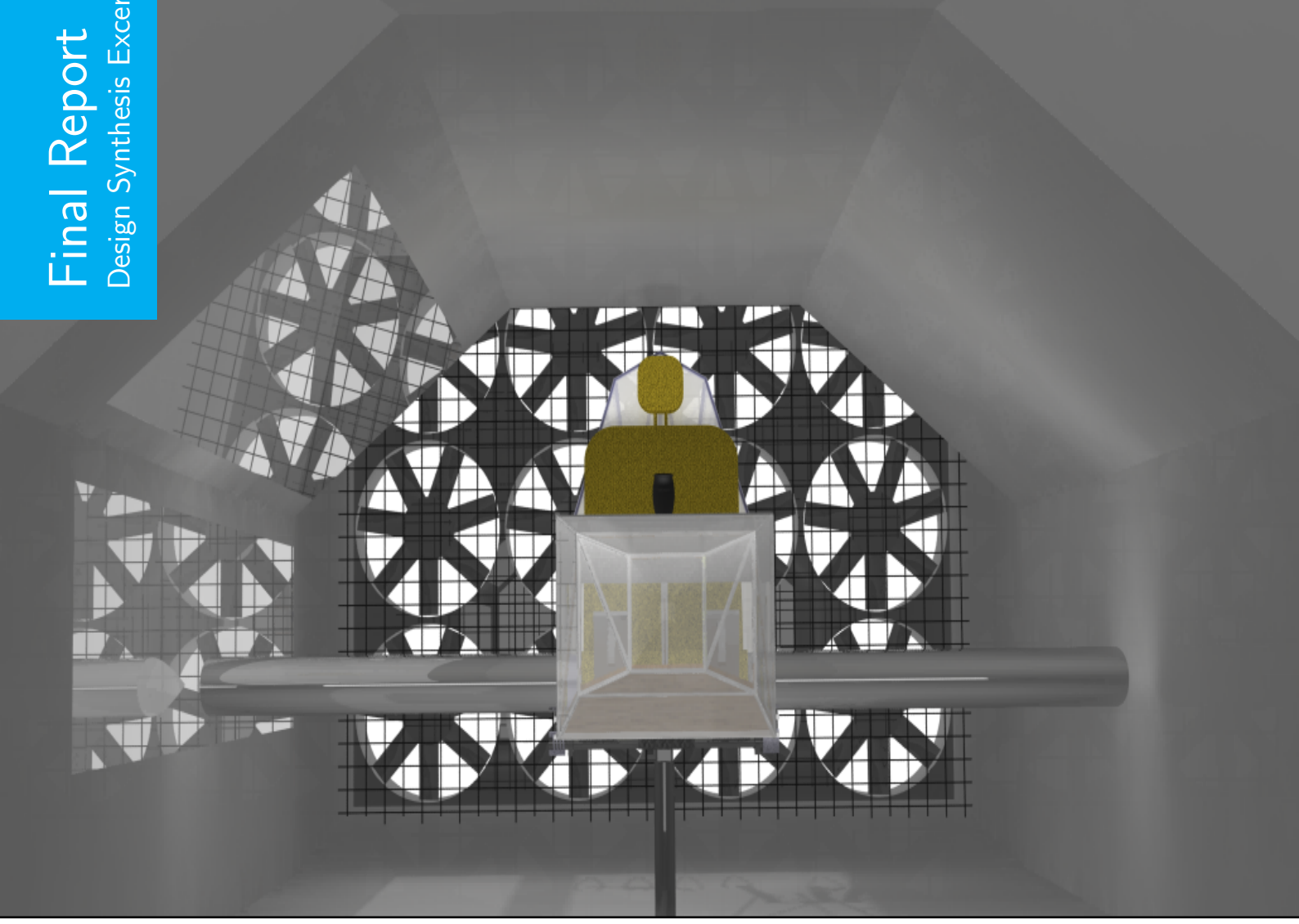

TU Delft Delft University of Technology

Aerospace Engineering

January 27, 2015

Preface

This is the fourth report of the 2014 autumn Design Synthesis Exercise (DSE) at the Delft University of Technology. The goal of this report is to work out the concept that was selected in the midterm report and arrive at a final concept. Conclusions will be drawn on the performance and feasibility of this concept.
We would like to thank Dr. Ir. Rene van Paassen, Ir. Daniel Baldacchino and Ir. Mohammmed Al Harbi for their tutoring and coaching.

DSE group F07, January 2015

Contents

List of Figures

List of Tables

List of Contributions

Chapter	Description	Author(s)	Other Contributors
1	Introduction	Simon S	
2	Configuration & Layout		
2.1	Final Design	Simon V.	
2.2	Changes wrt. Preceding Designs	Simon V.	Ivo
3	System Functions	Rick, Cas	Simon S., Simon V.
4	Airflow Generation System Design	Simon S.	
5	Aerodynamic Analysis		
5.1	Aerodynamic Model	Ivo	Olivier
5.2.1	Rudder & Elevator Effectiveness	Olivier	
5.2.2	Aileron Effectiveness	Olivier, Ivo	
6	Structural Analysis		
6.1	Method	Simon V.	
6.2	Main Wing Design	Simon V.	
6.3	Tail wing design	Cas	Simon V.
6.4	Fuselage Design	Amol	
6.5	Support Structure Design	Cas	
6.6	Structural Results	Cas, Simon V	
7	Stability & Control Analysis		
7.1	Analytical Model		
7.1.1	Model Layout	Rick	
7.1.2	Assumptions	Rick	Thijs
7.1.3	State Space Representation	Thijs	Rick
7.1.4	Stability and Control Derivatives	Thijs	
7.1.5	Initial Conditions	Rick	
7.1.6	Control Forces	Thomas	
7.1.7	Verification & Validation	Rick	Thomas, Thijs
7.1.8	Model Reliability	Rick	
7.2	Stability & Control Performance		
7.2.1	Motion Responses	Rick	Thijs
7.2.2	Aircraft-like Behaviour	Rick	Thijs
7.2.3	Control Forces	Thomas	
7.2.4	Discussion & Recommendation	Rick	
8	Sensitivity Analysis		
8.1	Fan Sensitivity Analysis	Simon S.	
8.1	Structural Integrity Sensitivity Analysis	Simon V.	
8.3	Motion Response Sensitivity		
8.3.1	Analysed Parameters	Thijs	
8.3.2	Analysis Results	Thijs	Olivier
9	Operations & Logistics		
9.1	Manufacturing	Rick	
9.2	Assembly & Integration	Rick	
9.3	Operational Life	Simon V.	
9.4	End-of-Life	Simon V.	
10	Electrical Systems		
10.1	Electrical Block Diagram	Simon S.	
10.2	Hardware Block Diagram	Amol	
10.3	Software Block Diagram	Thijs	
10.4	Data Handling Diagram	Ivo	Thijs
10.5	Communication Flow Diagram	Olivier	

Chapter	Description	Author(s)	Other Contributors
11	RAMS Analysis		
11.1	Reliability	Simon S.	
11.2	Availability	Simon S.	
11.3	Maintainability	Thijs	
11.4	Safety	Thijs	
12	Risk Assessment	Simon V.	
13	Market Analysis		
13.1	Entertainment Market	Simon V.	
13.2	Customer Analysis	Thomas	Simon V.
13.3	Market Introduction Strategy	Thomas	
13.4	NEMO Customer Analysis	Thomas	
13.5	Market Analysis	Thomas, Simon V.	
14	Return on Investment	Thomas	
15	Sustainability Assessment	Simon V.	
16	Post-DSE Planning	Ivo	Olivier, Rick
17	Compliance With Requirements	Simon S.	
18	Conclusion and Recommendations	Simon V., Cas	

Complementary tasks	Main contributor	Secondary contributor
3D modeller (CATIA)	Cas	Amol
ANSYS Fluent	Olivier	
ANSYS Mechanical	Cas	Amol, Simon V.
Logbook	Olivier	
Quality control	Simon V., Thijs	

List of Abbreviations

Abbreviation	Description
2D	Two Dimensional
3D	Three Dimensional
AC	Alternating Current
CFD	Computational Fluid Dynamics
CPU	Central Processing Unit
DC	Direct Current
DOF	Degree(s) Of Freedom
DSE	Design Synthesis Exercise
FBS	Functional Breakdown Structure
FEA	Finite Element Analysis
FFD	Functional Flow Diagram
FSI	Fluid Structure Interaction
GPU	Graphical Processing Unit
HDMI	High-Definition Multimedia Interface
HMD	Head Mounted Display
HWBD	Hardware Block Diagram
MMOI	Mass Moment Of Inertia
MTBF	Mean Time Between Failure
OS	Operating System
RAM	Random Access Memory
RAMS	Reliability, Availability, Maintainability and Safety
SF	Safety Factor
SSD	Solid State Drive
SWOT	Strengths, Weaknesses, Opportunities and Threats
U.S.	United States
USB	Universal Serial Bus
w.r.t.	with respect to

List of Symbols

The list of symbols is presented below, units are as specified unless indicated otherwise.

Symbol	Description	Unit
A	blade effective area	$[m^2]$
A	cross-sectional area	$[m^2]$
A	Aspect ratio	$[-]$
$A_{enclosed}$	enclosed area	$[m^2]$
A_{ibeam}	cross-sectional area of I-beam	$[m^2]$
A_{min}	minimum required cross-sectional area	$[m^2]$
b	wing span	$[m]$
C_c	dimensionless damper coefficient	$[-]$
C_D	3D drag coefficient	$[-]$
C_d	2D drag coefficient	$[-]$
C_{h_e}	dimensionless hinge moment elevator	$[-]$
C_{h_δ}	slope of $C_h - \delta$ curve	$[\frac{1}{rad}]$
$C_{h_{\delta_t}}$	slope of $C_h - \delta_t$ curve	$[\frac{1}{rad}]$
C_L	3D lift coefficient	$[-]$
C_l	2D lift coefficient	$[-]$
$C_{l_{\alpha,control}}$	slope 2D lift coefficient curve control surface	$[-]$
C_k	dimensionless spring stiffness	$[-]$
C_{M_α}	dimensionless moment contribution due to mass due to pitch angle	$[-]$
C_{M_ϕ}	dimensionless moment contribution due to mass due to roll angle	$[-]$
$\bar{c}$	mean aerodynamic chord	$[m]$
c	chord	$[m]$
$\bar{c}_e$	mean aerodynamic chord elevator	$[m]$
c_{u1}	fan inlet swirl	$[m/s]$
c_{u2}	fan outlet swirl	$[m/s]$
D	drag	$[N]$
DF	diffusion Factor	$[-]$
d	arm	$[m]$
d_{ail}	aileron lift increase arm	$[m]$
E	Young's modulus	$[Pa]$
F	failure cumulative distribution function	$[-]$
F_{HL}	horizontal leaning force	[N]
F_{VL}	vertical leaning force	[N]
F_y	force in y-direction	$[Pa]$
f	failure probability density function	$[-]$
H_e	hinge moment elevator	$[Nm]$
h_w	web height	$[m]$
I	moment of inertia	$[m^4]$
$I_{annular}$	moment of inertia of annular beam	$[m^4]$
I_{min}	minimum required moment of inertia	$[m^4]$
I_{xx}	mass moment of inertia about x	$[kg\ m^2]$
I_{xx}	moment of inertia about x	$[m^4]$
I_{yy}	mass moment of inertia about y	$[kg\ m^2]$
I_{yy}	moment of inertia about y	$[m^4]$
I_{zz}	mass moment of inertia about z	$[kg\ m^2]$
I_{zz}	moment of inertia about z	$[m^4]$
k	spring stiffness	$[N/m]$
L	beam length	$[m]$
L	lift	$[N]$
l_{arm}	distance hinge to aerodynamic centre	$[m]$
l_c	distance hinge to aerodynamic centre	$[m]$
$L_{C_{X_1}}$	length member C_{X_1}	[m]
$L_{C_{Z_1}}$	length member C_{Z_1}	[m]

L_{cone}	length of the nose cone in X-direction	[m]
$L_{I_{X_1}}$	length member I_{X_1}	[m]
$L_{N_{Y_2}}$	length member N_{Y_2}	[m]
$L_{N_{Z_2}}$	length member N_{Z_2}	[m]
M_A	moment about A	$[Nm]$
$M_{control}$	control moment	$[Nm]$
M_{max}	maximum moment	$[Nm]$
M_{roll}	rolling moment	$[Nm]$
$MTBF$	mean time between failure	$[hour]$
m	mass	$[kg]$
n	rotational velocity	$[1/s]$
p	roll rate	$[rad/s]$
p_t	total pressure	$[Pa]$
P	applied load	$[N]$
P_{fan}	Fan power	$[W]$
Q	Volumetric flow rate	$[m^3/s]$
Q_{design}	Design volumetric flow rate	$[m^3/s]$
Q_{max}	Maximum volumetric flow rate	$[m^3/s]$
r	yaw rate	$[rad/s]$
q	pitch rate	$[rad/s]$
q_b	basic shear flow	$[N/m]$
q_s	combined shear flow	$[N/m]$
q_s0	constant shear flow	$[N/m]$
R	radius	$[m]$
R	reliability	$[-]$
R_1	outer radius	$[m]$
R_2	inner radius	$[m]$
R_A	reaction force at location A	$[N]$
R_B	reaction force at location B	$[N]$
r	local blade radius	$[m]$
r_t	tip radius	$[m]$
r_h	hub radius	$[m]$
S	wing area	$[m^2]$
S_{ail}	area behind aileron trailing edge	$[m^2]$
S_e	elevator surface area	$[m^2]$
SF	safety factor	$[-]$
S_y	shear force	$[N]$
S_z	shear force	$[N]$
s	distance	$[m]$
s_e	control stick deflection	$[m]$
T	torque	$[Nm]$
t	thickness	$[m]$
t	time	$[s]$
$t_{annular}$	thickness of annular beam	$[m]$
t_f	flange thickness	$[m]$
u	blade velocity	$[m/s]$
u	airspeed	$[m/s]$
V	airspeed	$[m/s]$
V_h	horizontal tail airspeed	$[m/s]$
W	weight	$[N]$
W_U	user weight	[N]
w_2	flow outlet velocity	$[m/s]$
w_2	flange width	$[m]$
w_m	axial flow velocity	$[m/s]$
w_γ	angle velocity distribution function	$[m/s]$
w_{u1}	inlet relative flow velocity	$[m/s]$
w_{u2}	outlet relative flow velocity	$[m/s]$

x	location along hub circumference	$[m]$
x	x-location	$[m]$
Y	von-Mises stress	$[Pa]$
$\hat{y}$	y-location stress calculation	$[m]$
y	location along hub thickness	$[m]$
y	y-location	$[m]$
$\hat{z}$	z-location stress calculation	$[m]$
α	angle of attack	$[rad]$
α_h	horizontal tail angle of attack	$[rad]$
$\dot{\beta}$	yaw rate	$[rad/s]$
β	sideslip angle	$[rad]$
γ_1	blade inlet angle	$[rad]$
γ_2	blade outlet angle	$[rad]$
γ	blade angle	$[rad]$
Δ	increase	$[-]$
δ_a	aileron deflection	$[rad]$
δ_e	elevator deflection	$[rad]$
δ_r	rudder deflection	$[rad]$
δ_{te}	elevator trim deflection	$[rad]$
ζ	damping ratio	$[-]$
η_{axial}	fan efficiency	$[-]$
θ	angle	$[rad]$
θ	pitch angle	$[rad]$
λ	rate parameter	$[-]$
ρ	density	$[kg/m^3]$
Σ	summation	$[-]$
$\sigma_{bending}$	bending stress	$[Pa]$
$\sigma_{tensile/compressive}$	tensile/compressive normal stress	$[Pa]$
σ_x	normal stress	$[Pa]$
τ	shear stress	$[Pa]$
τ_{yz}	shear stress	$[Pa]$
ϕ	flow coefficient	$[-]$
ϕ	roll angle	$[rad]$
ψ	pressure coefficient	$[-]$
ω_d	damped frequency	$[rad/s]$
ω_n	natural frequency	$[rad/s]$

Abstract

In the early 20th century, a first generation of flight simulators made their entrance. These simulators relied on wind and respective models of aircraft for its operations. Although these types of simulators have been abandoned in favour of more sophisticated full flight simulators, combining an old concept of a wind reliant simulator with modern technology like a head mounted virtual reality display could provide a less costly alternative for a basic flight experience. A basic concept for this type of simulator was created that needs to be analysed in order to determine its feasibility and performance.

This report describes the process of analysing the performance and feasibility of the concept dubbed Aeolusim. The configuration of the simulator is detailed and the changes that have been made since the last design phase are elaborated on. These changes include the airframe structure, the airfoils used and the support structure.
System functions are describes using both a functional flow diagram, detailing the time dependent flow of functions, and a functional breakdown diagram, detailing the system functions in a hierarchical and time independent way.
The airflow is generated by 12 axial fans in a 4x3 rectangular configuration. The fans were designed according to a method that aims to construct an optimal blade profile distribution for a given flow condition. This condition is the desired volumetric flow rate, and all other parameters are iteratively determined. The final result of this approach is a blade design with a volumetric flow rate of $5.3\frac{m^3}{s}$ per fan and an ideal nominal efficiency of 51.3%. This combined with the wind tunnel design yields a airflow velocity of 12.4 $\frac{m}{s}$ in the section were the simulator is present. The wind tunnel design consists of a open return wind tunnel with a diffusion angle of 7.3°. It has an inlet of 3 meters length, an simulator section of 6 meters and a diffusion section of also 6 meters. Height of the tunnel in the simulator section is 1.9 meters, but due to the non rectangular shape the area is only 5.14 m^2. The total area at the inlet and at the fans is 7.04 m^2 and 9.72 m^2 respectively, both being rectangular in shape. Aerodynamic characteristics have been analysed using XFoil and ANSYS Fluent. It was found the wake created by the pilot was of such influence on the airflow over the rudder that an aerodynamic fairing has been added behind the pilot. Also, the effect of the wall of the wind tunnel on the tip vortices has been found to be very small.
Structural characteristics have been analysed using ANSYS Mechanical APDL. The fuselage consists of a truss structure covered with a fabric, where the main wing is made of a combination of aluminium and wood; and the tail wings of wood covered with fabric. This configuration is chosen because a user is expected to lean/sit on the wing but is not expected to be in the vicinity of the tail wings. The latter would require the user to jump over the main wing, which has a main chord of one m. The complete simulator is suspended on a universal joint which incorporates spring-damper subsystems to both limit and filter the simulator's motion response. The structural integrity of the complete system was designed such that it is able to cope with all expected loads during its operational life. These include the aerodynamic forces and the loads caused by user interaction. The minimum safety factor found during stress analysis were 3.87, 2.56 and 1.97 for the wing, fuselage and support structure, respectively. Other load cases such as bumping in to the wing had safety factors reaching values in the 100s, indicating an over-designed structure. This however could not be overcome, since the design was limited by production and cost factors, rather than the applied load. The stability and control characteristics are analysed by simulation the motion responses by creating a state space system. The control forces the pilot feels are also calculated by calculating the hinge moment of the control surfaces and, with that, calculating the control force on the pilot. An initial assessment of the Aeolusim's motion response concluded that it is able to either simulate aircraft-like behaviour, when compared to a Cessna Citation II or reach the maximum possible deflections. Large deflection angles are favourable for the entertainment value of the Aeolusim, while aircraft-like behaviour is an amicable feature for any simulator. The latter case however urged an undesirable decrease in the maximum deflection and has therefore been disregarded in the design. This will lead to maximum deflection of 10, 20 and 9.4 degrees , reached after 2.27, 2.3 and 2.5 seconds for pitch, roll and yaw, respectively.
The sensitivity of the design is analysed. This is done by changing key parameters of the design such as airspeed or mass and analysing the change of the model results. An important conclusion that was drawn from the model, is that the Aeolusim's design is inherently sensitive to a shift in the centre of gravity. A small offset in the $x-$ or $y-$direction (body axis frame) leads to very large and unwanted deflections.
The operations and logistics around the Aeolusim are described by going through the life phases of the simulator. A manufacturing, assembly and integration plan is presented. The operational life is elaborated on and the end of life procedure is described.
The electrical systems are described extensively. Both hardware and software diagrams are presented. Also included are a data handling diagram and a communication flow diagram. An electrical block diagram, showing the electrical systems and their connection, is also presented.

The RAMS characteristics are presented. The reliability had been estimated by examining the reliability of the separate parts. Availability had been determined by how long the simulator can be in operating condition. The maintainability has been assessed by addressing the maintainability of the separate parts. The safety was determined in a similar fashion.
A risk assessment was done by identifying technical and organisational risks. These risk were given a severity and a likelihood of occurrence. Each risk has been accompanied with a mitigation strategy and a risk map is presented.
The possible markets for the Aeolusim to enter have been analysed. Porter's analysis has been applied to a possible costumer and a market introduction strategy has been made using a SWOT analysis. It was found the entertainment market was the most viable market to enter.
The return on investment has been determined. This was done by defining the cost of the simulator and activities around the creation of the simulator. The possible revenues were then determined which resulted in a return of investment result for a worst, normal and best case. Only the best case scenario yielded a slight profit due to the very low expected sale numbers.
The sustainability strategy has been outlined and, with that, the sustainability of the design has been assessed.
Needed project steps that need to be taken to arrive at a finished product are determined and ordered in a diagram and a Gantt chart. The needed resource allocation for these design steps has been defined as well.
Finally, the design's compliance with the requirements is assessed. It is found that the power and production cost requirements are exceeded by a slight margin.

After extended analysis a final concept has be generated. This concepts fulfils most of the requirements. However, the power usage is slightly too high. It is determined that, given more power, the quality of the simulator can be improved even further. With this final concept a design team can move ahead to make a detailed design and finally build the simulator.

1 Introduction

In 1910, Eardly Billing obtained a patent on a flight simulator. This simulator used wind energy for its operation and had controls much like airplanes of that time. The Billing flight simulator was suspended on a pivot point and relied on wind to create aerodynamic forces on its wings and control surfaces, thus generating the motions of the simulator. This type of simulator has been abandoned, however, and current motion based simulators rely on hydraulic or electric power for generation of the simulator motion. Still, there are a number of advantages to a wind-driven simulator that make it interesting to take a new look at these types of simulators [1]. The control surfaces can be tuned to accurately resemble an aircraft's feel. Also, when the cockpit is open, the feel of the wind can enhance the realistic feel. Finally, the motion can be generated by a low-cost mechanism instead of by a 4 to 6 degree of freedom high-precision mechanical, electric or hydraulic drive.

The purpose of this report is to provide an understanding of the methods and results of the final phase of the conceptual design, and plan for further development, of a low-cost wind-driven flight simulator.

The structure of the report is as follows. A grand overview of the total system will be presented in Chapter 2. Additionally, in Chapter 3, a summary of all the functions and their relations of the total system. Following from this the method and performance of the airflow generation system has been put to paper in Chapter 4. Then in Chapters 5, 6 and 7 the same has been done for the aerodynamic, the structure and the stability and control designs respectively. With all technical design values established, their sensitivity is test in Chapter 8. The operations and logistics concept has been put in Chapter 9. Chapter 10 provides an overview of the electrical systems of the Aeolusim. Furthermore in Chapter 11 an analysis to determine the reliability, availability, maintainability and safety (RAMS) of the systems has been detailed. An overview and accompanying plan to mitigate risk that comes with a design has been included in Chapter 12. In Chapter 13 an in-depth analysis of the markets possibly suitable for the Aeolusim is performed. The economic investment and return prospectus of the design is presented in Chapter 14. The first being an breakdown of the cost of producing the design, and the latter being predictive scenarios of an eventual return of investment. A plan for any further development and production is printed in Chapter 16. A final overview of the requirements and the degree in which they are complied with, are also included in Chapter 17. Finally, in Chapter 18 a final conclusion and recommendations for the future are.

2 Configuration and Layout

The AEOLUSIM is a wind driven flight simulator aimed at the entertainment market. Its configuration is shown in Figure 2.1, with all important parts labeled. One specific element, the actual simulator, is separately shown in Figure 2.2 in a similar fashion. Both will be discussed in Section 2.1, with the complete 3D planforms are shown in Appendix G.
The configuration is based on the initial design of the AEOLUSIM, discussed in the preceding design reports (Reference [2] and [3]). Three components have been changed w.r.t. these reports: the airfoil, fuselage and support structure. The changes made for these elements will be discussed subsequently in Section 2.2.

2.1 Final design

The simulator is located in an open return wind tunnel, see Figure 2.1. An open wind tunnel located in a bigger enclosed room. The geometry of the wind tunnel is optimised to provide the maximum airflow velocity for the minimum power required. The simulation section is 1.9 m in height and 6 m in length. The complete wind tunnel is 15 m in length, to provide for a steady and laminar flow.
The airflow is generated by 12 fans, with custom designed fan blades for high efficiency. They are positioned aft of the AEOLUSIM in a four by three matrix. The airflow is guided back to the entrance of the wind tunnel trough the room where the wind tunnel is located, creating a continuous flow (Section 4.2.1).

Located aside the wind tunnel is the operator control booth. This room will provide the operator with a clear view of the simulation section. In addition, this room will also be the AEOLUSIM's entrance. A possible queue is to be positioned near the window, to provide the users with a clear view on the simulation section. The entrance to the wind tunnel itself is located near the nozzle of the wind tunnel. Locations near the test section do not allow for easy entrance due to the tilted shape of the simulation section ceiling (Figure 2.1). The AEOLUSIM can be made wheelchair accessible, an important factor for the entertainment industry. The limiting factor will be the windtunnel: The small scale does not allow for much space to help someone from a wheelchair to the AEOLUSIM. A possible design recommendation would be to design a flexible wind tunnel. This design should be able to create space (e.g. lift the top and outer wall, walls 1 and 2 in Figure 2.1), and thus allow the operator to help someone with, for instance, a disability, to enter the AEOLUSIM.

The simulator is in turn positioned on top of a support structure, a universal joint and allows for three degrees of freedom: pitch, roll and yaw motion, see Section 2.2. Integrated in this supporting structure are spring and damper subsystems which both limit and filter the simulator's motion response. To ensure a safe and stable vehicle upon entering, a locking mechanism is to be engaged when the simulator is not operational. This mechanism consists of four pistons, located near both wingtips and in front, and aft of the simulator. The positions are illustrated in Figure 2.1.

The fuselage of the simulator itself, Figure 2.2, consists of a load bearing beam structure with a canvas skin, sized in Chapter 6. The skin increases the aerodynamic performance and serves the aesthetics of the airframe whilst keeping production costs relatively low. A fairing is positioned on top of the rear fuselage between the pilot and the vertical tail. This fairing reduces the turbulent airflow behind the pilot, therefore improving the airflow velocity about the vertical tail, as detailed in Section 5.2. All wings have a 0 degree incidence angle and use the NACA0015 airfoil. The simulator's control surfaces are relatively large because of the small scale of the AEOLUSIM. The ailerons take up about 50% of the main wing (i.e. 50% of the main wing chord, between 22% and 92% the effective wingspan). The tail surfaces are, in turn, fully movable. Two horizontal tailwings act as elevator, and one vertical tailplane as rudder. The point of rotation for the elevator and rudder are located inside the fuselage, 50 cm in front of the leading edge. This configuration, in combination with the fully movable wings, allowed for larger stick and pedal forces for the pilot, providing the desired feedback on the control input.

2.2 Changes Made With Respect to Preceding Designs

Airfoil
An initial aerodynamic assessment in Reference [3] selected the Kennedy and Marsden airfoil for the main wing, based on its high stall angle and zero angle of attack lift coefficient. This airfoil is close to optimal if a combination of a vertical degree of freedom (DOF) and a high pitch angle are required. This approach prevented that the airfoil would be the limiting factor in the analyses of possible concepts. However, the concept that was concluded in the trade-off of Reference [3] does not have a vertical DOF, and the maximum pitch angle, equal to the angle

of attack, of the initial design was only 14.9 degrees. In addition, the shape did not allow for an easy integration of high lift surfaces such as an aileron due to the sharp curve at the trailing edge. It was therefore considered to opt for a less complex airfoil, whilst still having to perform at angles of attack reached by the AEOLUSIM, see Chapter 7.
A secondary aerodynamic assessment resulted in a NACA0015 airfoil. This symmetric airfoil has a high score on manufacturing and is thick enough to include the internal structure and the hinge for the aileron, even for small chords.

Fuselage
Reference [3] did not define a fuselage configuration. Three possible configurations have been considered,

1. monocoque fuselage; and
2. fully exposed truss structure; and
3. truss structure covered with a sheet of fabric.

The monocoque option was considered for its simplicity, aesthetics and aerodynamic performance The option of a composite structure was disregarded, since its production cost follows an exponential curve [4] and production volume is expected to be relatively low. This would in turn result in high production costs, unfavorable for the top-level requirement of a maximum unit price tag of €35.000,-.
A truss structure is expected to have relatively low mass and low production costs, when compared to a monocoque structure. A fully exposed truss structure however, greatly affects the aerodynamic characteristics of the fuselage. This performance can in turn be increased by covering the structure with a sheet of, for instance, fabric or canvas. In addition, this will improve the aesthetics of the simulator whilst increasing the mass. This mass increase and its effect is, however, expected to be negligible since the AEOLUSIM does not require to lift itself.
Based on a qualitative trade-off and engineering judgement, the covered truss structure was selected as the chosen configuration, as shown in Figure 2.2. This option would limit the production costs whilst having the desirable performance.

Support structure
In the preceding report a preliminary assessment for the support structure concluded that a gimbal support was for the AEOLUSIM. This support structure is shown in Figure 2.3. A secondary analysis using CATIA V5R20[1] and ANSYS R15[2] concluded that this type of support structure can be optimised. This optimisation is shown in the same respective figure and affects the following parameters:

Mass Moment of Inertia The optimised structure has fewer mass and its geometry has a less complex shape. This yields a lower mass moment of inertia for the simulator, resulting in a more apt *dynamic* response. This response may in turn be tuned with the spring-damper subsystem, if necessary.

Production Costs The complex shape of the initial design is expected to increase production costs of the specific part. The optimised structure, however, is significantly more simplistic. This shape results in lower stresses, less mass and therefore lower production costs.

These advantages where enough reason to opt for the optimised structure. This structure is able to rotate over 3 axes, shown in Figure 2.3. The fuselage is attached to the support-fuselage interface indicated in the Figure. It allows for roll pitch and yaw about the $x-$, y and $z-$ axis respectively. Motion is both filtered and limited by rotational spring-systems, to be sized per motion in Chapter 7.

[1] *www.catia.com*
[2] *www.ansys.com*

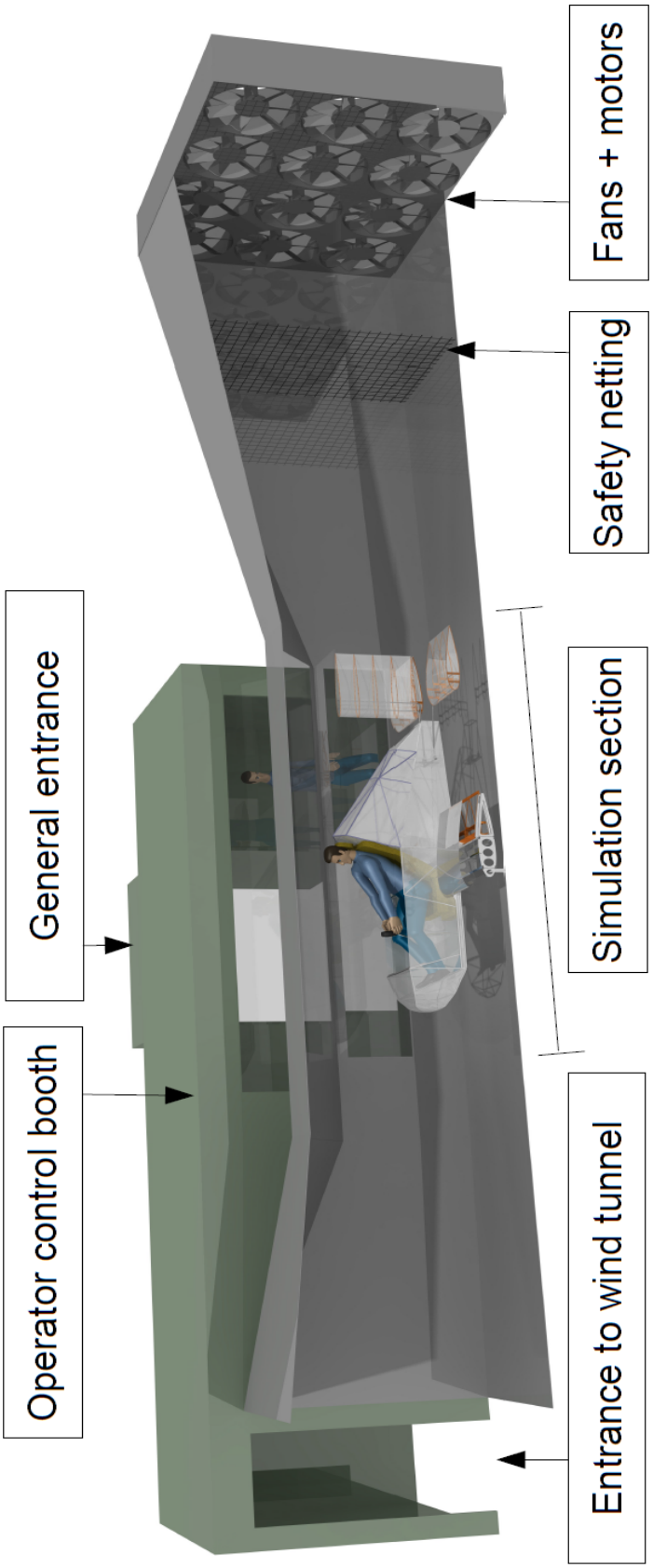

Figure 2.1: Configuration of the Aeolusim

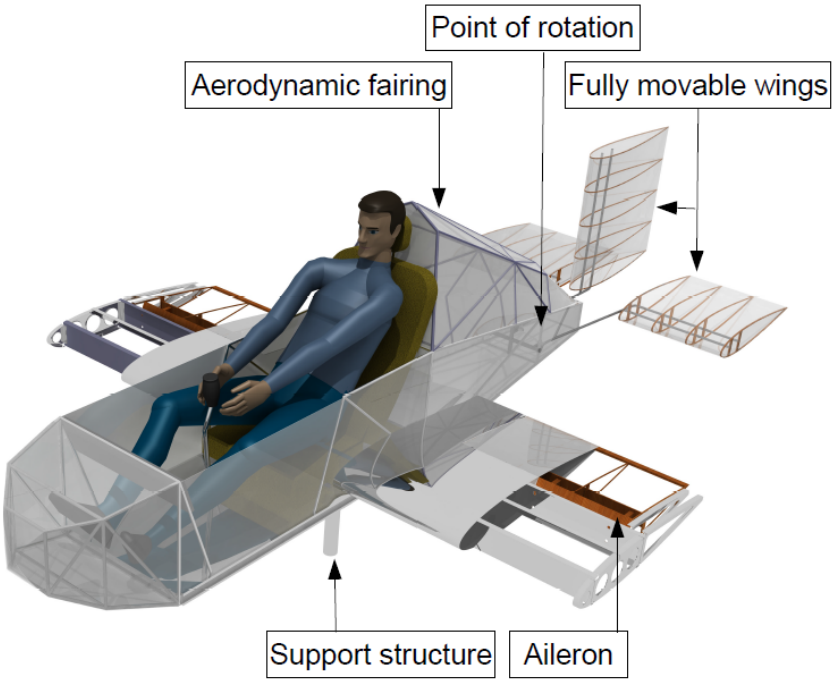

Figure 2.2: Configuration of the simulator

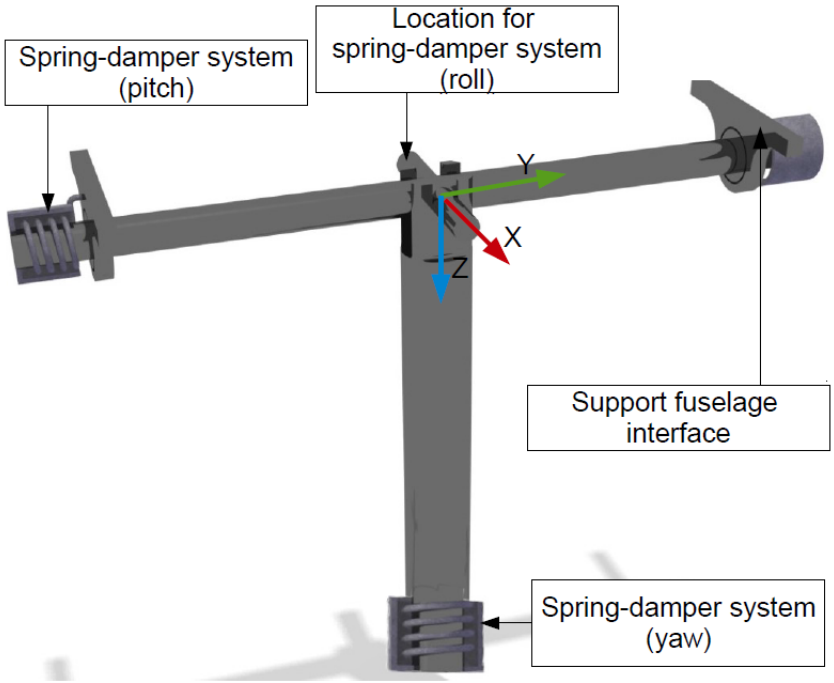

Figure 2.3: Support structure

3 System Functions

The Aeolusim has to perform several functions which are ordered in two ways. Firstly, they will be presented in a Functional Flow Diagram (FFD), Figure 3.1, showing the essential functions in a chronological order. Secondly, they are expressed in a Functional Breakdown Structure (FBS), Figure 3.2, which is a hierarchical representation. Time independent functions are also included.

The FFD aims to represent the order of events necessary for the systems to perform optimally. This means not only the operation, but also tending to the technical health of the system. Total system operations have been split into seven parts:

- System Start
- Pilot Entry
- Simulation Preparation
- Simulator Operation
- Simulation End
- System Shutdown
- Maintenance

During the System Start phase, the system will be powered up and tested. If any problems occur, the maintenance phase will be started.
When the System Start phase is complete, the Pilot Entry phase may commence. In this phase, a pilot enters the simulator, is secured and puts on the head mounted display.
Then, the Simulation Preparation is executed. Here, the user or operator can set up a simulation and the environment is rendered. The fan will then be powered up and the lock mechanism disengaged.
Now, the Simulator Operations phase is active. This is the phase where the user experiences the simulation and the simulator is free to move. While the simulation is running, the attitude and angular velocity and acceleration are monitored. If the safety limits are exceeded, the emergency shutdown is initiated. The user and operator also have the ability to initiate the emergency shutdown at any time.
At the end of the simulation, the End Simulation phase will be initiated. Here, the simulation is terminated and the simulator is locked in place so the pilot can exit safely. At the end of this process, either a new simulation can be initiated or the user or operator can decide to shut the system down. If the system was shut down using the emergency shutdown, the System Shutdown phase has to be initiated. In this case, a new simulation con not be chosen and a new pilot cannot enter the simulator. When the user chooses to start a new simulation, the Simulation Preparation phase starts again. When a new pilot takes over, the current pilot exits and the "Pilot Entry" phase is started.
If the system is shut down, the System Shutdown part will start. This part deals with shutting down the system and checking it for any damages sustained during operations. At the end of this phase the maintenance schedule is checked to see if the Maintenance phase needs to be initiated.
If maintenance is required, the Maintenance phase is initiated. Any part that is deemed to need maintenance, either as a result form inspection or because it is scheduled, is inspected thoroughly. After assessment, any faults are repaired. If replacement parts are not on hand they may need to be ordered. The system is then tested again and if it passes the test it is ready for use again.

An FBS is used to identify the hierarchical order of system functions, where each function was (indirectly) derived from the FFS. The FBS is shown in Figure 3.2. The tree is split up in five main functions,

Perform operations all functions required for the Aeolusim hardware to operate without simulating an virtual world.

Provide virtual experience All functions required for the simulation

Provide safety functions required to ensure the safety of the user, operator and the simulator itself.

Ensure maintainability ensure that the Aeolusim can be maintained and repaired, if needed.

Provide power provide the resources required to operate the Aeolusim (i.e. electricity for subsystems and kinetic energy for air).

These generalised, and fairly self explanatory, functional terms provide the context of what the product can and can not do. As when the Aeolusim is unable, due to damage, to fulfil one of the listed functions the system may be deemed inoperable or downright dangerous.

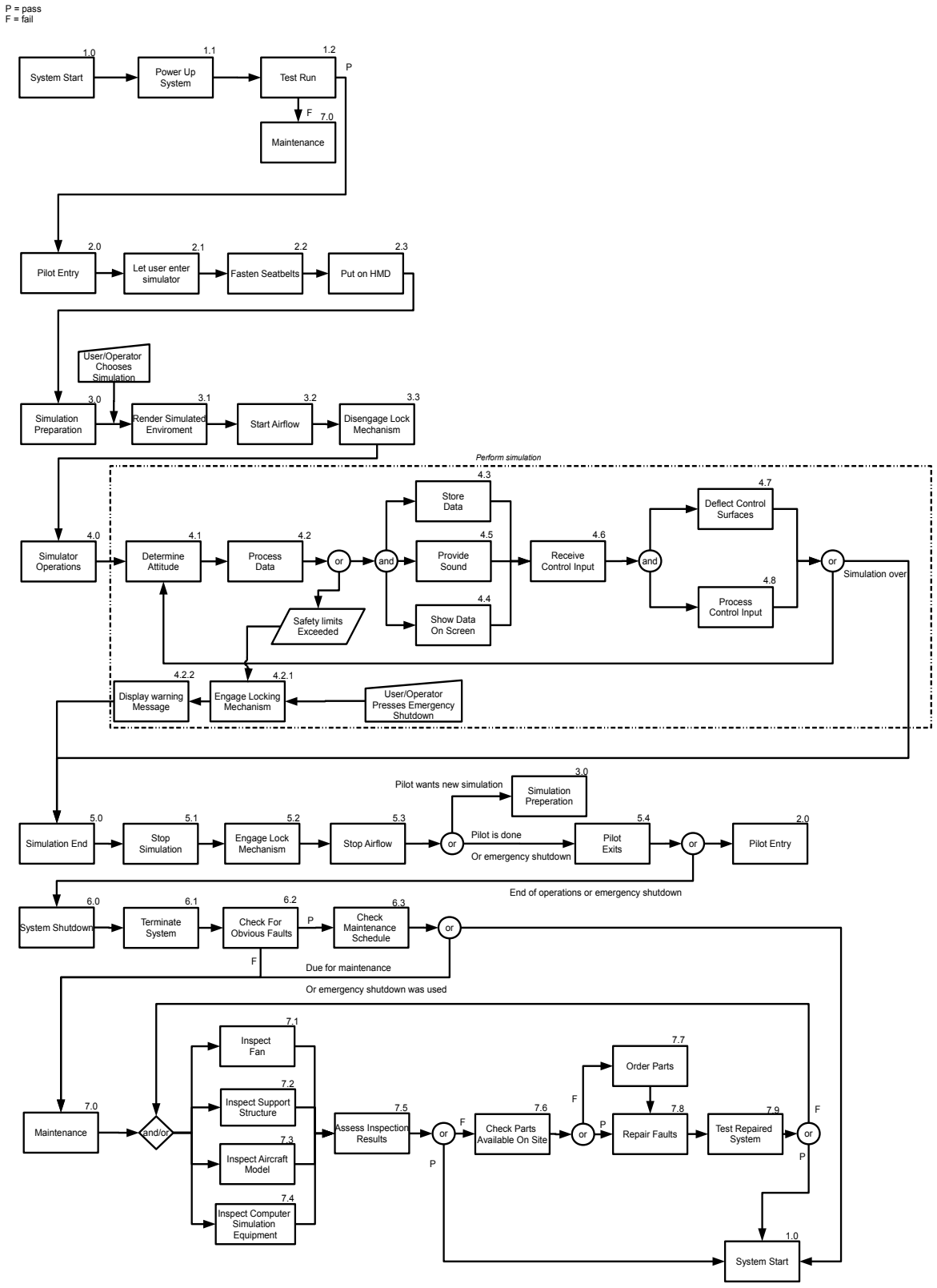

Figure 3.1: Functional Flow Diagram

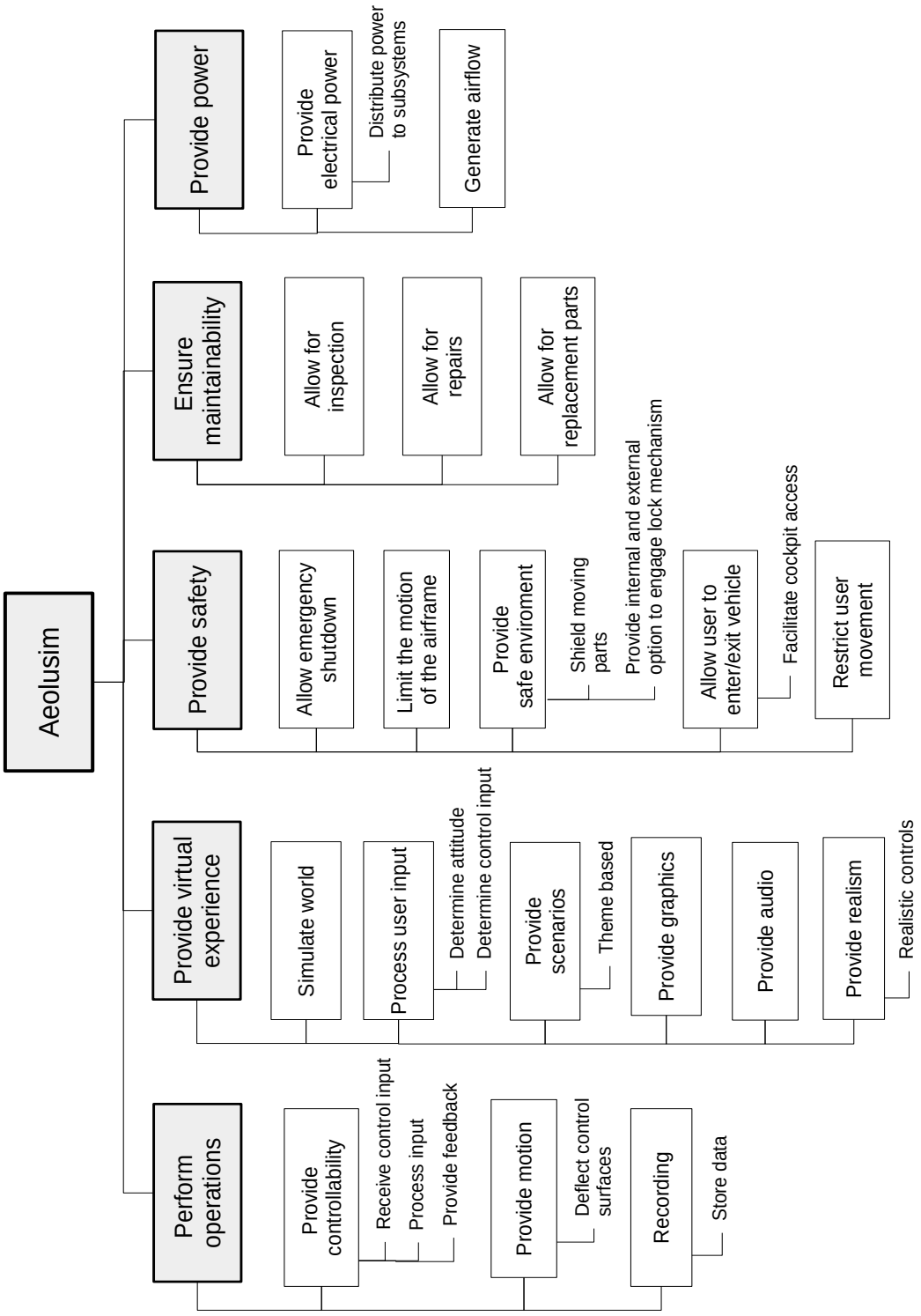

Figure 3.2: Functional Breakdown Structure

4 Airflow Generation System Design

In this chapter the airflow generation system, the fans and the wind tunnel, will be designed. This will be done through first explaining the method and range of applications of the fan design in Section 4.1. And the results of the design process for both the wind tunnel and the fan are presented in Section 4.2

4.1 Fan Design

In previous phases of the AEOLUSIM design the fan design was excessively based on existing designs. As these fans were not specially designed to generate the airflow for the AEOLUSIM they are not of optimum efficiency. Therefore an effort will be made to create a fan specially suited to the design's demands. These demands are high airflow rate against an as low as possible pressure increase with maximum efficiency. First an overview of the method used will be given in Subsection 4.1.1, followed by the verification procedure in Subsection 4.1.2. A proposed validation method is presented in Subsection 4.1.3, and finally an argumentation on the reliability of the method is included in Subsection 4.1.4.

4.1.1 Design Method

The approach taken for this fan design is based on the method as presented in Reference [5]. This method aims to compute the optimum blade profile distribution according to desired flow conditions for high volumetric flow axial fans. The design point is structured around the choice of volumetric flow rate Q_{design}, all other parameters will be changed and iterated in order to achieve the desired performance. To facilitate this analysis assumptions were made;

FN-1 Incompressible flow

FN-2 Inviscid flow

FN-3 Steady flow

FN-4 Fluid has axial entry into the fan

FN-5 Parabolic blade angle distribution

FN-6 Constant blade thickness

Incompressibility [**FN-1**] can be assumed since, even for axial fans, the airflow velocities will not exceed Mach 0.3. This will be further illustrated in Subsection 4.1.2, where one will see that the 100 $\frac{m}{s}$ limit will not be passed. Inviscid flow [**FN-2**] assumption is made only for Equation 4.11, but absolutely not for the rest of the method. Whether viscous forces are truly negligible is highly debatable, but the error introduced by this assumption has been investigated and will be accounted for. The steady flow assumption [**FN-3**] is valid for an isolated cascade row, but if more cascade rows are placed in succession the introduction of relative motions will cause unsteadiness. The relevance and justifiability of the other assumptions will be explained when they become relevant.

The design process starts with simplifying the three-dimensional flow to a more readily analysable format. This is done by "rolling out", in a manner of speaking, the fan into a infinite cascade as illustrated in Figure 4.1. Essentially going from three dimensional flow to a two dimensional situation.

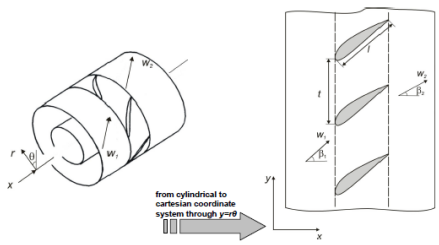

Figure 4.1: Cylindrical to infinite rectilinear cascade conversion [6]

This cascade can be further simplified to facilitate a mean-line calculation, taking a single element out of the two dimensional cascade to create a one dimensional model. This mean-line calculation marks the beginning of the

numerical design process as it determines the first velocity components and accompanying angles. These values are then used to expand the design to, first a two-dimensional cascade and finally, a full three-dimensional design. The mean-line calculation assumes that the fluid has axial entry into the fan **[FN-4]**. This assumption is valid if there are no disturbances in the upstream part of the flow, such as vanes, and will lead to a shockless entry due to a zero incidence angle, creating the velocity diagram in Figure 4.2.

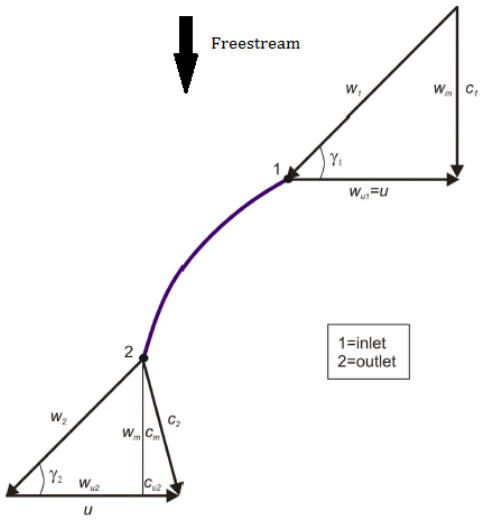

Figure 4.2: Velocity Diagram [5]

As can be seen in this figure the axial entry of the fluid leads to a zero tangential component of the absolute flow velocity $c_{u1} = 0$, thus there is no swirl introduced at the inlet. This implies that $w_{u1} = u$. The inlet angle is determined by Equation 4.1

$$\gamma_1 = atan(\frac{w_m}{u}) \tag{4.1}$$

Where u and w_m are defined by Equations 4.2 and 4.3.

$$u = 2\pi rn \tag{4.2}$$

$$w_m = \frac{Q_{design}}{\pi(r_t^2 - r_h^2)} \tag{4.3}$$

where r is the local radius of the blade, n the rotational velocity in rotations per second, r_t the tip radius and r_h the hub radius.

Additionally the outlet angle will need to be determined. This angle should be chosen as to maximize airflow and efficiency. To achieve this, an expression for maximum flow rate needs to be established. The equation derived in Reference [5] is:

$$Q_{max} = 2 \cdot \pi \cdot r \cdot n \cdot A \cdot tan\gamma_2 \tag{4.4}$$

Equation 4.4 implies that the airflow is maximum when the outlet angle $\gamma_2(r) = 90°$ as the flow rate becomes infinite. As this value is radius dependant it can only be applied at one cross section. To find the optimal location one must consider that at an outlet angle of 90 degrees, as follows from Figure 4.2, $w_{u2} = 0$ and $c_{u2} = u$, i.e. c_{u2} is maximum. As $c_{u2}r$ is a direct indicator of blade loading while c_{u2} expresses losses these values should be limited. This leads to the conclusion that the 90 degree outlet angle should be applied where radius and rotational velocity are minimum, namely the root chord of the blade. With this established it is possible to recursively determine the remaining outlet radii through Equation 4.5.

$$\gamma_2 = atan(\frac{1}{\frac{2\pi n}{rw_m}(r^2 - (x(\frac{r_t}{r_h})^x(r - r_h)^{1.35} + 1)r_h^2)}) \tag{4.5}$$

In this equation the value of x determines the shape of the pressure distribution over the blade. It is established in Reference [5] that $x = 0$ stands for the more conservative design approach which assumes that the fan operates in a free-vortex flow. This assumption states that there exists a constant pressure distribution over the blade, implying that $c_u r = const$. This assumption is not made in the current approach however, as its effects are not negligible. Therefore the remaining choices are $x = 1$ or $x = 2$, as increasing the value of x over 2 yields too high pressure increases to merit their application. The value of $x = 1$ yields a linear pressure distribution inverse of the hub ratio ($\frac{r_t}{r_h}$), A value of $x = 2$ is thus obviously parabolic. One of the major conclusions of Reference [5] states that the implementation of a parabolic pressure distribution produces the most efficient design. In accordance with this conclusion the value of $x = 2$ has been selected for the AEOLUSIM fan design as well. With the value for γ_2 and using Figure 4.2, w_{u2} can be computed as stated in Equation 4.6.

$$w_{u2} = \frac{w_m}{tan(\gamma_2)} \tag{4.6}$$

Using the known leading and trailing edge angles, the intermediate blade angles can be computed. To achieve this assumption **[FN-5]** is implemented. This assumption can be made since according to Pascu and Epple [7] this is valid for ducted axial fans. The equation for the angle distribution at a single chord is shown in Equation 4.7.

$$\gamma_y = Ay^2 + By + C \tag{4.7}$$

As is evident there are three unknowns (A,B,C) and only two knowns (γ_1 and γ_2), thus necessitating the introduction of a third "known". In Figure 4.3 this variable is shown.

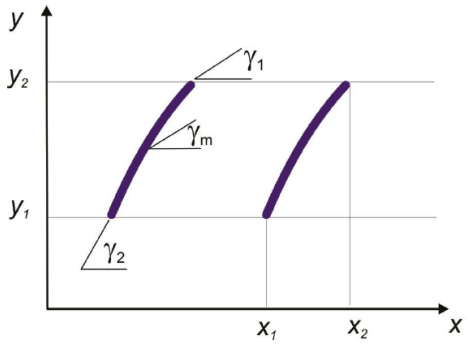

Figure 4.3: Chord Construction Method [5]

This point (y_m, γ_m) enables Equation 4.7 to be analytically solved. With this expression for the angle distribution it is a formality to numerically construct a curve for the chord shape. The point (y_m, γ_m) is chosen and then iterated to smooth as much as possible the curve of the velocity distribution over the blade as given in Equation 4.8. Furthermore, attention should be given to the fact that the chord at each radius should correspond to the maximum value set by the hub dimensions.

$$w_\gamma = \frac{w_m}{sin(\gamma_y)} \tag{4.8}$$

To apply a thickness to this chord, assumption **[FN-6]** will have to be implemented. This assumption states that the thickness distribution is constant over the blade. This assumption is valid at low pressure application as shown in Figure 4.4. The ϕ in this figure is defined by Equation 4.9.

$$\phi = \frac{w_m}{u} \tag{4.9}$$

At this point the fan blades can be given dimension, but the efficiency and other characteristics remains to be determined. First the diffusion factor is determined, Equation 4.10. This diffusion factor is a first indication of fan efficiency. It can be visualized as the deceleration(diffusion) of the fluid from $max(w_\gamma)$ to w_2, where $max(w_\gamma)$ is the maximum airflow velocity on the blade top surface. As illustrated in Figure 4.5 this value should be kept low to minimize wake losses. The diffusion factor is not definitive in determining the efficiency however, and values up to a maximum of 0.7 will be deemed acceptable.

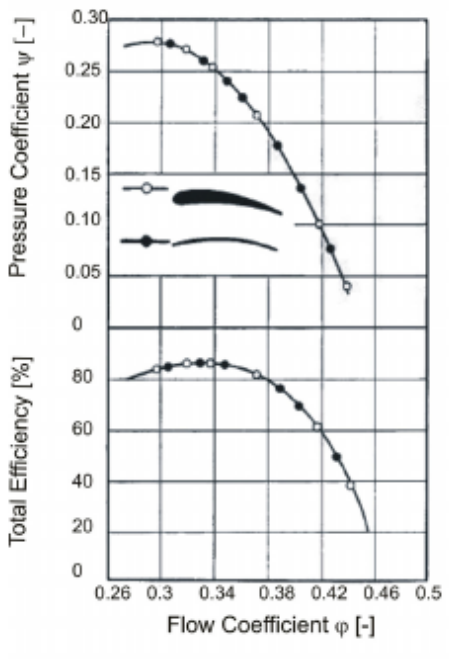

Figure 4.4: Relative Efficiency Airfoil-Constant Thickness [8]

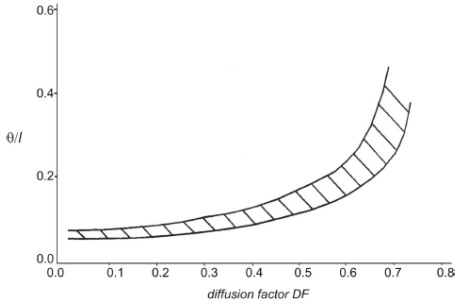

Figure 4.5: Diffusion Factor - Wake Thickness(θ) Relation [6]

$$DF = \frac{max(w_\gamma) - w_2}{max(w_\gamma)} \tag{4.10}$$

All that remains is to determine the fan efficiency and, by extension, the expected power consumption. The formula provided for the fan efficiency in reference [5] is shown in Equation 4.11. It integrates the efficiency from root to tip of the blade at different imposed flow rates on the design.

$$\eta_{axial} = \frac{1}{\pi(r_t^2 - r_h^2)} \int_{r_h}^{r_t} [1 - \frac{1}{2} \frac{\phi_{section}^2}{(1 - \frac{\phi_{section}}{tan\gamma_{2,average}})} - \frac{1}{2}(1 - \frac{\phi_{section}}{tan\gamma_{2,average}})] 2\pi r dr \tag{4.11}$$

$$P_{fan} = \frac{\Delta p_t Q}{\eta_{axial}} \tag{4.12}$$

The efficiency can then be used to determine the power consumption through Equation 4.12. As can be seen, all values will have been calculated except the total pressure change Δp_t. Bernoulli's theorem cannot be applied since it has been shown from experimental data that it consistently overestimates the pressure increases. This means that Δp_t will have to be determined in another way. Methods, however, that take into account changing airfoil shape are both rare and time-consuming. The Δp_t will thus be determined through comparison with similar fan designs. This approach is not ideal since the main focus of the design method presented is to distinguish

itself from more conventional methods and designs, making the comparison unreliable. A full computational fluid dynamics (CFD) analysis to accurately determine the pressure changes over the fan is therefore highly recommended for the final design.

4.1.2 Verification

The method of verifying the code is to, block by block, reproducing the values and graphs presented in reference [5]. There are three main areas from which all others follow: the camber distribution, the relative velocities and the efficiency. The inputs defined in the reference material are presented in Table 4.1.

Table 4.1: Fan Design Reference Input [5]

Variable	**Value**	**Unit**
Hub Radius	0.147	m
Tip Radius	0.280	m
Rotational Velocity	3000	rpm
Volumetric Flow Rate	4	$\frac{m^3}{s}$
Number Of Blades	8	-
Air Density	1.05	$\frac{kg}{m^3}$

The camber lines will first be tested. Comparing Figure 4.6 and the $x = 2$ curve in Figure 4.7 it can be seen that they are nigh identical. Small differences that might exist can be accredited to slightly different values used for y_m and γ_m used during optimisation. Also it can be seen that the x-value range increases in the reference material, something that has been actively avoided in the computed values. The increase in x-range in the $x = 2$ curve is likely due to the fact to be able to more accurately compare to the reference fan design with which the reference material compares. It can be noted that the axii are different, this is due to a difference in personal preference of the origin. Their identical nature merits the conclusion that the model up until this point is correct and it is possible to proceed with determining more complex values. Also seen in Figure 4.7 is a curve marked reference. This curve belongs to an off the shelve axial fan created for high airflow rates in cooling purposes. The method used was checked against this existing design in reference [5]. Meaning that the curves against which the verification is performed in this report are both verified and validated.

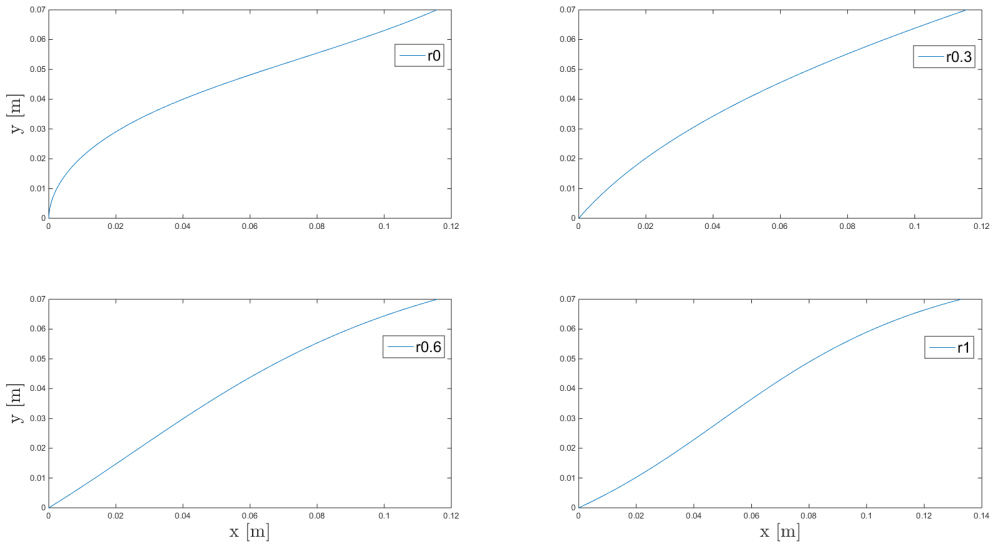

Figure 4.6: Computed Camber Lines

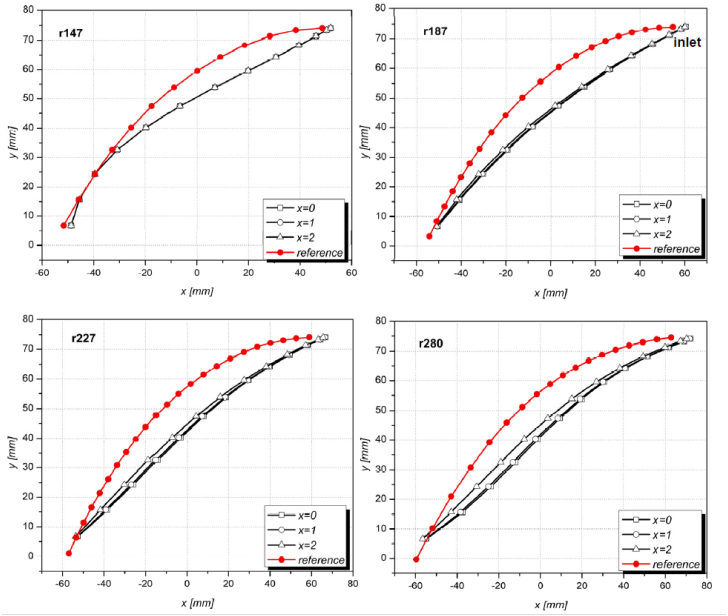

Figure 4.7: Reference(x=2) Camber Lines [5]

Also for the velocity distribution over the blade, presented in Figure 4.8 and Figure 4.9 it can be seen that the model is correct, as both curves show similar gradients and absolute values. The difference between the computed and the $x = 2$ curve increases slightly when moving to the tip. This can be accredited to the difference explained for Figure 4.6 and Figure 4.7.

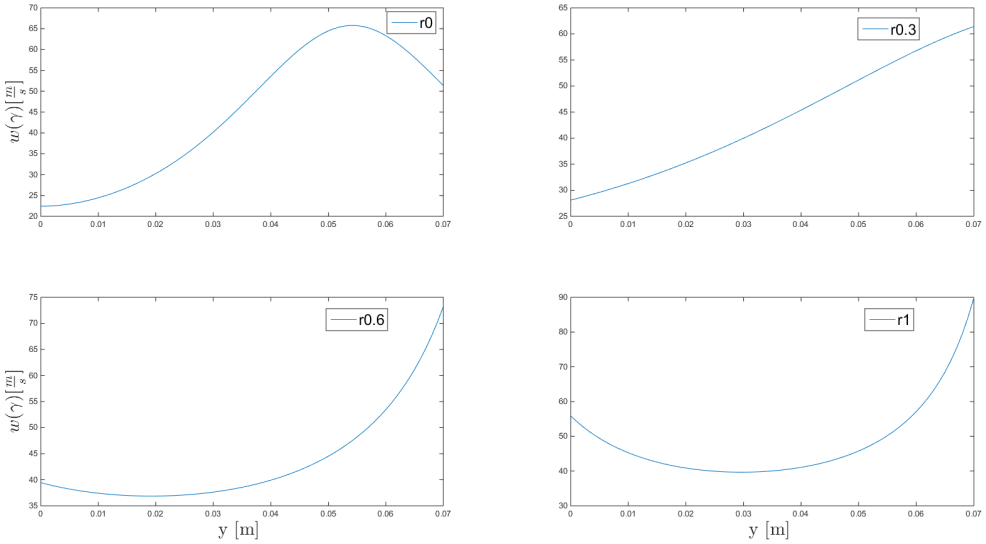

Figure 4.8: Computed Velocities Over The Blade

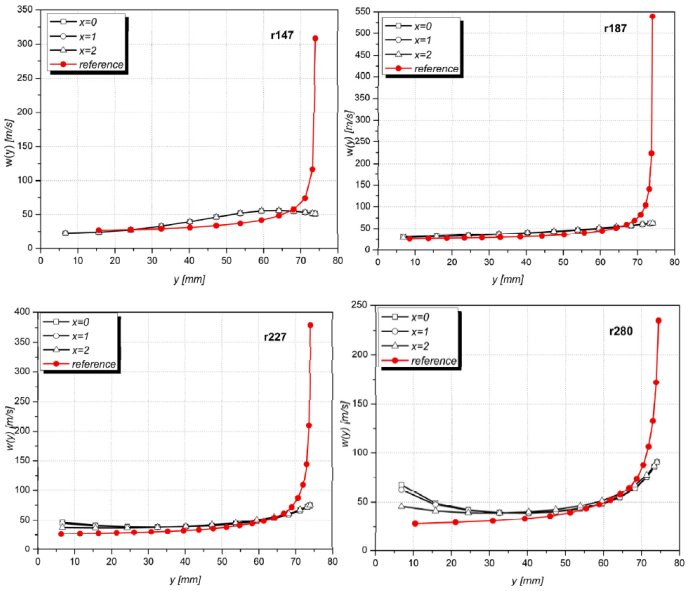

Figure 4.9: Reference(x=2) Velocities Over The Blade [5]

The final, and arguably most important, part of the verification efforts consist of comparing the ideal total fan efficiency. The different curves can be found in Figure 4.10 and Figure 4.11. Again the slightly different values, most evident at Q=0 and Q=8, can be explained through the slightly different choice in the optimization parameters y_m and γ_m. As all graphs have been deemed sufficiently similar verification can be deemed successful.

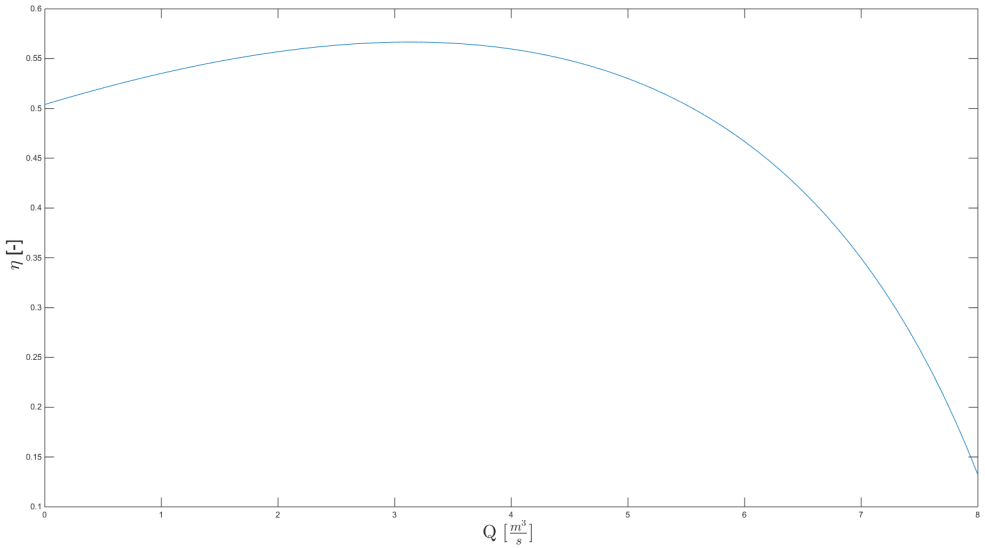

Figure 4.10: Computed Efficiency

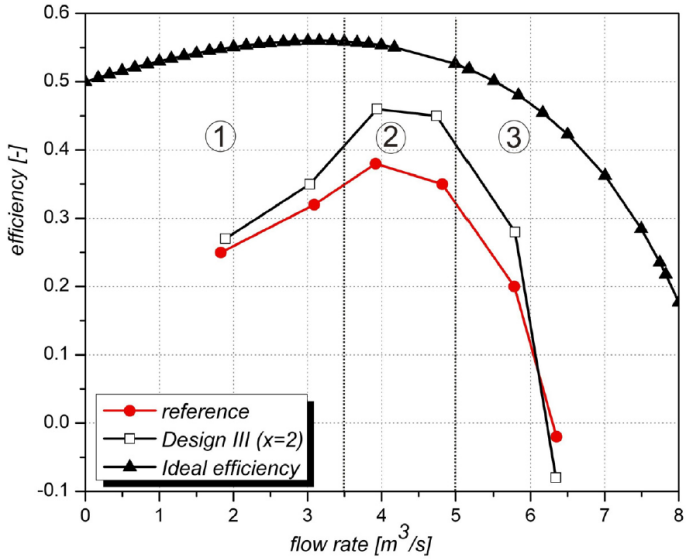

Figure 4.11: Reference(Ideal) Efficiency [5]

4.1.3 Validation

The proposed validation strategy entails a prototype test. To attain complete insight into the design's performance, different flow rates should be evaluated. Proposed test flow rates are 2, 3, 4, 5.3, 5.7, 6, 6.5 and 7 $\frac{m^3}{s}$ as these flow rates cover the expected range of the design. All the test should be performed at the design rotational velocity of 900 rpm. Tested parameters should be the power consumption of the electrical drive and the total pressure increase over the fan. With these parameters the true fan efficiency can be obtained, which can be compared to the computed value. If, taking all assumptions into account, these curves are similar the design and the design model will be validated.

4.1.4 Reliability

The design approach itself has been chosen due to the proven qualities of said approach. In Reference [5] the method is extensively tested against a comparable design used in industry. It was shown that an absolute total efficiency increase of 9% was achievable. This value was obtained through both CFD analysis and prototype testing. Although the test was done with only one reference fan, the efficiency values cannot be denied. These remain remarkably high for axial fans and merit the application of the method.

That the method is usable does not mean it has no shortcomings however. Foremost of these is the method of obtaining the efficiency. This method does not account for losses such as shock losses as soon as the fan operates away from its design point, friction losses, and any mechanical losses. From among these, only mechanical losses do not influence the pressure and can thus be separately accounted for. As can be seen in Figure 4.11 the true efficiency is an absolute 9% lower than the computed ideal efficiency, but this expected to be mainly due to mechanical losses as proven in subsection 4.2.2. Also regarding the efficiency is the fact that at zero airflow the efficiency is 0.5. This is obviously wrong as efficiency at that point should be zero as well. It can also be seen that there is a serious mismatch at high airflow rates. This all leads to the conclusion that the efficiency curve is only reliable in the region near the design point.

The other main shortcoming has been touched upon earlier in Subsection 4.1.1, namely the issue of pressure increases over the fan. Since no reliable method of determining these was found and consecutively implemented, the pressure increases remain in the domain of accurate guesswork. Although the current guess is moderately reliable the method would certainly benefit from a more consistent form of pressure estimation, one that does not immediately necessitate CFD analysis.

Also the possible effects of placing multiple fans in a rectangular configuration have not been taken into account. It is recommended that in further stages of design possible effects that might interfere with the efficiency are investigated. It is expected that these effects are minimal due to the duct length around the fans.

In conclusion it can be said that the method is very reliable in determining an optimum blade shape suited for

a design volumetric flow rate. Even the efficiency can be estimated quite reliably with the aid of additional empirical data and some understanding of the assumptions made. The lack of solid pressure increase data is troublesome but can be overcome, as not to invalidate the entire method.

4.2 Airflow Generation System Performance

To properly asses the performance of the airflow generating system its two major constituent parts must be evaluated. In Subsection 4.2.1 the wind tunnel design will be presented, and in Subsection 4.2.2 the final dimensions and performance prediction of the fan system will be explained.

4.2.1 Wind Tunnel Design

Before the fan itself will be sized, first the wind tunnel must be designed. In part the design depends on the physical dimensions and limitations of the aircraft model and in part on aerodynamic considerations. The length of the "test section" or simulation section is determined by the model and is set at 6 meter length. The cross sectional shape is show in Figure 4.12. The accentuated area is part of the tunnel but can be removed to achieve a 2% increase in airflow velocity.

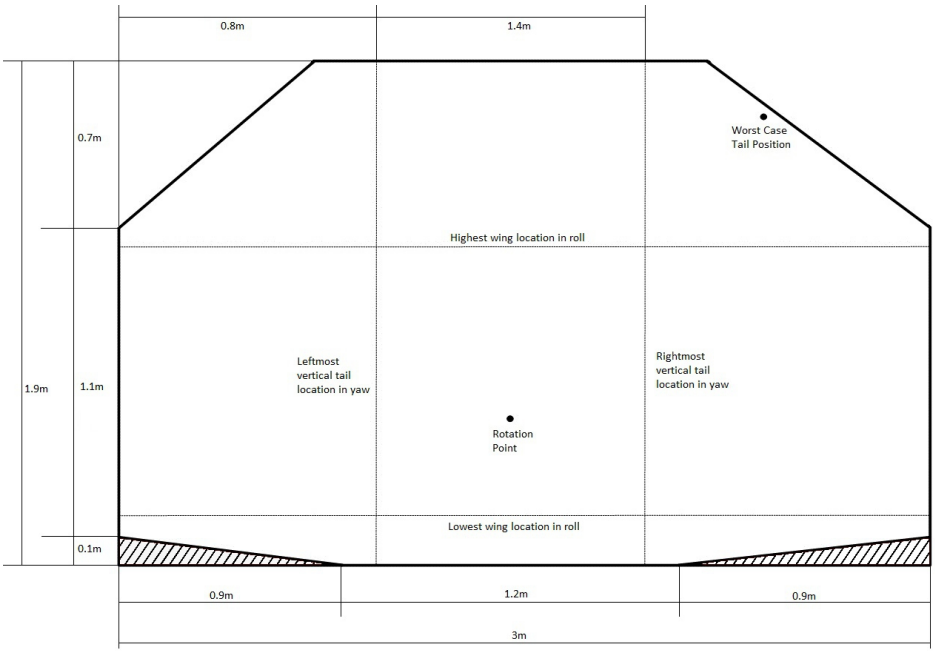

Figure 4.12: Wind Tunnel Cross Section At The Test Section

The cross-sectional area has been calculated to be 5.14 m^2 to still facilitate all movements of the model. The wind tunnel will be open-return to save building cost and minimize disturbance of the airflow. An example of an open-return wind tunnel has been included in Figure 4.13[1].

This particular wind tunnel design does not incorporate a both expensive and large closed tunnel. Also the placement of the fan behind the test section yields a flow with almost no vorticity. In Figure 4.14 a side view of the wind tunnel, with indication of four stations and the length between these stations, is presented.

Air gets sucked in at the inlet(station 1), is undisturbed until it passes through the test section(station 2-3). After which there is an expansion(station 3-4) of the flow to settle it until it passes through the fan. The flow will then proceed out of the exit into the reservoir outside the tunnel. Here the flow settles completely, reinforcing the redundancy of pressure increases over the fan, until it enters the inlet once more and the loop is complete. At the four stations the pressure and airflow velocity has been computed through use of flow continuity and Bernoulli's

[1] http://www.grc.nasa.gov/WWW/k-12/airplane/Images/tunoret.jpg

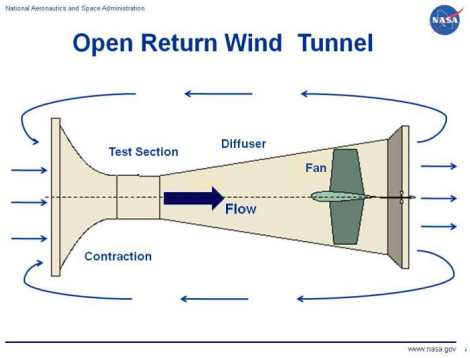

Figure 4.13: Wind Tunnel Example

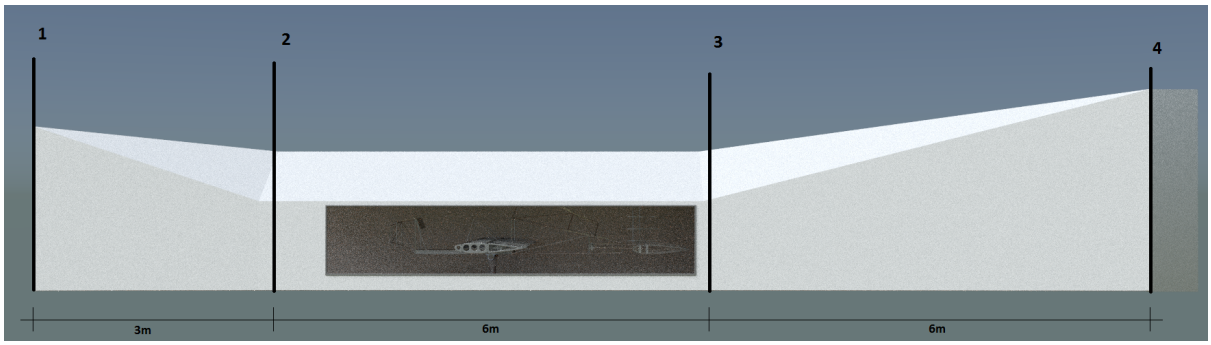

Figure 4.14: Wind Tunnel Side View

pressure equations, Equation 4.13 and 4.14 respectively.

$$A_1 \cdot V_1 = A_2 \cdot V_2 \tag{4.13}$$

$$p_t = p_s + \frac{1}{2}\rho V^2 \tag{4.14}$$

Where A is the cross sectional area, V the airflow velocity, p_t the total or atmospheric pressure, p_s the static pressure and ρ the air density. The values of each of these parameters, except p_t and ρ since they are assumed constant, at each station has been presented in table 4.2. The atmospheric pressure is a constant 101325 Pa at sea level and ρ is assumed constant in Subsection 4.1.1. In Subsection 4.2.2 the total volumetric flow rate of the fan configuration is determined to be 63.3 $\frac{m^3}{s}$. The values in Table 4.2 are calculated under the assumption that the model present between stations 2 and 3 does not create significant disturbances at station 3, and that the contraction between station 1 and 2 and expansion between station 3 and 4 of the flow adheres to the assumptions made in Subsection 4.1.1.

Table 4.2: Wind Tunnel Pressure And Velocity Distribution

Station	Area $[m^2]$	Flow Velocity $[\frac{m}{s}]$	Static Pressure $[Pa]$
1	7.04	9.03	101275
2	5.14	12.4	101231
3	5.14	12.4	101231
4	9.72	6.54	101299

The values for the diffusion angle is 7.3 ° at the ceiling of the wind tunnel. There seems to be no clear consensus[2][3][4]

[2] http://www.academia.edu/4954487/Design_and_fabrication_of_subsonic_wind_Tunnel_testing_machines_for_Nigerian_Universities_IJETR011847

[3] http://www.grc.nasa.gov/WWW/k-12/WindTunnel/windtunnel_report.html

[4] http://www.icas.org/ICAS_ARCHIVE/ICAS2004/PAPERS/104.PDF

on what the maximum angle for diffusers may be, although they all seem to be less than 10°. The choice of material for the wind tunnel walls is wood, as it is cheap and versatile. Although nearly any material can be used as friction losses at such low airflow velocities are low. At the test section both at the left and right side will be a cut out in the wood to accommodate a plexiglass window.

4.2.2 Fan System Performance

The main goal of the fan performance analysis is to provide an airflow velocity in the test section of at least 11.5 $\frac{m}{s}$ with a maximum power consumption of 30 kW. Although a higher airflow velocity takes precedence over lower power consumption. A quick calculation yields that this means a minimum of 5.1 $\frac{m^3}{s}$ that each of the 12 fans will need to provide. This has been chosen as the starting point on the design, one that will be iterated if a larger volumetric flow rate is achievable within the power restriction. The final iteration converged on a volumetric flow rate of 5.3 $\frac{m^3}{s}$. The accompanying data will be summarized and discussed here.

In Figure 4.15 the blade leading and trailing edge angles are shown, γ_1 and γ_2 respectively. And in Figure 4.16 the angle distribution along the blade is shown. The function of these graphs is to assure that the camber lines will be both smooth and continuous.

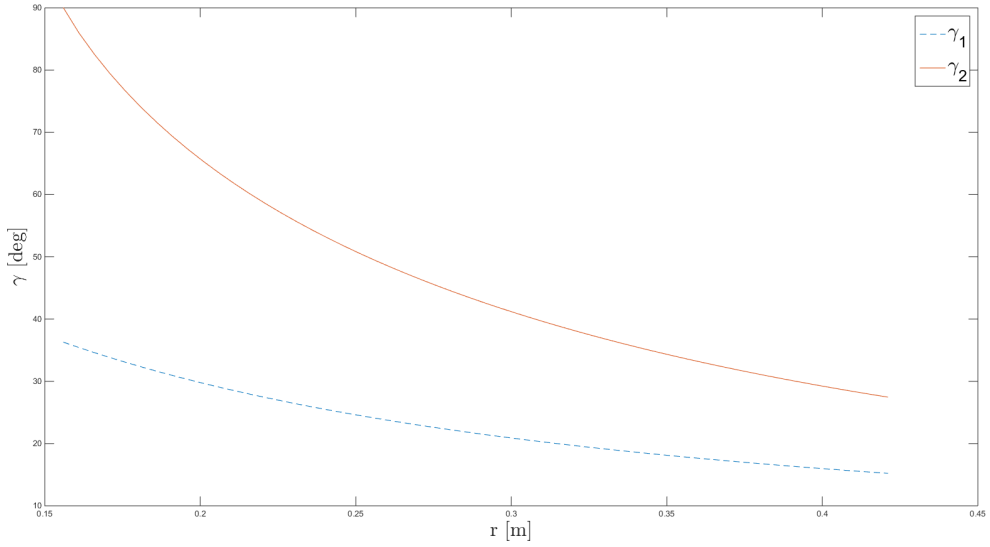

Figure 4.15: Leading And Trailing Edge Angles

As evident from Figure 4.16 the blade is evaluated at four sections to ease optimisation. These sections have been chosen at the root (0r), at 0.3 blade radius, at 0.6 blade radius and at the tip (1r). Corresponding to the final absolute values of 0.156, 0.231, 0.311 and 0.425 meters from the rotational axis respectively. Following the optimisation process the produced camber lines and velocity distributions are shown in Figure 4.17 and Figure 4.18.

Shown in Figure 4.19 the diffusion factors communicate that at the root has high diffusion which quickly drops to more acceptable values when approaching the tip. This means most of the losses occur at the root, leading to slightly lower efficiency. This is necessary however as the design is focused on generating maximum airflow rate, and is thus sacrificing pressure increases.

A more definitive statement on efficiency is made in Figure 4.20. Alas as stated in subsection 4.1.1 an estimate on the total pressure increase needs to be made to arrive at a usable power consumption prediction. As gathered from reference material[5][6] realistic values range from 100 to 300 Pa. It has therefore been decided that a pressure increase of 200 Pa is acceptable for this analysis. It is expected that the true value will be near this estimated one although an error of about 25% is not beyond reason.

[5] http://www.krugerfan.com/brochure/Axial/TDA-L%20LEA001.E2%20New.pdf
[6] http://www.airtradecentre.com/RO/EN/documentation/I06.013.0-AXIAL-~Axial-wall-fans

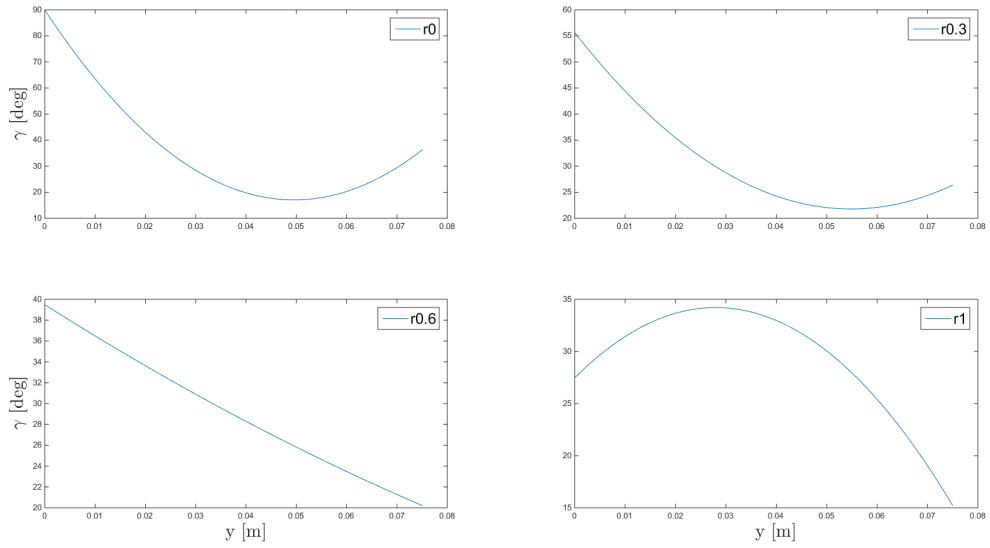

Figure 4.16: Blade Angle Distributions

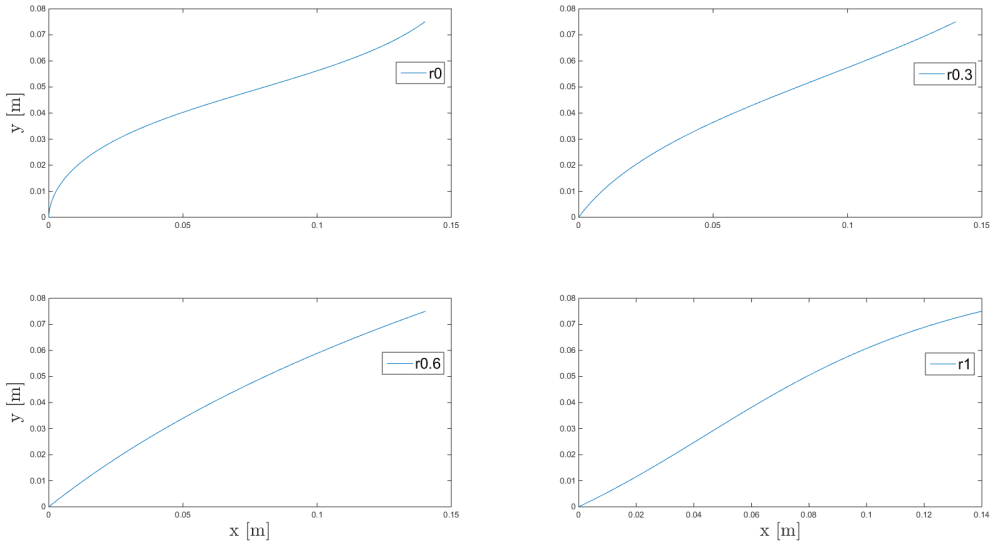

Figure 4.17: Blade Camber Lines

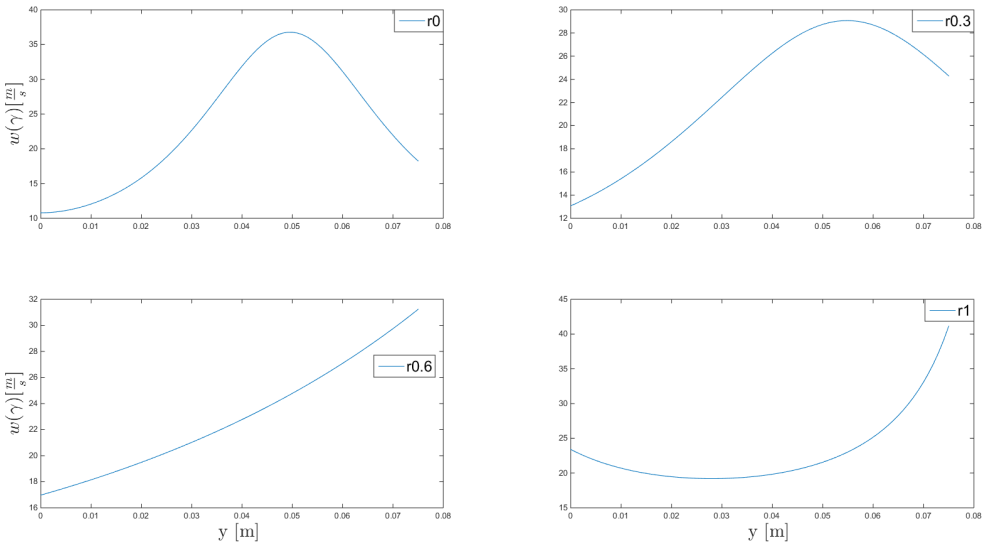

Figure 4.18: Blade Velocity Distributions

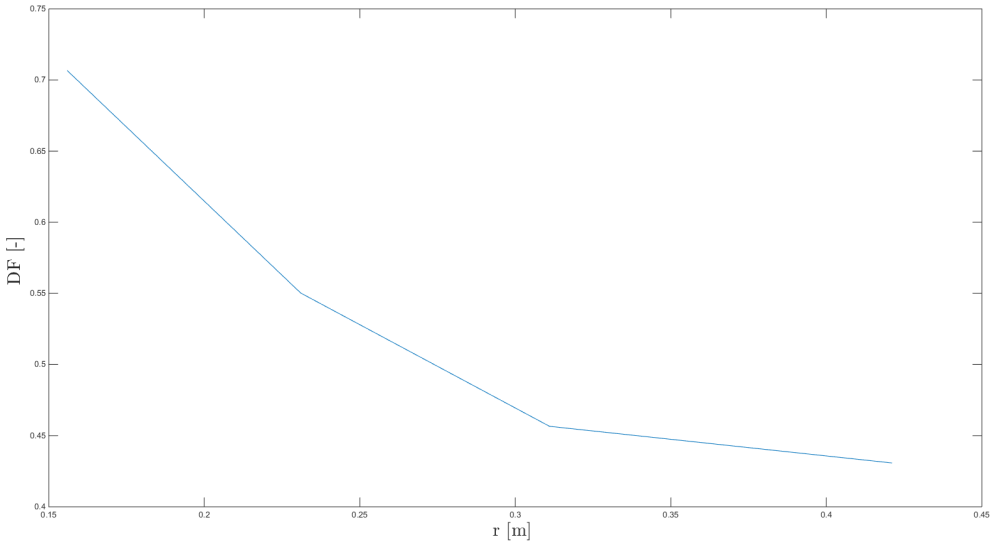

Figure 4.19: Diffusion Factors

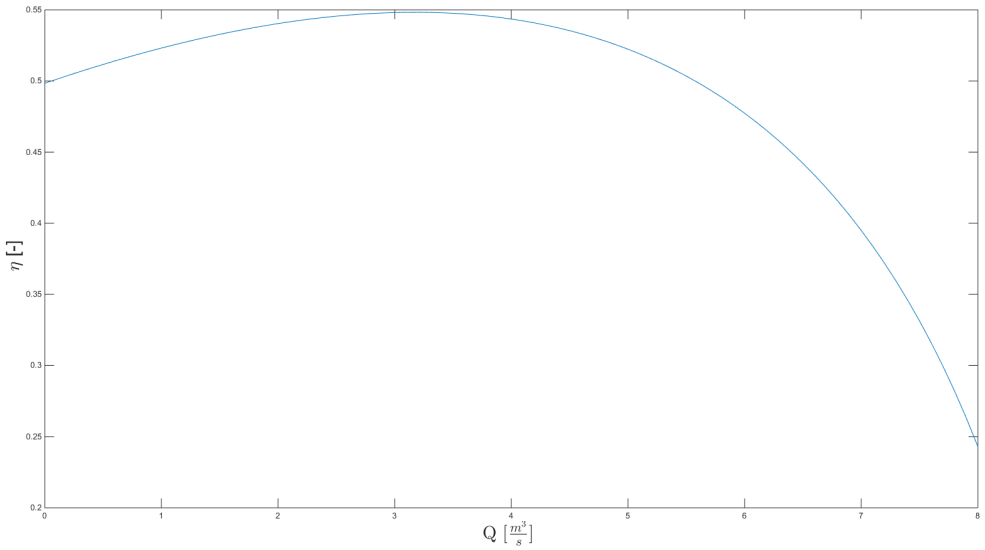

Figure 4.20: Fan Efficiency Curve

Table 4.3: Final Fan Design Characteristics

Variable	**Value**	**Unit**
Hub Radius	0.156	m
Tip Radius	0.425	m
Hub Depth	0.075	m
Rotational Velocity	900	rpm
Volumetric Flow Rate	5.3	$\frac{m^3}{s}$
Number Of Blades	7	-
Blade Thickness	0.005	m
Blade Chord	0.1588	m
Nominal Total Efficiency	0.5118	-
Nominal Power Consumption	2.0712	kW
Nominal Airflow Velocity	12.4	$\frac{m}{s}$

The final design model parameters are summarized in Table 4.3, and a visualisation of the hub and blade can be found in Figure 4.22

As can be seen it has been possible to increase the airflow velocity from 11.5 to 12.4 $\frac{m}{s}$ with a power consumption of 2071.2 Watts. This value however is a measure of the kinetic energy of the drive shaft and not the electrical. The loss which is most influential is the power loss associated with transferring electrical energy to kinetic energy in the electric motor. As a rule these motors do not have a 100 % efficiency, and thus the required electrical power will be higher. According to CE requirements, which are needed for any electrical equipment to be traded in the EU, the minimum efficiency of electric motors of 2.2 kW motors needs to conform to the IE2 efficiency level as of january first 2015 and IE3 as of january first 2017. It seems prudent to anticipate this change in efficiency requirements and choose a motor with a IE3 efficiency level. This means the minimum efficiency of a 6 pole motor needs to be at least 84.3 % [9]. This three phase motor will placed in accordance with Figure 4.21. A reference electrical motor is a Fuji Three-Phase Standard Series[7]

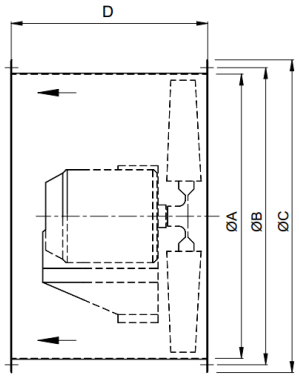

Figure 4.21: Example Of Electric Motor Placements

The imperfect efficiency means that the obtained value from the design method still needs to be adjusted. Dividing the ideal power consumption by the minimum fan efficiency and multiplying that by the total number of fans yields the expected true power consumption of approximately 29.5 kW.

This marks the end of the blade design, but there are some additional geometric properties to determine. One of these is the necessity of a duct and supporting structure. A duct is necessary to validate the assumptions made in the design model and also to limit fan downstream interaction. Although no detailed study has been made to quantify these swirl interaction effect, it can be said that they are not beneficial for pressure recovery. The duct length has been set to 650 mm, a ratio of 0.76 with respect to the diameter of the fan. The distance between the tip of the blades and the duct wall should be kept as small as possible, distances as small as 1 mm are common practice [5]. This will however necessitate a slight rounding off at the tip, but the influence of such a procedure is negligible. The blades and the hub will be made out of steel to counter the blade loading and cause no stress mismatch at the hub. The final area of consideration is the fan housing structure. The sizing of this structure however depends highly on the pressure increase over the fan, as this also dictates the thrust. It has not been deemed an essential design point as the structure can simply be constructed using beams. And is thus not included in this phase of fan design.

[7] http://www.fujielectric.com/products/motor/products/three.html

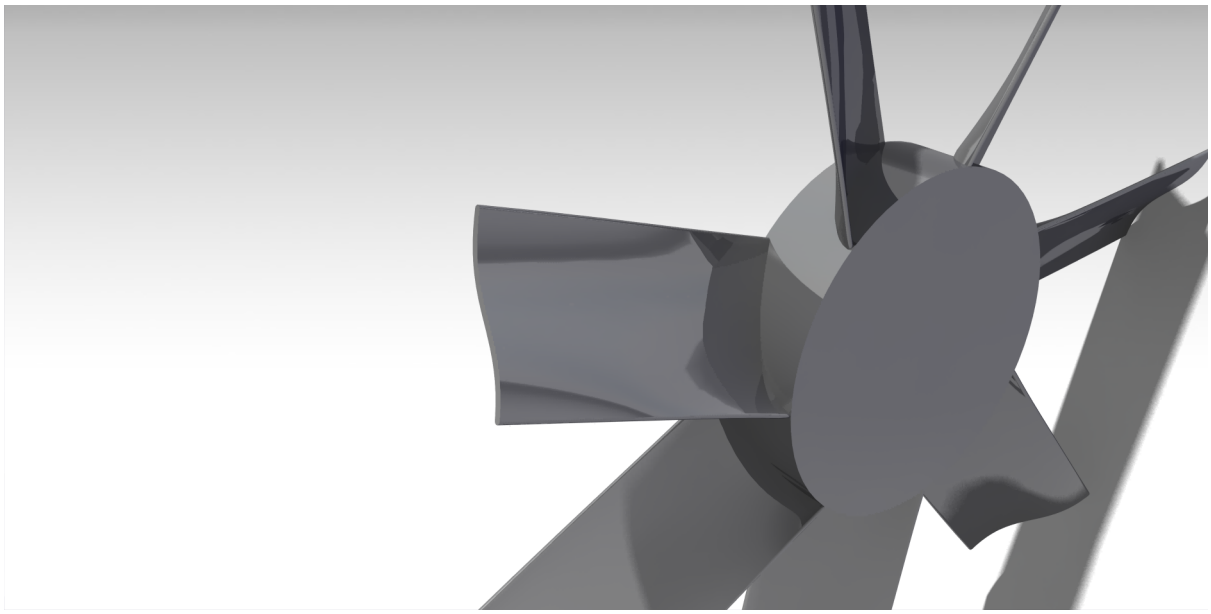

Figure 4.22: Final Fan Design Render

5 Aerodynamic Analysis

In this chapter the aerodynamic performance of the simulator is analysed. It focuses on the study of the vortices and its influence on the control surfaces: is the decrease in velocity or pressure over these surfaces substantial? In Section 5.1 the model that was used in order to determine the aerodynamic performance characteristics is discussed and verified. In Section 5.2 the results of the analysis will be presented and differences examined.

5.1 Aerodynamic Model

The purpose of airflow generation is to give the pilot the ability to enforce movement on the simulator using the control surfaces. Therefore, it is important that the effectiveness of the control surfaces is evaluated. To achieve this, disturbances in the flow are identified. The main objective of the aerodynamic design is to prevent that the control surfaces are not effective due to disturbances in the flow. A model of the airflow over the simulator has to be made to identify disturbances in the flow, at the locations of the control surfaces. Also, the aerodynamic characteristics of the wing have to be determined as they are used to calculate the loads the structure needs to take. Further, the aerodynamic analysis gives the increase in lift of a wing if the ailerons are deflected. As the clearance between the wing tips and the wall of the wind tunnel is small, the wall may have significant influence on the aerodynamic characteristics of the wing and wall interaction needs to be taken into account in this phase of the design.

This section describes the physical phenomenon that is modelled as a start. After that, the actual model is explained and the verification procedure of this model is described. This section is concluded with a review on the reliability of the model.

5.1.1 Physical Model

The airflow created by the fans over the flight simulator in the wind tunnel is modelled. Two different airflows are modelled: the airflow over just the wings and the airflow over the entire simulator, including support structure and wind tunnel. Next to that, the ailerons and the lift force that is created by deflecting these is modelled.

The flow over the wings is modelled the wall at 0.1 meter and at 0.5 meter. The model of the wing with the wall at 0.1 meter is analysed to identify at what distance from the wing tip the ailerons should be located to be fully effective. The comparison between the airflow over the wing with the wall at 0.1 meter and at 0.5 meter is made to determine whether there is a large difference in flow conditions over the wings if the wall is located further from the wings. If the difference is significant, the effectiveness of the ailerons should be analysed separately at neutral position and during roll and yaw, as the distance from the wings to the wall becomes larger during roll and yaw.

The effectiveness of the control surfaces is dependent on the airflow over the control surfaces, which may be influenced by the walls and the support structure. If the airflow over the ailerons, rudder and elevator is disturbed by the support structure or any other part of the Aeolusim, the forces and moments created by the control surfaces may be different than predicted by the control and stability analysis. By simulating the airflow over the complete flight simulator, including the control surfaces, the support structure and the wind tunnel, the properties of the flow near the control surfaces can be evaluated. The velocity and pressure distribution of the flow over the control surfaces is determined by the aerodynamic analysis.

The last thing that is modelled effect of deflecting the ailerons The increase in C_L caused by deflection of the ailerons at a range of angles of attack is calculated by this model. This value is used to analyse roll motion in Section 7.1.6.

5.1.2 Numerical model

The design of the wing and of the complete flight simulator is created in CATIA V5 Release 20[1], later referred to as CATIA, after which it is imported in ANSYS® Fluent, Release 15.0 [2], later referred to as ANSYS Fluent. ANSYS Fluent is a CFD program that can give numerical solutions to fluid flow problems using the Navier-Stokes equations. The solution that is obtained using this numerical simulation gives the aerodynamic characteristics of the wing and gives the velocity and pressure distribution of the entire flow over the Aeolusim. To get a solution

[1] *www.catia.com*
[2] *www.ansys.com*

of the flow in ANSYS Fluent, different choices for the settings in the program have been made. The design model consists of the specific combination of these settings, the computational domain, the flight simulator model and the equations underlying ANSYS Fluent. The choice for the computational domain and the settings in Ansys Fluent is described briefly.

The computational domain is a rectangular cuboid representing the test section of the wind tunnel. The boundaries of this cuboid are treated as walls. The width of the cuboid is 3 meters, the height is 1.9 meters and the length is 8.5 meters. The cross-sectional shape of the wind tunnel is simplified to a rectangle and the contraction section and the diffusion section of the wind tunnel are not included in the simulation. The inflow condition is a uniform, straight, steady flow of 12.4 m/s.

For the creation of the mesh a trade-off between accuracy and calculation time has been made. The size of the elements of the mesh is small near the surfaces of the flight simulator and near the walls of the wind tunnel. Also locations where vortices will occur, such as in the flow behind the simulator, a refined mesh is used. A refined mesh at these locations is likely to result in higher accuracy of the result. The minimum cell size is set to 1 mm, the maximum cell size is set to 250 mm. For smoothing of the mesh the high setting is used, so a high number of iterations is used to smooth the mesh. A coarse relevance centre is used.

The solver that is used is a pressure based solver. A consideration between accuracy and calculation time resulted in the choice of the k-epsilon model as the viscous model. For the near-wall treatment, non-equilibrium wall functions are used.

The increase in lift of a wing if the aileron is deflected is calculated using the airfoil analysis code XFOIL version 6.94 [3]. The NACA 0015 airfoil is loaded into XFOIL and a plain flap is created. The airfoil with flap is used as a model for the actual airfoil with aileron. The 2D lift coefficient C_l is calculated at the range of angles of attack from -20 to 20 degrees and a range of aileron deflection from 0 to 10 degrees, using a viscous flow simulation. A Reynolds number of $8.5 \cdot 10^5$ is used for the simulation, resulting from an airspeed of $12.4 m/s$ and a chord length of 1 meter. The increase in lift coefficient of the particular aileron deflection angles is then calculated by subtracting C_l with no aileron deflection from C_l with aileron deflection. This is done over the whole range of aileron deflection angles and angles of attack. The ailerons are located outside the influence of the wing tip vortices and thus the increase in 2D lift coefficient can be used to predict the increase in 3D lift coefficient C_L over wing area in front of the trailing edge of the aileron. Then, the rolling moment M_{roll} is calculated using Equation 5.1. Here, ρ is the density of air, V is the airspeed, S_{ail} is the wing area behind the aileron trailing edge, ΔC_L is the increase in lift coefficient due to aileron deflection, and d_{ail} is the arm of the increase in lift ΔL to the rotation point.

$$M_{roll} = \frac{1}{2}\rho V^2 S_{ail} \Delta C_L d_{ail} \tag{5.1}$$

5.1.3 Verification & Validation

ANSYS Fluent is a leader in CFD modelling and is one of the most used commercial CFD codes. The verification manual [10] shows the results of the verification of the code by ANSYS Inc. It also allows any user to check the verification procedure as performed by ANSYS Inc. Therefore, the code is deemed to give solid results. However, misuse of even top quality software can lead to erroneous results. Therefore, the method of using ANSYS Fluent as described in Section 5.1.2 needs to be verified. The procedure for verification is the lift and drag coefficients of the 3D wing, without wall interaction, is determined at a single angle of attack with use of the ANSYS Fluent model. The result is compared to the 3D lift coefficient calculated using the DATCOM method. The results of the verification are presented in Table 5.1. Appendix E shows the convergence plot of the verification. It took 100 iterations and about 90 minutes for the simulation to converge. The values of C_D are close, the difference between the values of C_L is larger. An explanation might be that the DATCOM method has lower accuracy for thick airfoils, relative to thin airfoils [11]. It is also possible that the settings in ANSYS Fluent can be optimized further, or that such error is inherent to a CFD analysis using ANSYS Fluent. However, the difference is deemed small enough to verify the simulation of ANSYS Fluent using the method as described in 5.1.2 and at the Reynolds number of the actual 3D wing.

Validation of the model needs to be done with a wind tunnel test. A complete model of the airframe and support structure needs to be placed inside a wind tunnel, after which the flow conditions over the control forces need to be determined. Also the force that is created by deflecting the ailerons, and the total force that is exerted on the support structure can be determined at various angles of attack. These results can be compared by the predictions of the model to validate the model.

[3] *http://web.mit.edu/drela/Public/web/xfoil/*

Table 5.1: Verification results of a rectangular wing with a NACA 0015 airfoil at an angle of attack of 10 degrees.

	ANSYS Fluent Model	DATCOM	Deviation
C_L	0.49	0.43	14%
C_D	0.057	0.056	1.8%

5.1.4 Reliability

As stated, ANSYS Fluent is considered a suitable program for these type of airflow simulations. The reliability of the solution is mainly dependent on the user of the software. For this analysis, the software is used by inexperienced users in a limited time frame. However the decisions for the settings are made carefully, the lack of experience and time might have led to a model that has some flaws. More experience and time gives the opportunity to recognize certain signals that indicate errors in the model that may not have been detected in the current analysis. Overall, the reliability of this model is considered to be high, the improvement that could be made to this model is considered small.

5.2 Aerodynamic Performance

Now the design models have been described, the analysis can be started and results can be evaluated. The first analysis is about the aerodynamic influence of the structure and the pilot on the control surfaces at the tail. The same analysis will also yield the total lift and drag force on the support structure The second analysis is about the aileron and the effect of the wall nearby the wing tips on the air-stream. The last analysis concludes with the 2D lift-creation capabilities of the aileron.

5.2.1 Rudder & Elevator Effectiveness

The rudder and elevator effectiveness is dependent on the airflow velocity over the respective surfaces. The total 3D body has been analysed in ANSYS Fluent in order to check the influence of the turbulent flow behind the pilot and the structure on these control surfaces. This is done for two different cases: one where behind the pilot an aerodynamic fairing is added, and one without this fairing. In Figure 5.1 the 3D plot of velocity streamlines over the centre section plane of the simulator without fairing at neutral position can be seen.

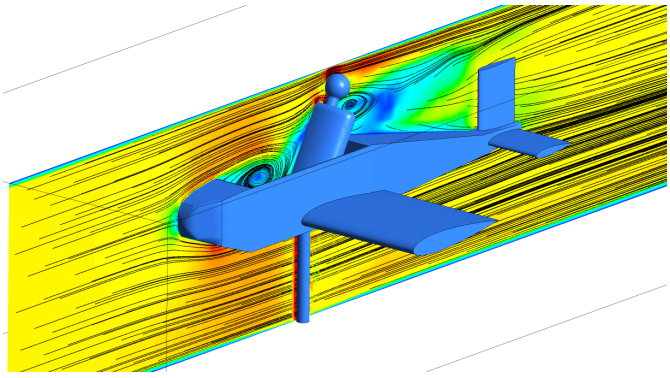

Figure 5.1: Airflow streamlines over simulator without fairing at neutral position

The wake behind the pilot is clearly visible and will have a great impact on the velocity over the vertical tail. In order to get measurement values, a section plane is created just in front of and perpendicular to the tail. At this section plane the velocity magnitude contour plot is created and can be found in Figure 5.2.

In Figure 5.2 the airstream velocity at the vertical tail is measured to be approximately 5 m/s, which means a decrease of more than half of the inlet velocity which was initially set at 12 m/s.
A less significant decrease in velocity can be observed at the horizontal tail which is the result of the main wings' wake. There the average velocity is approximated to 10.5 m/s. In both situations these decreases in velocity affect the controllability of the simulator and should be accounted for.
In order to decrease the turbulent flow over the tail an aerodynamic fairing is placed behind the pilot. The analysis is repeated and the results are shown in Figure 5.3.

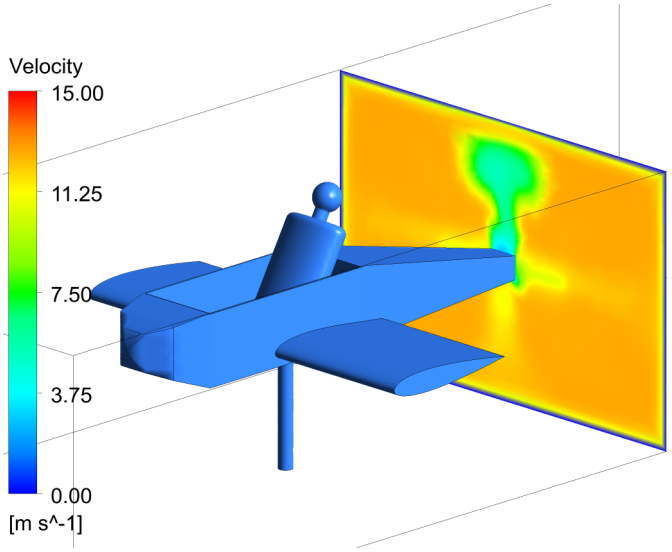

Figure 5.2: Velocity magnitude in front of taiplane of Aeolusim *without* aerodynamic fairing behind pilot

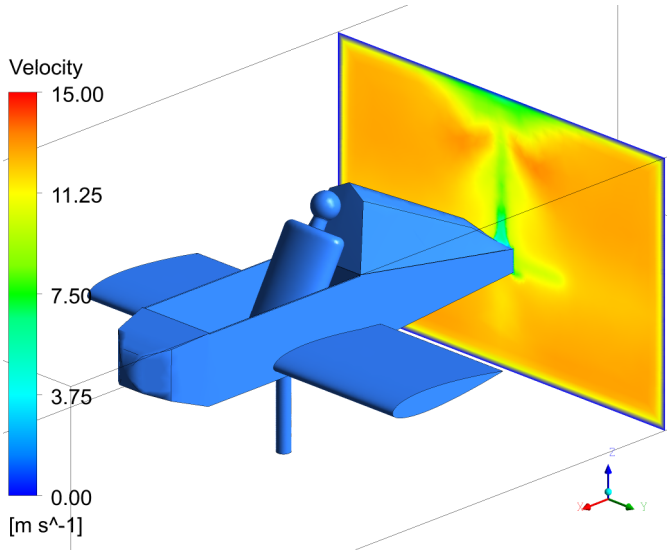

Figure 5.3: Velocity magnitude in front of tailplane of Aeolusim *with* aerodynamic fairing behind pilot

When Figure 5.2 is compared to Figure 5.3, a significant difference in turbulent flow can be observed. With the fairing added the velocity at the vertical surface is around 7.5 m/s, which means an increase of 50% with respect to the motion-base without the fairing. In the lift-formula, the velocity is found squared. Thus, the created force and moment are increased by 125% by only adding the fairing. This increase in performance is considered more valuable than the added weight and cost for and therefore this design is chosen.
ANSYS will also compute the lift and drag coefficients and forces through this analysis. The lift and drag forces on the support structure for the motion-base with fairing for zero angle of attack are $L = -5.8N$ and $D = 49N$ with corresponding coefficients: $C_L = -0.07$ and $C_D = 0.56$. The explanation for the lift being almost zero is due to the symmetric airfoils which at zero angle of attack will not generate any lift.

Due to the fact that the fans have a fixed position and power setting, the airflow velocity vector will be of the same magnitude and direction for every position of the simulator's motion base. As a result, the wake vortices originated behind the structure and pilot will differ substantially for different roll, pitch and yaw angles. Therefore, for the max positive pitch angle (10 degrees) the same analysis is done and a velocity plot in front of the tail is made as can be seen in Figure 5.4.

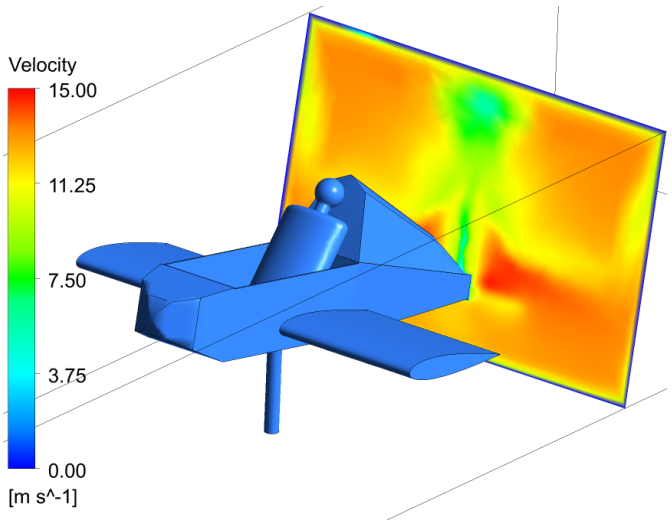

Figure 5.4: Velocity magnitude in front of tailplane at pitch angle of 10°

For this configuration, the velocity at the vertical tail surface is measured to be 7 m/s. Although the rudder on this surface will be slightly less effective, the pilot will still be able to yaw while pitching.
For the aerodynamic loading case the new lift force generated in this configuration equals 250 Newton, the drag force 68 Newton and the corresponding C_L and C_D values are 2.87 and 0.80 respectively.

5.2.2 Aileron Effectiveness

In order to have a clear view of the aileron effectiveness, research has been conducted for the interaction between the wing and walls of the wind tunnel. Using the design model described in Section 5.1 results in the form of ANSYS plots are presented.
First, a section plane is created aligned with the inlet of the wind tunnel and perpendicular to the wind tunnel wall through the centre of the aileron surface. This can be seen in Figure 5.5.

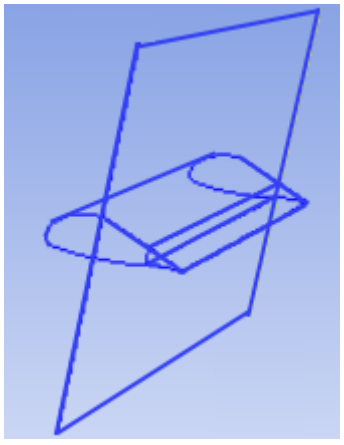

Figure 5.5: Section plane for tip vortex analysis

The vorticity magnitude as seen from this section plane over the surface of the wing is plotted for two different cases: one where the wing tip is at a 0.5 meter distance from the wind tunnel wall and the other where this distance is only 0.1 meter. The inlet airspeed is set at 12 m/s. The results are given in Figure 5.6.

As can be seen, the tip vortex for the wing-wall distance at 0.1 meter is weaker than when distanced 0.5 meter from the wall. This actually confirms that it acts more like a infinite wing when getting closer to the wall. However, this difference is very small and can be neglected as the lower and upper limit for the vorticity magnitude were manually defined (zoomed in) in ANSYS in order to make differences visible.
A better look at the influence of the tip vortex on the performance of the aileron can be shown by plotting the

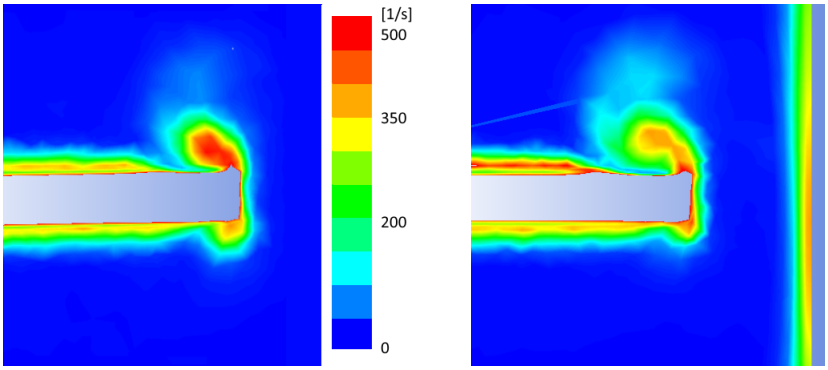

(a) wing-wall distance = 0.5m (b) wing-wall distance = 0.1m

Figure 5.6: Vorticity magnitude of tip vortex in [1/s]

pressure distribution over the wing. In Figure 5.7 the gauge pressure distribution on top and bottom of the wing is shown.

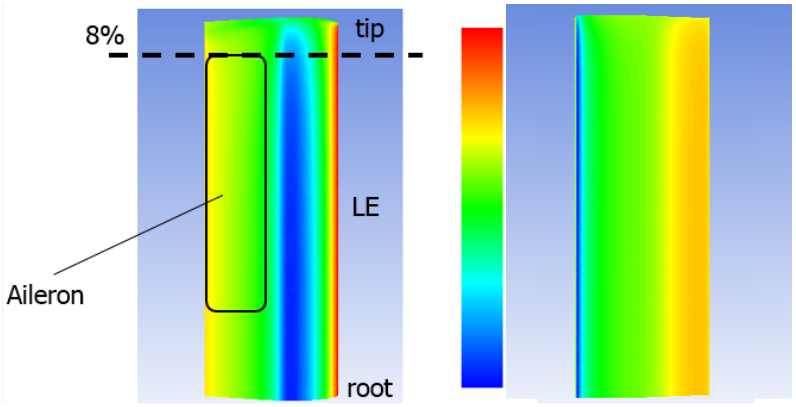

(a) Top-view (b) Bottom-view

Figure 5.7: Static gauge pressure distribution over wing

As can be clearly seen in the top-view (Figure 5.7a) the gauge pressure at the tip is almost zero which would mean no lift is created there. The aileron surface will therefore have no effect at this position. This area is approximately 8% of total wing surface. Therefore, it is chosen to end the aileron surface at 92% of the wingspan as seen from the root.

Unlike the elevator and rudder which are fully movable surfaces, the aileron is only part of the main wing. Therefore when changing the deflection of the aileron the camber of the actual wing is deformed and the lift creation-characteristics are changed. In order to analyse this change in lift due to the aileron XFOIL is used. The aileron is hinged at 48% of the chord from the leading edge at half the thickness. In the range of aileron deflection angles from 0 to 10 degrees the increase in lift coefficient of the airfoil is calculated. Figure 5.8 shows the model of the airfoil with a 10 degree aileron deflection angle that is created by XFOIL and is used for analysis. The $C_l - \alpha$ curves of the NACA 0015 with no aileron deflection and with 10 degrees aileron deflection is shown in Figure 5.9. Deflection of the aileron increases C_l over the whole range of angles of attack. It decreases the positive stall angle and makes the negative stall angle more negative. From the $C_l - \alpha$ curves, ΔC_l can be calculated, where ΔC_l is the increase in C_l for an aileron deflection relative to no aileron deflection. Figure 5.10 shows ΔC_l versus α for an aileron deflection of 10 degrees. An increase in positive α results in ailerons that are less effective, since the $C_l - \alpha$ curves of the airfoil with and without aileron deflection are closer to one another. The relationship between ΔC_l and δ_a is close to linear in the range of δ_a from 0 to 10 degrees, for angles of attack between -10 and 10 degrees. For purpose of illustration, Figure 5.11 shows the curve of ΔC_l versus δ_a at an angle of attack of 10 degrees. Figure 5.12 shows the rolling moment M_{roll}, that is created if the left aileron is deflected 10 degrees downward, and the right aileron is deflected 10 degrees upward, for a range of angles of attack.

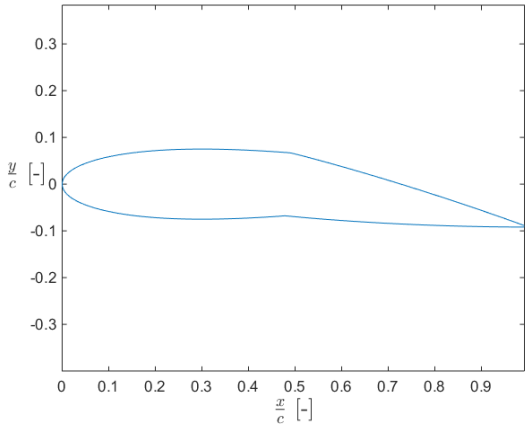

Figure 5.8: XFOIL model of NACA 0015 with aileron deflected 10 degrees.

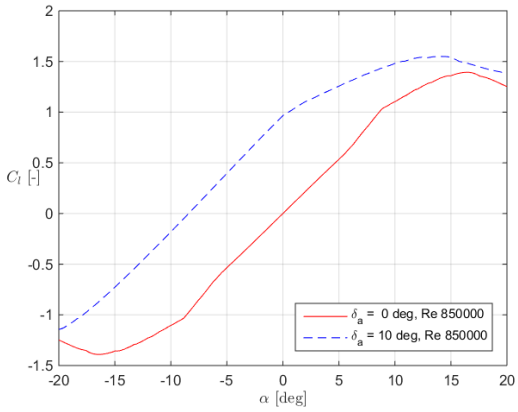

Figure 5.9: XFOIL prediction of $C_l - \alpha$ curve of the NACA 0015 airfoil with zero aileron deflection and with 10 degrees aileron deflection.

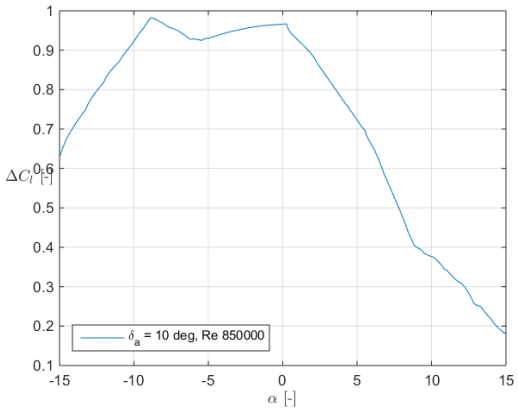

Figure 5.10: Increase in C_l for aileron deflection of 10 degrees relative to no aileron deflection for a range of angles of attack.

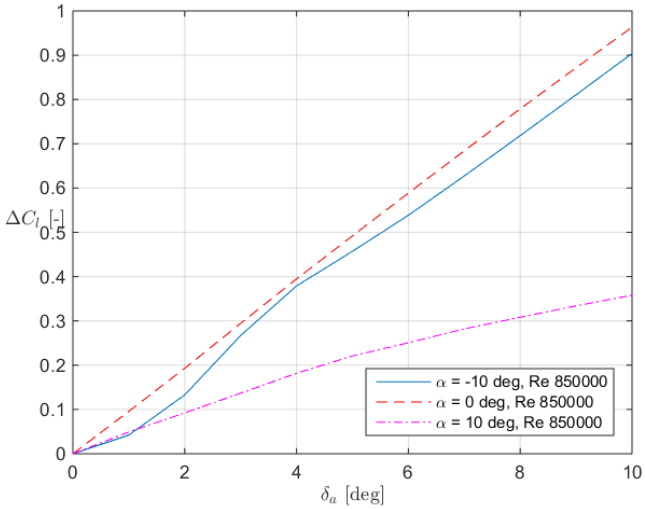

Figure 5.11: Increase in C_l versus δ_a for angle of attack of 10 degrees.

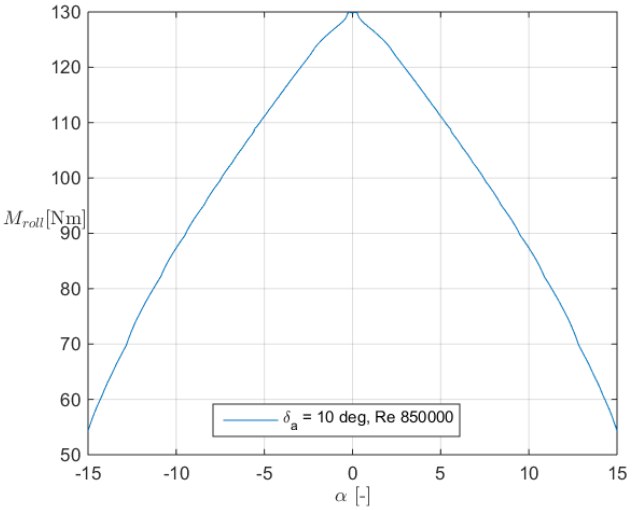

Figure 5.12: Rolling moment for aileron deflection of 10 degrees.

6 Structural Analysis

The initial design of the Aeolusim was based on aerodynamic performance and aesthetics requirements, as stated in Chapter 2. During its operational life the Aeolusim may not show signs of structural failure as a consequence of the expected normal operating loads. A design capable of withstanding the loads is to be analysed in order to obtain output values for its weight, production costs and mass moment of inertia (required for Chapter 7.1). Section 6.1 explains the method of approach that has been utilized to perform the analysis for all elements. Section 6.2 shows the design process, application and results of the method, for the main wings. Similarly, this is shown for the horizontal and vertical tail planes in Section 6.3, for the fuselage in Section 6.4 and the supporting structure in Section 6.5. The structural analysis has been performed while optimising for the following key concepts:

SA-1 The structure may not fail under the expected operating loads.

SA-2 The structure may not exceed a reasonable deflection.

SA-3 The structure is to be optimised w.r.t. production costs

Failure [**SA-1**] is defined as either plastic deformation or buckling and its respective deformation [**SA-2**] has been assessed based on engineering judgement.
As listed in [**SA-3**], production costs and mass moment of inertia are key concepts. Production costs will have to be minimised in order to achieve the top level requirement of a €35000,- overall price tag per unit. Production costs are assumed to depend on the number of specific parts, their complexity, production method and the used material (mass).

This chapter shall discuss the sizing of the the main wing, tail surfaces, support structure and fuselage in Section 6.2 to 6.4, respectively. Before doing so the method to analyse the structural integrity is explained in Section 6.1. Final output values, such as mass and production costs of the Aeolusim will be concluded in Section 6.6.

6.1 Method

The structural analysis was performed with a three dimensional model created in CATIA V5 Release 20[1] and analysed using ANSYS®Mechanical Release 15[2], in this chapter referred to as ANSYS.
ANSYS is a Finite Element Analysis (FEA) program. Its results are dependent on the mesh size. A bigger mesh, thus smaller elements, yields more accurate results whilst consuming more computational resources.
Standard configurations have been used to automatically generate an appropriate mesh in ANSYS (i.e. using the *'coarse'*, *'medium'* or *'fine'* settings).
An initial and first run of each part was performed with an auto-generated 'coarse' mesh. This mesh was manually refined by defining a maximum element size of 1 mm about a sphere of influence where one would expect stress concentrations. A second run was performed using the 'medium' settings, similarly refined about the points where the first run indicated high stress levels. Computational resources did not allow for a smaller (overall) mesh size in the current design phase.
Sharp edges, which may appear near flanges, can introduce artificial stress singularities. The output of the finite element model will increase its von-Mises stress at that specific location for bigger mesh sizes: reaching for example 1000 MPa for a mesh size of 1 mm and an applied load at the stiffener of the main wing of 100 N. These singularities arise as a limitation of the finite element model [12]. A quick workaround was found to 'smoothen' sharp edges by introducing a local radius. This did not always do the trick. Persistent stress singularities were therefore neglected from the analysis based on engineering judgement.

To analyse each structure, standard settings have been used in ANSYS. Static structural mechanics was analysed using the Static Structural Mechanics Toolbox in combination with the built in ANSYS Parametric Design Language (APDL) solver whilst accounting for standard Earth gravity components. Dynamic (time response) mechanics were deemed beyond the scope of the current design phase.
Contacts between two parts have been simulated using contact surfaces. Forces were applied over an area of at least 1 cm^2 (or as large as the structure allowed if this could not be achieved), since singular point forces are not to be expected in reality.

[1] *www.catia.com*
[2] *www.ansys.com*

Verification
Analogous to ANSYS Fluent, see Section 5.1.3, ANSYS Mechanical is verified by ANSYS inc. Its respective verification is shown in Reference [13]. Based on this reference ANSYS Mechanical was deemed to give solid results. However, misuse of even top quality software can lead to erroneous results. Several simple load cases have been used to verify the use of the respective software. For these results please refer to the preceding design report (Reference [3]).

Model Reliability and Validation
The reliability of a solution obtained using any finite element analysis is highly dependent on the user of the software. For this analysis, the software was used by inexperienced users in a limited time frame. Decisions made while configuring the software have been made carefully. Nonetheless, the lack of experience and limited time frame might have led to a model that has some flaws. More experience and time will provide the opportunity to recognize areas of improvement. An area of improvement that can already be indicated is to improve the method of surface contact. The current method uses the entire surface-to-surface interface of two adjacent parts as surface contact. This would result in accurate results for a glued structure. The contact area will be relatively lower for riveted, or bolted, structures - dependent on the respective rivet spacing. Incorporating this would include stress concentrations due to rivet pockets, and improve the simulation of the stress distribution because of the skin for said configurations.
Including the effects of rivets would however add little to this analysis, since its main outputs are production costs, weight and mass moment of inertia. The small scale and the little loads acting on the structure are expected to allow for fairly reasonable estimates for the costs of riveting. In addition, the used raw material is expected to increase by as little as a few percent due to the effects of the rivet pockets and the Aeolusim's small scale.
Overall the model has been kept simple and its respective reliability is considered to be high enough for the current design phase. Validation of its result is to be performed using a test with strain gauges, specifically located at several points where the model indicates high stress levels.

6.2 Main Wing

This section shall describes the sizing of the main wing. Subsection 6.2.1 describes what load cases the wings are expected to be exposed to. The design of the wing is not only dependent on the load cases, but also on the manufacturability. This is discussed in Subsection 6.2.2, where a configuration for the wing is chosen and sized to comply to the requirements of structural integrity and manufacturability. After the sizing, a stress analysis is performed in Subsection 6.2.3. A review of the design is discussed in Subsection 6.2.4.

6.2.1 Load Cases

The main purpose of the wing is to generate aerodynamic forces that will induce a control moment. Its respective aerodynamic loads were defined in the aerodynamic analysis of the wing. In the entertainment industry, however, it is expected that the likelihood of someone applying a force, lean or possibly even sit on the wing during the Aeolusim's lifetime is likely (rated $50-70\%$ in the risk assessment, Chapter 12). Even with visual aids such as warning stickers there is bound to be someone who 'did not see' or 'forgot' the warning. This event would have a catastrophic impact if the structure is not designed for this load. To ensure robustness of the Aeolusm during its operational life, this load case has been taken into account.
The maximum loads applied at the wing are derived from Chapter 5 and the top level requirements (maximum pilot weight of 95 kg). The load cases are defined as follows,

Aerodynamic A	Maximum lift force (pitch up and ailerons positively deflected)
Aerodynamic B	Minimum lift force (pitch down and ailerons negatively deflected)
Misuse 1	Bumping into the wing with a maximum 10 *kg-f*
Misuse 2	Sitting on the wing with a 95 *kg-f*

The aerodynamic load cases occur when the simulator is operational: the spar is clamped at the root. Misuse, on the other hand can only occur when the simulator is in a stationary and locked position: clamped at the root and simply supported by a piston at the tip. It is assumed that loadcase '*Misuse 2*' occurs between 10 to 50 cm with respect to the leading edge. This assumption was made because of the limited space and curvature of the wing to position, for example, one's foot. In stead it is assumed that the front part of the wing (< 10 cm) has to carry one third of the pilots weight when he or she is sitting on the wing. Locations exceeding the 50 cm were not taken into account. The ailerons start at that specific location, and putting one's (full) weight at a location 50 cm from the leading edge would be intentionally damaging the system.

6.2.2 Wing Design

Analytical models for the main wing could not be verified because of the author's unfamiliarity with classical plate and shell theory (the Kirchhoff–Love theory) to incorporate the contribution of the skin. The latter turned out to be a significant factor when incorporating a three dimensional model in a finite element analysis, possibly due to the AEOLUSIM's small scale. Analysis has therefore been performed directly using CATIA and ANSYS, as explained in Section 6.1. The resulting design of the wing is shown in Figure 6.1. It consists of two spars, two ribs, a stiffener and three skin plates (top, front and bottom). All components will be made of aluminium 7075-T6, as selected in the previous design report (Reference [3]). Parts are to be connected using blind rivets. These blind rivets are relatively simple to use, and are therefore chosen to limit production cost. The aileron consists of wooden ribs covered with a canvas skin. Wood was chosen because of its low density and easy production. A specific type of wood is yet to be selected. The loads acting on the aileron are relatively small, which makes wood a viable choice. Technical drawings with dimensions of all respective parts are included in Appendix G.

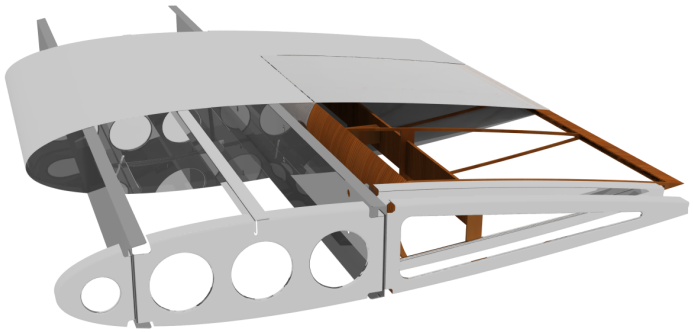

Figure 6.1: Wing structure. Half of skin has been omitted for illustrative purposes.

A configuration with two spars was chosen to ensure the stability of the wing when someone is leaning on the wing. The stiffener was in turn required to reduce the internal stress when someone is sitting on the wing (loadcase *'Misuse 2'*). The segments of the ribs are relatively simple parts. They can be made of sheet metal by rubber forming. The male dyes necessary for this production are to be made out of wood. These dyes are therefore inexpensive since their shape does not require much skill in wood craft to be made. This production process will allow all parts of the ribs (front, middle and aft) to be created with one press, using multiple dyes, thus reducing the number of hours required to, for instance, rent the press. The skin is to be rolled into form over a male die, preferably wood to reduce cost. Stretch forming is proposed to obtain the curvature of the leading edge. The spars and L-beam (stiffener) can also be made of sheet metal by using guided bending methods such as folding (especially suitable for the spars) or v-shape punching for the L-beam. An L-beam made through extrusion is an option, however this production method is assumed to be more expensive based on the required equipment. In addition, the longeron has a L-shaped cross-section ($20mm$x$20mm$x$1mm$) which might allow buying it as an off the shelve part. A quick investigation at multiple suppliers yielded minimum cross-sectional dimensions for an 'aluminium angle beam' of $20mm$x$20mm$x$1.6mm$ for 2.22 GBP per meter[3] (€2.95, January 27th 2015). Clear estimates for the earlier production methods to compare this with the off-the-shelve parts could not be obtained. It is however expected that the latter is favourable nevertheless.

Stress analysis of the wing structure, results presented in Section 6.2.3, concluded that the internal stresses are small, such that production limits for the geometry become dominant. The structure has therefore been sized for this minimum thickness. No clear information could be found about the minimum thicknesses and bend radii of the specific processes. The following assumptions have therefore been made:

SAW1 The minimum thickness for rubber forming and to allow the end-product to be riveted is 1 mm

SAW2 The minimum thickness for guided bending and to allow the end-product to be riveted is 1 mm

SAW3 The minimum skin thickness for (rolled) aluminium is 0.5 mm

Assumptions **SAW1** and **SAW2** have been made based on engineering judgment, whereas assumption **SAW3** was based on assumptions made in Reference [14]

Production costs for the main wing have been determined based on the used raw material and an estimation for the production costs. Exact numbers for production cost depend on the volume and complexity of the part

[3] http://www.metals4u.co.uk/

and may require a bid from a manufacturer. Nonetheless, it is expected that a male dye to rubber form a metal sheet cost approximately €80,- per male dye (material and manhours), which can be recycled for multiple units. Rubber forming is preferably done by an external party, or at a rented press. One complete wing (both left and right) will require 16 parts to be rubber formed over three separate male dyes (front rib-section, middle rib-section and aft rib-section). It is expected that renting a rubber press cost €110,- per hour, including the operator's man hour. If all parts can be pressed in one hour, which is likely for only 16 parts, this would result in €360,-. The same reasoning is applied to the forming of the spars, however they would not need dyes to be formed. It is expected that this would result in an expected forming cost of €110,-. The material costs are in turn obtained using CES Edupack 2014[4] and found to be €1.60 and €1.- for aluminum and wood (average per kg), respectively. The resulting material cost are shown in Table 6.1. As expected, raw material costs are relatively inexpensive. It is, however, impossible to acquire raw materials without prior production. To incorporate this, take scrap material into account and allow for contingency, the total material cost was multiplied by a factor of 15. Thus resulting in a total material cost of €286.48.

Assembly of the main wing is budgeted to take about 2 days by one person. Assuming a normal working day (8hrs) and a nominal payment of €40,- per hour (including VAT and company share in health care etc.) results in an assembly cost estimate of €640,-. To allow for contingency and equipment use this result has been multiplied by 1.5 to conclude a final estimate of €960,-.

The total cost of the main wing are a summation of material costs (€286.48), forming costs (€110 + €360) and assembly costs (€960,-). This summation yield a total estimate of €1716,48.

Table 6.1: Material cost per part of one complete wing (left and right

Part	**Mass [g]**	**Material cost [€]**
Front rib section (x4)	35	0.06
Middle rib section (x4)	138	0.22
Aft rib section (x8)	127	0.20
Front spar (x4)	219	0.35
Aft spar (x2)	249	0.40
Longeron (x2)	113	0.18
AL skin (x2)	2300	3.68
Rib aileron (x2)	11	0.02
Front bumper aileron (x2)	11	0.02
Spar aileron (x2)	202	0.2
Canvas skin (x2)	600	3

6.2.3 Stress Analysis

As previously stated, the wing was sized using finite element analysis. The load cases previously defined in Section 6.2.1 can be applied at a multitude of positions on the predefined wing structure. Analysis has therefore been performed for several locations, all indicated in Table 6.2 (Body Axis Frame).

The resulting maximum von-Mises stress, deformation and the corresponding safety factor with their respective locations are presented in Table 6.3. As this table shows, the maximum von-Misses stress occurring in the wing is 9.28×10^7 Pa, resulting in a safety factor of 3.87. This implies an over-design, even when looking at the desired safety factor of 2. However, the loads acting on the wing are so small that wing structure was designed to meet the expected minimum dimensions required for its production method. For that reason, the high safety factors are acceptable. The maximum deflection is 0.61 mm, which is almost unnoticeable and will not affect the wing shape. Two load cases are highlighted to explain some phenomena that occur in the structure of the wing. First of all, the case in which a 95 kgf load is applied right on the stiffener (*Misuse 2C*). This loadcase causes peak stresses in and along the stiffener, see Figure 6.2a. The stiffener distributes the load via the ribs to the spars. The skin also carries some stresses to relieve the stiffener and thus counteracts large peak stresses.

Figure 6.2b shows the total deformation of the structure. The maximum deflection is located where the force is applied. The aileron also shows quite a deflection, this effect will be addressed later.

Multiple aerodynamic load cases have been analysed. The output for load case *Aerodynamic C*, where the wing is positioned at maximum pitch and the aileron is deflected, is shown in Figure 6.3. The stresses throughout the

[4]http://www.grantadesign.com/education/edupack/edupack2014.htm

Table 6.2: Load application for the Finite Element Analysis

Loadcase		**Point of load application**
Misuse 1	A	Between the outer and middle ribs, on the leading edge in the negative $x-$direction
	B	At the middle rib on the leading edge in the negative $x-$direction
Misuse 2	A	On the front spar in the middle of the wing in the positive $z-$direction
	B	Halfway between front spar and stiffener in the middle of the wing in the positive $z-$direction
	C	On top of stiffener in the middle of the wing in the positive $z-$direction
	D	Five cm in front of the front spar in the middle of the wing in the positive $z-$direction
Aerodynamics	A	Pitch up and ailerons positively deflected
	B	Pitch down and ailerons negatively deflected

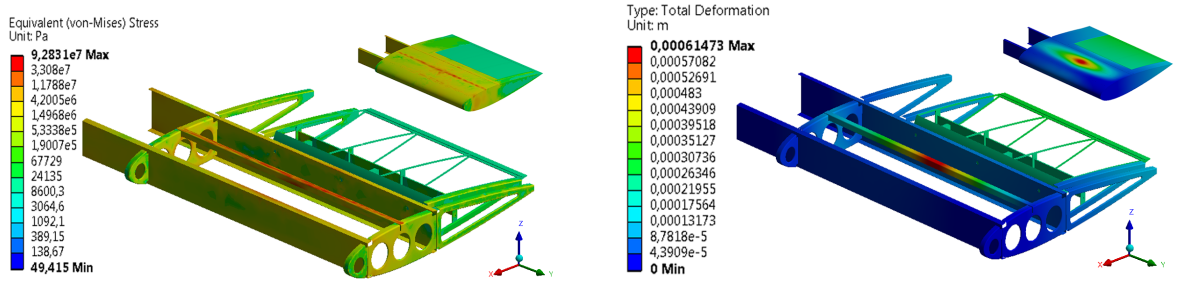

(a) von-Misses stress distribution

(b) Total deformation

Figure 6.2: Output for loadcase Misuse 2C

wing are so small that the aerodynamic forces will not cause any failure. This loadcase is, however, the primary loadcase during the Aeolusim's lifetime. A fatigue analysis has therefore been performed for the most critical aerodynamic load case using the current model[5]. The wing structure will experience a maximum of $6,000,000$ load cycles during the Aeolusim's 5000 hr lifetime, if, for example, a single pitch or roll manoeuvre lasts three seconds and all other maneuvres are neglected from the analysis. This assumption would result in the absolute worst case scenario, not to be expected in reality. Nonetheless, using the fatigue toolbox in ANSYS yielded a remaining safety factor of *7.9* after one billion cycles. This is a positive result. However, it does not take the effects of riveting into account. For this reason it is expected that the structure is able to cope with the number of cycles expected, but additional research using FEA and more computational resources are required to provide certainty.

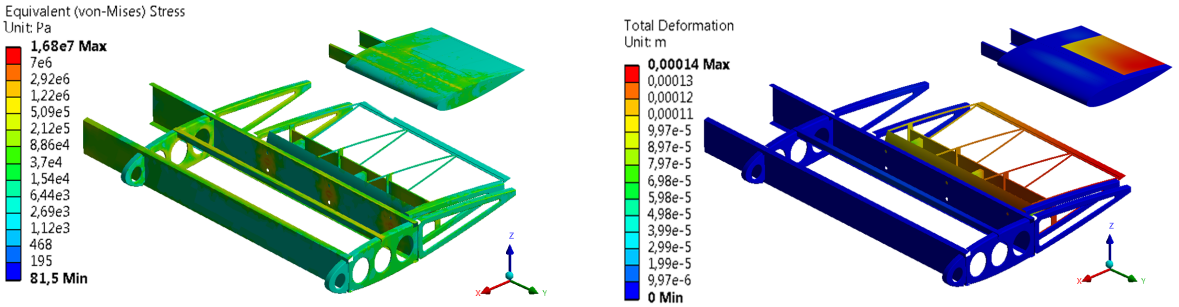

(a) von-Misses stress distribution

(b) Total deformation

Figure 6.3: Output for loadcase Aerodynamics C

[5]For the limitations of the current model, see Section 6.2.4

The results often showed a maximum deformation in the trailing edge of the aileron. This was due to the fact that the aileron is suspended at three rotation points and attached to the rear spar with small mechanisms, see Figure 7.15 for a clear view. If no loads were applied at the aileron, it deflected due to its own weight. These deflections are however so small that they are almost unnoticeable. In Figure 6.2b the colour of the aileron indicates a larger deformation with respect to the colour which is found in a large part of the wing.
Due to the small size of the mechanism that linked the aileron to the rear spar, stress concentrations arose at their attachment points. These stresses ranged from 2.16 MPa to 2.21 MPa, indicating that the structure will not yield. The stress concentrations can be clearly seen in the rear spar in Figure 6.3a. During the load case where the aileron was deflected this stress reduced to 1.68 MPa, because of the lift counteracting its weight.

Table 6.3: Maximum Von-Mises stress, deformation and minimum safety factor with their respective location.

Load case		σ (Pa)	**S.F. (-)**	**Location**	ν (mm)	**Location**
Misuse 1	A	1.18×10^7	30.4	Force application	0.10	Force application
	B	5.30×10^6	67.8	Rear spar at root	0.19	Rear aileron
Misuse 2	A	2.11×10^7	17.0	Attachment of skin to front spar	0.13	Force application
	B	6.01×10^7	5.98	Attachment of skin to stiffener	0.49	Force application
	C	9.28×10^7	3.87	Attachment of skin to stiffener	0.61	Force application
	D	9.83×10^6	36.6	Skin above front spar at mid	0.10	Force application
Aerodynamics	A	1.75×10^6	205	Stiffener	0.18	Rear aileron
	B	1.96×10^6	183	Bottom skin at root	0.20	Rear aileron

For all load cases a buckling check is done with ANSYS. The result is a number with which the current load has to be multiplied before the structure buckles. The most critical load case is *Misuse 2C* where the rib buckles at a load of almost 20 times higher, as clearly seen in Figure 6.4. The deformation is scaled down to give a good representation of the buckling rib, since a deformation of 1 m (see legend) would distort the picture too much. Based on this analysis it may be concluded that the wing structure is not very sensitive to buckling.

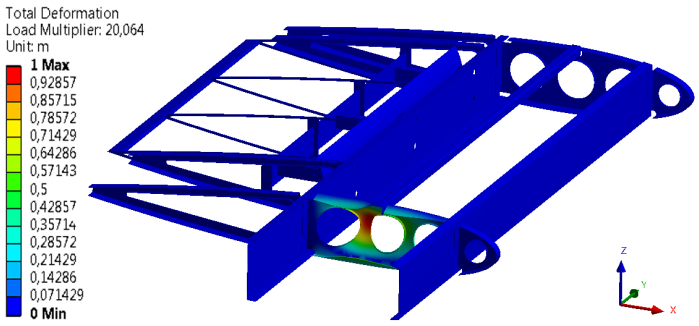

Figure 6.4: Buckling

6.2.4 Design Review

During the design, cut-outs were introduced in specific elements of the ribs. These cut-outs are fairly often used in the Aerospace industry to save mass. For the AEOLUSIM, however, mass is of lesser significance since it does not need to lift itself. These cut-outs will save weight, and therefore reduce mass moment of inertia for a more apt motion response, though they will increase production cost. A sensitivity analysis later performed concluded that a 100% increase in the mass moment of inertia has little effect, see Section 8.3. It may therefore be concluded that the cut-outs are relatively inefficient for the design at hand and are to be removed from future designs to save cost. All in all, if the structure is able to cope with the exerted loads with these cut-outs, it will also do so

without them (as it will become more rigid). It is to be investigated what the minimum required thicknesses are for production, such that the use of raw material (therefore cost) can be optimised.

A secondary structural analysis of the main wing is to be performed whilst incorporating the rivets used for bonding. This will yield more accurate results, taking into account the peak stresses due to the rivet pockets. In addition, Fluid Structure Interaction (FSI) Analysis will allow for a more accurate force prediction in the aerodynamic load cases.

6.3 Tail Section

For the Aeolusim to be able to pitch and yaw, it has to feature appropriate control surfaces that can create these motions. For this design, a conventional tailplane with full movable elevators and rudder is chosen. The structure of this tailplane has to be able to withstand the aerodynamic loads on it, whilst not deflecting too much to retain its aerodynamic shape. The minimum allowed safety factor is 1.5 and the maximum allowed deformation is set at 10% of the chord thickness. The elevators and rudder have a NACA0015 airfoil and a chord of 0.8 m, resulting in a maximum thickness of 12 cm. The maximum allowed deformation is thus 1.2 cm. A leading factor in designing the tail, as well as the rest of the structure, is the production cost, which will be highlighted later on.

6.3.1 Load Cases

The load cases that were used to analyse the tail are as follows. Both the elevator and rudder are supported at their hinge and standard earth gravity is applied. Since the lift force created by the elevator will not exceed its weight, the limiting load case is the one where the elevator creates a downward lift force. For the rudder, a force in the positive y-direction is chosen. In this case the direction should not matter since the structure is symmetrical.

6.3.2 Tail Design

The resulting design of the tail structure can be seen in Figure 6.5. Since the loads are very small, the rudder and elevator are made of fabric-covered wooden frames, whilst the internal spars are aluminium beams.

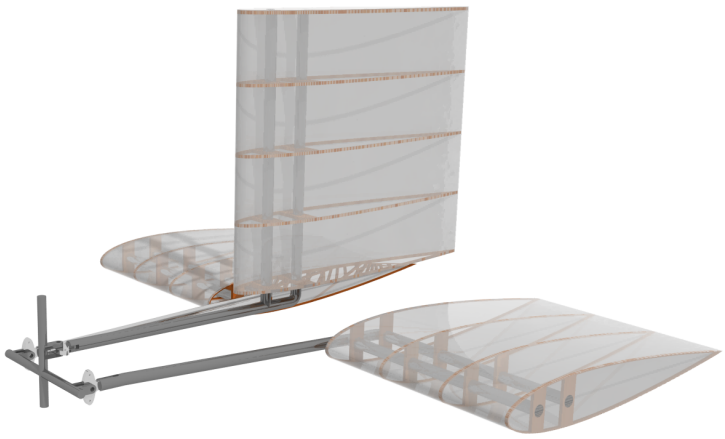

Figure 6.5: The tail structure

Two internal spars are chosen, so the ribs will not rotate about an axis. Also, standard annular beams are cheap and can easily be bent and welded together. Since the tail surfaces rotate about a point in front of the wing, relatively large moments will arise at its connection to the fuselage. The distance also creates a large deformation and thus fairly thick beams with a radius of 14 mm have to be used to make sure the deflection of the structure stays within the predefined limits. To keep production cost low, the same parts are used for the rudder.
The ribs can be cut from 8 mm thick wooden plates and produced in halves. These halves are then glued together and onto the spars. Finally the structure is covered with as polyester fabric. The spar is connected to the fuselage with the same mechanism used in the ailerons. Using similar parts also reduces cost and simplifies the design. It is made sure that this particular part can handle all loads, whether it is used in the tail or in the aileron.

The costs are estimated by determining the parts, man hours and machining costs that are needed to produce

the tail. Three annular beams of each 2 m length cost €70 [6], a wooden plate of 2.44x1.22 m to saw all the ribs from costs €29[7] and the skin is estimated at €2.50 per kg, resulting in a total of €4.90. The fabric is not bought per kg, but per square metre and to obtain the small surface the tail needs a safety factor of 10 is used on the raw material cost. The total material cost comes down to €148.
Employee costs are budgeted €40 per hour. The annular beams have to be bent and welded which is estimated to last 2 hours. Sawing the halve ribs will take about 6 hours and draping the skin takes around 4 hours. The final assembly of the tail planes will take another 6 hours, which brings the total cost of the assembly to €720. The total cost of the tail is a final €868.

Table 6.4: Tail cost

Part	Mass (kg)	Production cost (€)
3 Spars	5.72	150
26 Halve ribs	0.57	269
Skin	1.94	209

6.3.3 Tail Analysis

Both the horizontal and vertical tail have been analysed with ANSYS for several load cases. The resulting Von-Mises stress and deformation are shown in Figures 6.6 and 6.7.

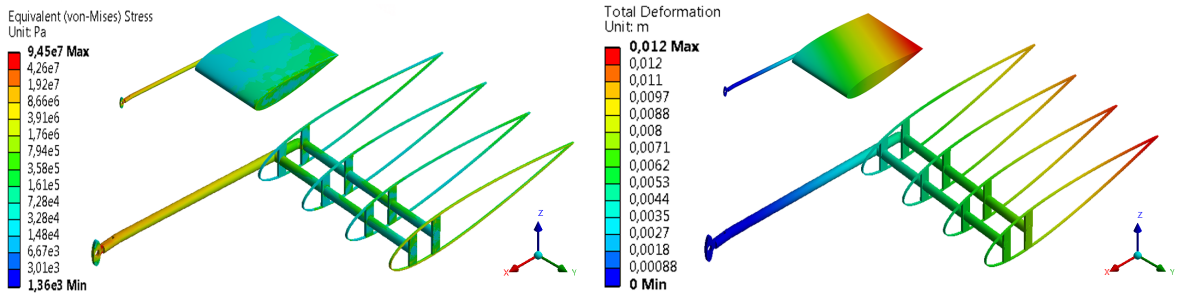

(a) Stress

(b) Deformation

Figure 6.6: Structural analysis of the horizontal tail

The maximum stress in the horizontal tail occurs where the spar is linked to the fuselage. This was already expected due to the sharp edges of the part that links them together and due to the moment created by the arm of the force. The maximum stress however is 9.45×10^7 Pa resulting in a minimum safety factor of 3.8.
In Figure 6.6b it is clearly seen that the maximum deformation happens in the most outboard side of the trailing edge of the elevator. This is due to the suspension point being inboard and ahead of the elevator. The maximum deflection is 1.2 cm which is exactly the predefined limit and this deflection limits the design of the spars.

The maximum stress the vertical tail experiences is 1.16×10^8 Pa which is severely higher than the maximum stress in the horizontal tail. This is due to the fact that higher peak stresses arise in the mechanism that links the rudder to the fuselage. The weight causes a shear force that is applied at a smaller area, compared to the elevator. The minimum safety factor of 3.1 indicates the structure will not fail.
The maximum deformation of the rudder is 2.6 mm, which is allowed and significantly smaller than the deformation of the horizontal tail. This is due to the vertical part of the spar of the rudder being mainly in compression and the horizontal part in bending, while the elevator experiences bending around 2 axes.

A buckling analysis has been done on the tail as well. Apparently, the skin of the horizontal tail buckles when the load is multiplied 174 times as seen in Figure 6.8a. This however is a strange result since the skin is made of nylon and not a metal sheet. This is a limitation of ANSYS, since it can not analyse non-linear materials very well. The vertical tail however shows out of plane buckling of the spar when the load is multiplied 833 times as seen in Figure 6.8b. The tail is regarded to be safe with respect to buckling.

[6] $http://www.metals4u.co.uk/aluminium/tube/38.1mm-x-3.2mm-(-1-12od-x-10swg-)/detail.asp?prd_id=987$

[7] Gamma Catalogus; Multiplex hardhout 9mm 244x122cm fsc

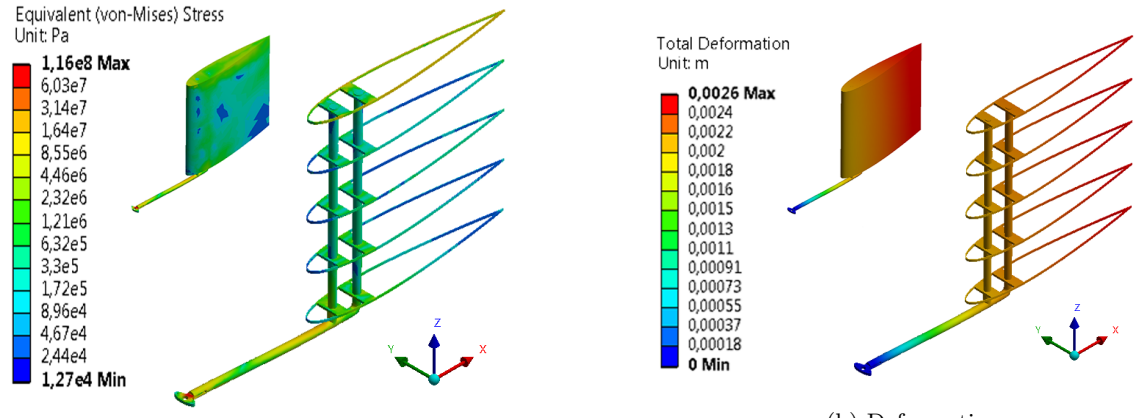

(a) Stress

(b) Deformation

Figure 6.7: Structural analysis of the vertical tail

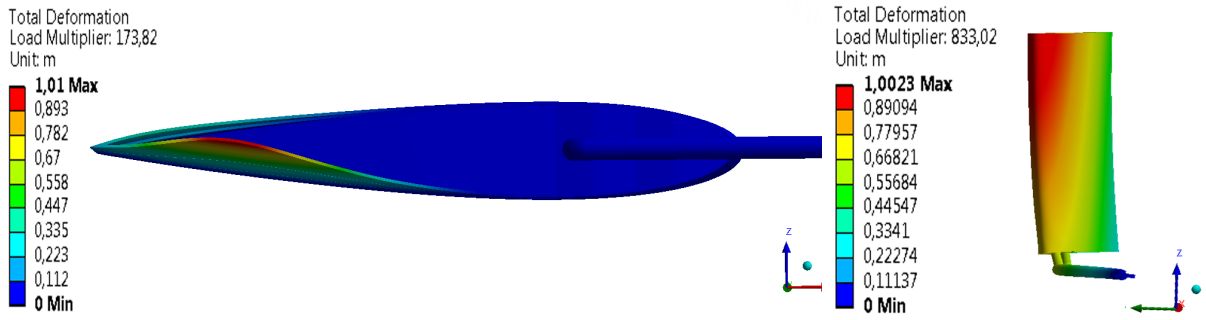

(a) Buckling of the horizontal tail

(b) Buckling of the vertical tail

Figure 6.8

6.3.4 Review of Tail Design

The current design for the tail features wooden ribs and a fabric skin, but other possibilities have to be researched as well. Since the aerodynamic loads at the tail are so small, even tail planes of solid styrofoam might be strong enough. The limiting factor in the current design turned out to be the deflection of the spars. The spars therefore cannot be removed, but the wooden ribs could be replaced.

6.4 Fuselage Design

The fuselage is a complex truss structure that serves as the body of the airframe, where all control surfaces and support structure are mounted to and where the user operates the simulation. The members of the truss members need to be sized for optimal weight and structural integrity. In order perform this sizing, the fuselage was analysed with ANSYS for several load cases, which required the fuselage to have an initial configuration and sizing parameters, some of which were established in Chapter 2 and Chapter 7.1. The sizing terms that were still unknown, were most relevant to structural integrity. The objective of this section is to illustrate how these initial dimensions were estimated. First, Subsection 6.4.1 will illustrate the assumptions used to aid in the analytical model. Second, the failure criteria are defined in Subsection 6.4.2. The limiting load case selection for the analytical model is performed and elaborated in Subsection 6.4.4. Next, the results for each limiting load case presented in Subsection 6.4.5. Furthermore, the results of the ANSYS simulations and iterations will be displayed in Subsection 6.4.6. Finally, the cost breakdown of the fuselage will be shown in Subsection 6.4.7.

6.4.1 Assumptions

The analysis of systems can often become tediously complex. This can be simplified within reasonable accuracy, by using assumptions and a design approach. For the structural design models, the relevant assumptions are listed below:

SFA-1 The analytical model complies with linear elasticity and moment theories.

SFA-2 The stress derivations comply with Euler bending and buckling.

SFA-3 The fabric sheet is not load bearing.

SFA-4 For the analytical model, the truss structure is simplified with hinge joints.

SFA-5 Material properties are considered to be homogeneous.

Note that assumption [**SFA-4**] will only allow for the approximation of the curve of the internal energy, as many boundary conditions for the entire structure are unknown. While the presence of boundary values will be neglected, the curve itself provides benefits for the estimation of failure cases (extrema in internal stresses).
These assumptions are accompanied by the following design choices and their argumentation:

- The thickness of any member will not be lower than 1 mm to allow for machining error.
- To account for inaccuracies, the yield criterion will have a safety factor of $SF = 1.5$.
- All adjacent, similarly oriented truss members have the same cross-sectional dimensions to allow for continuous, longitudinal internal load distributions.
- Size dimensions will be single decimal accurate in millimetres as higher accuracies are costly to produce.
- Users will have no access to the structure aft of the wing, therefore the members here will not be considered for user loads.

6.4.2 Failure Criteria

The failure criteria are the circumstances that are the primary cause to a catastrophic end of the Aeolusim. These criteria are present under the limiting load cases, which were analysed in compliance with [**SA1**]. The following analysis will respect the axis reference system defined in Chapter 2. Utilizing Beam Theory, as described in the Reference [15], the failure criteria can be derived from stress analysis, starting with the equivalent stress exceeding the yield stress:

$$\sigma_{bending} = \frac{S_y\,\hat{y}x}{I_{zz}} + \frac{S_z\,\hat{z}x}{I_{yy}} \tag{6.1}$$

$$\sigma_{tensile/compressive} = \frac{S_x}{A} \tag{6.2}$$

$$q_s = q_b - q_{s0} = -\frac{S_z}{I_{yy}}\int_0^s tyds - \frac{S_y}{I_{zz}}\int_0^s tzds + \frac{T}{2A_{enclosed}} \tag{6.3}$$

$$\tau = \frac{q_s}{t} \tag{6.4}$$

Where $S_{x,y,z}$ are the forces in their respective directions, q_s is the shear flow distribution in the cross section of the beams, $I_{xx,yy,zz}$ is the area moment of inertia, t is the local thickness of the cross-section, A is the cross-sectional area and $A_{enclosed}$ is the enclosed cross-sectional area of the beam. Note that all annular beams are dual axis symmetric over the cross section, $I_{zz} = I_{yy} = I$. Furthermore, $S_{y,z} * x$ is a moment contribution where x is the x-directional moment arm. The terms $\hat{x}$ and $\hat{y}$ represent the coordinates of the stress calculation with respect to the centroid. The Cartesian subscripts represent a beam with its longitudinal dimension in the X-direction. For other directions, the subscripts and direction terms need to augmented accordingly. Equations 6.1, 6.2, 6.4 and 6.3 are all contributors to the von-Mises criterion 6.5, which governs the yielding limit for combined equivalent stresses:

$$Y = \sqrt{(\sigma_x)^2 + 3(\tau_{yz})^2} \tag{6.5}$$

The second mode of failure is buckling. The highest allowable load for a member of length L with elastic modulus E is:

$$P_{crit} = \frac{4\pi^2 EI}{L^2} \tag{6.6}$$

When investigating the parameters of Equations 6.5 and 6.6, one can note that most of the truss structure members share several similarities. Material properties are constant as per assumption [**SFA-5**]. Similarly, the applied forces (i.e. user weight and leaning forces) are considered to be constant as only the largest loads are investigated. The cross sectional sizes (area, enclosed area, area moment of inertia and local thickness) of similarly oriented members, are all equal to each other as per design choices in Subsection 6.4.1. This shows that the variables most prone to be different between truss members, are the length of each beam and which force is applied. The dimensions of the beam can therefore allow for an optimised analysis strategy, which is listed below to satisfy the failure criteria:

SFC-1 Members subjected purely to longitudinal loads can only fail at the lowest cross-sectional area.

SFC-2 The smallest critical buckling load is located in the beam with the largest length.

SFC-3 The largest equivalent stress can be located in the beam with the largest moment arm.

If the analysis for the failure criteria is performed, it soon becomes clear that there are too many unknowns in the cross-section, resulting in an indeterminate problem. As the cross-sectional shape of the truss members was still unknown, their definition will be performed in order to forge relations for the cross-sectional parameters. The plan of approach for the von-Mises criteria therefore involved setting up an initial template for the cross section, after which the dimensions would be iterated manually until the equivalent stress no longer exceeds the yield stress. The templates can be viewed in Figure 6.9:

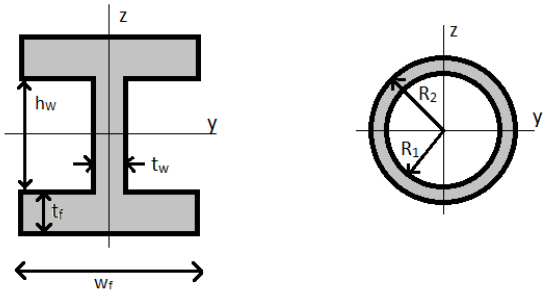

Figure 6.9: Template of cross-sections with relevant dimensions

The templates involve the cross-sections for annular beams and I-beams. The annular beams will be present for most of the truss structure. The I-beam will be placed in locations with cut-outs due to their known performance under bending stresses. This design choice is based on engineering judgement.

The relevant parameters are: flange thickness t_f, flange width w_f, web thickness t_w, web height h_w, outer radius R_2 and inner radius R_1. In both configurations, the cross sections are dual axis symmetric, which leads to the relations given in Equations 6.7:

$$\hat{z} = \frac{2 \cdot t_f + h_w}{2} \tag{6.7a}$$

$$\hat{y} = \frac{w_f}{2} \tag{6.7b}$$

$$t_{annular} = R_2 - R_1 \tag{6.7c}$$

$$A_{ibeam} = (2 \cdot t_f \cdot w_f) + (t_w \cdot h_w) \tag{6.7d}$$

$$A_{annular} = \pi(R_2^2 - R_1^2) \tag{6.7e}$$

$$I_{yy_{ibeam}} = \frac{2}{12} w_f \cdot t_f^3 + \frac{1}{12} t_w \cdot h_w^3 + 2w_f \cdot t_f \cdot \left(\frac{1}{2} \cdot (t_f + h_w)\right)^2 \tag{6.7f}$$

$$I_{zz_{ibeam}} = \frac{1}{12} h_w \cdot t_w^3 + \frac{2}{12} t_f \cdot w_f^3 \tag{6.7g}$$

$$I_{annular} = \frac{\pi}{4} \cdot (R_2^4 - R_1^4) \tag{6.7h}$$

Note that all adjacent I-beams will have the same dimensions in order to allow for better connection surfaces and load distributions. If loads were to be applied in the middle of the beams, the internal shear forces and moments have to be determined. Free Body Diagram 6.10 illustrates all the relevant forces, where the end points were assumed to be simply supported. This is an extension of assumption [**SFA-4**]:

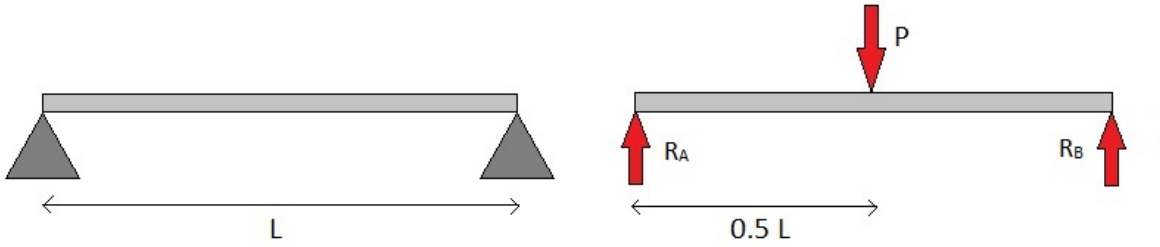

Figure 6.10: Statically determinate annular beam

The forces R_A and R_B are the reaction forces in the hinges, while P is the applied force, which can be either S_z or S_y. Using analysis methods from Reference [16]:

$$\Sigma F_y = 0: \quad R_A + R_B = P$$
$$\Sigma M_A = 0: \quad R_B L = \frac{1}{2} PL \leftrightarrow$$
$$R_A = R_B = \frac{1}{2} P$$
$$M_{max} = \frac{1}{4} PL$$

Combining Equations 6.8 and 6.1:

$$\sigma_{bending_{annular}} = \frac{\frac{1}{4} PL \cdot (R_2 - \frac{1}{2} t_{annular})}{I_{annular}} \tag{6.9}$$

In order to make Equations 6.1, 6.2, 6.4 and 6.3 easier to apply to circular objects, the linear Cartesian terms were converted to a cylindrical reference system with:

$$y = R\cos\theta \tag{6.10a}$$
$$z = R\sin\theta \tag{6.10b}$$
$$ds = R\sin\theta d\theta \tag{6.10c}$$

Combining Equations 6.4 and 6.10 results in a more appropriate form for calculations. The resulting equation is listed below:

$$\tau_{yz} = \frac{S_z sin(\theta) + S_y sin(\theta) - \frac{1}{2}\pi}{2\pi Rt} + \frac{T}{2\pi R^2 t} \tag{6.11}$$

6.4.3 Load Case Identification

The simulator is expected to be subjected to several load cases. Each of these load cases is defined by the magnitude, location and orientation of external forces and moments on the body of the simulator. A list of these external forces is defined below:

SFL1 Aerodynamic loads

SFL2 User weight

SFL3 Reaction loads

The aerodynamic loads consist of the lift and drag contributions of all profiles (airfoils, airframe and control surfaces), and their associated moments and torques. The user weight loads are applied in specific conditions at set locations and directions. The reaction loads are defined as the normal force contributions of the supporting structure and their associated moments and torques.

The load cases can now be defined as a combination of the external forces and are all considered for their respective failure types. These cases are collected into two categories: standard flight and non-standard interactions, both of which are elaborated below:

Standard Flight
The loads present in this configuration are [**SFL1**], [**SFL2**] and [**SFL3**] and make up the load cases where the AEOLUSIM is performing its standard operations, such as horizontal flight and manoeuvring flight (roll, pitch and yaw). The aim of these cases is to investigate the effects of loads under an angle on the structural members in various flight manoeuvres. These are expected to be the most critical load cases for the structural members under standard flight conditions, due to the added forces from control surface deflections. The maximum deflection in each degree of freedom is investigated.

Non-standard Interactions
The loads present in this configuration are [**SFL2**] and [**SFL3**]. The non-standard interactions consist of several situations where the user applies forces to the airframe that don't contribute to the simulation, such as leaning or sitting on different locations of the airframe. The aim of these cases is to investigate the effects of non-standard user interactions on the members of the fuselage for both the vertical and horizontal loads where they are applicable. As it is difficult to predict and control the behaviour of people, the fuselage needs to be sized for several factors that allow for human error. In these cases, the pilot weight is a purely vertical load onto the fuselage.
The non-standard interactions were approached as the more critical load cases as the forces exerted by users were far larger in magnitude than the aerodynamic forces.

6.4.4 Limiting Load Case Identification

The limiting load cases that will be investigated for the analytical model can now be selected from the above categories, specifically the non-standard interactions categories. This selection will stay true to the failure criteria of Subsection 6.4.2.

Load Case I
The first load case is defined as user loads at the edge of the nose, which creates the largest moment arm for the I-beam. This can be visualised in Figure 6.11 as a user leaning in a horizontal direction (X and Y axis), or the user suspending himself on the nose (Z axis).

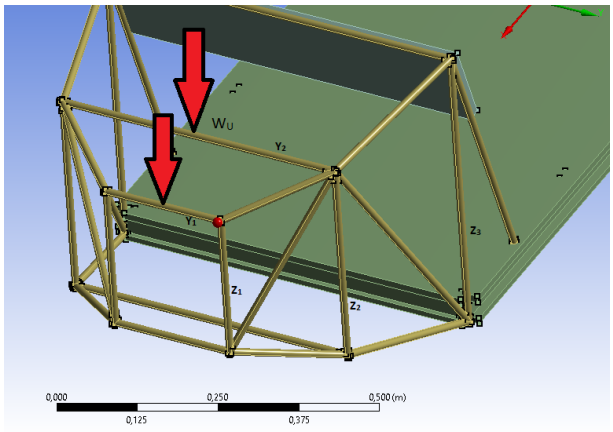

Figure 6.11: Load case I

This suspension is performed by sitting on the nose, where the user's weight is divided over member $N_{Y_{1,2}}$ and subsequently, the adjacent members. This is the largest vertical force present on a horizontal annular beam. The forces are applied in the centre of the beams. Note that the user might shift his weight, which makes it unclear how his weight will be distributed. It is therefore assumed that any member or joint may be subjected to the user's full weight.

Load Case II
The second load case is defined as the user entering the AEOLUSIM from one of the sides. Which side is chosen is arbitrary as the simulator is symmetric in the XZ plane. During entry, the user may pull himself up against the side of the airframe. The load distribution on the relevant members can be visualized in Figure 6.12. This action applies a vertical force on the longest horizontal annular member as well as the longest vertical member of the cockpit. The vertical pulling force will be assumed to be similar to the vertical leaning force, followed by the remainder of the user weight to be applied on a single X-direction I-beam.

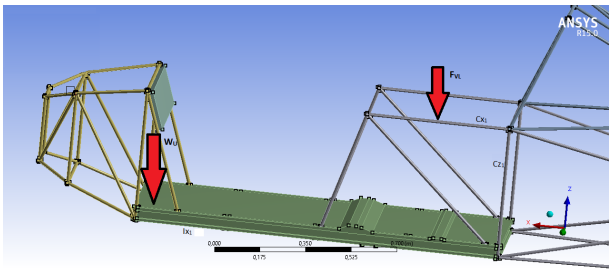

Figure 6.12: Load case II

Note that there is a diagonal bar that would prevent the user to step at the rear end of the cut-out, as can be seen in Figure 6.12. The remainder of the user weight is therefore applied adjacent to the above mentioned diagonal bar. Additionally, it is assumed that the loaded I-beam carries the equivalent stresses by itself.

Now that the limiting load cases have been identified, the relevant parameters for both are displayed in Table 6.5.

Table 6.5: Parameters for load cases

Parameter	Symbol	Value	Dimension
User weight	W_U	931.95	N
Horizontal leaning force	F_{HL}	150	N
Vertical leaning force	F_{VL}	350	N
Length member N_{Y_2}	$L_{N_{Y_2}}$	0.475	m
Length member N_{Z_2}	$L_{N_{Z_2}}$	0.35	m
Length member C_{X_1}	$L_{C_{X_1}}$	0.55	m
Length member C_{Z_1}	$L_{C_{Z_1}}$	0.5	m
Length member I_{X_1}	$L_{I_{X_1}}$	1.4	m
Length of the nose cone in X-direction	L_{cone}	0.4	m

The term N denotes that the beam is present in the nose, whereas C denotes annular cockpit beams. Lastly, term I denotes an I-beam. The horizontal and vertical leaning force are based on the rounded average of performed measurements, where a sample size of 9 adult men were mimicking leaning actions against a weight scale.

6.4.5 Results of Analytical Model

In order to obtain proper initial sizes for the fuselage members, the limiting cases were investigated analytically for both the I-beams and the annular beams. The analytical model follows suit to each failure criterion mentioned earlier and will investigate both load cases. In compliance with the design choices in Subsection 6.4.1, the members in the tail will not directly be subjected to user loads. With the prevalence of multiple failure criteria, the results might have overlapping dimensions (both buckling and yield are functions of the area moment of inertia). The structure will therefore be sized for the dimensions where no failure occurs, in other words the highest minimum will be chosen.

Using the above parameters, the solution for criterion [**SFC-1**] can be calculated. Using Equation 6.2, the lowest

required cross sectional area for vertical tensile/compressive loads becomes:

$$A_{min_Z} = 3.89 \cdot 10^{-6}\ m^2$$

For horizontal members, the applied load F_{HL} can be in either X- or Y-direction, respective to the direction mentioned in the subscript. The result:

$$A_{min_{X,Y}} = 5.84 \cdot 10^{-5}\ m^2$$

When analysing for [**SFC-2**], the load cases are considered separately. In load case I (with superscript identifier and applied load direction in subscript identifier), Equation 6.6 can be used to calculate the required area moment of inertia for member N_{Z_2} (longest member under largest load).

$$I^I_{min_Z} = 1.23 \cdot 10^{-10}\ m^4$$

For buckling in member N_{Y_2} (longest member under largest load), the applied load is once again the leaning force, which leads to:

$$I^I_{min_{X,Y}} = 4.32 \cdot 10^{-11}\ m^4$$

Looking at load case II, the members investigated will be C_{Z_1} and I_{X_1}, performing under loads F_{HL} and F_{VL}.

$$I^{II}_{min_Z} = 3.28 \cdot 10^{-11}\ m^4$$

For buckling in member N_{Y_2} (longest member under largest load), the applied load is once again the leaning force, which leads to:

$$I^{II}_{min_{X,Y}} = 3.39 \cdot 10^{-10}\ m^4$$

For the analysis of criterion [**SFC-3**], the load cases will be investigated separately as well. In load case I, the maximum moment arm is equal to: $L_{cone} + L_{I_{X_1}} = 1.8\ m$, which will mostly contribute to bending stresses in the I-beams. Due to the symmetry of the load case, it can be assumed that each I-beam has to carry half the stresses. Considering the user weight, while using Equation 6.1, 6.3 and 6.5

$$\begin{aligned}
t_f &= 0.005\ m \\
w_f &= 0.025\ m \\
t_w &= 0.002\ m \\
h_w &= 0.026\ m \\
A_{I-beam} &= 3.02 \cdot 10^{-4}\ m^2 \\
I_{yy_{I-beam}} &= 6.35 \cdot 10^{-8}\ m^4
\end{aligned}$$

For the analysis of member N_{Y_2}, the polar form of Equation 6.5 can be used to calculate the equivalent stresses for the bending moment caused by the one half of the user weight that's carried by this member. In similar fashion to the I-beam, the cross-sectional parameters of the annular beams were manually iterated to optimally approach the yielding stress. This results in:

$$\begin{aligned}
R_{2_Y} &= 0.008\ m \\
R_{1_Y} &= 0.0063\ m \\
A_{annular_Y} &= 8.03 \cdot 10^{-5}\ m^2 \\
I_{annular_Y} &= 2.06 \cdot 10^{-9}\ m^4
\end{aligned}$$

For the Z-direction member N_{Z3}, the applied load F_W creates a compressive load. The results are:

$$\begin{aligned}
R_{2_Z} &= 0.002\ m \\
R_{1_Z} &= 0.001\ m \\
A_{annular_Z} &= 9.42 \cdot 10^{-6}\ m^2 \\
I_{annular_Z} &= 1.18 \cdot 10^{-11}\ m^4
\end{aligned}$$

If we were to consider a leaning force in the Y-direction, both I-beams will carry the stresses again, but in a different orientation. The result of this orientation adds a relatively large Steiner term to the area moment of inertia. In other words, the horizontal case will qualitatively not be the failure case and therefore does not require further investigation.

For the second load case, only a single I-beam (I_{X_1}) is assumed to carry all the stresses. The resulting dimensions become:

$$
\begin{aligned}
t_f &= 0.005\ m \\
w_f &= 0.021\ m \\
t_w &= 0.002\ m \\
h_w &= 0.030\ m \\
A_{ibeam} &= 2.70 \cdot 10^{-4}\ m^2 \\
I_{yy_{ibeam}} &= 6.93 \cdot 10^{-8}\ m^4
\end{aligned}
$$

For member C_{X_1}, which carries F_{VL}, the results are:

$$
\begin{aligned}
R_{2_X} &= 0.0076\ m \\
R_{1_X} &= 0.0066\ m \\
A_{annular_X} &= 4.46 \cdot 10^{-5}\ m^2 \\
I_{annular_X} &= 1.13 \cdot 10^{-9}\ m^4
\end{aligned}
$$

For the Z-direction member C_{Z1}, the applied load F_{VL} creates a compressive load. The results are:

$$
\begin{aligned}
R_{2_Z} &= 0.002\ m \\
R_{1_Z} &= 0.001\ m \\
A_{annular_Z} &= 9.42 \cdot 10^{-6}\ m^2 \\
I_{annular_Z} &= 1.18 \cdot 10^{-11}\ m^4
\end{aligned}
$$

Now that all relevant dimensions have been approximated, they can be used as inputs for ANSYS Mechanical. Due to the different assumptions used, the analytical model and the ANSYS results may differ. Whether the initial dimensions cause the structure to be over- or under-designed, they will be augmented accordingly until an optimum is reached, or the minimal production dimensions are reached.

6.4.6 Performance Analysis of the Fuselage

The fuselage truss structure has been analysed as explained in Section 6.4 and several results were obtained. For every load case the resulting maximum von-Mises stress, maximum deformation and minimum safety factor with their respective locations are presented in Table 6.6.

Parameter S.F. represents the safety factor that is present in the structure when subjected to the resulting stresses. As the table shows, the maximum absolute stress that occurs in the nose is $1.40 \times 10^8\ Pa$, resulting in a safety factor of 2.56. This m that the nose is over-designed, since a safety factor of 1.5 was assumed to be sufficient. The current structure is however designed to be as cheap as possible and so production costs are kept low by using standard minimum thickness materials, that apparently will not fail under the specified loads. For that reason, the high safety factors are acceptable. The maximum deflection is 4.89 mm which is almost unnoticeable and will not affect the overall shape or the user experience.

Two load cases are highlighted to explain some phenomena that occur in the structure of the fuselage. In the first load case, it can be clearly seen in Figure 6.13a that the highest stress occurs in and along the nose members where the user weight is applied. This member distributes the load through the adjacent members towards the

Table 6.6: Fuselage performance results for its respective load cases

Load case	σ (Pa)	**S.F. (-)**	**Location**	ν (mm)	Location
I	1.40×10^8	2.56	Force application	4.89	User weight application
II	6.85×10^7	5.24	Leaning force application	0.09	Leaning force application
Standard roll	1.42×10^7	25.28	At pilot seat	0.39	Nose
Standard yaw	1.33×10^7	26.99	At pilot seat	0.36	Nose
Standard pitch	1.51×10^7	22.97	At pilot seat	0.44	Nose

I-beam and floor plate. Comparing this case to load case 2, the maximum stress is higher in the I-beam due to the fact that the moment arm is longer. In Figure 6.13b the total deformation of the structure is seen. The maximum deflection is located where the force is applied.

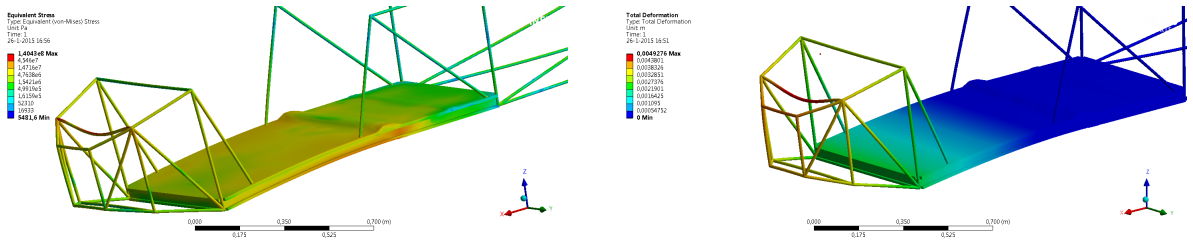

(a) Stress distribution (b) Total deformation

Figure 6.13: Load Case I

A few standard flight load cases where analysed as well. Load case *Standard pitch*, where the wing is positioned at maximum negative pitch and the aileron is at its largest deflection, can be seen in Figure 6.14. This is considered the manoeuvre with the highest aerodynamic loads. The stresses from the wing onto the fuselage are so small that the aerodynamic forces will not cause any failure. The most significant load present is the weight of the user positioned onto the seating arrangement of the cockpit. A fatigue analysis was also performed for this load case. If a pitching manoeuvre is estimated to last five seconds, the fuselage structure will be capable of sustaining a maximum of 5.2×10^7 cycles.

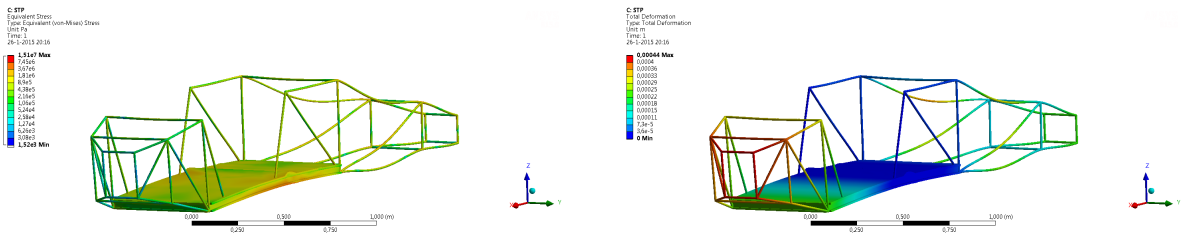

(a) Stress distribution (b) Total deformation

Figure 6.14: Standard pitch

For all load cases a buckling check is done with ANSYS. The result is a number with which the applied load has to be multiplied before the structure buckles. In other words, the lower this multiplier term, the closer the structure is to the buckling limit. The most critical load case (1) demonstrates where a nose member buckles at a load of about 34 times higher, as clearly seen in Figure 6.15. The deformation is scaled down to give a good representation of the buckling member, since a deformation of 1 m (see legend) would distort the picture significantly. It can be concluded that the fuselage structure is not very sensitive to buckling.

The total mass of the fuselage truss members are summed up to be 28.9 kg.

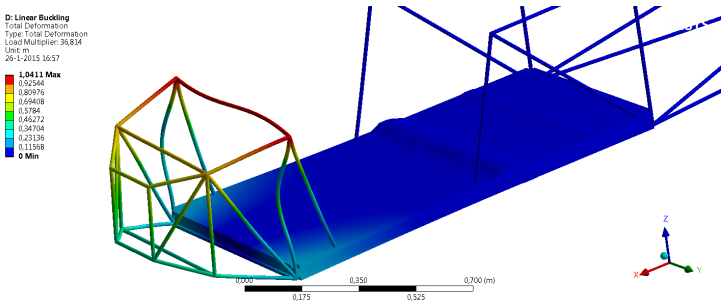

Figure 6.15: Buckling of load case 1

6.4.7 Production Costs of the Fuselage

Now that the configuration and topology of the truss structure is established, an estimation can be made of what the manufacturing costs will be. This estimation is taken with respect to the I-beam, the annular beams and the assembly of all the elements.

The beams themselves can be purchased by manufacturers [8], at prices based on shapes, cross-sectional sizes and lengths. For dimensions similar to those of the annular beams in the AEOLUSIM, the price per 5 meters is approximately 6.72. Considering that the total length of all annular members is equal to 25.4 m. The total cost for annular beams becomes 34.14, which is equal to €45.53.

The I-beams will be created by welding flat plates together, which themselves will be acquired in similar fashion to the annular beams. The relevant flat plates have an approximate cost of 17.65 per 5 meters, where three plates are required to make one I-beam. This will require a weld length of over 24m. The combined length of all I-beams in the fuselage amounts to 5.8 m. Therefore, the total cost for the I-beams becomes 20.47, which is equal to €27.28.

The canvas required to cover the fuselage is geometrically approximately 50 m^2 large. The price per square meter of polyester brushed fabric is \$1.31 [9]. This amounts to a total cost of \$65.63, which is equal to €58.19.

The time required to perform all these welds and machining will amount to an approximate of 2 workdays, each of 8 hours, performed by one person and a nominal payment of €40, − per hour (including VAT and company share in health care etc.). This results in an assembly cost estimate of €640, −. To allow for contingency and equipment use this result has been multiplied by 1.5 to conclude a final estimate of €960, −.

The total cost of manufacturing the fuselage is thus equal to €1091.

6.5 Supporting Structure Design

An important part of the AEOLUSIM is its supporting structure. As already explained in Chapter 2, it consists of two beams that are free to rotate about their axes and the fuselage is attached with two bearings. On each axis a spring damper systems is attached to stabilise the system.

The lower beam of the can be bought for €41.50 [10] and has to be milled so the upper beam can be attached to it. This will take around an hour of machining, which is estimated at €110 per hour, including the operator. Also one hour is needed to polish and oil the contact surfaces. The upper beam which will be the pitch axis is bought at a price of around €20.70 [11] and is adapted to suit the fuselage attachment in 2 hours.

The support structure has to be able to rotate around its three axes. To allow for yaw, a pneumatic cylinder is used to support the entire structure whilst barely creating any friction. Such a cylinder is estimated to cost €100. The roll axis is welded to the pitch axis and is locked onto the bottom of the support structure. Their contact surfaces have to be oiled up to reduce friction. To allow for pitch two bearings are used to transfer the

[8] http://www.metals4u.co.uk/aluminium/flat/25.4mm-x-6.3mm-(-1-x-14-)/detail.asp?prd_id=263
[9] http://www.alibaba.com/product-detail/100-polyester-brushed-fabric_60117613839.html?s=p
[10] $http://www.metals4u.co.uk/aluminium/round/63.5mm-(-2-12-)/detail.asp?prd\_id = 346$
[11] $http://www.metals4u.co.uk/aluminium/round/31.8mm-(-1-14)/detail.asp?prd\_id = 331$

Table 6.7: Support structure cost

Part	Mass (kg)	Production cost (€)
Lower beam	11.73	191.50
Upper beam	0.57	100.70
2 Bearings (pitch)	-	200
Cylinder bearing (yaw)	-	100
Spring-dampers	-	1500

loads from the fuselage to the pitching axis. By using two bearings it is also made sure the airframe will not slide sideways. The bearings are budgeted at €200, since they have to be able to carry the loads and moments caused by the airframe.

The spring and damper mechanisms are part of the detailed design phase, since entire studies can be done on viscous damping mechanisms and so it is deemed outside the scope of this conceptual design. No reference mechanisms could be found that are applicable in this concept and so it is assumed that the parts have to be custom designed. However, an initial mock-up is made, consisting of a rotational spring that attaches to two objects, one reference and one mobile object. Surrounding the spring is a cylinder with a highly viscous fluid inside that has to travel through tiny holes or openings so friction is created, causing damping. An initial cost estimation for the spring damper mechanisms is €1500, because they are custom parts.

After assembly, the total cost of the support structure is rounded off and estimated at €2,210.

6.5.1 Load Case

All forces acting on the airframe pass through the supporting structure. These forces include the weight of the airframe and the pilot, the lift created by the wings, elevator and rudder and the drag. These forces are modelled in ANSYS as remote forces, which means they have an external location. The weight for example is located at the centre of gravity and its maximum distance with respect to the rotation point is used as limiting load case. The forces and their respective locations with respect to the rotation point are presented in Table 6.8.

Table 6.8: Limiting load case for the support structure

Load	Force (N)	(x,y,z) w.r.t. rotation point (cm)
Mass	2000 (z-)	(0,-5,20)
Wing lift	250 (z+)	(0,20,10)
Drag	68 (y-)	(0,20,10)
Elevator lift	32 (z+)	(0,-226,46)
Rudder lift	10.5 (x+)	(0,-216,70)

6.5.2 Analysis

The support structure is analysed without its bearings to simplify the model. The resulting stress and deformation found in the limiting load case are shown in Figure 6.16. The maximum deformation is located at the tips of the pitch axis, since the load is applied at those ends. A deflection of 1.1 mm is negligible and safe enough for the support structure. The maximum stress is found in the connection of the pitch axis to the roll axis and is 1.27×10^8 Pa. This results in a safety factor of 1.97. A fatigue analysis is also done, where one cycle is taken as the loading and unloading of the pilot. Since a ride in the Aeolusim lasts five minutes, the support structure has to withstand 60,000 cycles. Even after this many cycles the safety factor is still 1.53.

In Figure 6.16b it is clearly seen that large stresses arise in the pitch axis. This is due to the bending moment created by the weight of the airframe. It is also seen that the centre of the beam is lighter than the outside due to torsion, which is caused by the centre of gravity not being above the support structure. This offset also creates a moment in the bottom beam which is allowed to yaw. The beam shows a clear neutral axe indicated by the green colour. The torsion created by the rudder is minimal and is hardly noticed.

The support structure is also checked for buckling, since its beams are mainly subjected to compression or bending. The load has to be multiplied with a factor of 217 as can be seen in Figure 6.17. The deformation is

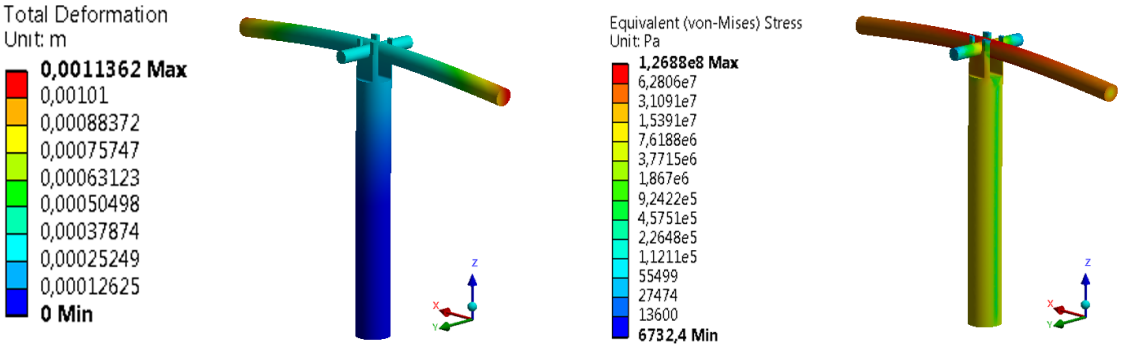

(a) Deformation

(b) Stress

Figure 6.16: Support structure

auto-scaled and is out of proportion, but nonetheless out of plane buckling can be seen. The thick bottom beam of the support however is very effective against buckling.

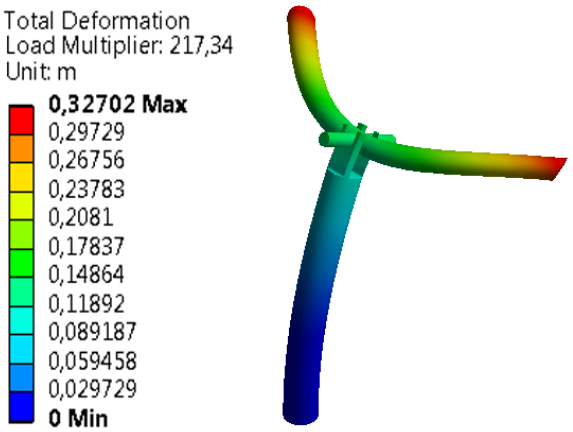

Figure 6.17: Buckling of the support structure

6.5.3 Review of Design

The design of the spring damper mechanisms is a very tedious process. If rotational mechanisms turn out to be ineffective or too expensive, a design with longitudinal spring dampers can be chosen. These will have to be attached to the airframe and the support structure, introducing new loads. The entire design would then have to be recalculated.

6.6 Structural Results

All parts have been analysed and their costs have been determined. The final values are presented in Table 6.3.

The resulting moment of inertias can be seen in Table 6.10.

Table 6.9: Mass and cost of the Aeolusims structural parts

Part	Mass [kg]	Cost [€]
Airframe	31.2	1,019.00
Counterweight	49.5	100.00
Wings	11.0	1,716.50
Tail	9.0	868.00
Support	6.7	2,212.20

Table 6.10: Mass moment of inertias

Mass moment of inertia	$[kg \cdot m^2]$
I_{xx}	17.02
I_{yy}	68.73
I_{zz}	78.93
I_{xy}	0.14
I_{yz}	2.45
I_{xz}	-0.08

7 Stability & Control Analysis

The Aeolusim needs to be controllable like a real aircraft. For that reason, the simulator response to control input needs assessment. The movement of the Aeolusim is naturally high-pass filtered by passive spring and damper mechanisms, that limit the motion of the simulator. These spring damper system greatly influence the stability of the Aeolusim, and the combination of the spring damper mechanisms and the aerodynamic surfaces determines how the simulator will respond to control inputs. The objective of the stability and control analysis is to determine and tweak the response of the simulator to control inouts. Section 7.1 describes the model that is used to analyse the stability & control characteristics. In this section, the layout of the model is presented. Next, the assumptions made to create the model are given and elaborated on. Afterwards, the elements of the model are explained with the neutral position calculation, the state space implementation and the control forces. The verification of the model is presented and a validation method is recommended. Finally, the reliability of the model is discussed.
The performance of the Aeolusim will be discussed in Section 7.2. This section discusses the maximum deflections that can be achieved and elaborates on the aircraft like behaviour of the Aeolusim. The control forces are analysed as well. Finally, a recommendation is given.

7.1 Analytical Model

A common way to determine the response of an aircraft on control inputs is with a state space system containing stability and control derivatives. Since the stability of the Aeolusim is also dependent on the spring damper mechanisms and its own weight, these factors will have to be included in the state space system. The simulator that features a fully movable horizontal tail that acts as elevator, a fully movable vertical tail that acts as a rudder and a wing with ailerons. Therefore, the model will feature these characteristics as well.

7.1.1 Model Layout

An overview of the model that is used for Stability & Control is presented in Figure A.1 in Appendix A. The inputs and outputs of the model are presented in Table A.1. Figure 7.1 shows the reference frame that is used. In this figure, the origin is located at the rotation point. A rotation of ϕ radians about the $x-$axis will be referred to as roll, pitch is defined as a rotation of α radians about the $y-$axis. Rotations of β radians about the $z-$axis will be referred to as yaw.

The Aeolusim's movement is dependent on aerodynamic factors as real aircraft are. There are, however, several other factors that influence its behaviour. Any translational motion is held back by the support structure, therefore the simulator can only rotate around the $x-$, $y-$ and $z-$axes. As the simulator rotates, the springs will generate a force opposite to the angular deflection of the simulator. The dampers will generate a force opposite to the angular velocity of the movement.

Another important factor that influences the simulator movement that is not a factor in real aircraft is the mass. The simulator is designed to have its centre of mass exactly above the point of rotation. When the simulator pitches or rolls, the centre of gravity will move around the rotation point. This is illustrated schematically in Figure 7.2. The mass causes a moment about the rotation point in the direction of the movement and is therefore destabilising.

If the centre of gravity is not directly above the rotation point in its ideal neutral position, the mass will cause a moment around the rotation point causing the simulator to move from its ideal neutral position until a new neutral position is reached. The ideal neutral position is defined as is where, without control inputs, the $xy-$plane of the simulator's body fixed axis system is parallel to the floor and $x-$axis points into the airflow. When the mass is not directly above the rotation point, a new neutral position will be reached, i.e. the simulator will have a non-zero static pitch and/or roll angle without control input. If this is the case, these angles are added to the results from the state space simulation. The way these angles are calculated is discussed in Section 7.1.5.

7.1.2 Assumptions

To create the model, a number of assumptions have been made. These assumption were made to simplify the model without compromising the accuracy of the results. The assumptions made were as follows:

- SC-1 - The equations of motions can be linearised around a neutral position

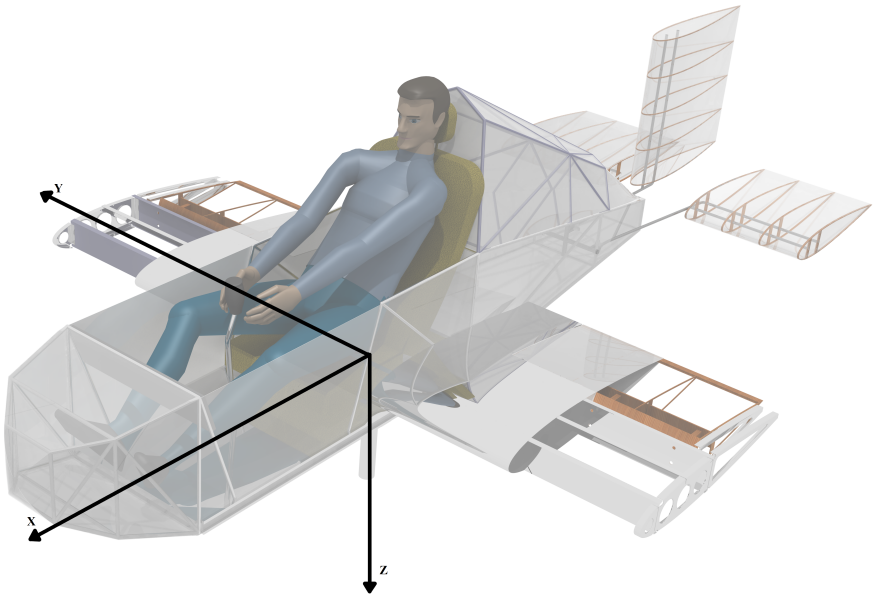

Figure 7.1: Reference frame used for the Stability and Control analysis

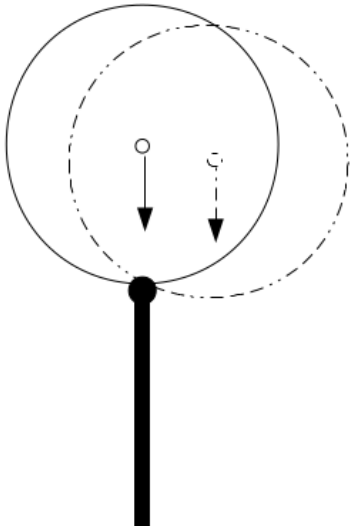

Figure 7.2: Effect of mass balanced about a point of rotation around x or y axis

- SC-2 - The airspeed is constant.
- SC-3 - The angle of attack is equal to the pitch angle.
- SC-4 - Control forces can be linearised around the maximum deflection control surfaces.

Assumption SC-1 was made to allow the equations of motion to be put in state space matrices. For this assumption to be valid, offset angles from the neutral position have to be small ($< 30^o$). This will not pose problems as the requirements in Reference [1] state that offset angles will not be higher than 30^o.

The airspeed is determined by the airflow the fan generates. Since the fan will generate a constant velocity airflow, it can be assumed the airspeed will not change during manoeuvres (Assumption SC-2). The impact of this assumption is discussed in Section 7.1.3.

Since the airflow from the fans will always be parallel to the ground, assumption SC-3 is valid. The consequences of this assumption is elaborated on in Subsection 7.1.3

Assumption SC-4 was made to allow linearisation of the control force equations around the maximum deflection of the control surfaces. Due to the small deflection angles of the rudder and elevator, which are NACA0015 airfoils, of up to 10^o, it can be seen from the Cl-α curves of these airfoils that the Cl changes linearly with angle of attack. This principle is different for the aileron deflection. The aileron is 50% of the main wing chord and causes a change in Cl when deflected to 10^o. This deflection change is also linear, which is explained in Section 5.2.2.

7.1.3 State Space Representation

In order to create the State Space matrices, the longitudinal and lateral equations of motion have been linearised and put in matrix form. Subsequently, the matrices are simplified using the assumptions provided in section 7.1.2. From these simplified matrices, it can be seen what stability and control derivatives have to be determined.

General Linearised Equations of Motion
The matrix in Equation 7.1 contains the linearised, dimensionless longitudinal equations of motion. All stability and control derivatives in the matrix will be calculated in Subsection 7.1.4. For the meaning of the standard stability and control derivatives is refer to Reference [17] This matrix is an adapted version of the longitudinal stability matrix that can be found in reference [17]. The matrix is adjusted because the original matrix has been derived for real aircraft. As the AEOLUSIM is a simulator that rotates around the attachment point of the pivot instead of its centre of gravity, the mass will cause a positive pitching moment when α is positive (see Figure 7.2). The contribution of the dimensionless mass to roll and pitch is included as C_{M_p} and C_{M_q}, respectively. The spring damper system that restricts the pitching moment is included in the system such that the springs cause a negative pitching moment for a positive α, and the dampers cause a negative pitching moment for a positive pitch rate. The dimensionless spring and damper coefficient are defined to be C_k and C_c, with subscripts ϕ, α and β for roll, pitch and yaw, respectively. The subscripts p, q and r denote a dependence on roll rate, pitch rate and yaw rate, in that order.

$$\begin{bmatrix} C_{X_u} - 2\mu_c D_c & C_{X_\alpha} & C_{Z_0} & C_{X_q} \\ C_{Z_u} & C_{Z_\alpha} + (C_{Z_{\dot\alpha}} - 2\mu_c)D_c & -C_{X_0} & C_{Z_q} + 2\mu_c \\ 0 & 0 & -D_c & 1 \\ C_{m_u} & C_{m_\alpha} - (C_{k_\alpha} - C_{M_\alpha}) + C_{m_{\dot\alpha}} D_c & 0 & C_{m_q} - C_{c_q} - 2\mu_c K_y^2 D_c \end{bmatrix} \begin{bmatrix} u \\ \alpha \\ \theta \\ \frac{q\bar{c}}{V} \end{bmatrix} = \begin{bmatrix} -C_{X_{\delta_e}} \\ -C_{Z_{\delta_e}} \\ 0 \\ -C_{m_{\delta_e}} \end{bmatrix} \delta_e \quad (7.1)$$

Equation 7.2 shows the lateral equations of motion. These equations are linearised and configured for the AEOLUSIM specifically. As with the set of longitudinal equations of motion, the matrix in Equation 7.2 is configured to implement the additional mass moment when the AEOLUSIM is under a roll angle and the moments caused by the spring damper systems restricting yaw and roll.

$$\begin{bmatrix} C_{Y_\beta} + (C_{Y_{\dot\beta}} - 2\mu_b)D_b & C_L & C_{Y_p} & C_{Y_r} - 4\mu_b \\ 0 & \frac{1}{2}D_b & 1 & 0 \\ C_{l_\beta} & -(C_{k_\phi} - C_{M_\phi}) & C_{l_p} - C_{c_p} - 4\mu_b K_X^2 D_b & C_{l_r} + 4\mu_b K_{XZ} D_b \\ C_{n_\beta} + C_{k_\beta} & 0 & C_{n_p} + 4\mu_b K_{XZ} D_b & C_{n_r} - C_{c_\beta} - 4\mu_b K_Z^2 D_b \end{bmatrix} \begin{bmatrix} \beta \\ \phi \\ \frac{pb}{2V} \\ \frac{rb}{2V} \end{bmatrix} = \begin{bmatrix} -C_{Y_{\delta_a}} & -C_{Y_{\delta_r}} \\ 0 & 0 \\ -C_{l_{\delta_a}} & -C_{l_{\delta_r}} \\ -C_{n_{\delta_a}} & -C_{r_{\delta_r}} \end{bmatrix} \begin{bmatrix} \delta_a \\ \delta_r \end{bmatrix} \quad (7.2)$$

However, since these derivatives assume the AEOLUSIM to have six degrees of freedom, some changes have to be made in the matrices.

Simplification of the Equations of Motion
The simulator will not move in either $x-$, $y-$ or $z-$direction. The stability derivatives that are calculated in Subsection 7.1.4 do not take into account that for every force on the AEOLUSIM there is a reaction force from the supporting structure. As a result, the net force is zero and a couple moment is left. In the matrices of

Equation 7.1 and Equation 7.2 that means that the force derivatives that generate a displacement are set to be zero, and the force derivatives causing a moment should not be changed since they represent the couple.

As stated in assumption SC-2 (Subsection 7.1.2), there is no variation in airspeed. Because of this, the first row of the symmetric equations can be removed. The first column can be removed as well as it is dependent on the airspeed variation. Because α and θ are always equal, as stated in assumption SC-3, the column and row pertaining to θ can be dropped from the equation.

State Space Form
Equations 7.4 and 7.3 show the result of the adjustments and simplifications. The equations are given in the form $\mathbf{P\dot{x}} + \mathbf{Qx} = \mathbf{Ru}$, so the time dependent and time independent parts are split.

$$\frac{V}{c}\begin{bmatrix} 2\mu_c & 0 \\ C_{m_{\dot{\alpha}}} & -2\mu_c K_y^2 \end{bmatrix}\begin{bmatrix} \dot{\alpha} \\ \frac{q\bar{c}}{V} \end{bmatrix} + \begin{bmatrix} 0 & -2\mu_c \\ C_{m_\alpha} - (C_{k_\alpha} - C_{M_\alpha}) & C_{m_q} - C_{c_q} \end{bmatrix}\begin{bmatrix} \alpha \\ \frac{q\bar{c}}{V} \end{bmatrix} = \begin{bmatrix} 0 \\ -C_{m_{\delta_e}} \end{bmatrix}\delta_e \tag{7.3}$$

$$\frac{V}{b}\begin{bmatrix} -2\mu_b & 0 & 0 & 0 \\ 0 & \frac{1}{2} & 1 & 0 \\ 0 & 0 & -4\mu_b K_X^2 & 4\mu_b K_{XZ} \\ 0 & 0 & 4\mu_b K_{XZ} & -4\mu_b K_Z^2 \end{bmatrix}\begin{bmatrix} \dot{\beta} \\ \phi \\ \frac{pb}{2V} \\ \frac{rb}{2V} \end{bmatrix} + \begin{bmatrix} 0 & C_L & 0 & -4\mu_b \\ 0 & 0 & 1 & 0 \\ C_{l_\beta} & -(C_{k_\phi} - C_{M_\phi}) & C_{l_p} - C_{c_p} & C_{l_r} \\ C_{n_\beta} + C_{k_\beta} & 0 & C_{n_p} & C_{n_r} - C_{cr} \end{bmatrix}\begin{bmatrix} \beta \\ \phi \\ \frac{pb}{2V} \\ \frac{rb}{2V} \end{bmatrix} = \begin{bmatrix} 0 & 0 \\ 0 & 0 \\ -C_{l_{\delta_a}} & -C_{l_{\delta_r}} \\ -C_{n_{\delta_a}} & -C_{r_{\delta_r}} \end{bmatrix}\begin{bmatrix} \delta_a \\ \delta_r \end{bmatrix} \tag{7.4}$$

The linear equations from Equations 7.3 and 7.4 can be rearranged to the state space form $\mathbf{\dot{x}} = \mathbf{Ax} + \mathbf{Bu}$, where $\mathbf{A}$ is given by Equation 7.5 and $\mathbf{B}$ is given by Equation 7.6.

$$\mathbf{A} = -\mathbf{P^{-1}Q} \tag{7.5}$$

$$\mathbf{B} = \mathbf{P^{-1}R} \tag{7.6}$$

7.1.4 Stability and Control Derivatives

The stability derivatives in Equations 7.3 and 7.4 will be determined using Datcom methods, which are implemented by the Digital Datcom code. A parser has been written to translate a file with simulator data to a file that can be used as input for the Digital Datcom.

Using reference [17], the dimensionless mass (μ) and dimensionless mass moment of inertia (K) can be calculated. The dimensionless spring and damper constants have been determined with Equations 7.7 and 7.8. Equation 7.9 and 7.10 show the calculation of the dimensionless weight contributions in longitudinal and lateral direction respectively.

$$C_k = \frac{k}{\frac{1}{2}\rho V^2 S d} \tag{7.7}$$

$$C_c = \frac{c}{\frac{1}{2}\rho V^2 S d} \tag{7.8}$$

$$C_{M_\alpha} = \frac{W}{\frac{1}{2}\rho V^2 S}\left(\frac{z_{cg}}{\bar{c}} + \frac{\sqrt{z_{cg}^2 + x_{cg}^2}}{\bar{c}} sin(\alpha_0)\right) \tag{7.9}$$

$$C_{M_\phi} = \frac{W}{\frac{1}{2}\rho V^2 S}\left(\frac{z_{cg}}{b} + \frac{\sqrt{z_{cg}^2 + y_{cg}^2}}{b} sin(\phi_0)\right) \tag{7.10}$$

In these equations, $d = \bar{c}$ for longitudinal constants, and $d = b$ for the lateral stability derivatives. δ is the initial offset angle in lateral or longitudinal direction as calculated in Section 7.1.5.

The control derivatives have been determined from the definition of the control derivatives (see Equation 7.11), where the moment generated by the control surfaces ($M_{control}$) at maximum deflection δ is made dimensionless. Again, for longitudinal control derivatives $d = \bar{c}$ and $d = b$ for control derivatives in lateral direction.

$$C_{M_{control}} = \frac{M_{control}}{\delta \frac{1}{2} \rho V^2 S d} \tag{7.11}$$

Since the vertical and horizontal tail will be fully movable and symmetric and $M_{control}$ can be calculated with Equation 7.12, Equation 7.11 can be reduced to Equation 7.13

$$M_{control} = C_{l_{\alpha,control}} \delta \frac{1}{2} \rho V^2 S l_c \tag{7.12}$$

$$C_{M_{control}} = C_{l_{\alpha,control}} \frac{l_c}{d} \tag{7.13}$$

where l_c is the distance from the aerodynamic centre of the control surface to the rotation point, $d = \bar{c}$ for longitudinal moments and $d = b$ for control derivatives in lateral direction.

The force caused by the ailerons has been determined by finding the lift of the wings without aileron deflection and with a maximum aileron deflection δ using XFoil. This change in lift ΔL causes a change in moment with an arm from the rotation point of the Aeolusim to the aerodynamic centre of the respective control surface, which has been made dimensionless using the definition of the control moments (Equation 7.11).

7.1.5 Initial Conditions

The mass and moment of inertia gained from the structural model does not include the pilot, which is a large part of the mass. Therefore this has to be added. To calculate the total mass, the mass of the pilot is simply added to that the airframe. For the mass moment of inertia, data was used from Reference [18] to incorporate the mass moment of inertia of a sitting person of the right weight into the moment of inertia of the rest of the airframe. This was done by adding the moment of inertia of the pilot (including a Steiner term) where applicable to that of the structure.

When the centre of gravity is not directly above the rotation point, the simulator will rotate until the spring moments are sufficiently high to counteract the moment of the Aeolusim. The rotation that occurs due to the c.g. offset is illustrated in Figure 7.3. The ξ in the figure represents the offset angle from the ideal neutral position. If there is equilibrium, the angle ξ is equal to α_0 in longitudinal direction or φ_0 in lateral direction.

The moments caused by the weight and the springs are the only contributions in lateral direction. The moment equilibrium in lateral direction is shown in Equation7.14.

$$\sqrt{z_{cg}^2 + y_{cg}^2} W sin(\gamma + \xi) - k_r \xi \tag{7.14}$$

The angle $\gamma[rad]$ is defined as the angle between a vertical line through the rotation point and the line from the rotation point to the centre of gravity (see Figure 7.3). When the centre of gravity is located directly above the point of rotation, $\gamma = 0$. The angle that the simulator rotates due to a nonzero γ because of its weight $W[N]$ is defined to be $\varphi_0[rad]$. The spring contribution has been accounted for by $k_r[\frac{Nm}{rad}]$, which is the stiffness of the spring that restricts the rolling motion.

A centre of gravity offset in longitudinal direction has a similar effect. In this case however, the wing and horizontal tail have a contribution which depends on the angle of attack of the simulator. This moment is defined in Equation 7.15 for the main wing, the moment caused by the horizontal stabiliser (M_h) is calculated in the same fashion. The moment equilibrium in longitudinal direction is shown in Equation 7.16.

$$M_w = (C_{l_{0,w}} + C_{l_{\alpha,w}} \xi) \frac{1}{2} \rho V^2 S_w l_w \tag{7.15}$$

$$M = \sqrt{z_{cg}^2 + x_{cg}^2} W sin(\gamma + \xi) - k_p \xi + M_w + M_h \tag{7.16}$$

As stated earlier, the value of ξ where the moment is zero is the new equilibrium position. The angles α_0 and φ_0 are added to the pitch and roll angles gained from the state space simulation to find the actual pitch and roll angle.

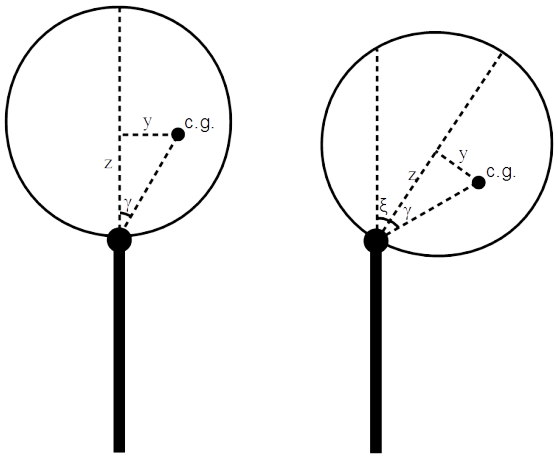

Figure 7.3: Effect of c.g. offset from the rotation point at zero rotation (left) and new neutral position (right)

7.1.6 Control Forces

The attitude of the Aeolusim is determined by the deflection of the stick and pedals. The user will provide this deflection and requires direct feedback to know that he is deflecting the control surfaces. This feedback is a translation of the hinge moment created by the control force due to the deflection of the control surface. In most aircraft the forces the pilot experiences are only a small part of the total hinge moment of the control surfaces or no part at all. This effect is apparent due to high wing loading and air velocity [17] creating too large hinge moments for the pilot to cope with. In the case of the Aeolusim, the control forces due to the hinge moments will be very small due to the low air velocity and the small control surfaces.

The control forces of the Aeolusim are all determined for maximum deflection of the control surfaces. If the pilot can cope with these forces, he should be able to handle the forces caused by deflecting the control surfaces less. The following method is explained for the elevator control force, but the method used to determine the aileron and rudder control forces are the same. Deviations to the method used for either the aileron or rudder, this will be mentioned.
The maximum deflection of the flight stick and pedals needs to be determined as a first step. The maximum allowable flight stick and pedals displacement distances are 40 *cm* [17]. In case of the Aeolusim, the maximum displacement for the flight stick and pedals are set to 20 *cm* due to space limitations in the fuselage. The determination of the maximum deflection of the control surfaces is done next. Since the rudder, elevator and aileron control surfaces will all be symmetrical airfoils, the maximum deflection is defined to be 10° to prevent flow separation. The flow separation occurs at the stall angle of the control surfaces, this is explained in section 5.1. The maximum control surface deflection is used to calculate the change of the deflection with change in flight stick deflection, in this case for the elevator: $\frac{d\delta_e}{ds_e}$. This derivative relates the change in hinge moment created by the control surface with the control forces the pilot experiences as can be seen in Figure 7.4. This relation is presented in equation 7.17 as stated in [17].

$$F_e = -\frac{d\delta_e}{ds_e} H_e \tag{7.17}$$

The hinge moment is determined by calculating the lift force the control surface generates at maximum deflection. The lift coefficients for the control surfaces are determined via the DATCOM method for the elevator and rudder and in Section 5.2.2 for the ailerons. The lift force is applied at the aerodynamic centre of the control surface. Placing the hinge a certain distance away from the aerodynamic centre, l_{arm} in equation 7.19, creates the hinge

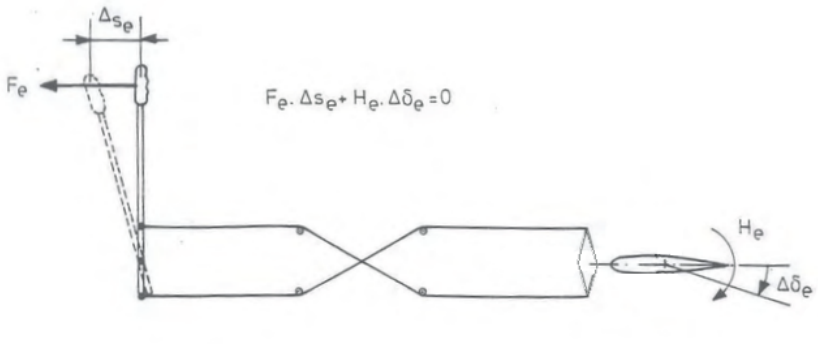

Figure 7.4: The relation between stick and elevator deflection, adapted from [17]

moment.

$$L = 0.5\rho V_h^2 S_e C_L \tag{7.18}$$

$$H_e = -L * l_{arm} \tag{7.19}$$

The hinge moment is made dimensionless by dividing by $\frac{1}{2}\rho V_h^2 S_e \bar{c}_e$ as seen in equation 7.20:

$$C_{h_e} = \frac{H_e}{\frac{1}{2}\rho V_h^2 S_e \bar{c}_e} \tag{7.20}$$

The hinge moment coefficient is in turn dependent on the angle of the horizontal tail, the elevator deflection and the trim tab of the elevator as seen in equation 7.21.

$$C_{h_e} = C_{h_e}\left(\alpha_h, \delta_e, \delta_{t_e}\right) \tag{7.21}$$

Combining the hinge moment (equation 7.17) with equation 7.20 gives the total stick force due to a maximum elevator deflection, as given in equation 7.22. Equation 7.21 has been linearised around the maximum deflection of the control surface, which is valid because of assumption SC-4 in Section 7.1.2. The hinge coefficients have been adapted to shortened notations for its dependencies, as shown in equation 7.20.

$$F_e = -\frac{d\delta_e}{ds_e}\frac{1}{2}\rho V_h^2 S_e \bar{c}_e \left(C_{h_\alpha}\alpha_h + C_{h_\delta}\delta_e + C_{h_{\delta_t}}\delta_{t_e}\right) \tag{7.22}$$

The trim tab is normally used to relieve control forces for the pilot. However a possible trim tab for the Aeolusim is ineffective because the small size of the elevator would only allow for a very small trim tab to be made. The added entertainment or realism by adding a trim tab is also negligible. Equation 7.22 is therefore used without the trim tab contribution. Because the entire horizontal tail is deflected for pitching manoeuvres, there is no difference between the angle of attack of the horizontal tail and elevator. The contribution of the horizontal tail $C_{h_\alpha}\alpha_h$ are omitted. These reasons cause equation 7.22 to be reduced to equation 7.23:

$$F_e = -\frac{d\delta_e}{ds_e}\frac{1}{2}\rho V_h^2 S_e \bar{c}_e C_{h_\delta}\delta_e \tag{7.23}$$

As one can see, the hinge coefficient is only dependent on the deflection of the elevator in equation 7.23.

The control forces and stick and pedal deflections for the rudder and ailerons are based on Figure 7.5. It can be seen from the picture that the hinges of the control surfaces are connected to the flight stick and pedals with wires. A forward deflection of the flight stick will result in a downwards deflection of the elevator, causing pitching up of Aeolusim. Deflecting the pedals by extending the right leg will cause the rudder to deflect to the right and the Aeolusim to yaw to the right as well. If the pilot deflects the flight stick to the left, the right aileron will deflect downwards and the left aileron will deflect upwards. This causes the Aeolusim to roll to the left.

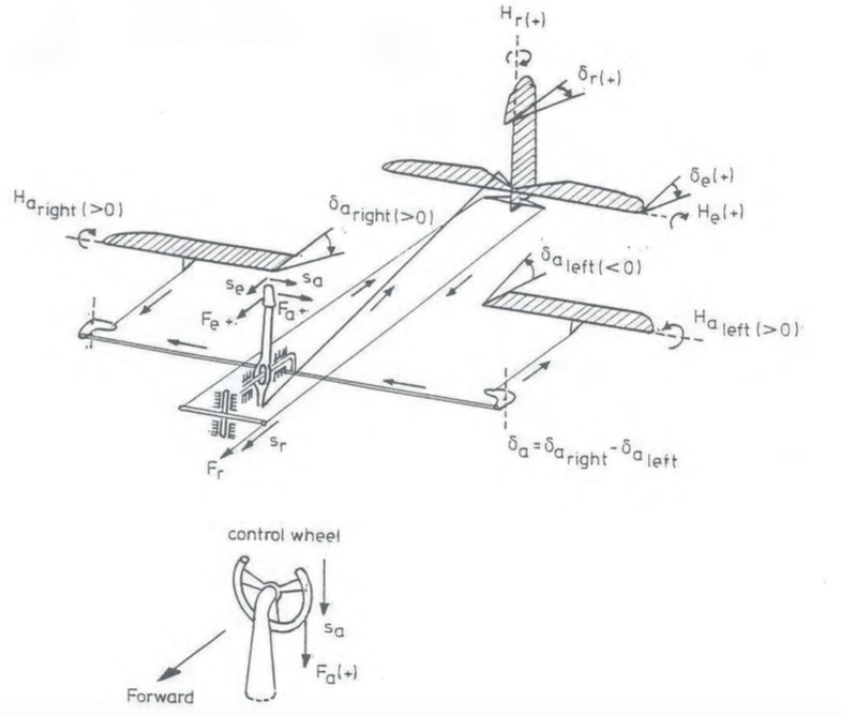

Figure 7.5: The relation between control surfaces and input deflection [17]

7.1.7 Verification & Validation

Two aspects of the model have to be verified. First it has to be proven that the method of obtaining the stability and control derivatives is valid. After that, it will be shown that the state space system is correctly implemented. Finally the control forces method is verified. Since the control derivatives have been determined directly from the control forces, these have been verified using unit verification.

To verify the stability derivatives, the method of inputting and obtaining data into and out of the Datcom program was verified. This was done using the known data from the Cessna Citation II. Entering its data into the created Datcom input parser and retrieving its results with the created Datcom output parser indeed yielded the correct stability derivatives.

To verify the state space system, first the state space without added AEOLUSIM specific coefficients like the spring stiffness was verified. Then, the addition of these coefficients in the model was verified.
To verify the first case, an existing model was used. This model was verified and validated in Reference [19]. This model used the coefficients for the Cessna Citation II. These coefficients were also entered in the Stability & Control model. As can be seen in Figure 7.6 and Figure 7.7, the outputs for both models are equal in both the symmetrical and asymmetrical case.

To verify the addition of the AEOLUSIM specific coefficients, the other coefficients were set to zero. In this case the resulting state space system would model a free damped vibration. The output of this system was compared to the output of Equation 7.24 which models a free damped vibration [20].

$$\alpha = Ae^{-\zeta\omega_n t}sin(\omega_d t + \varphi) \tag{7.24}$$

In this equation ζ is the damping ratio (Equation 7.25), ω_n is the natural frequency (Equation7.26), ω_d is the damped frequency for an underdamped system (Equation 7.27), φ is the phase shift and A is the amplitude.

$$\zeta = \frac{c}{2\sqrt{mk}} \tag{7.25}$$

$$\omega_n = \sqrt{\frac{k}{m}} \tag{7.26}$$

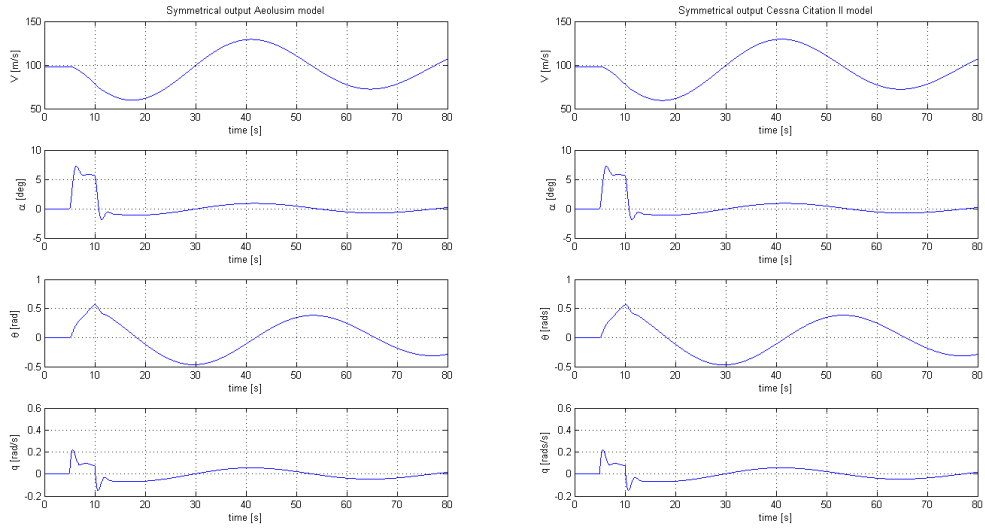

Figure 7.6: Symmetrical output for the Aeolusim and Cessna Citation II models

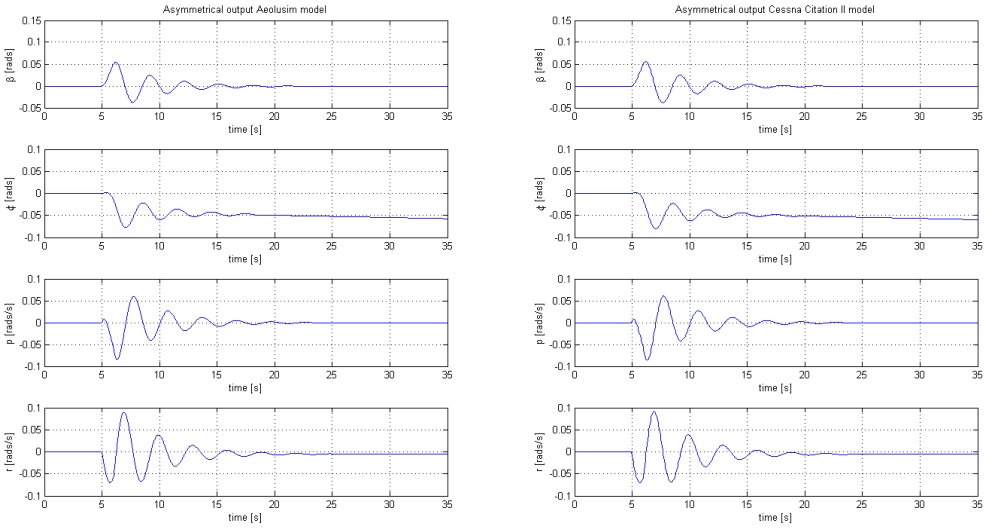

Figure 7.7: Asymmetrical output for the Aeolusim and Cessna Citation II models

$$\omega_d = \omega_n \sqrt{1 - \zeta^2} \tag{7.27}$$

As input, an initial offset of 0.2 *rad* (11.46 deg) has been used which will be the amplitude input for the free damped vibration. With an initial offset as input, the phase shift is $\frac{1}{2}\pi$.
It needs to be verified that the state space system with only the AEOLUSIM specific coefficients behaves as a free damped vibration. If this is the case both models should respond in the same way to a change in spring stiffness or a change in damping coefficient. Since only the change is of interest, the damping ratio and natural frequency of the vibration model have been multiplied by a certain factor so the output for both models for the initial spring stiffness and damping coefficient were equal. Afterwards, the spring stiffness was multiplied by eight and the results were plotted for both models. This was also done for a damping coefficient multiplied by eight and the original spring stiffness. The results for the pitching motion are presented in Figure 7.8. The verification was also done for yawing and rolling motion with similar results.

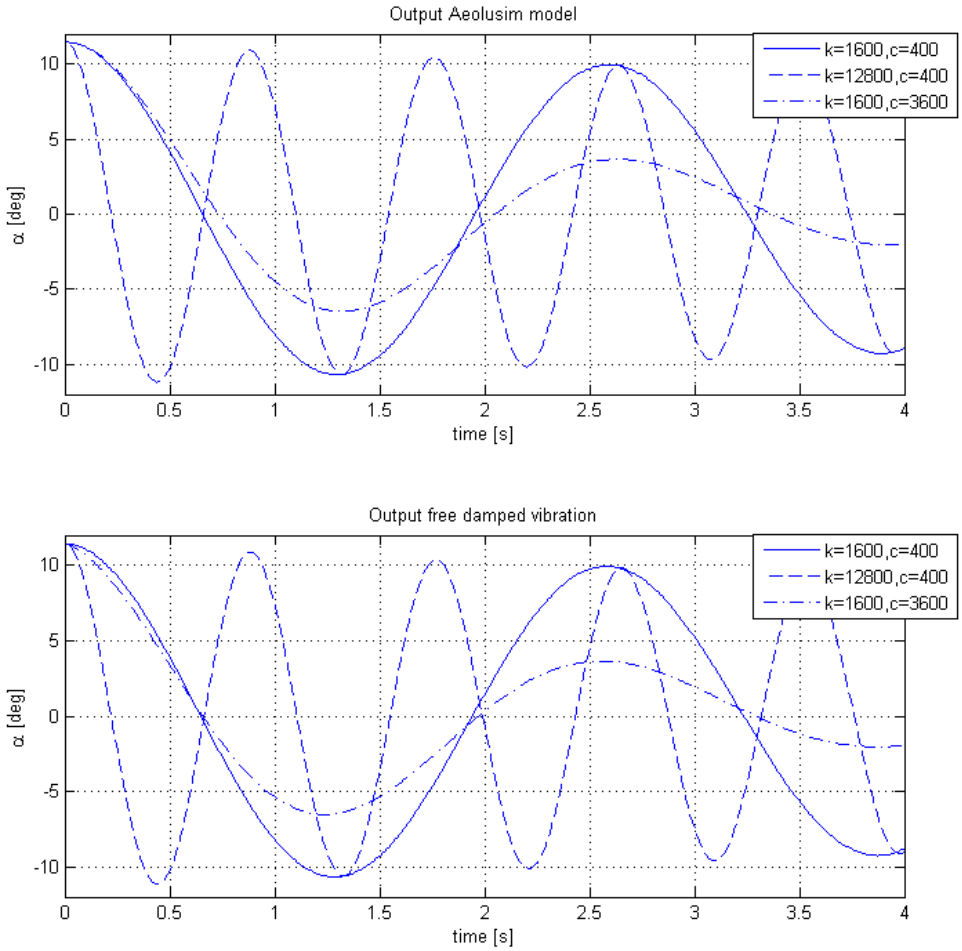

Figure 7.8: Time response to an initial offset of AEOLUSIM model and a free damped vibration

As can be seen, the models respond in the same way to a change in spring stiffness and in damping coefficient. Therefore, the AEOLUSIM specific coefficients have been implemented into the state space system correctly.

The verification of the control forces has been done using unit verification. Since the calculation of control forces is a series of straightforward calculations this is an adequate method of verification.

Since there are no existing wind driven simulators, let alone existing wind driven simulators with extensive available data, the validation of the model will have to be done by either building a working prototype or a scale model and running tests. These test results can be compared to the model output to validate it.

7.1.8 Model Reliability

Since the Datcom method is widely used to estimate the stability derivatives of an aircraft, it is determined to be very reliable. However, it is stated in Reference [21] that when an airfoil is used that has a higher thickness over chord ratio than 12%, the accuracy will diminish. Since the airfoils used in the AEOLUSIM have a thickness of 15% of the chord, the accuracy diminishes somewhat. The results from the Datcom method were compared to the results with the same input but a NACA-0012 airfoil (which has a 12% thickness to chord ratio) there were changes but these were not dramatic.
The state space system used in the model is also widely applied to model aircraft behaviour. The addition of AEOLUSIM specific coefficients, however, is not. Since it was verified these coefficients were entered into the model correctly, it can still be considered a reliable method.

7.2 Stability & Control Performance

Important aspects of the Stability & Control parameters have been determined to be the angles the simulator can achieve in all directions, the degree to which the system behaves like a real aircraft and the control forces the pilot needs to exert. For the simulator motion to be like a real aircraft, the spring stiffness and the damping coefficients may need to be changed. This will adversely impact the maximum angles that can be achieved in pitch and roll. To find an optimum, a trade-off will have to be done between aircraft like behaviour and maximum pitch and roll angles.

7.2.1 Motion Responses

Due to wind tunnel geometry, the maximum allowed deflections are 20°, 10° and 10° for roll, pitch and yaw, respectively.

To obtain the maximum deflections that can be achieved, the spring stiffness and damper coefficients have been optimised to achieve a maximum angle while remaining within the wind tunnel's constraints. The used spring and damper values can be found in Table 7.1. The resulting model output is presented in Figure 7.9, Figure 7.10 and Figure 7.11.

	Spring Stiffness $[\frac{Nm}{s}]$	Damping Coefficient $[\frac{Nm}{s^2}]$
Pitch	1000	850
Roll	650	930
Yaw	200	900

Table 7.1: Used spring stiffnesses and damping coefficients for the maximum motion response

The maximum deflection of the control forces is used, which is 10° for all control surfaces. The maximum roll angle has to be limited to 20°. Since the rudder does not only cause a yaw angle but also a roll angle, this has been taken into account in determining the maximum roll angle.

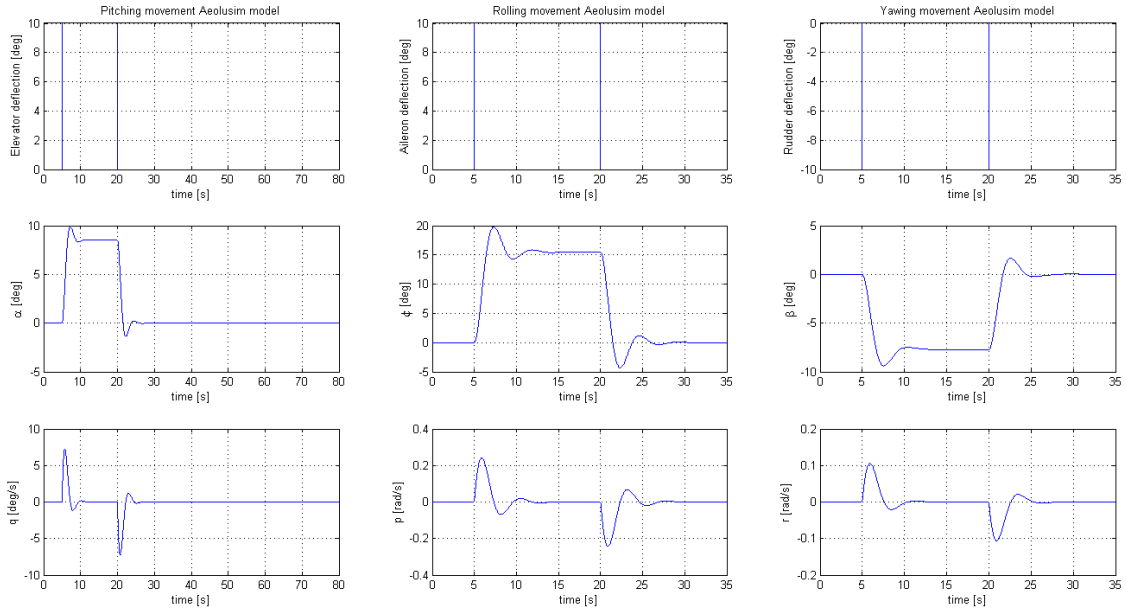

Figure 7.9: Output in all angles for maximum deflections spring settings

As can be seen, the deflections in all directions are very close to their maximum. The time it takes to reach these deflections is between two and three seconds for all directions. For the short period motions, there is an acceptable eigenmotion visible. The Dutch roll however, has a very low frequency and a very high damping. In the short period graph, a phugoid is seen in the Cessna's graph. This is something the Aeolusim cannot replicate since the velocity does not vary. In the Dutch roll plot, the roll does not go to zero for the Cessna this is

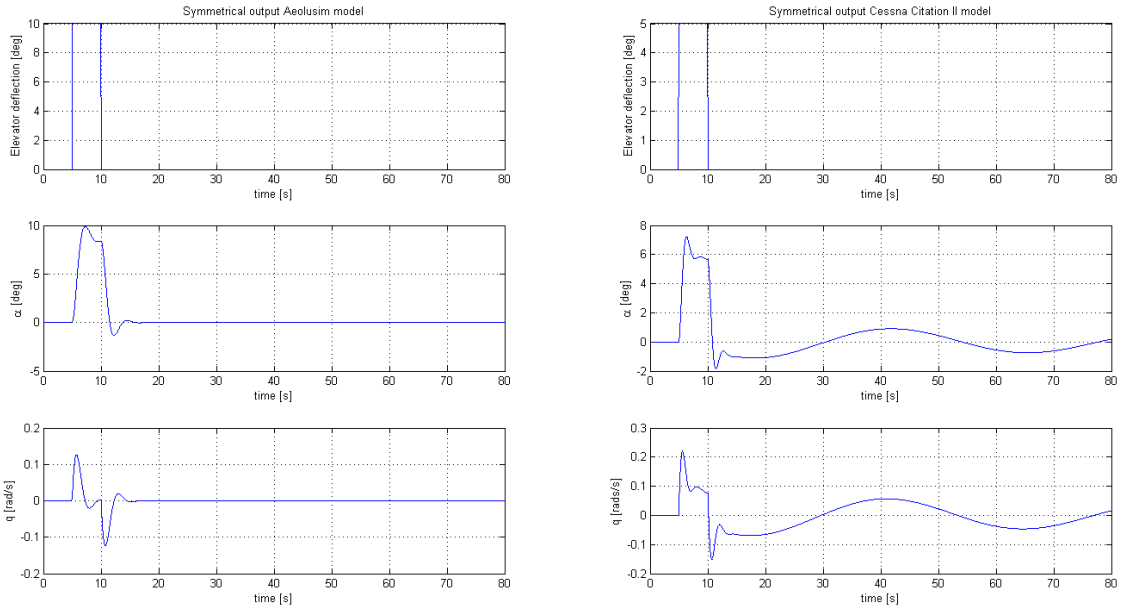

Figure 7.10: Output for maximum deflections spring settings for short period input

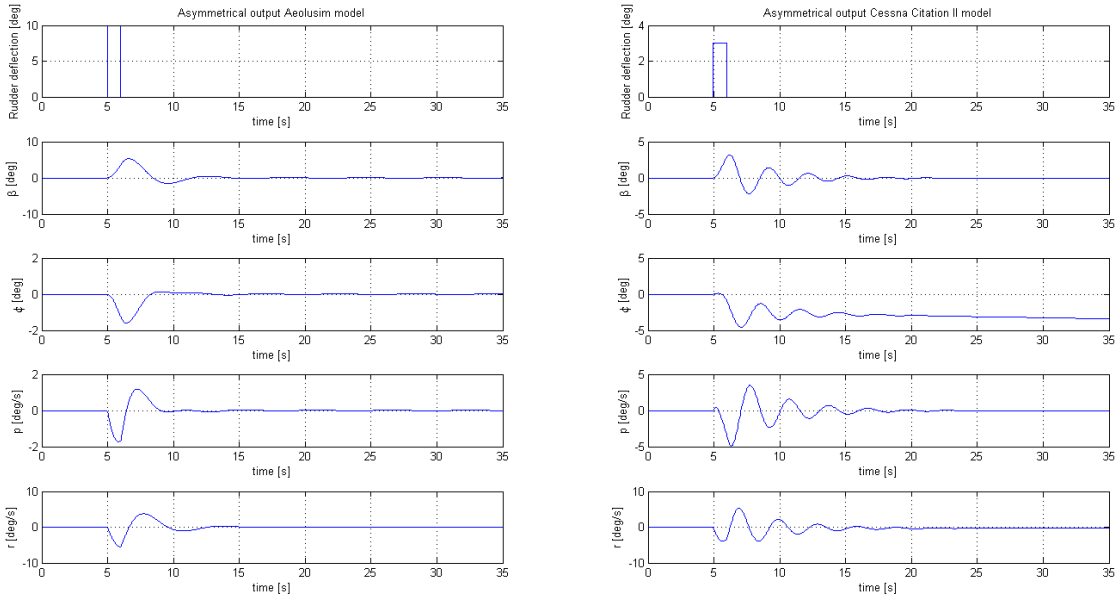

Figure 7.11: Output for maximum deflections spring settings for Dutch roll input

because it has an unstable spiral motion. The AEOLUSIM does not have an unstable spiral motion and therefore does return to zero.

7.2.2 Aircraft-like Behaviour

To simulate aircraft motions, the spring stiffness and damper coefficients have been optimised such that the model response resembles that of the response of the Cessna Citation II eigenmotions. The used spring and damper values can be found in Table 7.2. The resulting model output is presented in Figure 7.12, Figure 7.13 and Figure 7.14.

As control input, the maximum deflection have been used for a short duration to determine the eigenmotions.

	Spring Stiffness $[\frac{Nm}{s}]$	Damping Coefficient $[\frac{Nm}{s^2}]$
Pitch	1200	850
Roll	800	400
Yaw	650	600

Table 7.2: Used spring stiffnesses and damping coefficients for the aircraft like motion response

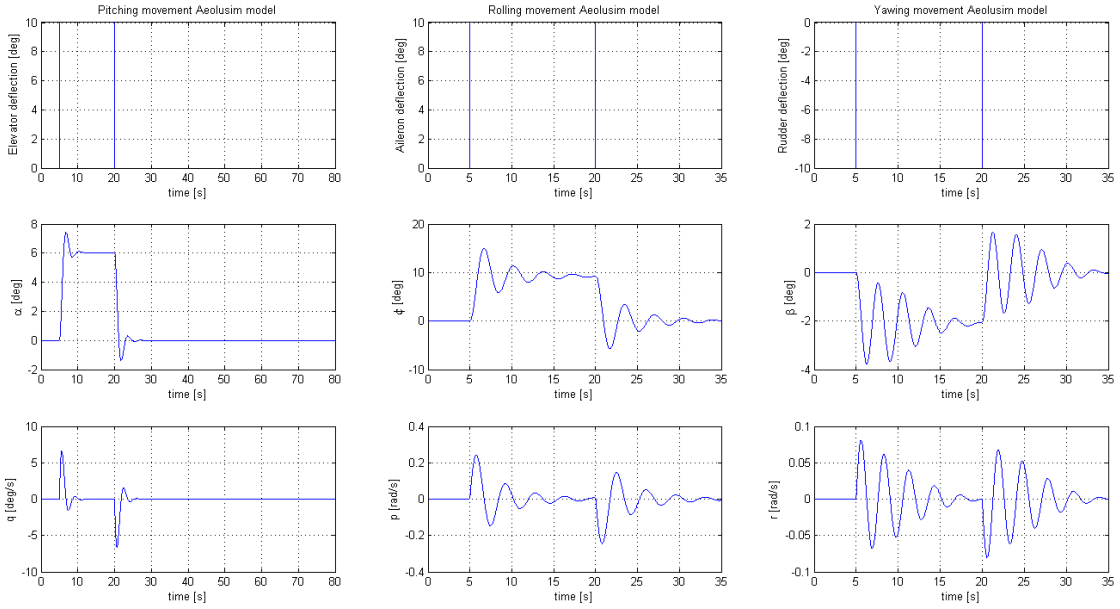

Figure 7.12: Output in all angles for aircraft-like motion spring settings

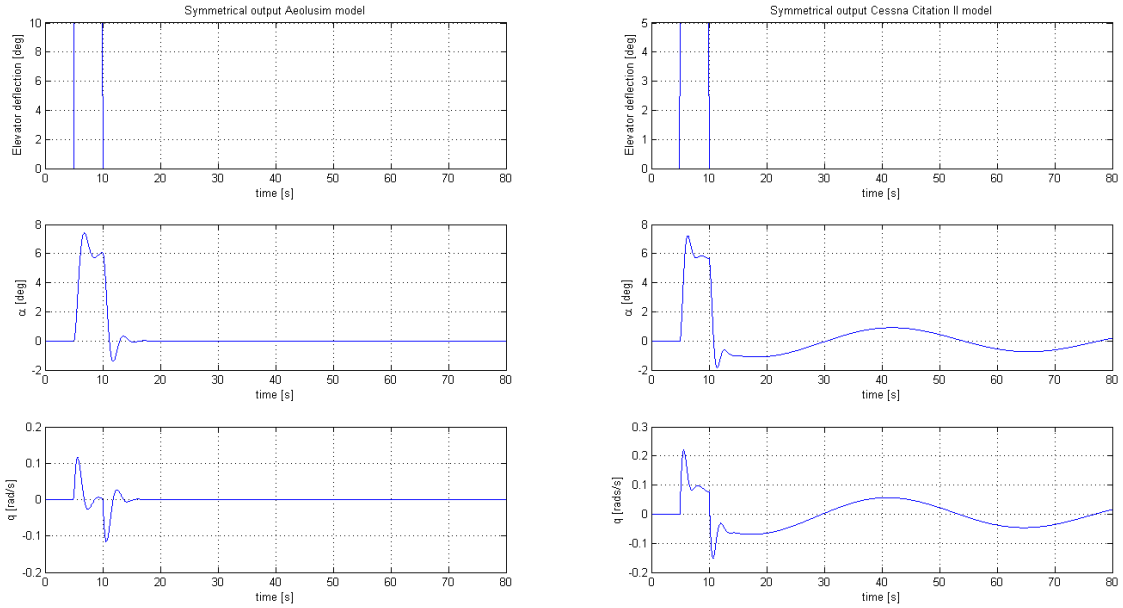

Figure 7.13: Output for aircraft-like motion spring settings for short period input

As can be seen, both in longitudinal and lateral directions, the motions of the simulator are very similar to the Cessna's motions. However, since the spring stiffness had to be increased to obtain similar frequencies, the maximum deflection that can be obtained is lower now. This is especially the case for yawing motion. Also, in

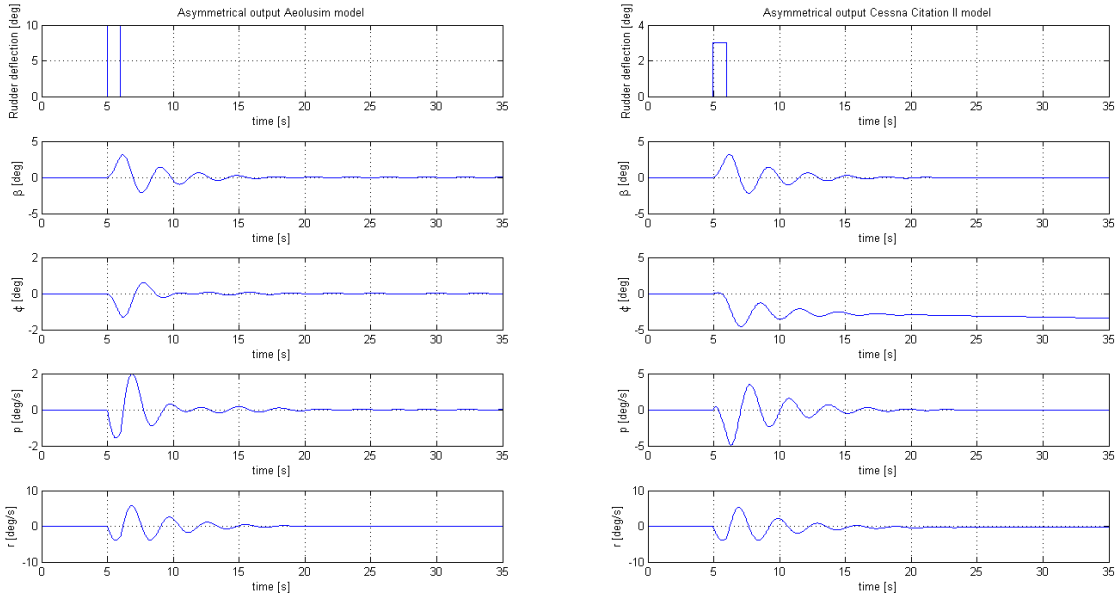

Figure 7.14: Output for aircraft-like motion spring settings for Dutch roll input

roll and yaw, the damping is very low. This would possibly cause an uncomfortable situation. These factors would greatly reduce the entertainment value of the Aeolusim.

7.2.3 Control Forces

In this section the control forces are determined and presented, after which they will be checked with the control force requirements. With satisfactory control forces, the layout of the control surfaces and hinges will be presented. The layout will also include the connection between the hinges and the control stick and pedals.

Using the method as described in Section 7.1.6 and after several iterations, the lift forces generated by the control surfaces are determined to be:

- Ailerons Lift Force : 62.8 N
- Elevators Lift Force: 31.9 N
- Rudder Lift Force : 10.5 N

Converting these lift forces to the hinge moments requires a certain hinge arm. The hinge arm is the distance between the aerodynamic centre of the control surface, which is located at a quarter chord of the control surface, and the hinge point, around which the control surface rotates. Because the chords of the elevators, ailerons and rudder are 0.8 m, 0.5 m and 0.8 m respectively, these moments would be very small if the hinge is placed inside the control surfaces. The maximum hinge arm would be 0.2 m, 0.125 m and 0.2 m for the elevators, ailerons and rudder respectively. The resulting control forces the pilot experiences are too low according to the limit of at least 1.3 kg as defined by the U.S. military regulations in reference [17]. The military regulations have been chosen in this regard to increase the user experience by giving feedback when starting to deflect the control stick and pedals. The British and American Civil Airworthiness Regulations, as can be seen in Table 7.3, regulate the maximum forces a pilot should encounter. Aside from the low hinge moment, a more practical reason for placing the hinge in the fuselage is that the hinge would not fit inside of the control surface profile. The hinge would have to be placed in the nose of the NACA0015 airfoil of the elevators and rudder. The elevators and rudder are at maximum 12cm in thickness at the aerodynamic centre, making this impossible. For these reasons, the hinges of the elevators and rudder are placed in front of the control surfaces inside the fuselage as seen from the nose of the Aeolusim.

After several iterations where the hinge arms were changed, the aileron and elevator control forces have been found to be acceptable and within the British and American Civil Airworthiness Regulations limits. The hinge arm required to have acceptable rudder control forces would be too large (1.6 m) to put on the Aeolusim. The large hinge arm combined with the rudder deflection of 10° would require the elevators to be placed away from the

	Requirement according to U.S. Civil	Requirement according to British Civil
Rudder pedals	82 kg (short intervals) 9 kg (short intervals)	82 kg (short intervals) 22.5 kg (long intervals)
Elevator control	35 kg (short intervals) 4.5 kg (short intervals)	22.5 kg (short intervals) 2.6 kg (long intervals)
Aileron control	27 kg (short intervals) 2.3 kg (short intervals)	

Table 7.3: The maximum control forces for long and short duration [17]

fuselage centreline so much, that they would hit the wind tunnel, limiting the yawing motion of the AEOLUSIM. Due to this reason the hinge arm of the rudder has been set at 0.5 m in front of the rudder's leading edge, equal to the hinge arm of the elevators. Due to the large force created by the ailerons, the hinge arm is only 0.04 m in front of the ailerons' leading edge.

The resulting control forces, using the above determined hinge arms and the method as explained in 7.1.6.

- Aileron Control Force : 22.5 N
- Elevator Control Force: 21.4 N
- Rudder Control Force : 7.03 N

As one can see the rudder control force the pilot experiences in the pedals is too low for the U.S. military regulation: the control forces for the aileron, elevator and rudder should be higher than 1.3 $kg = 12.75$ N. The low rudder control force can be increased by using a spring behind the hinge. This spring can add a constant force, but also a variable force. For the AEOLUSIM a variable force will be added. This will give the pilot a better feedback because the spring force is increased for longer pedal deflections.
The connection between the control surfaces and the hinges can be seen in Figures 7.15 and 7.16 for the aileron, elevator and rudder. The hinges are connected to the controls using steel cables as shown in Figure 7.5.

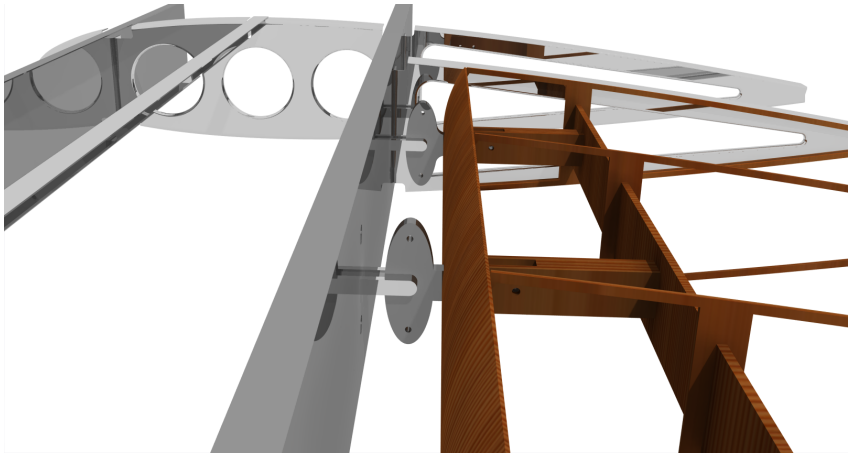

Figure 7.15: The link between the aileron control surface and the aileron hinge

7.2.4 Discussion & Recommendation

From the results in Section 7.2.1 and Section 7.2.2, it is clear that both large deflections and aircraft like motions are possible. However, different spring stiffeners and damping coefficients are needed in both cases. This means a choice needs to be made between the two.
Since the AEOLUSIM is aimed at the entertainment market, it is determined that big deflections are more attractive to a user than aircraft like motion with small deflections. Therefore, the choice is made to use the spring and damper values that were used to obtain maximum deflection. These settings will also give a proper short period motion and something resembling a Dutch roll.
If more power could be used to generate the airflow, a higher wind speed could be obtained or a larger wind

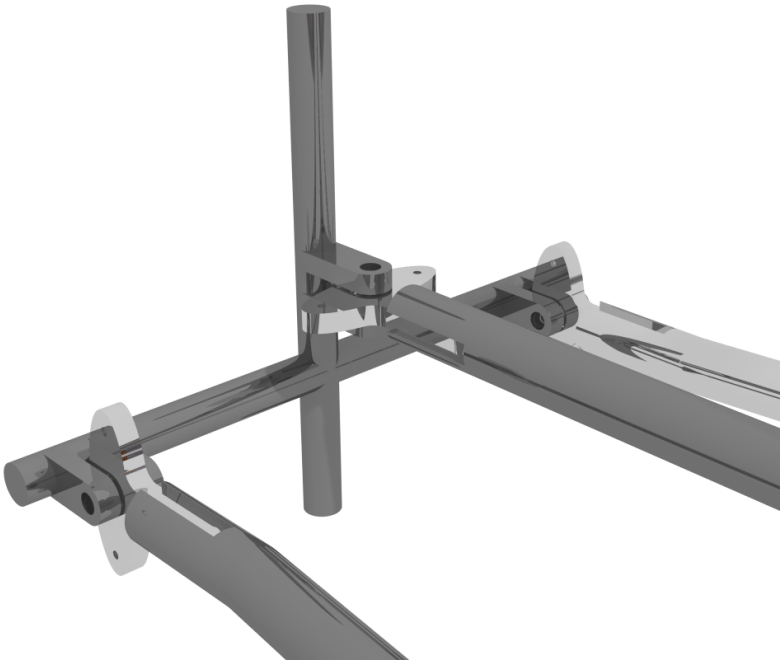

Figure 7.16: The link between the elevator and rudder control surface and their hinges

tunnel could be made. With either of these changes, the control surfaces can be made more effective. This would enable the Aeolusim to have both aircraft-like behaviour and large deflections, vastly improving the quality of the simulator.

8 Sensitivity Analysis

In this chapter the sensitivity analysis on the AEOLUSIM will be performed. Since the sensitivity analysis is performed at the same time as the performance analysis, the values that are taken as initial values in this chapter may not be the same as the final values from the performance analysis. This is not a problem however, as the sensitivity analysis focusses on the change of parameters.

Section 8.1 discusses the sensitivity of the fan, Section 8.2 elaborates on the structural sensitivity and Section 8.3 contains the sensitivity analysis for the motion responses.

8.1 Fan Sensitivity Analysis

the main problem with determining sensitivity of the fan model is the fact that only one input, the volumetric flow rate Q_{design}, is used to determine all other parameters. this single starting point really defeats the purpose of an extensive numerical sensitivity analysis as changing, for example, only the rpm really does not make much sense from a design standpoint. Nevertheless a select few values, among which is the rpm, is used as a variable input to the model. These values are listed in table 8.1.

Table 8.1: Fan Model Inputs

Variable	Value	Unit
Hub Radius	0.156	m
Tip Radius	0.425	m
Rotational Velocity	900	rpm
Volumetric Flow Rate	5.3	$\frac{m^3}{s}$

These values will all be systematically increased and decreased to asses the sensitivity. The outputs are the calculated design characteristics, the increase in pressure, the efficiency and the power consumption. These three values determine all aspects of the fan operation, and are thus best suited as a measuring point for the sensitivity. The final judgement on the sensitivity will take into account that some values will almost never be a design input. All values will both be increased and decreased with a fixed percentage of 10 %. First the hub radius was varied, changing this value obviously changes the bladed area of the fan. The pressure increases of all have been estimated with a empirical formula based on bernoulli's theorem and checked with Reference [22]. The results are summarized in table 8.2.

Table 8.2: Fan Model Sensitivity

Input Change	Pressure Increase Change	Efficiency Change	Power Change
Hub Radius +10 %	+7%	-1%	+6%
Hub Radius -10 %	-5%	-3%	-3%
Tip Radius +10 %	+26 %	+8%	+15%
Tip Radius -10 %	-21 %	-28%	+4%
Rotational Velocity +10 %	+21%	+3%	+17%
Rotational Velocity -10 %	-21%	-7%	-13%
Volumetric Flow Rate +10 %	0%	-8%	+23%
Volumetric Flow Rate -10 %	0%	+3%	-13%

These are the values that can be checked using the numerical model, yet there is an other parameter that is vulnerable to change during production. And, more importantly, will impact performance if changed. This parameter is the blade angle distribution, especially the leading edge angles. These are defined with enough accuracy that production errors may cause a slight drop in efficiency due to the fact that wrong angles will cause shock losses. These effects will not be prevalent until the angle deviates from its intended value with a value of over 1 degree. Although not terribly sensitive, attention should be given to the fact that this particular part of the design is produced with enough accuracy. In Conclusion the results show that the model, and thus the

design, is not very vulnerable to small changes. These changes can be alleviated, albeit slightly, by changing other parameters as well, further reducing sensitivity to change. This means that future versions of the design will not need to perform extensive design alterations or compensation exercises to reach acceptable measures of performance.

8.2 Structural Integrity Sensitivity Analysis

The structural integrity is determined by the applied load. Chapter 6 designed the structure for the maximum load cases of user interaction (for example, someone leaning or sitting on the main wing). This load was derived from the maximum allowable pilot weight of 95 kg. If the client requests to increase this upper limit the respective loads will increase as well. This sensitivity analysis shall discuss the effects of a 10% increase in pilot mass in a qualitative manner.

Main Wing
Current safety factors for the main wing range from 3 to 244. Based on these safety factors it may be concluded that the current geometry of the main wing is able to cope with the increase in pilot mass.

Tail wings
The load cases of the tail wings are not directly affected by the pilot weight. The user is not expected to come in the vicinity of the tail wings, as this would require the user to 'jump' over the main wing which has a chord length of 1 m.

Support Structure The support structure is designed as a pivot point for the entire simulator. An increase in pilot weight would increase the mass the support structure is to counteract. The current lowest safety factor is 1.97, see Section 6.5. A 10% increase in pilot mass would result in an additional 9.5 $kg - f$. A drop in safety factor is undesirable, as it would not allow for much contingency. A redesign of the support structure is therefore advised.

Fuselage
The fuselage is designed with loadcases analogous to the main wing. Its design yielded a minimum safety factor of 2.56 for the loadcase of someone sitting on the nose of the simulator (Section 6.4. An increase in pilot mass would result in higher internal stresses. However, a drop below a safety factor of 2 is not to be expected for a 10% increase in pilot mass.

8.3 Motion Response Sensitivity

In this chapter the sensitivity analysis on the Aeolusim will be performed. Since the sensitivity analysis is performed at the same time as the performance analysis, the values that are taken as initial values in this chapter may not be the same as the final values from the performance analysis. This is not a problem however, as the sensitivity analysis focusses on the change of parameters.

Both the maximum roll, pitch and yaw deflections and the eigenmotions of the simulator are greatly influenced by the spring stiffnesses of the spring damper system. Since the main focus of the Aeolusim will be the entertainment market and not the flight simulator market, the focus in this sensitivity analysis will be on the effect of changes to the maximum rotation rather than to the eigenmotions.

First, the reason why a sensitivity analysis is performed will be explained. The second part explains what aspects will be analysed. The last part will present and discuss the results of the sensitivity analysis.
The performance analysis of the Aeolusim has been done, but changes to the design can still occur. The sensitivity analysis plays an important part in this respect, because it tests the robustness and feasibility of the current design. The focus on the sensitivity analysis in this chapter is on the feasibility aspect of the simulator. The feasibility is of crucial importance in weighing whether to bring the Aeolusim to market, and when it will be put to the market. The feasibility will be tested by changing certain parameters of the Aeolusim, which will be detailed in the next section.

8.3.1 Analysed Parameters

The Aeolusim has been analysed for a change in various aspects. Below is a list of which variables have been analysed and why these have been analysed:

- Mass Moment of Inertia - The main goal of the AEOLUSIM is to provide the user with a realistic flight experience. This is partly achieved by the displacement of the AEOLUSIM. Changing the mass moment of inertia will affect the acceleration and peak displacement of the AEOLUSIM.
- Mass - The mass of the AEOLUSIM determines for a large part the amount of roll and pitch which can be achieved. This is because the mass helps the AEOLUSIM create a larger displacement. Changing the mass will thus affect the rolling and pitching motion.
- Location of tailplanes - The tailplanes of the AEOLUSIM are the control surfaces. Changing the location of these tailplanes changes the moments they provide, and thus changes the maximum angular acceleration, velocity and displacement.
- Location of the main wings - Moving the main wing changes the distance between the ailerons and the rotation point, so the pitch moment will be affected.
- Size of the main wings - Changing the size of the main wing changes the lift force, so the pitch moment will be affected.
- Centre of Gravity offset - Since the mass generates a moment about the rotation point, changing distance and angle between the rotation point and centre of gravity will cause this moment to change.
- Velocity - All forces on the AEOLUSIM directly depend on the velocity, so changing this factor has influence on the performance of both pitch and roll and yaw.
- Hinge locations - The control forces depend on the location of the hinges. Since there are requirements on the magnitude of the control forces, the influence of the hinge locations is determined.

8.3.2 Analysis Results

This section shows and discusses the results from changing the parameters listed in 8.3.1.

Mass Moment of Inertia
Four mass moments of inertia have influence on the parameters in the state space system of the model. All four have been changed separately in order to determine the severity of changes in these parameters. Since the current performance will increase when the mass moments of inertia decrease, this scenario is not analysed in the sensitivity analysis.

The influence of the mass moments of inertia I_{xx}, Iyy and I_{zz} is shown in Table 8.3 for a maximum aileron, elevator and rudder deflection, respectively. It is clear that none of these parameters has an influence on the stabilised angle, since this angle only depends on the mass (except in the case of the yawing motion), spring stiffness and applied moment. The factor that is affected is the peak deflection. This behaviour is due to the fact that an object that rotates with a higher mass moment of inertia is harder to stop. If the peak deflection were to become too large due to a large mass moment of inertia, it could easily be solved by increasing damping coefficients of the spring damper mechanisms. The last mass moment of inertia that is tested is Ixz. However, the influence of I_{xz} is so small that multiplying it with a factor 10 does not yield significant differences. For that reason, this parameter was not included in Table 8.3

Mass Moment of Inertia	Initial performance			Doubled Mass Moment of Inertia		
	stabilised angle [^{o}]	peak angle [^{o}]	time s	stabilised angle [^{o}]	peak angle [^{o}]	time s
I_{xx}	24.6	29.4	3	24.6	33.1	4
I_{yy}	16.8	18.6	4	16.8	21.0	5
I_{zz}	11.7	16.7	4.3	16.8	18.3	6

Table 8.3: Angular deflection comparison for the current Moments of Inertia versus increased Moments of Inertia

Mass
The mass has been determined for two extreme cases. The first is a maximum pilot weight and a simulator weight increase of 10%. The second case is the minimum required pilot weight and a simulator that is 10% lighter than expected.

Clearly, the mass has a large influence on the pitch and roll performance, as expected. In order to solve this problem, a solution that is used in sailplanes can be taken over. When a light user operates the AEOLUSIM an additional mass has to be added, preferably example under the chair.

Location of the Tailplanes
The horizontal and vertical tailplanes will be moved together, such that the interaction between them will not

Rotation	Initial performance		10% Maximum Mass Increase		10% Minimum Mass Decrease	
	stabilised	peak	stabilised	peak	stabilised	peak
roll angle [^{o}]	24.6	29.4	35.9	40.6	9.6	12.9
pitch angle [^{o}]	16.8	18.6	19.3	20.7	8.3	9.6
yaw angle [^{o}]	11.7	16.7	11.7	16.7	11.7	16.7

Table 8.4: Angular deflections for the maximum weight+10% and minimum weight−10%

change. Also, it is assumed that the centre of gravity does not move. Both the $z-$location and the $x-$location of the tailplanes will be changed. The arm to the centre of gravity in $x-$direction will move $\pm 10\%$, and the arm in $z-$direction will move $\pm 0.4m$. It was chosen to not express this in a percentage for the reason that the $z-$arm is already quite small, so a small displacement would have resulted in a misleadingly high percentage.

The changes in pitch, roll and yaw angle due to a relocation in $x-$direction of the horizontal tail are listed in Table 8.5. It can be seen that the pitch and yaw deflection angles increase when the tail arm increases, and vice versa. Obviously, this is due to the increased moment arm.

Rotation	Initial performance		10% $x-$arm Increase		10% $x-$arm Decrease	
	stabilised	peak	stabilised	peak	stabilised	peak
roll angle [^{o}]	24.6	29.4	24.6	29.4	24.6	29.4
pitch angle [^{o}]	16.8	18.6	17.7	19.5	12.6	14.4
yaw angle [^{o}]	11.7	16.7	15.4	20.4	9.2	14.2

Table 8.5: angular deflections for changes in the $x-$arm of the tailplanes

Table 8.6 shows what happens to the deflection angles when the tailplanes are moved in the $z-$direction. It can easily be explained that the maximum roll angle increases when the tail is moved upward: the vertical tail has a moment arm with respect to the rotation point which causes a roll deflection. Increasing this arm generates a larger moment.

The increase of the maximum pitch angle due to lowering the tail surfaces seems counter-intuitive. Drag of the horizontal tail causes a pitching moment, and lowering the tail surfaces would decrease this pitching moment. However, examining the output from the Digital Datcom program showed that the increase in pitch was due to an increase in C_{m_α} caused by interaction between the wing and the horizontal tail. The horizontal tail is now located in the wake of the wings. These wings generate downwash, due to which the horizontal tail experiences a negative angle of attack. Since the tail is a symmetric airfoil, it generates negative lift and thus a positive pitching moment. In the original setting, the tail surfaces are not located in the wake of the wings.

It can be seen that the extra pitch angle is not very large for an extremely large relocation of the horizontal tail. For that reason it can be assumed that the extra pitch angle will not cause the simulator to hit the wind tunnel as the pitch angle will always be within the safety margins.

What can however cause the Aeolusim to hit the top or bottom of the wind tunnel at pitch-up or pitch-down is the change in vertical location of the vertical tail. The margins in the wind tunnel have been kept small to generate an as high as possible air velocity. The vertical tail is therefore sensitive to changes in relocations in $z-$direction.

Rotation	Initial performance		$0.4m$ $z-$arm Increase		$0.4m$ $z-$arm Decrease	
	stabilised	peak	stabilised	peak	stabilised	peak
roll angle [^{o}]	24.6	29.4	25.1	29.9	18.4	23.2
pitch angle [^{o}]	16.8	18.6	16.5	18.3	19.0	20.8
yaw angle [^{o}]	11.7	16.7	11.7	16.7	11.7	16.7

Table 8.6: angular deflections for changes in the $z-$arm of the tailplanes

Location of the Main Wings

The location of the main wings is varied along the $x-$axis in two directions, and varied along the $z-$axis in only the upward direction. This is because the wing cannot be located lower than its current location.

Changing the $x-$location of the main wings only has an influence on the peak and stabilised pitch angles (see Table 8.7). When the horizontal location of the wing changes, the moment the wings generate about the rotation point changes and has a significant influence on the maximum pitch angle. Also the $z-$location of the wing is sensitive to relocations, as can be seen in Table 8.8. The roll angle can increase when the wings are placed too high due to the wing-fuselage interaction, possibly causing the simulator to hit the wind tunnel. For these reasons, it is important that the wings are accurately placed.

Rotation	Initial performance		10% $x-$arm Increase		10% $x-$arm Decrease	
	stabilised	peak	stabilised	peak	stabilised	peak
roll angle $[^o]$	24.6	29.4	24.6	29.4	24.6	29.4
pitch angle $[^o]$	16.8	18.6	19.0	23.4	10.5	14.9
yaw angle $[^o]$	11.7	16.7	11.7	16.7	11.7	16.7

Table 8.7: angular deflections for changes in the $x-$arm of the wings

Rotation	Initial performance		$0.2m$ $z-$arm Increase	
	stabilised	peak	stabilised	peak
roll angle $[^o]$	24.6	29.4	30.5	34.9
pitch angle $[^o]$	16.8	18.6	17.8	19.6
yaw angle $[^o]$	11.7	16.7	11.7	16.7

Table 8.8: angular deflections for changes in the $z-$arm of the wings

Size of the Main Wings
The chord and span of the main wings are separately varied by 10%, in order to determine the sensitivity to these parameters.

Table 8.9 shows what happens when the span is changed. The size of the wind tunnel depends on the size of the wings, so when during design the span of the wings increases, this will be paid with a loss of velocity and thus smaller maximum deflection angles. Since there is only a decimetre margin between the wings and the walls of the wind tunnel, the wings of the Aeolusim should not increase more than a decimetre in length. The Digital Datcom code was unable to determine the stability derivatives when the wing would be 10% shorter, so it is unknown what this will do to the performance. This has to be determined by wind tunnel testing.

	Initial performance		10% Span Increase		10% Span Decrease	
	stabilised	peak	stabilised	peak	stabilised	peak
velocity $[m/s]$	11.9		10.62		13.58	
roll angle $[^o]$	24.6	29.4	18.7	23.1	–	–
pitch angle $[^o]$	16.8	18.6	12.4	14.0	–	–
yaw angle $[^o]$	11.7	16.7	7.5	12.5	–	–

Table 8.9: Velocity and angular deflections for changes in the span of the wings

In Table 8.10 it is shown what the maximum angular deflections are when the chord of the main wing changes. A 10% change in the chord length does not seem to have a very large influence, except that the pitch angle may increase a little when the chord is decreased. This change however is so small that the margins of the wind tunnel are sufficient to allow a decrease in chord length.

Size of the Tail Surfaces
The size of the tail surfaces is varied by changing the chord and span by 10% simultaneously, such that the ratio between chord and span is unchanged and the total surface is changed 21% Table 8.11 shows the effect of changing the surface of the horizontal tail. As one would expect, this only has an effect on the maximum pitch angles and not on roll and yaw. Depending on the increase surface, this might become a problem for a serious increase in tail surface. For that reason, care should be taken that the tail surface does not become much larger during production.

The effect of increasing and decreasing the size of the vertical tail is shown in Table 8.12. It has become clear that a significant increase in the vertical tail size does not have much effect on the roll angle, and as could be expected it has no effect on the maximum pitch angle. However, an increase in span of the vertical tail can cause

Rotation	Initial performance		10% chord Increase		10% chord Decrease	
	stabilised	peak	stabilised	peak	stabilised	peak
roll angle [^{o}]	24.6	29.4	24.6	29.4	24.6	29.4
pitch angle [^{o}]	16.8	18.6	16.3	18.1	17.3	19.1
yaw angle [^{o}]	11.7	16.7	11.7	16.7	11.7	16.7

Table 8.10: angular deflections for changes in the chord of the wings

Rotation	Initial performance		10% $x-$arm Increase		10% $x-$arm Decrease	
	stabilised	peak	stabilised	peak	stabilised	peak
roll angle [^{o}]	24.6	29.4	24.6	29.4	24.6	29.4
pitch angle [^{o}]	16.8	18.6	19.2	21.0	14.5	16.3
yaw angle [^{o}]	11.7	16.7	11.7	16.7	11.7	16.7

Table 8.11: angular deflections for changes in the tail surface of the horizontal tail

the vertical tail to hit the wind tunnel when the AEOLUSIM pitches down. Therefore it is important that the vertical tail is manufactured with precision, as a few centimetres extra span could cause damage to the wind tunnel.

Rotation	Initial performance		10% $x-$arm Increase		10% $x-$arm Decrease	
	stabilised	peak	stabilised	peak	stabilised	peak
roll angle [^{o}]	24.6	29.4	26.6	31.0	23.2	27.6
pitch angle [^{o}]	16.8	18.6	16.8	18.6	16.8	18.6
yaw angle [^{o}]	11.7	16.7	14.5	19.5	9.3	14.3

Table 8.12: angular deflections for changes in the surface of the vertical tail

Velocity
When the velocity increases, all control surfaces will generate a larger force and thus a larger moment. This impacts the maximum rotation angles as well as the stick forces. The results of both reducing and increasing the velocity with 10% is shown in Table 8.13.

Clearly a small increase in velocity induces a large increase in deflection angle. However, the likeliness that the velocity will increase by accident is close to zero. The fans will be designed for maximum efficiency, and any design or production error will probably cause a lower velocity and not a higher velocity. For that reason, the system can be considered sensitive to changes in velocity, but it is not a very high risk. Lower velocity results in lower deflection angles which may influence the experience but will not cause the system to break in any way.

First, an aerodynamic analysis is done in order to check the difference in flow velocity over the control surfaces. Both the increase and decrease in inlet velocity yield approximately the same percentage decrease of velocity over the tail surfaces with respect to the normal case. Therefore aerodynamically speaking the inlet velocity sensitivity is negligible.
Increasing or decreasing the airflow velocity with 10 % will result in a 20 % increase or decrease in control forces respectively. The AEOLUSIM is thus relatively sensitive to velocity decrease looking at the control forces. Since the control forces should be kept above 12.75 N as stated in 7.1.6, the velocity decrease may not decrease control forces beyond this amount. The upper limit for control forces is farther away than the lower limit, also stated in 7.1.6, making the AEOLUSIM not sensitive for velocity increases when considering control forces.

Hinge distance
The hinge distance is important to convert the forces generated by the control surfaces to the control forces in the flight stick and pedals as explained in Section 7.1.6. Because the forces acting on the control surfaces are relatively low due to the low airflow velocity, the control forces for the pilot are low as well. This implies that a decrease in hinge arm is unwanted and will result in a smaller control force. If a larger control force is required or the hinge arm is increased for manufacturing reasons will not result in control force problems. The changes in control forces due to changes in the hinge arm can be seen in Table 8.14.

Centre of Gravity Offset

Parameter	Initial performance		10% Velocity Increase		10% Velocity Decrease	
	stabilised	peak	stabilised	peak	stabilised	peak
roll angle $[^o]$	24.6	29.4	31.2	35.6	18.9	23.3
pitch angle $[^o]$	16.8	18.6	22.0	23.8	12.9	14.7
yaw angle $[^o]$	11.7	16.7	15.8	20.8	8.0	13.0
F_a $[N]$	10.1		12.4		8.5	
F_e $[N]$	19.9		24.1		16.5	
F_r $[N]$	12.3		14.9		10.2	

Table 8.13: angular deflections and stick forces for changes in the velocity

Parameter	Initial performance	10% Hinge arm Increase	10% Hinge arm Decrease
F_a $[N]$	10.1	11.3	9.2
F_e $[N]$	19.9	21.9	17.9
F_r $[N]$	12.3	13.5	11.1

Table 8.14: Stick forces for changes in hinge arms

If the rotation point is not located exactly below the centre of gravity, the neutral position of the simulator will have a pitch and roll angle. Table 8.15 shows what happens when the offset changes $10cm$ in all three directions. For the $x-$offset and $y-$offset only pitch and roll are listed, respectively. This is because there is no direct influence on the other neutral and maximum angles.

Offset	Rotation	Initial performance		10% arm Increase		10% arm Decrease	
		Neutral position	peak	Neutral position	peak	Neutral position	peak
x	pitch angle $[^o]$	0	18.6	16.3	31.0	-16.3	-1.6
y	roll angle $[^o]$	0	29.4	47.1	74.8	-47.1	-19.7
z	roll angle $[^o]$	0	29.4	unstable		0	12.5
	pitch angle $[^o]$	0	18.6	unstable		0	12.3
	yaw angle $[^o]$	0	16.7	unstable		0	16.9

Table 8.15: angular deflections for changes in the initial centre of gravity offset

As could be expected, a shift in centre of gravity can have disastrous results. When the centre of gravity lies $10cm$ before the rotation point, apparently the neutral position will be 16.3^o pitch-down and the range of pitch angles lies between -31^o and -1.6^o. Similar results are obtained when the centre of gravity has a y offset or different z offset. Since the likeliness of an offset in $x-$ or $y-$direction between the centre of gravity and the rotation point, there should be the option to add mass to the front or to the back. This will increase the mass moment of inertia of the Aeolusim, but as proven in the paragraph about the mass moment of inertia, this does not have to be a problem. However, this does not prevent the centre of gravity from shifting during flight. The main cause of a shifting centre of gravity would be the user leaning forward or sidewards for example. As this is not allowed to happen, the user movement should be restricted with a restraint, e.g. one of the type that can be found in roller coasters. Unfortunately, this behaviour cannot be prevented. The behaviour is caused by the moment caused by the mass offset. Generally, three cases can be considered. The first case is where the mass causes no moment. In the case of the Aeolusim, this is infeasible. For the mass to never have a moment contribution about an axis (not even when the simulator rotates), it should lie on that axis. A requirement of the Aeolusim is that all motion is generated aerodynamically. This means the supporting structure is passive, and thus that there are fixed rotation axes. With different users entering the simulator the centre of gravity location becomes variable, and for that reason the centre of gravity cannot be designed to always lie exactly on a rotation axis. The second case is a case where the mass has a stabilising moment. As shown in Section 7.2, the spring stiffnesses needed for aircraft-like behaviour are too high to generate significant deflections. If the mass of the Aeolusim were to generate a stabilising moment, the deflections would be much lower and close to non-existent. This could be solved by decreasing the spring stiffnesses, but that would result in very slow deflections and extremely unrealistic eigenmotions. The third case is the case where the mass has a destabilising moment. This is the case that is chosen to be used in the Aeolusim, and the result of this decision can be seen in Table 8.15. From the pitch performance in Section 7.2, it can be concluded that the horizontal tail will not be

able to stabilise the aircraft, and for that reason trim tabs will not be an option.

9 Logistics & Operations

After the Aeolusim's design is finalised, its lifetime can be categorised as follows,

1. Manufacturing
2. Assembly and Integration
3. Operational life
4. End-of-life and disposal

The four phases listed define the operational and logistics concept of the Aeolusim. The manufacturing phase is detailed in Section 9.1 and the assembly and integration phase in Section 9.2. Section 9.3 discusses the operational life of the Aeolusim. Finally, the end-of-life and disposal is elaborated on in Section 9.4.

9.1 Manufacturing

For manufacturing, a lean manufacturing approach will be taken. Because of this, the Aeolusim's components will be off the shelf products where they can be. Because the expected sale numbers are low, all parts will be ordered from an outside manufacturer. This is because creating a manufacturing facility at the factory to manufacture the needed parts would mean there would be no activity in this facility for large portions of time and cause a lot of unnecessary waste.

To define what parts need to be manufactured, the Aeolusim has been broken down into its general parts. The three basic structures of the Aeolusim are the airframe, the supporting structure and the wind tunnel. The airframe structure consists of the following parts:

- Fuselage, consisting of the frame and any covering panels.
- Cockpit, consisting of the control panel, the seat and the control stick.
- Main wings, consisting of the spars, ribs, ailerons and covering panels.
- Tail, consisting of the vertical and horizontal tail ribs, spars, covering panels, the elevators and rudder.
- Electrical system, consisting of the power cables needed in the fuselage, attitude determination system and any connection the VR system needs.
- Actuator connections, consisting of any rods and cables needed to connect the control stick to the actuators.

All parts of the airframe will be custom ordered, the joining of the parts will be done during the assembly.
The support structure consists of the frame and the springs and dampers. The joint is also part of the support structure.
The wind tunnel consists of the fans and the wind tunnel structure. The fan blades are custom designed and can not be off the shelf. Thy will be ordered from an outside manufacturer. The other fan parts will be off the shelf products. The wind tunnel will only need on-site assembly.
The computer is made from off the shelf products and will only need to be assembled and integrated on site.

9.2 Assembly & Integration

The assembly process of the Aeolusim is very important to plan. Production costs can run very high and these are one of the most important factors when pricing the product. If the production process is planned properly and is accounted for in the design choices, it can be made more efficient reducing expenses and allowing a lower selling price. The assembly process has been charted in a flow diagram in chronological order as seen in Figure 9.1.

To determine the most efficient order of assembly, the broken down system, as defined in Section 9.1, is analysed. This is done in order to learn which parts can be created in parallel and to estimate the complexity of the larger parts that make up the system. Then, the diagram can be made which shows the most efficient method of assembly.

Figure 9.1 shows the flow diagram of the assembly process. The process is planned in such a manner, that work can be done efficiently by no more than three teams of workers with low needed storage capacity. The large

arrow shaped blocks indicate that the parts for that component are delivered at that time. Work will mostly revolve around the fuselage as all the parts excluding the fan will have to be attached to the fuselage at some point. Therefore, many tasks cannot be done in parallel. An optimal plan was created to work around this issue and only in the installation phase will there be only one task to do, which can obviously be only the installation. The ordered products should arrive in time to be assembled so no delays are caused. However, they should not arrive too soon and fill up storage space. This could cause storage costs to be unnecessarily high. To assure the needed storage capacity stays as low as possible without causing delays due to missing components, the components are planned to arrive one assembly phase before they are needed.
Because the expected sales are low, the assembly time can be reasonably long. Since the daily wage of a worker is higher than the daily cost of production space, it is cheaper to increase the production time than to increase the workforce to decrease the production time. Therefore, the choice has been made that there will be one team of two workers who will work on all tasks on the fuselage and two separate workers who will do the tasks that can be run in parallel. When only two tasks are available the two separate workers will work as a team. This means the phases as shown in the assembly flow diagram will be around four days and the entire assembly and integration process excluding phase zero will be around 36 days.

9.3 Operational life

The AEOLUSIM operational life can be catagorised by its respective operation and maintenance.

Operation
The operational life of the AEOLUSIM consists of its daily use and maintenance. Even though the simulator will be designed such that it is safe enough to operate without operator, safety regulations require an operator nonetheless.
Operation of the AEOLUSIM will not require extensive technical expertise. Neither will the simulator require an operator's full attention, as is has been designed to operate safely on its own. The operator's main task will be to perform daily checks, activate the AEOLUSIM and initiate the emergency procedure should any endangering event occur.

As briefly mentioned, daily use should commence with an equivalent to a 'pre-flight checklist', i.e.:

1. Ensure that control stick and pedals are not limited in their motion.
2. Ensure that control surfaces deflect accordingly.
3. Globally check the structural integrity: both visually and by applying forces on selected locations (i.e. points located on the wing, the fuselage).
4. Ensure software integrity with test simulation

This pre-flight checklist is to be performed once per day to ensure that failure of critical components is noticed in an early stage.
A positive result will be followed by normal system functioning, as shown in Figure 3.1. Intermediate checks between users are not necessary since the system would have proven to be operational beforehand.

Maintanance
Logistics become an important factor when concerning maintenance. Three key components have been analysed to predict whether a solid line of supply can be established,

- Availability
- Accessibility
- Alternatives

Availability, the issue whether parts exist, can become an an issue for the custom made parts. Since these are usually made by one specific company, deals will have to be made to anticipate maintenance needs. These specific parts may therefore experience a limited *availability* and longer lead times (*Accessibility*). However production methods described in Chapter 6 are widely used within the industry, and are not expected to cause critical delays. Production costs will benefit from off-the shelf products, and as a result so will the expected maintenance costs and maintenance period.
Alternatives may include setting up an own production facility, although this might prove overly costly for the low volume of products expected. Another alternative may be to include an optional stockpile of frequently needed spare parts with each purchase of the AEOLUSIM.

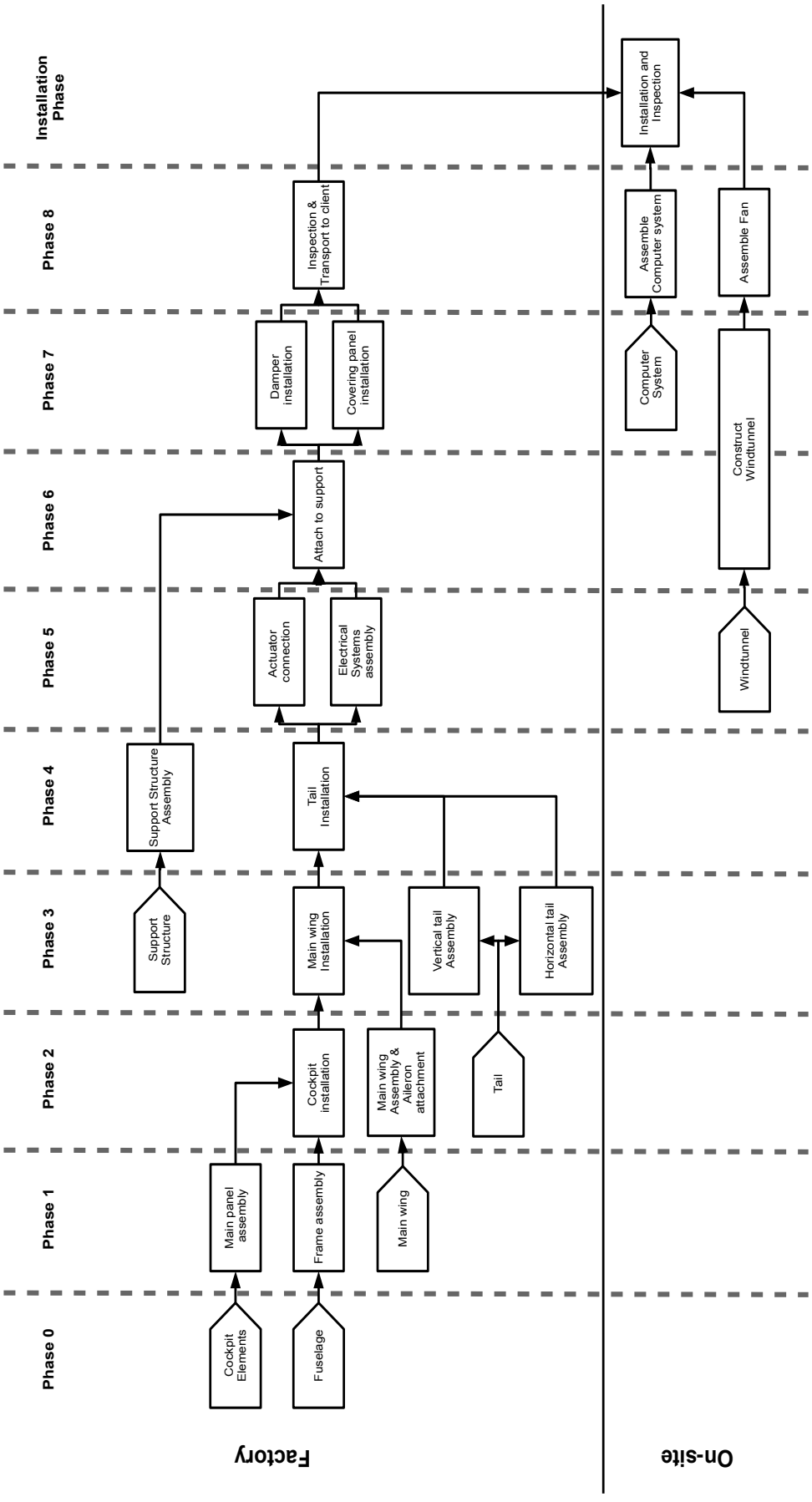

Figure 9.1: Assembly & Integration Diagram

Inspection is categorised in two levels. As previously stated, daily inspections are to be performed by the operator. Periodic in-depth inspections are to be performed by an Aeolusim maintenance engineer. The periodicity of these inspections is to be assessed using the reliability of each respective part (Section 11.1). The spring damper support structure currently shows the lowest reliability: its respective reliability drops to 70% after a six month period. Since the spring-damper support structure is one of, if not, the most critical component, in-depth inspection intervals are based in this reliability.

9.4 End-of-Life

The simulator is to be designed for a lifetime of five years. After this period it is expected that maintenance costs will exceed the operational benefit. An end-of-life disposal strategy has been defined in compliance with the sustainability philosophy of Chapter 15. This is to be done by separating parts that may be recycled or degraded to waste. Raw materials such as steel (fuselage) and aluminum (wings) are to be recycled. The wood used in the vertical- and horizontal tail, ailerons, the fuselage and wind tunnel may be recycled, if a possible coating will allow this. If this is not the case, it must be reviewed if it is possible to remove the coating and recycle the products individually. Sub-parts such as the chair and head mounted display are to be decomposed to reusable parts as much as possible. Remaining parts are to be disposed correctly.

10 Electrical Systems

In this chapter the totality of electrical systems is summarized. This is done in the following structure: In Section 10.1 an overview of the electrical systems and the total power consumption will be given. A summary of the computer hardware required for the simulation and control is given in Section 10.2. Section 10.3 gives the accompanying software diagram. The internal and external communication of the computer system is provided in Section 10.4 and 10.5 respectively.

10.1 Electrical Systems Overview

In this section the relations between the different constituent electrical components of the Aeolusim are listed and shown in a diagram, Figure 10.1. Note that this is a very high level look at the electrical systems, more detail on the individual components can be found in the other sections in this chapter.

Electrically speaking the system is not very complex. As it is wind driven and spring damped, electrical systems are not required to govern the movement. The Power source consists of a grid power connection (230V/50Hz NL) [23]. Conversion to a lower voltage is necessary to operate the computer system. This computer system regulates and distributes power to the simulation equipment. Namely the visual systems, the attitude determination systems, the cockpit systems and the fan. The fan is only regulated, as it requires more power than can safely pass through the computer system, and is therefore also directly connected to the grid. As stated in Subsection 4.2.2 a 6 pole motor is used, these require a simple grid connection at the relatively low power output of 2 kW. The total energy consumption per component and the grand total have been listed in table 10.1

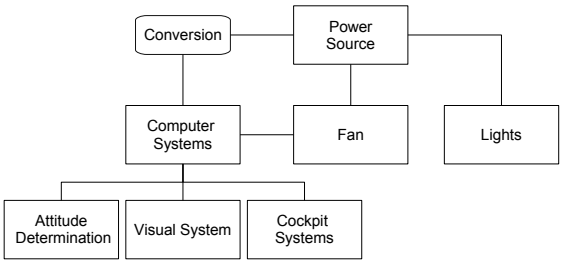

Figure 10.1: Electrical Block Diagram

Table 10.1: Total Power Distribution

Component	**Power Consumption in Watts**
Computer System	314.1
Attitude Determination System	5
Visual System	11
Cockpit Systems	10
Fan	29483
Lights	30
Total	29853.1

10.2 Hardware Block Diagram

In order to obtain a clear overview and improve the understanding of the hardware interactions of the system, a Hardware Block Diagram (HWBD) can be outlined. This schematic can effectively communicate the functions and relations of hardware elements or components, the logical progression of signals, the input and output channels and actions of the simulator. The components are all subdivided into blocks that are specific to a certain function or operational parameters and are listed below for the Aeolusim:

- Electronic hardware
- User interface
- Power management
- Moving parts

The elements and functions of the electronic hardware will be portrayed in Subsection 10.2.1, followed by the user interface in Subsection 10.2.2. Afterwards, the power management components will be listed in Subsection 10.2.3, while the moving parts will be discussed lastly in Subsection 10.2.4.

10.2.1 Computer Hardware

The electronic hardware consists of the elements that allow for the processing of signals and the computation of appropriate responses. In the case of the Aeolusim, these components are the Central Processing Unit (CPU), the Random Access Memory (RAM), the Solid State Drive (SSD), the Graphics Processing Unit (GPU), the audio card and the rotary motion sensors that are placed on the control stick and pedals.

The CPU is the centre of all logical processes, receiving and transmitting digital information to and from several other components. The RAM temporarily stores digital information that is required in active processes. The SSD serves as a long term storage of information (such as log files), but also contains the operating system and software for the electrical hardware and the simulation. The GPU performs processes that allow visual media devices to display information, while the audio card does the exact same for audio devices. The rotary motion sensors detect physical angular deflections and transmit them to the CPU in digital format.

10.2.2 User Interface

The user interface consists of components that relay information to and from the user, usually as the result of logical processes or user interaction. Additionally, this is where the user controls the mechanical motions of the Aeolusim. These components are the Head Mounted Display (HMD), the headset, the emergency switch and the flight controls.

The HMD and headset serve as the primary devices to relay information to the user. The flight controls are the physical elements that the user can interact with to pilot the Aeolusim. The emergency switch allows the user to quickly end the operation in case of an emergency.

10.2.3 Power Management

The power management consists of elements that generate and relay power to the appropriate subsystems and their respective components. For the Aeolusim, these elements are the electrical grid and the AC/DC (alternating current, direct current) converter.

The electrical grid is the simulator's source of power, which is provided as an alternating current. The AC/DC converter serves as a device that transforms the alternating current into a direct current for hardware elements that can only operate on a direct current.

The headset and HMD are USB-powered or battery powered and therefore do not need a constant connection to the power grid.

10.2.4 Micro Controllers

Micro controllers are programmable to output specific voltages at certain pins, which is needed to be able to send signals to the fan and the locking mechanisms. The CPU communicates with both micro controllers, to be able

to shut down the fans and activate the locking mechanism and receive a confirmation signal that the operation has succeeded.

The power consumption of all relevant members are displayed in Table 10.2:

Table 10.2: Maximum power consumption of hardware elements

Part	Value [W]	Reference Model
CPU	140	Intel i7 5820-K [1]
SSD	0.1	Samsung 850 EVO 250GB [2]
GPU	170	MSI GeForce GTX 760 [3]
HMD	11	Sony Wearable HDTV [4]
Microcontrollers	4 (total)	TI Tiva TM4C123gXL

The resulting diagram can be seen in Figure 10.2:

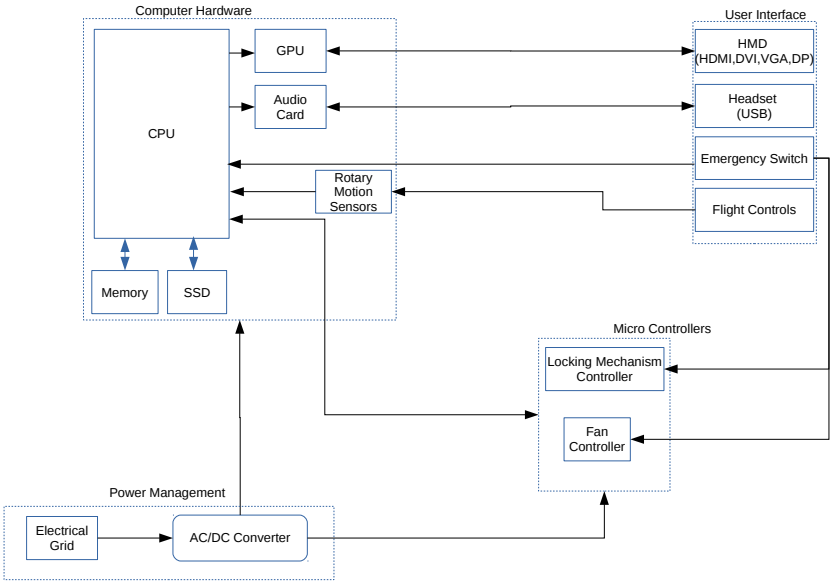

Figure 10.2: Hardware Block Diagram

10.3 Software Block Diagram

The software block diagram (Figure 10.3) shows the software components of the system, and the interaction between these components. Inputs and outputs of the system are indicated with a fat outline. The diagram focusses on the software parts that are specific for the Aeolusim. Since a third party program such as FSX or X-Plane can be used to provide visual and audio simulations, the software block diagram will not go into detail on those aspects of the software.

Three divisions have been identified: at the lowest level there is the kernel and the operating system (OS), which have been taken together for conciseness. Sensor input is handled by the kernel and OS and sent to the Application, the second division. Both the OS and the Application send data to the third division, which has the label 'Presentation'. This includes the screen on which the simulation and errors are displayed as well as the sound system. The division 'Kernel/OS' is placed at the bottom of the diagram as it acts on a lower level than the Application and the Presentation.

The 'Kernel/OS' division handles the sensor input and booting and shut down signals. After boot, the operating system will have to automatically start the Application, and in the same way shut down the application on a shut down signal. Not included in the diagram are options for example for updating the software and providing

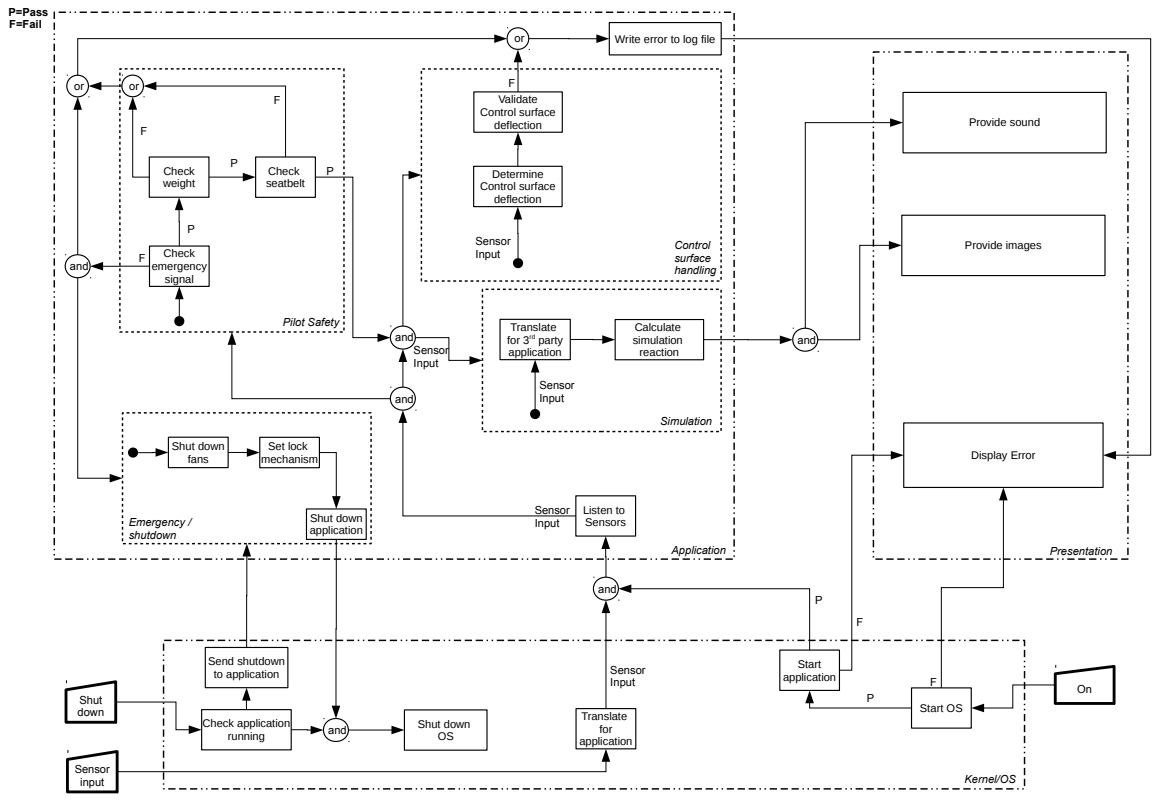

Figure 10.3: Software Block Diagram

remote access. Updates can be handled by the operating system and the update package, as the update package can be an executable that updates specific files of the program and may perform compilations. Remote access can be provided by third party programs if deemed necessary.

The Application is the part where all calculations regarding the AEOLUSIM take place. The software diagram acts as a flow chart, where the data flow between the software components is shown. Data flow is modelled by an arrow, the data itself is provided next to the arrow. When there is no data provided, it indicates that previous data has been passed on. The Application has been divided in four modules. The first module is by default the module that checks the safety of the user in the simulator. This is done by checking if the weight of the user does not exceed the maximum weight that is set in the requirements of the AEOLUSIM, checking if the seatbelt is fastened and making sure no emergency signal is input. When either of these checks fails, the fans will be shut down, the simulator locked and the application shut down by the 'Emergency / Shutdown' module. Also, a log will be provided describing what went wrong and the user will see an error on the screen. If all checks pass, the sensor information will be forwarded to a module that provides the visual simulation. This module will translate the sensor output to input that can be handled by a third party program. Translation may include multiplying the deflection angles by a certain factor if that contributes to a better user experience. The third party program will provide the visual and audio simulations. The diagram also provides a module that determines and validates the control surface deflections. When these would become too high, an error will be shown on the user screen.

The third division, 'Presentation', is the software that translates the output of the third party simulation program to be viewed on the screen and heard through the sound system. As the 'Presentation' is in charge of the visuals, this is the part where errors will be displayed.

10.4 Data Handling Diagram

The data handling diagram (Figure 10.4) shows a high-level illustration of the data flow through the system. Shown is how all input signals are converted such that they can be processed by the CPU. This can be done for

example by an additional micro controller, or by stock sensors that output to USB. This signal is sent from the USB port to the CPU, which processes the data. The output of the CPU is sent to hardware components to further process the data. The calculations regarding visuals will mainly be done by the GPU, and is output via HDMI to the head mounted display.

Fans can be shut down by a micro controller that receives a signal from the computer and converts it to an analogue signal. The locking mechanism is activated similarly; a micro controller handles the locking signal from the computer system.

The SSD is provided for the operating system, applications and log files to be stored on.

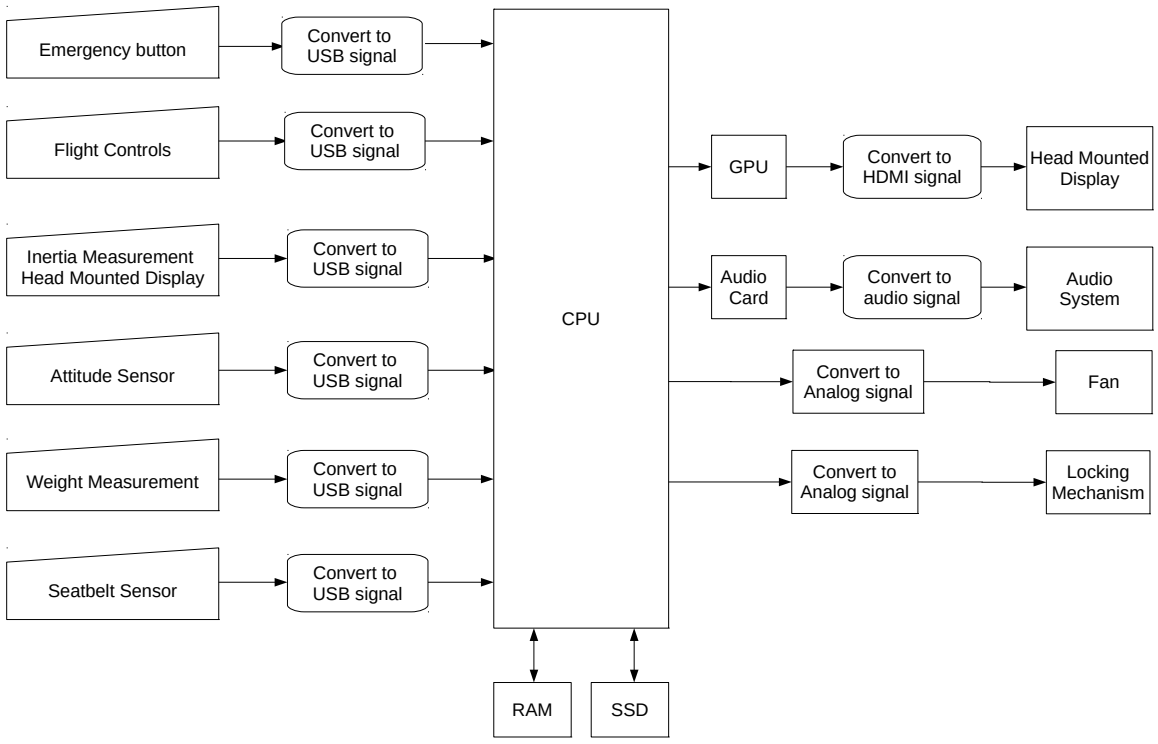

Figure 10.4: Data Handling Diagram

10.5 Communication Flow Diagram

The intention of this section is twofold: firstly, it copes with the safety communication from and to the user, and secondly, it gives an impression of what the user should do before 'take-off'. In Figure 10.5 an overview is presented of the procedures that are described in this section. This figure can be used for the construction and design of the safety system controller.
In order to facilitate the elaboration of the operation procedures, a distinction is made between two states:

- **SAFE** - The fan engine is off; the motion system is in its neutral position and locked. The head-mounted display is off. The wind tunnel gate is unlocked.
- **START** - The fan system is set idle. The user is seated and the seat belt is fastened. The head-mounted display and audio headset are active. The motion system is unlocked; the spring-dampers are loaded. The tunnel gate is locked. The simulation is ready to start.

10.5.1 General Procedure

The procedure starts from the SAFE state, reached after starting up the simulator.

SESSION START PROCEDURES

1. User enters through gate wind tunnel.
2. User enters cabin via door and sits down.
3. User puts on audio headset
4. Audio message of closing the gate when gate sensor gives signal.
5. Operator closes gate
6. Audio message of fastening seat belt when seat belt sensor gives signal.
7. User fastens seat belt.
   - From now on, the seat belt must remain fastened until the end of the session. If the seat belt is unlocked, then go to SESSION STOP EMERGENCY.
8. Audio message of putting on head-mounted display
9. User puts on head-mounted display.
10. Visual message of pressing the start button.
11. User presses Start on the stick.
12. START state is active
    - From now on, the cabin door must remain locked until the end of the session. If the cabin door is unlocked, then go to SESSION STOP EMERGENCY.
    - From now on, when the infrared sensors at the wind tunnel entrance notice something crossing its path, then go to SESSION STOP EMERGENCY.
13. Countdown from 3 to 0, game starts.

The simulation stops when one of these four things occur:

- End of game ⟶ Go to SESSION STOP
- Stop button on stick pressed ⟶ Go to SESSION STOP
- Violation of safety measures ⟶ Go to SESSION STOP EMERGENCY
- Emergency button pressed (inside or outside) ⟶ Go to SESSION STOP EMERGENCY

SESSION STOP

1. Audio message that stick should be released.
2. Motion base returns to settled position, lock mechanism activated.
3. Shut down fans.
4. Door unlocks.
5. Tell user they can unfasten their seat belt.
6. Return to SAFE state.

SESSION STOP EMERGENCY

1. Audio message that stick should be released.
2. Motion base returns to settled position, lock mechanism activated.
3. Shut down fans.
4. Door unlocks, and seat belt unfastens automatically
5. Audio notification of what went wrong.

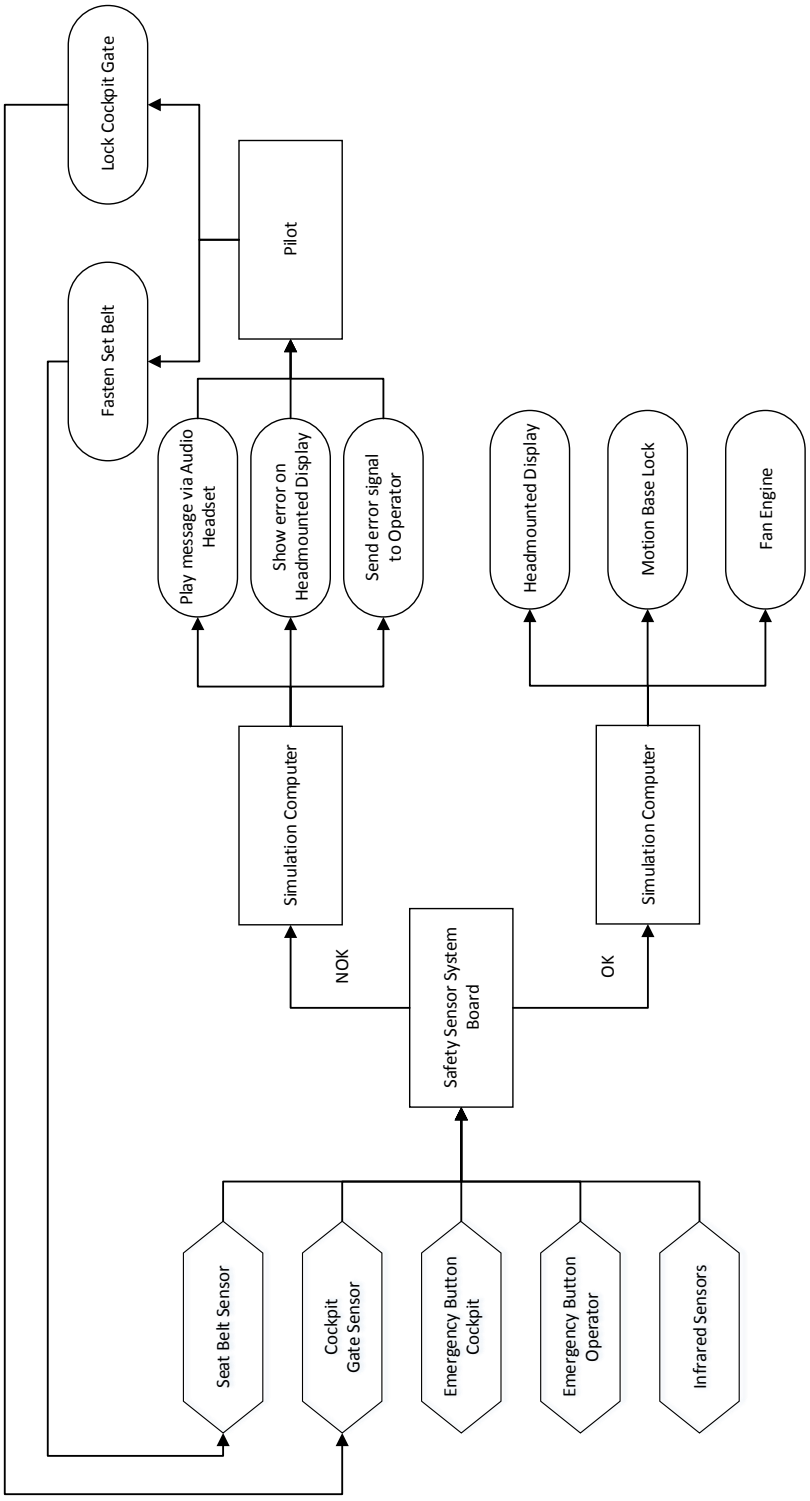

Figure 10.5: Communication flow diagram

11 RAMS Analysis

The RAMS analysis provides a way to determine the quality of the product. Section 11.1 estimates the reliability of the Aeolusim, and the availability is discussed in Section 11.2. Closely related to the availability is the maintainability, which is covered in Section 11.3. The safety aspects of the Aeolusim are presented in Section 11.4.

11.1 Reliability

The reliability of the total system is dependent on its constituent parts. The reliability of the Aeolusim has been determined by examining the reliability of the following parts: The fans, the spring support system, the computer system, the fuselage structure, the wing structure and the mechanical control system. The reliability estimates of these parts can be found in Subsection 11.1.2 through 11.1.7, and are preceded by a presentation of the method used in Subsection 11.1.1.

11.1.1 Reliability Determination Method

This analysis has been done by constructing reliability curves. This method provides an analytical estimate of failure probability and time [24]. It defines reliability as the probability that the part will not fail after a certain time. As shown in Equation 11.1,

$$R(t) = 1 - F(t) \tag{11.1}$$

where $F(t)$ is defined by Equation 11.2.

$$F(t) = \int_t^\infty f(t)dt \tag{11.2}$$

The failure probability density function $f(t)$ is an approximation of the failure behaviour of a component. There are many different functions that may be used, but for the purposes of this analysis a negative exponential has been chosen as shown in Equation 11.3. This function is the most suitable for the current general analysis. True reliability tests should be performed; the true reliability functions will follow from this.

$$f(t) = \lambda e^{-\lambda t} \tag{11.3}$$

Where λ is given by;

$$\lambda = \frac{1}{MTBF} \tag{11.4}$$

and $MTBF$ equal the mean time between failure. The values of this constant is based on the required reliability as prescribed by their respective design philosophies. Aides used in this process include the technical risk map and the production plan. Relating Equation 11.1, 11.2 and 11.3 leads to a simple equation relating reliability and time, as shown in Equation 11.5

$$R(t) = e^{-\lambda t} \tag{11.5}$$

The reliability of the components will be plotted over the entire design lifetime of 5000 hours. Finally, it must be remarked that in the assessment of the mean time between failure it was assumed that the proper procedures of use are followed during operational life. This means that errant behaviour is not accounted for as it cannot be measured or compensated for. With errant behaviour actions such as actively trying to break the control stick or throw objects in the fan are meant. Following proper procedures means that such things, accidental or intended, will not happen. Furthermore, it is important to re-emphasize that the reliability curves shown in the following subsections are design goals not established data.

11.1.2 Fan

The fan reliability relies on the quality of the driving electric motor and the immovability in any but the radial direction of the blades and hub. The main reason of external wear in these components is usually foreign particles in the flow. As the fan system has been designed to only move pure air the impact of this factor is almost negligible. Motor failure is also not a true concern as electric motors usually are quite robust due to minimal heat production and lubrication requirements. The part first expected to fail are the bearings, but as the airflow is assumed to be clean the mean time between failure is still expected to be high. The hub is direct driven by the motor thus eliminating any wear vulnerable belt drives. This all leads to a expected mean time between failures of 2500 hours. The reliability curve is shown in Figure 11.1

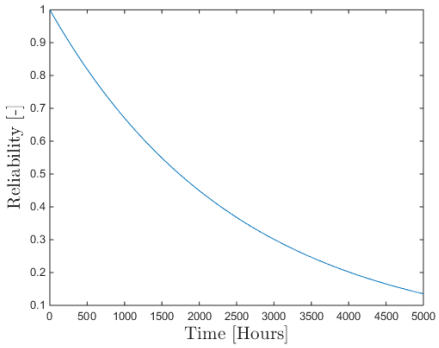

Figure 11.1: Fan System Reliability

11.1.3 Spring Damper Support Structure

The reliability of the support structure is mainly dictated by the fatigue of the springs and dampers. After a number of cycles the springs will start to lose their stiffness, ultimately leading to failure. Fatigue of the load bearing structure is of less concern as it designed in the same manner as the fuselage structure. The relative fragility of the system yields an expected mean time between failures of 1000 hours. In Figure 11.2 the corresponding reliability curve can be found.

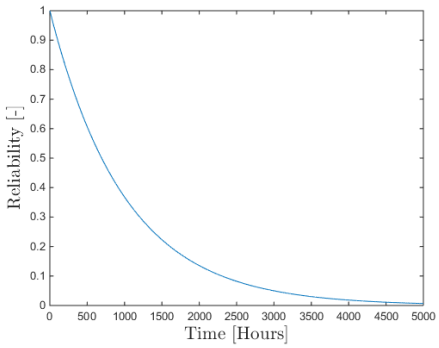

Figure 11.2: Spring Damper System Reliability

11.1.4 Computer System

Computer systems are known for their high reliability, often clocking in more than 8000 hours before the first hardware failure. Software failures are slightly more common, but are usually associated with changes in said software. As there is no expected need to change any software during the design operational life the mean time between failures will still be very high. That being said it is still expected that a software crash might occur due to the fact that almost no software is fully bug-free. The expected mean time between failure of the computer systems is therefore 4000 hours. The accompanying curve is illustrated in Figure 11.3.

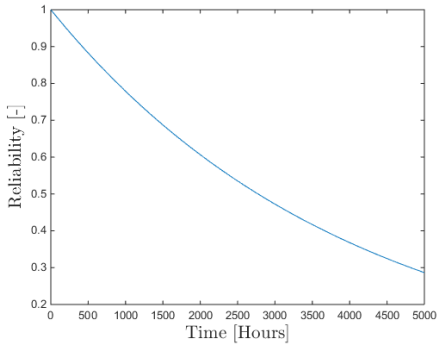

Figure 11.3: Computer System Reliability

11.1.5 Fuselage Structure

Since the fuselage structure has been designed according to the safe-life philosophy, meaning that with proper use no maintenance is needed during its design lifetime of 5000 hours. The design even has some considerations built in regarding accidental improper use, further reinforcing its already reliable status. Giving a mean time between failure of 8000 hours. As illustrated in Figure 11.4.

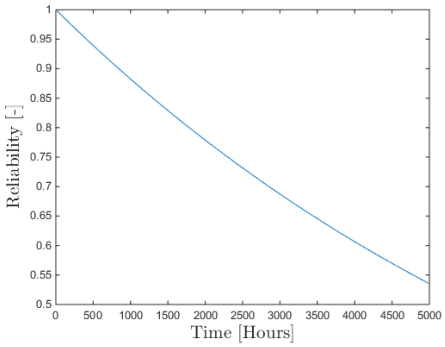

Figure 11.4: Fuselage Structure Reliability

11.1.6 Wing Structure

The wing design follows the same philosophy as the fuselage and has therefore the exact same reliability, a mean time between failures of 8000 hours.

11.1.7 Mechanical Control System

The mechanical control system is a relatively simple system for operating the control surfaces. Less complexity usually means more reliability, and that is definitely true in this case. Fatigue may be an issue since this is arguably the most intensely used part of the total system, as it is the direct link with the pilot. Failure is expected after a modest 3000 hours. Which leads to the reliability curve as plotted in Figure 11.5.

11.2 Availability

The availability of the Aeolusim is dictated by the measure by which it can be kept in operating condition, and is thus heavily dependant on the robustness of the design and the speed of maintenance. There are few factors or conditions that might interfere with the availability. If the open return wind tunnel is connect to the outside environment severe weather conditions may interfere with availability as it is not designed for outside use, and the open return wind tunnel will function better when placed in a closed room. Availability is improved due to the presence of an operator. This operator can fix small issues which will arise in a very timely manner, eliminating the need for a full maintenance process every time something small fails. Mind these small failures

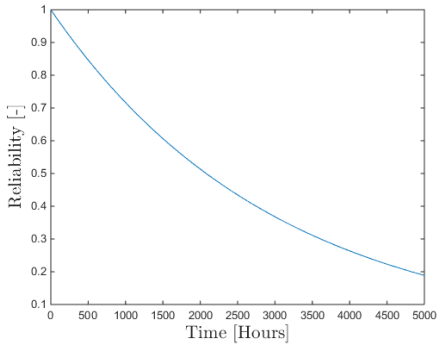

Figure 11.5: Control System Reliability

are not structural in nature, but more along the line of loose cables and minor software errors. Although the set requirement of a 1000 hours of operation time per year is a steep one, confidence in the fact that this is achievable is possible.

11.3 Maintainability

The maintainability of the product is determined by how easily parts of the system can be repaired or replaced. Two aspects of maintenance are considered important. The first is preventive maintenance, which focusses on preventing failure. The second aspect is corrective maintenance, where the system has failed and parts have to be fixed.

Fan
As stated in Subsection 11.1.2, the part of the fan that is expected to fail first are the bearings. The fan blades are not expected to fail due to the clean airflow. However, maintenance will be expensive when they do fail, as the fan blades are custom made. When a blade breaks or fails in an other way, the complete fan will have to be replaced. This has a large impact on the time between diagnosis and start of maintenance.

Spring Damper Support Structure
The spring damper systems in the support structure will be encapsulated by the structure for user safety. This encapsulation will be removable to allow easy access to the systems. The systems may not be off the shelve products, so in case of failure the replacement time can be long due to the time delivery can take. At the half-yearly inspections the state of the spring damper systems should be determined in order to prevent failure and allow ordering of replacement systems to anticipate to possible failure or replace the system before failure occurs.

Computer System
Due to the high reliability of computer systems (see section 11.1.4), the maintenance will mainly consist of updates to and upgrades of the operating system or application software. These updates can be handled mostly by the software and can therefore take place overnight, limiting the downtime to the times the system would not be used anyway. In order to reduce the maintenance time after a total crash, a system image should be made after setting up the system. This way, restoring the computer to a functioning state can be done without having to reconfigure the complete system again.

Fuselage and Wing Structure
It is expected that the fuselage and wings will not need maintenance in the first 5000 hours (Section 11.1.5). However, since serious fuselage or wing failure may require correctional maintenance taking several days, regular inspections are needed to prevent this situation. Small cracks in the structure can be fixed by for example applying patches, which can be done outside the peak hours. Corrective maintenance however may cause the Aeolusim to be unusable for more than a day.

Mechanical Control System
Since the mechanical control system only consists of a few cables and cable guides, maintenance will not be time consuming. Frequent inspection should prevent the cables from snapping and thus having to perform reparations during peak hours. Replacing the cables in time is considered to be a small task that can be done at the end of a regular day.

11.4 Safety

In order to ensure the safety of both the operator and the user of the Aeolusim, several safety measures have been taken which will be summarized in this section. These measures are divided into four elements. The first element is general safety, the second paragraph covers user safety and the third paragraph discusses the safety of the operator.

General Safety
General safety covers the safety of the developers, the user, the operator and any third party that may be involved, such as spectators or other people in the building. To guarantee the safety of these people, only non-toxic materials have been used and highly flammable or radioactive materials have been avoided. The buildings where the Aeolusim will be developed, manufactured and operated should be ventilated and well lit for the sake of the developers, manufacturers and any person using the simulator. In order to prevent any fire, the building in which the simulator will be placed should comply to the local emergency safety regulations. As the Aeolusim company does not supply these buildings, the company will not bear responsibility for the state of these buildings.

Between the fans and the simulator will be a netting to make sure users or operators will not be harmed by a fan.

All safety critical components will be checked regularly, as stated in subsection 11.3. This prevents the user, operator or any third party from getting harmed by broken or (due to failure) unshielded parts.

User Safety
Most safety measures have been targeted specifically at the user of the system, as the user will be the one exposed to the simulator. To prevent the user from falling out the simulator during operation, the user will be strapped using a five point seat belt. This seat belt should be removable by the user without help from an operator, in case of an emergency. However, it should not be allowed to take off the harness during operation in any other case. For that reason there will always be an operator in a separate cabin that is directly connected to the wind tunnel, supervising the simulator.

A user should be able to safely enter and exit the Aeolusim, and the simulator should be able to stop at any time when the user becomes unwell or in case of an emergency. Therefore a locking mechanism is provided (Chapter 2) that can be locked by the user from inside the Aeolusim. The operator is able to lock and unlock the mechanism from inside the operator cabin.

Operator Safety
The operator should supervise the simulator during operations to make sure users will not misuse the Aeolusim and to ensure the safety of the user. For the operator to be safe, there will be a cabin next to the wind tunnel with a view to the simulator. From this cabin, the Aeolusim can be operated. There should be a button in the cabin to operate the locking mechanism.

12 Risk Assessment

The Aeolusim is to be designed such that it meets its intended purpose: *"Providing a realistic in flight experience"*. However, with the design and its operation, uncertainties arise. These uncertainties are coupled to specific risks, affecting either the economics, design, use or the lifetime of the product. This chapter shall discuss the optimisation of the Aeolusim by accounting for risks and providing risk mitigation strategies. The assessment is performed in compliance with the ISO 31000:2009 standard (Reference [25]).

All identified risks are listed in Appendix C. Each listed risk event is described by a risk statement identifying the risk source and the event that could impact on the project's objective. Examples, including mitigation strategies, are treated later in this chapter.
The impact of each risk event was in turn assessed using a likelihood and consequence framework, consistent with the ISO 31000:2009 standard. Any risk event having a likelihood of occurrence greater than 80% is rated as *Extremely Likely*, between 50-70% as *Likely* between 30-50% as *Probable*, between 10-30% as *Improbable*, and below 10% as *Extremely Unlikely*.

The impact of the event, if it were to occur, is expressed in terms of *Catastrophic*, *Critical*, *Severe*, *Marginal*, or *Negligible* as follows:

Catastrophic	Event has a maximum impact on system; system can no longer function.
Critical	Event affects technical performance greatly.
Severe	Event affects technical performance considerably.
Marginal	Event affects technical performance marginally.
Negligible	Event has a very small or no impact on the system; technical performance remains (largely) unaffected.

The product of both the impact and the likelihood of the risk event can be visualised by a risk matrix. Table 12.1 shows the risk matrix of the risks listed in Appendix C. This matrix expresses the technical risk profile of each risk event as,

High risk (red)	Event poses a significant threat to the system. Risk mitigation is necessary.
Medium risk (yellow)	Event poses a significant threat to the system. Risk mitigation is optional, but preferred.
Low risk (green)	Event poses a little to no threat to the system. Risk mitigation is not necessary.

Table 12.1: Technical risk map for all risks listed in Appendix C

Extremely Likely			8		
Likely		20 b		16	13
Probable			4,6, 19e	1,7	12, 19a, 19b
Improbable		20c	15	2,5, 14	9, 10,17c, 17e, 19c
Extremely unlikely			3,11	18b, 18c, 20	17a, 17b, 17d , 18a, 19d
	Negligible	Marginal	Severe	Critical	Catastrophic

Risk events that are within the red region of Table 12.1 require mitigation. Two high risk events are highlighted as an example: Risk event 13 states that "the market might be too small to make a profit". The Aeolusim is a relatively expensive and specialised attraction, and alternatives have already found their niche in the market. The likelihood of this event is therefore rated as likely, and its impact catastrophic. This event can be mitigated by hiring a market firm as 'man in the middle'/market agent. This approach might result in a better market overview, thus attract new potential buyers.
Risk event 19a expresses that the spring-damper might fail. The spring-damper mechanisms are critical components, affecting the response of the simulator. As they are moving parts, it is expected that they will show signs of failure during the Aeolusim's lifetime. Its impact would also be catastrophic, since a simulator without this subsystem would stop functioning. This risk event can in turn be mitigated by regular inspection intervals, clearly defined by laboratory tests based on part degradation.
Risk mitigation strategies for all remaining risk events are shown in Appendix C.

13 Market Analysis

The entertainment market was considered the most favorable market for the Aeolusim to enter. Alternative markets have been considered in Reference [2], but where disregarded due to a small predicted market share. The market analysis presented in this chapter consists of three main parts: The current entertainment market is analysed in Section 13.1, the competition for musea and theme parks is defined in Section 13.2 and finally a strategy to find a launching customer is determined in Section 13.3.

13.1 Entertainment Market

The entertainment market has three main buyers for the Aeolusim: musea, theme- and amusement parks and specialized flight simulator entertainment firms. Private consumers are defined as secondary buyers. They do present themselves in the market, however, they are assumed to be scarce. The latter is expected because of the relatively high purchase cost of the product.

In-depth market analyses and forecasts with respect to the entertainment market can be purchased[1]. This was however deemed beyond the scope of the project at hand. The entertainment market has therefore been analysed using free and openly available annual reports of associations within the specific industry.

Recent growth
The year 2013 was the fourth consecutive year showing a gross growth in the number of visitors after the financial depression of 2008 [26]. Figure 13.1 shows the amount of visitors in the top 20 (defined by attendance) theme parks and musea in 2013, excluding waterparks. The average annual growth of the top 20 theme- and amusement parks is shown per region in Table 13.1. The North-American market showed a steady growth rate over the last 3 years, where the South-American market appeared to be increasing its growth rate annually. The Asia-Pacific and European regions are outliers. The latter region still suffers from the effects of the financial depression, whilst the Asia-Pacific growth rate is approximately twice the global growth rate [26]. A possible explanation could be the rapidly growing economies in the respective region with more people reaching middle class status [26] [27]. Table 13.2 shows the gross growth in museum visitors during 2013 (top 20 listed musea). This market has been growing as well with the Asia-Pacific region as an extreme outlier, again assumed to be due to the growing economies.

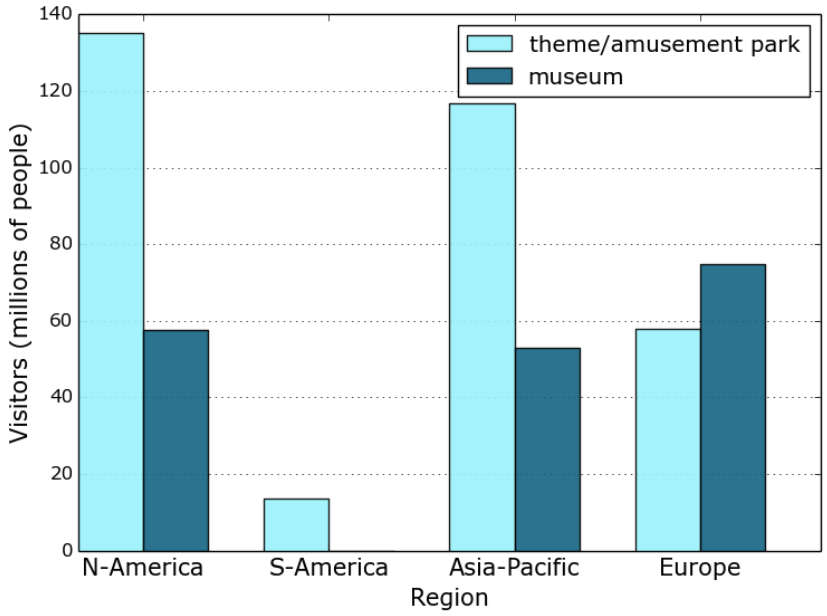

Figure 13.1: Number of visitor to theme and amusement parks and museums in 2013 based on Reference [26]

[1] The interested reader is suggested to visit *www.ibisworld.com* or *www.marketresearch.com*

Table 13.1: Top 20 theme and amusement park visitor growth rate per region [26] [28] [29]

	N-America	S-America	Asia-Pacific	Europe
2011	2.9 %	0.7 %	7.5 %	2.8 %
2012	3.6 %	2.6 %	5.8 %	-0.3 %
2013	2.7 %	3.8 %	7.5 %	-0.1 %

Table 13.2: Top 20 museum visitor growth rate per region [26]

	N-America	Asia-pacific	Europe
2013	1.6 %	27.6 %	4.6 %

Entertainment Market Forecast
The economies within the Asia-Pacific region are expected to continue to their growth [27], thereby boosting their local entertainment industry. China, for example, aims to establish 1000 new musea in the next 10 years [28].
The European theme parks are expected to stabilize over the coming years. The Theme Entertainment Associations Report of 2013 [26] states: "While awaiting increases in leisure spending that are forecast in Europe in the medium term, many are adopting a prudent approach to business activity, (..) limited capital expenditures and ways to boost visitors' per capita spending." This may in turn lead to difficulties for the Aeolusim in European theme parks.
The European musea, however, show steady growth. The Dutch Museum Association, for example, predict a growing market by 2026 (Reference [30]). This market will show a decline in the number of musea, but an increase in the amount of visitors and the budget of (Dutch) musea.

Clear estimates for market forecast of the Americas could not be obtained by the annual reports of the selected associations. It is however expected that these markets will continue to show signs of growth, based on a extrapolation of the gross growth between 2010-2013 and the forecast for other regions. The North-American growth will be accompanied by a demand for more technology in Musea, since the "(US) Government is shifting its attention to increasing the involvement of children and young people in museums' education work" (Museums Association, Reference [31]). This may be, in turn, a possible positive outlook for the Aeolusim.

Market for the Aeolusim
Even though the entertainment industry is growing annually, it is expected that a limited number of both theme parks and musea are going to be interested in a flight simulator attraction. Five of the 2013 top 20 musea in North-America are related to science and aviation, eight in Asia-Pacific and three in Europe [26]. Extrapolating this to the overall market suggests a variety of musea available as possible targeted buyers. Especially musea focusing on an interactive link between aviation and its visitors could benefit from the Aeolusim.
The user flux of a single simulator unit will possibly be a limiting factor for theme and amusement parks, since it is relatively limited when compared to that of other theme park attractions: The Goliath rollercoaster in The Netherlands has a passenger flux of 32 passengers per 1:32 min [32]. The expected minimal Aeolusim passenger flux is 1 passenger per 5 min.

The *International Association of Amusement Parks and Attractions* [2] (IAAPA) and the *American Society for Testing and Materials International F-24 Committee on Amusement Ride and Devices* [3] (ASTM F24) are associations with the aim to provide standards for amusement attractions. These associations have not been identified as certification authorities, though their qualification is assumed as an international prerequisite.
When designing the Aeolusim for the entertainment market, the certification of the ASTM F24 committee is adhered to. They publish their standards in the *Annual Book of ASTM Standard*. A copy of the F24 standards costs $120, which is deemed beyond the scope of the design synthesis exercise. Readers interested in these standards are advised to purchase a copy for full future reference. For the current project however, these requirements have been identified based on engineering judgement.

13.2 Customer Analysis

In order to provide an initial overview of potential buyers, one has to know the market they operate in and the wishes of their respective customers (end-user). A Porter's analysis was performed to facilitate in this assessment and analyse the competition within a specific market [33].

[2] *www.iaapa.org*
[3] *http://www.astm.org/COMMITTEE/F24.htm*

The Porter analysis has been applied to the entertainment market from the perspective of an arbitrary science museum as potential buyer. This will give an insight in the competitiveness of the entertainment market for musea and theme parks. A competitive market will force a museum to innovate and attract new customers. This in turn will be beneficial to launch the Aeolusim.

Competitive Rivalry - Low Risk
Defining competitive rivalry in the entertainment market is difficult. Most companies differentiate from each other by choosing a specific theme. If entertainment companies are located in close proximity to each other, the competitive rivalry may be increased. Due to the combination of proximity and differentiation of the entertainment companies, the competitive rivalry risk is deemed to be low. This is mainly because of the low number of aviation and science musea.

Threat of New Entrants - Medium Risk
Due to the good prospects of the market forecast, the threat of new entrants is medium. If high profits are to be made, new companies will try to gain market share [34]. Starting a museum or a theme park however has a high starting cost and needs approval from the (local) government. These entrance barriers will prevent a big increase in entertainment companies. The total threat of new entrants is therefore medium.

Threat of Substitute Products - Low Risk
Substitutes for musea and theme parks are scarce. The customers of musea wants to get the full experience of being in the museum, getting a tour and seeing real art or scientific pieces. Customers of theme parks are either alone or in a group and go for the theme park rides. There are no real substitutes for musea and theme parks, therefore the threat of substitute products is low.

Bargaining Power of Buyers - Low Risk
In case of the entertainment industry, the buyers are the visitors to the musea and theme parks. The bargaining power of these buyers is low: there are many customers which visit theme parks and museums and as such a (single) customer is expected to have little to no bargaining power. This risk is therefore low for the entertainment market.

The Bargaining Power of Suppliers - Medium Risk
The bargaining power of suppliers to companies in the entertainment business is medium. For the museum segment of the market, the bargaining power of suppliers is high due to the fact that there are relatively little suppliers and the pricing is not based on cost price [34]. In the case of theme parks however, there are many suppliers and the price is mainly determined by tenders. The bargaining power of suppliers in the theme park segment is therefore low.
The overall bargaining power of suppliers in the entertainment market is determined to be medium, with special note that this is very dependent on whether the musea or theme park segment of the market is chosen.

Results
The Porter analysis of the entertainment market concludes that the market has a low to medium competition for musea and theme parks. This competition will drive innovation for new attractions and expositions. The Porter analysis shows that the bargaining power for suppliers to musea and theme parks is medium. This will be of interest to the company selling the Aeolusim, which will become a supplier of musea and theme parks.
The difference between the theme park and museum segments of the entertainment markets are in the case of the Aeolusim negligible because it is a novelty item and there are little other suppliers of a flight simulator.

13.3 Market Introduction Strategy

In order to define a goal for the company bringing the Aeolusim to market, a SWOT analysis is performed. SWOT stands for Strengths, Weaknesses, Opportunities and Threats. The strengths and weaknesses are determined first and are based on the (technical) specifications of the Aeolusim. The Opportunities and Threats are based on the entertainment market. These strengths and weaknesses are combined to create the goal which can be pursued to market the Aeolusim.

The combination of a high level of immersion and the wish for more interaction wanted by museum visitors [35] results in the most applicable goal for the Aeolusim:

> '*Find a launching customer in the physics museum industry willing to attract museum visitors using a immersive interaction by 2016*'.

To determine an accurate strategy for finding a launching customer, the Science Center NEMO in Amsterdam is taken as potential customer as reference. NEMO has been chosen because of the information available and it's potential as a future customer.

Table 13.3: SWOT analysis of the Aeolusim for the entertainment market

Strengths	**Weaknesses**
Direct aerodynamic stick and pedal forces Low purchase and operating costs High level of immersion due to combination with HMD and moving simulator	Small 'user flux' for entertainment industry. Large surface footprint
Opportunities	**Threats**
More interaction wanted by museum visitors Low competition in market Growth in entertainment market	Limited amount of targeted musea and theme parks No brand recognition

13.4 NEMO Customer analysis

The NEMO Science Center in Amsterdam is a well visited museum, mostly by children. Their mission is to *'Show people in every phase of their life how fascinating, fun and useful science and technology is'*. The NEMO Science Center would be a great launching customer to showcase the Aeolusim and to engage people from all ages to get introduced to the concept of flying. To determine how to convince NEMO to be the launching customer for the Aeolusim, the Treacy and Wiersema model [36] was applied. This model allows to determine the client's management strategy.
Treacy and Wiersema state that organisations cannot please everyone. To come out ahead of your competition, companies have to make a choice of one of three value disciplines: operational excellence, product leadership and customer intimacy. Operational excellence focuses on making a company as efficient as possible. Product leadership is based on operating innovatively to get ahead of the competition. Customer intimacy, finally, focusses on the best customer experience possible in order to bind these customers and their word-of-mouth advertisement. From NEMO's 2013 financial overview [37] it becomes clear that customer intimacy is their highest priority. The NEMO's visitors grade the experience they had in the NEMO a 8,6 out of 10 mark. The Aeolusim is designed towards engaging people in a way that makes learning about flying fun, which suits the core values of the NEMO and its customer intimacy approach. When contacting NEMO Science Center, the focus should be on the impact the Aeolusim would have on the NEMO's customers experience. This of course does not mean that the other two value disciplines should be neglected, but they are of less importance.

The final step after the market and customer analysis has been performed, is to convince the NEMO Science Center to become a launching customer. By marketing the Aeolusim as a fun and safe way to experience and learn about flying for people of all ages, the NEMO's customer intimacy is directly addressed. This marketing strategy will help convincing their board that the Aeolusim will create a better overall user experience and increased customer growth, while maintaining their main principle of educating people about science and physics. This marketing strategy will be applied for all similar companies, which are the main targeted buyers of the Aeolusim.

13.5 Market opportunity

The market analysis concludes that the entertainment market is the best market to launch the Aeolusim. The market wants a fun and affordable way to introduce people to the concept of flying. The Aeolusim is to be designed such that is meets this specific market need.
The entertainment market is nevertheless expected to be very small, probably selling about ten Aeolusims in a best case scenario because of the limited potential buyers showing overlap with the Aeolusim's goal.

14 Return on Investment

In this chapter the return on investment is detailed for the Aeolusim. To be able to calculate the return on investment, the total cost breakdown structure for the Aeolusim is presented. The cost breakdown structure includes materials, products and production costs for the entire Aeolusim package. The development costs are presented further on in this chapter which, combined with the costs from the cost breakdown structure, allow for the return on investment to be calculated. All costs and return on investments can be found in Appendix B and Appendix D respectively. In Section 14.1 all the costs required to develop and produce the Aeolusim are detailed. Section 14.7 includes the business model of the Aeolusim. The expected return on investment for three different cases are determined in Section 14.8.

14.1 Cost Breakdown Structure

In this section the cost breakdown for the Aeolusim's post-DSE lifetime is given. The cost breakdown structure contains all the cost elements which contribute to the development, production and maintenance of the Aeolusim, as can be seen in Figure 14.1. First the research and development costs are detailed in Subsection 14.2. The production costs are explained in Subsection 14.3. The marketing costs are detailed in Subsection 14.4. The costs which are related to the operation of the Aeolusim are given in Subsection 14.5. In Subsection 14.6 the maintenance related costs are detailed.

14.2 Research and Development Costs

The research and development phase after the DSE is concluded consists of several phases: further design iterations, the detailed design, building and testing of the prototype and certification of the Aeolusim. In the detailed design phase an estimated 16000 hours of engineering is required to finish the design of the Aeolusim. This equals to ten engineers working 40 full weeks (in the normal scenario, see 14). Each engineer will approximately cost €50 per hour, combining to a total of €800.000. The prototype is estimated to cost 1.5 times the normal Aeolusim production cost, this accounts for possible manufacturing defects and other unexpected problems. Testing of the prototype will take approximately five hours a day for four weeks. During this time the testing facility and operator will have to be paid, accounting for a total of €21.000. The certification of the Aeolusim will be done for the entertainment industry as indicated by the market research 13 and is estimated to cost €15.000. The combined research and development cost will add up to approximately €900.000.

14.3 Production Costs

The production costs are made up of material costs and required man hours. An overview of the different materials and man hours per part can be found in Appendix B. The major costs for production are the fans, wind tunnel, Aeolusim and its support structure. The production cost of €37.700 for the Aeolusim differs significantly of the estimated €24.200 production cost in the baseline report [2]. The main reason for this difference are the fan and wind tunnel. The fan was expected to be bought as an off the shelf product and not custom designed, which drove up the price. The wind tunnel was not expected to be necessary, but due to airflow velocity it was included in the current design. The assembly staff will most likely consist of 4 people each earning approximately €40 per hour. Aside from the production costs, additional costs have to be made for the off the shelf products used for the Aeolusim. These products are the processing computer, flight simulator software, Head Mounted Display, Headset and the desk and chair for the operator.

14.4 Marketing Costs

To sell the Aeolusim an external marketing company should be hired. The hired marketing company should create awareness among potential buyers that the Aeolusim exists. A budget of approximately €100.000 has been accounted for this step in the marketing phase. When a potential launching customer has been found, €40.000 has been budgeted to finalise this sell and help the customer gain consumer awareness. The marketing costs are therefore expected to be €140.000.

14.5 Operation Costs

The operation costs are for the buyer of the Aeolusim, unless the Aeolusim is rented as explained in Section 14.7. The operational costs are a combination of the operator, electrical power, depreciation and insurance costs. The operator will cost around €35 per hour. The price for electricity in The Netherlands is about €0.18 per kWh excluding VAT, including energy tax for companies [38]. Therefore, the costs of electricity for the Aeolusim are about €5.40 per hour for 30 kW. The remaining €9.60 of the €50 are budgeted for depreciation and insurance.

14.6 Maintenance Costs

The maintenance costs of the Aeolusim are expected to be 10% of the total production costs per year. This results in a maintenance cost of €3.770 per year. These costs are for the company selling the Aeolusim. This may seem like a lot, but it is determined that it is better to have a maintenance budget overhead than shortage.

14.7 Earnings

To become a successful and profitable company, the Aeolusim will be sold and rented out. Giving companies the option to either rent or buy the Aeolusim will make it easier to attract customers.

Selling
The margin on the total production cost of €37.700 has been established at 100%. This margin can be further increased to make the Aeolusim more profitable, but to gain market share the initial margin of 100% is chosen and results in a €75.400 selling price

Leasing
Renting the Aeolusim can be a very attractive profit model. Sticking to the operational life of 1000 hours per year, the Aeolusim would be used approximately 83 hours per month. Setting the price at €100 per hour is conform market price [39] and with 83 hours per month would result in a gross earning of €8.330. Taking into account the operational and maintenance costs, which combined equal €3.770 per month, results in a total earning of €4.560 before interest and taxes.

14.8 Expected Return on Investment

For the expected return on investment a worst, normal and best case scenario have been estimated. These different scenarios have been changed in the amount of Aeolusim sold and the development time and therefore cost. To reduce the costs of the Aeolusim, it will be built to order which eliminates storage costs. The three scenarios all have a negative return on investment. As presented in Chapter 13, the amount of potential customers is limited to technical musea and theme parks, which result in low selling numbers. The three scenarios will be elaborated on and their cumulative cash flow will be presented.

Worst case scenario
In the worst case scenario it is assumed that after six years a total of 1 Aeolusim will have been sold and 1 will have been rented. The return on investment is negative for the first six years, as the total investment is €1.447 million and the total profit is €0.375 million, the total return on investment is 26%. This is combined with the development time of a full year. The total earnings and costs can be seen in Figure 14.2.

Normal case scenario
In the normal case scenario, it is assumed that after six years a total of 5 Aeolusims will have been sold and another 4 will have been rented. The expected return on investment for the normal case scenario is not positive over the first six years. The development time in the normal case scenario is 10 months. The return on investment over the first six years, with a total investment of €2.210 million and a total profit of €1.851 million, is approximately 84%. This can be seen in Figure 14.2.

Best case scenario
In the best case scenario, it is assumed that after six years a total of 10 Aeolusims will have been sold and another 9 will have been rented. The development time after the DSE before market launch is a mere eight months. The expected return on investment for the best case scenario looks more promising than the normal case scenario, with a total investment of €2.947 million and a profit of €3.128 million. This results in an expected return of investment of 106%, which is barely positive. The best case scenario can be seen in Figure 14.2.

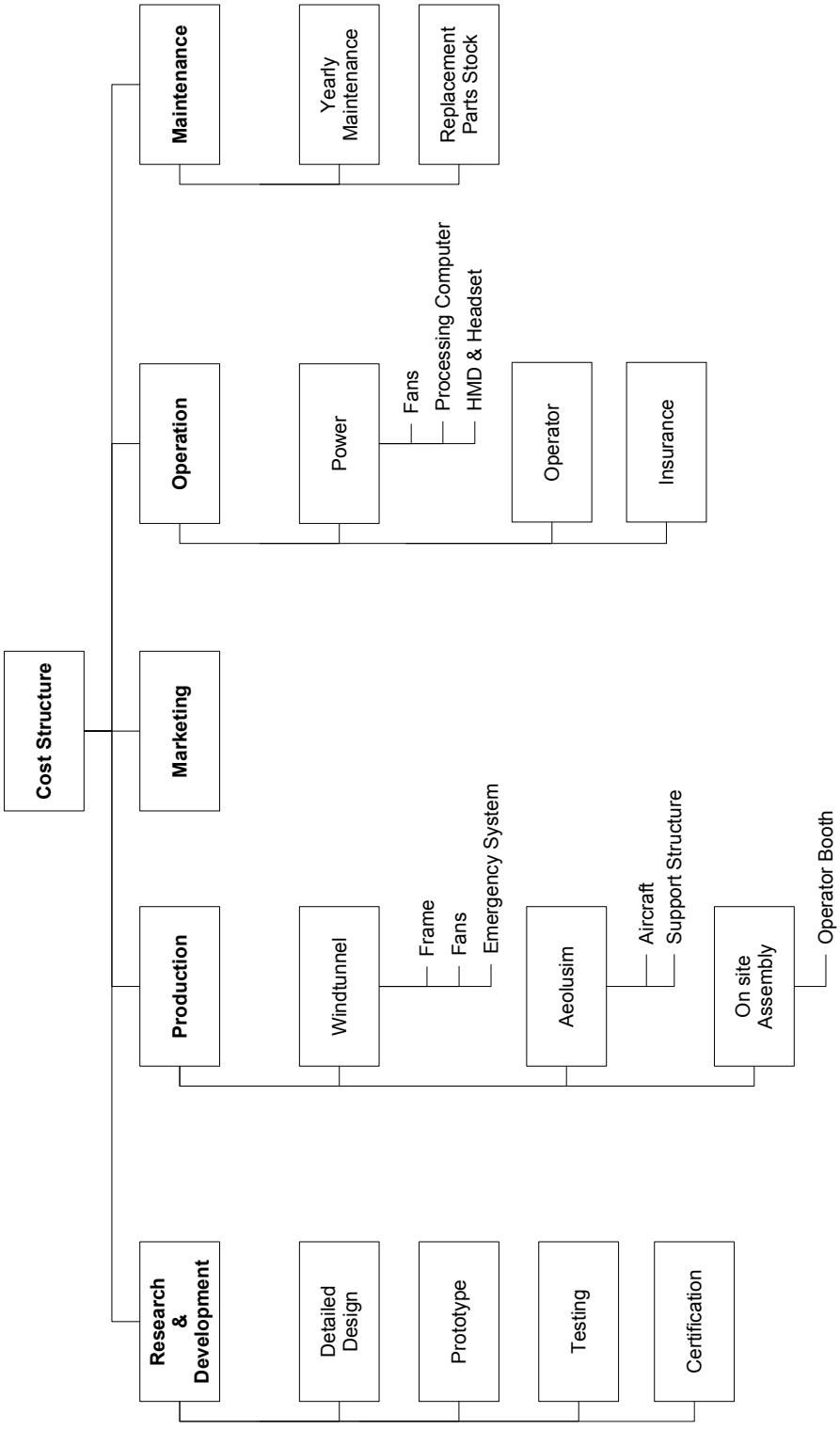

Figure 14.1: Cost Breakdown Chart

The expected return on investment is negative for the worst and normal case scenario. In the best case scenario a profit is to be made, albeit a very small profit. This is mainly due to the low selling numbers. The low selling numbers are the result of a small, and so far non-existing market and the relatively high operating costs. After getting a foothold in the entertainment market it is possible to expand to complementary markets, thereby increasing the offset numbers. Renting is a feasible strategy for gaining more attention as it gives companies a cheap way to obtain an Aeolusim and letting the end users come in contact with it.

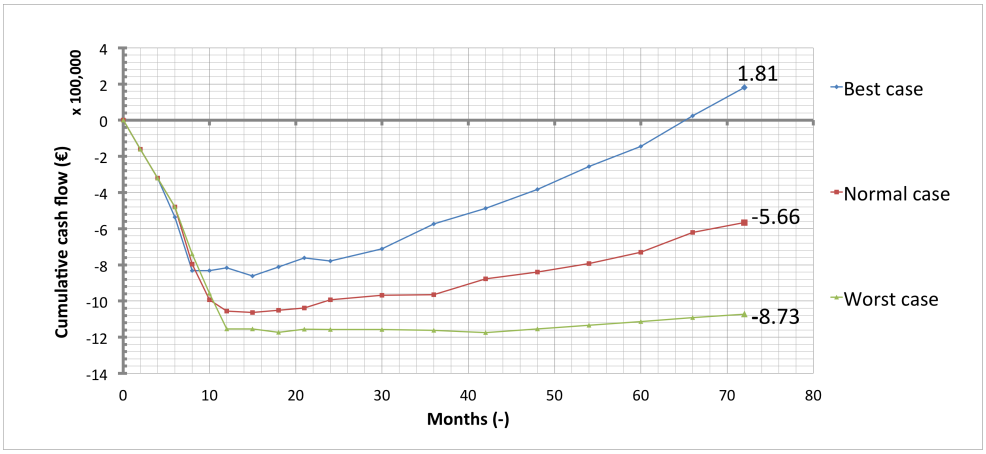

Figure 14.2: Cumulative Cash Flow for all three Case Scenarios

15 Sustainability Assessment

The international Institute for Sustainable Development defines sustainable development as:

> "The development that meets the needs of the present without compromising the ability of future generations to meet their own needs."
>
> Reference [40]

The sustainability philosophy of the Aeolusim was centered about this definition. To asses the design's compliance with this definition, the *Lowell Center Framework* was used (Reference [41]). This framework determines the product's compliance with the sustainability definition by focusing on key concepts. These concepts, adapted with respect to their relevance for the Aeolusim, are the following,

- the **need** for a healthy and safe product for both consumers and workers; and
- the **limitations** imposed on the environmental impact; and
- the **need** for an economically viable end product.

The assessment is divided into two parts: the sustainability of the design and operation and the sustainability of the manufacturing process in Section 15.1 and 15.2, respectively. The economical viability shall be discussed in Section 15.3

15.1 Sustainable Design

When considering sustainability during the design and manufacturing phase, an obvious area of concern is the use of materials. Poor material choice may cause harm to either customers, users or employees. In addition, some materials have a higher ecological footprint than others. For this reason, no toxic or relatively highly radioactive materials are to be used. In addition, parts relatively close to a possible fire source or the user are not allowed to be flammable or explosive.

The materials used in the Aeolusim are metal (Aluminium and Steel), wood (specific type yet to be determined) and a canvas/polyester fabric (specific type yet to be determined). Aluminium and steel are both 100% recyclable, with aliminum consuming only 5% of the energy initially invested in the product during the process [42]. Wood is in itself a sustainable product if, and only if, its origin is durable. The durability of the origin can be ensured by only using FSC certified wood[1]. A possible coating, such as varnish, may prevent the used wood from being recycled. A sustainable coating is to be selected such that it can be removed properly and disposed whilst limiting the environmental impact. The polyester fabric used for the fuselage and tail surfaces may prove harder to recycle due to the possible coating of the fabric to achieve the desired aerodynamic performance.

For a product to be sustainable, the end product has to be sustainable in its use as well. The latter is defined by the use of resources: electricity and materials during either operation or maintenance. Chapter 4 discussed the design of the fan subsystem, optimised for the design at hand. This chapter provided an estimated efficiency for the engines of 84.3%, and an nominal ideal[2] fan efficiency of 51%. Combining this yields an upper limit for the efficiency of 43.4%. In addition, only the kinetic energy in the airflow over the control surfaces can truly be called efficient, since the Aeolusim does not need to generate lift. This airflow is a relative low portion of the complete airflow accelerated by the fans, hence lowering the efficiency considerably. This devaluation of the efficiency is inherent to the concept of a wind driven simulator, as the wind tunnel has a minimum shape to facilitate roll, pitch and yaw manoeuvres.

The sustainability of the Aeolusim's maintenance can be optimised by allowing for repairs on site, whilst minimizing minimum waste material. For example, when one spring-damper system is broken it should be relatively easy to repair or replace this part without transporting the whole simulator. This results in a decrease of the ecological footprint, because fewer resources will be required.
It is an absolute necessity to prevent both customers and operators to be harmed by the simulator. This is done by making sure that customers have sufficient space in the simulator, and no protruding parts are present in the cockpit that can either harm the customer or allow the customer to harm the system. Wires are shielded properly such that customers and operators do not experience shocks and moving parts are shielded.

[1] *www.fsc.org*
[2] neglecting friction losses

The sustainability assessment concludes that the design of Aeolusim moderately sustainable. The majority of the parts in simulator can be recycled and are safe to use because of the chosen materials. Nonetheless, the system's energy efficiency is relatively low. However optimised for the concept of a wind driven simulator.

15.2 Sustainable Manufacturing

During production, waste of materials and energy should be kept to a minimum. This can be done by opting for the *lean manufacturing* method as mentioned in Section 9.1, minimizing the amount of custom parts, keeping production locations close to each other and making use of renewable sources of energy where possible. The safety of the workers is not only dependent on the used materials, but also on safety of the workplace. This applies to the selected external manufacturers as well as the post-DSE design team. A safe workplace is a workplace that is well lit and ventilated, and working hours are within reason. In order to ensure this, a realistic planning has to be made that takes the amount of workers and their working hours into account.

The sustainability assessment concludes that the manufacturing of Aeolusim has the potential to become sustainable.

15.3 Economical Feasibility of the Design

The *Lowell Center Framework* used in this assessment defines the economical feasibility as an important parameter to asses the sustainability of a project. If a project is not economically feasible, its use of resources is deemed to be not sustainable. Chapter 13 and 14 discussed the entertainment market and the expected return on investment, respectively. Both chapters conclude that the market is small and that alternative products have already found their niche. The relatively low efficiency and high purchase costs are expected to affect the amount of potential buyers. Chapter 14 defined three business scenarios, with only the 'best case scenario' showing a positive outlook for a period of six years. Based on the obtained market insight it may be concluded that the economical feasibility of the Aeolusim is low. Small profits are to be expected when weighed against the invested resources. It is therefore advised to discontinue further development from a sustainability point of view.

16 Post-DSE planning

This chapter presents the planning of all phases that follow the DSE until the first Aeolusim is produced. Section 16.1 presents the resource allocation, in which the budgets for technical resources during the following design phases are defined. All activities that need to be performed after the DSE to create the Aeolusim are presented in Section 16.2.

16.1 Resource Allocation

The technical resources for the remaining design are budgeted based on the values of the current design. The technical resources that are defined are: mass, electrical power, computing power and dimensions. A contingency is given for all budgets to account for the uncertainty in the current design. Table 16.2 gives an overview of the technical resources used in the current design, the contingency that is taken, and the budgeted value for further design phases.

16.1.1 Mass

The mass of the airframe is 105 kg, of which the wings are 11 kg and the mass of the fuselage is 67.5 kg. The mass of the support structure is 6.7 kg. The production limits determine the structural design of the wing and fuselage, and this resulted in a high safety factor for all load cases. In the analysis of connections in the wing structure, it was assumed that loads could be distributed over the complete surface of the connection. In further design phases, stresses at the connection points need to be calculated for the actual way of connection. The stress concentrations due to for example rivets at the connections might increase the mass. For that reason, a contingency of 10% is taken for the mass of the wing.
For the fuselage, the contingency due to uncertainty about the way of connecting the different parts is smaller than it is for the wing. It is likely that most connections will be welded. A contingency of 5% is set for the mass of the fuselage during further design.
The uncertainty about the mass of the support structure is mainly in the design of the spring-dampers. The design of the spring-dampers has to be performed during detailed design. As this can have a significant influence on the mass of the support structure, a contingency of 10% is taken for the mass of the support structure.

16.1.2 Electrical Power

The Aeolusim needs $29853W$ of electrical power. Almost all electrical power is used by the fans. As the fans are custom designed, the efficiency of the fans still needs to be validated. Most importantly, a more accurate prediction of the pressure increase over the fan needs to be made. To account for the uncertainty that exist about whether an airflow velocity of $12.4m/s$ can be achieved at a fan power consumption of $29.5kW$, a contingency of 15% is taken for the power consumption in the further phases of the design.

16.1.3 Computing Capacity

The computing capacity is dependent on the choice for the simulation software of the simulator. The computer should process the inputs from the pilot and the sensors of the Aeolusim, and create a visual and sound simulation for the head-mounted display. As the software design is not yet started and has to be performed in the post-DSE phase of the design, only an initial estimate is made for the computing capacity. This estimate is based on reference flight simulators and a high contingency is taken. The computing capacity of the Aeolusim is divided into three separate categories: RAM, GPU and storage.

As reference for the computing power, two existing flight simulators have been used. These flight simulators have no motion cueing system. The computing power of such a flight simulator is comparable to the required computing power for a wind driven flight simulator, since the Aeolusim's motion cueing system determined by the aerodynamic forces. For such a simulator, computing power is used primarily for processing and presenting the visual system.
The first reference simulator is the desktop flight simulator CAT III BATD that is produced by the company Precision Flight Controls Inc. and is approved by the FAA [43]. The second reference simulator is the cockpit simulator GTX MAX AATD, also produced by Precision Flight Controls Inc., which uses two computer systems: one master computer; and one computer for the visual system [44]. The computing power characteristics of these simulators are presented in Table 16.1.

Table 16.1: Computing power characteristics of two flight simulators. [43] [45] [46]

	RAM	**GPU**	**HDD/SSD**
CAT III BATD	4 GB DDR3 1066	nVidia GeForce GTS250 1GB DDR3	250 GB HDD
GTX MAX AATD Visuals PC	12 GB DDR3 1600	nVidia 650Titan 2GB GDDR3	256 GB SSD, 256 GB back-up
GTX MAX AATD Master PC	4 GB DDR3 1600	nVidia 650Titan 2GB GDDR3	240 GB SSD, 240 GB back-up

The budgeted value for computing power has been based on the values of Table 16.1 and include a contingency of 30%. For this reason, the budgeted RAM is a 12 GB DDR3 RAM. Based on the GPUs used by the reference flight simulators, a GPU with 2 GB GDDR5 Memory is to be used as maximum budgeted resource value. GPUs with these specifications are expected to fulfil the AEOLUSIM's need and be able to process a detailed visual system for its user. A 256 GB SSD for primary software storage will allow for low latency.

16.1.4 Wind Tunnel Dimensions

The size of the wind tunnel has a substantial influence on the space that is required to operate the AEOLUSIM. Therefore, a budget is defined for the dimensions of the wind tunnel. At the test section, the cross-sectional area of the simulation section of the wind tunnel is $5.14m^2$. The cross-sectional area has been made as small as possible, and the size and motion range of the AEOLUSIM have been the limiting factor. It is not expected that the size of the AEOLUSIM will change during further design. However, the height of the cross-sectional area might be too small to guarantee pilot comfortability. As this must be evaluated during further design phases, a contingency of 10% is taken on the area.
The length of the simulation section of the wind tunnel is $6m$. This is enough to have the airframe and support structure located in the simulation section, and have some clearance before and after the airframe. It is not expected that the length of the simulation section will increase, the 6 meters already contains enough contingency. The inlet nozzle of the wind tunnel has a length $3m$ and the diffusion angle at the ceiling of the inlet nozzle is 7.3 deg. As the effect of the diffusion angle on the airflow has not yet been analysed, a contingency of 20% is taken for the length of the wind tunnel, which can be used to decrease the diffusion angle.

Table 16.2: Values in current design and contingencies for technical resources.

Technical Resource	Unit	**Value current design**	**Contingency**	**Budgeted value**
Mass wing	[kg]	11	10%	12.1
Mass fuselage	[kg]	67.5	5%	74
Mass support structure	[kg]	6.7	10%	7.3
Electrical power	[W]	29853	10%	32800
RAM	[GB]	-	25%	12
GPU	[-]	-	25%	2 GB GDDR5
SSD	[GB]	-	25%	256
Wind tunnel simulation section cross-sectional area	$[m^2]$	5.14	10%	5.65
Wind tunnel simulation section length	[m]	6	-	6
Wind tunnel inlet nozzle length	[m]	3	20%	3.6

16.2 Project Development & Design Logic

Figure 16.1 shows the activities to be executed during the post-DSE phase of the project. Figure F.1 in Appendix F shows the Gantt chart of the post-DSE activities. The activities can be grouped in three phases: detailed design, testing and manufacturing.

In the first post-DSE phase, the concept that is created during the DSE-phase of the project is designed in more detail. In the detailed fan design a full CFD analysis will be executed to get a more accurate prediction of the pressure increase over the fan, and to get a prediction of the interaction between the fans. Using this result, the fan design is optimised. During detailed aerodynamic design, the effectiveness of the flow at the rudder needs to be improved. Also, nozzle needs to be included in the model and the effect of the propagation of the boundary layer of the wall needs to be analysed. The output of the detailed design phase is the complete design of the Aeolusim. Technical drawings are made of all parts of the Aeolusim, and with these a prototype can be built.

This prototype is then tested and the design is updated until the prototype meets all requirements. For the prototype testing, an element test of the fan is done and a test of the airframe is done. A prototype of just one fan is tested, and not of the entire wall of fans. The airframe and support structure are tested in a existing wind tunnel during this phase.

After certification for the Aeolusim is obtained, manufacturing of the simulator starts. A detailed manufacturing plan was presented in Chapter 9.

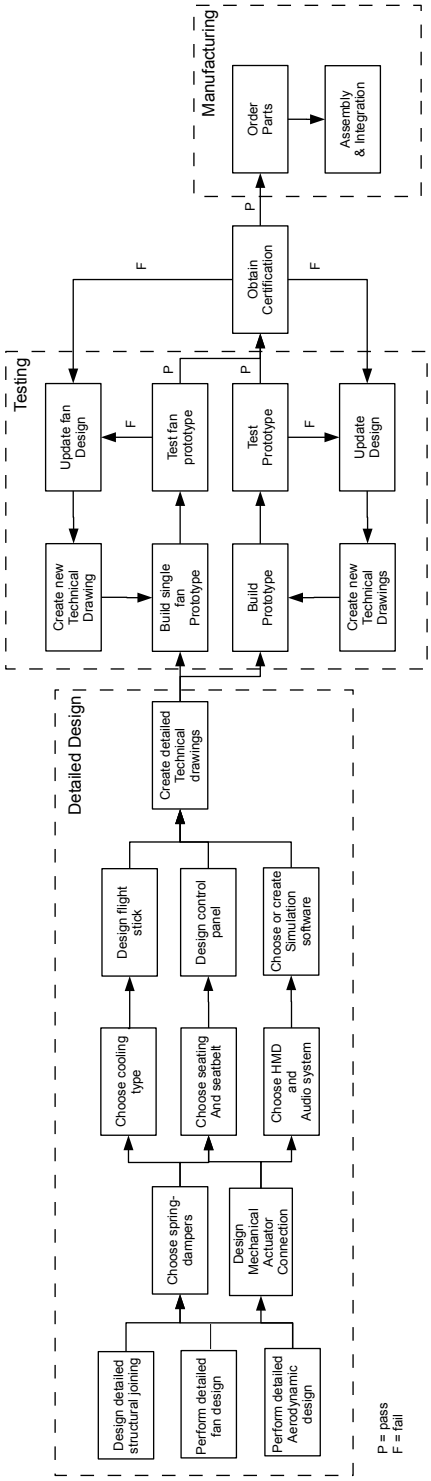

Figure 16.1: Post-DSE Activities

17 Compliance With Requirements

This chapter will pass the final verdict on whether the top level requirements were met. It will first offer an overview on which requirements were met in the form of a table, and consecutively an explanation will be given on why some requirements were not met. The compliance matrix can be found in Table 17.1.

Table 17.1: Compliance Matrix

Requirement	Compliance
Power	
Total power consumption $< 30kW$	✓
Cost	
Unit price tag < €35.000	
Running Cost < 50 €/h	✓
Performance	
Pilot Weight Range 35kg-95kg	✓
High pass filtered	✓
Realistic Control Forces	✓
3 to 6 Degrees of freedom	✓
Roll and Pitch movement	✓
Head mounted display	✓
Safety And Reliability	
Limit linear accelerations Normal operations $< 7\frac{m^2}{s}$	✓
Limit maximum linear accelerations $< 15\frac{m^2}{s}$	✓
Limit Rotational accelerations $< 1\frac{rad}{s}$	✓
Shielded moving parts	✓
Sustainability	
Recyclable Materials	✓
Environmentally Safe	✓

As evident one requirement has not been met: production cost. this may appear a failure but, as is often the case, the truth is more nuanced. The unit cost, totaling in at €37660,-, has gone over requirement. This is mainly contributed to the size of the entire system. Cost has gone up due to the fact that the wind tunnel had a too low budget to begin with. Cost saving has been a major focus during design, and it is expected that the Aeolusim will not become cheaper during the post-DSE phase.

The fan power consumption of 29500 Watts, as explained in Subsection 4.2.2, is unreliable. The final value for the expected power consumption given in Section 10.1 is 29853.1 Watts. As fan power consumption effectively determines the total power consumption, the total power consumption becomes unreliable. The final value may not be reliable, but it is representative. Meaning that it is likely that the power consumption requirement can be met in further stages of development.

18 Conclusion and Recommendations

The goal of this report is to present an understanding of the methods and results of the Aeolusim's conceptual design phase (hardware only). Following a preliminary conceptual design, system functions and relations were defined to guide the design process. Hereafter several aspects of the concept were analysed, either by creating and verifying new models, or by using existing software such as Xfoil, ANSYS Fluent and ANSYS Mechanical. These aspects include a custom fan design, an analysis of the aerodynamic performance, motion capabilities, control forces and structural integrity of the simulator. This resulted in a technically viable conceptual design for the Aeolusim.

The Aeolusim is a simulator located in an open return wind tunnel. Air is propelled through the wind tunnel by 12 ducted fans positioned in a 4 by 3 matrix, providing a aiflow velocity of $12.4 m/s^2$. These fans feature custom designed fan blades in order to boost the system's efficiency. All in all providing a volumetric flow rate of $5.3 m^3/s$ at a nominal design efficiency of 51.2 %. Incorporating the electrical motors yields a power consumption of 29.5 kW. The wind tunnel design consists of a open return wind tunnel with a diffusion angle of 7.3°. It has an inlet of 3 meters length, a simulator section of 6 meters and a diffusion section of also 6 meters. Height of the tunnel in the simulator section is 1.9 meters, but due to the non rectangular shape the area is only 5.14 m^2. The total area at the inlet and at the fans is 7.04 m^2 and 9.72 m^2 respectively, both being rectangular in shape. The simulator itself has a span of 2.8 m and a fuselage length of $3.6m$ and is suspended by a support structure. This support structure is a universal joint, allowing the simulator to pitch, roll, and yaw, respectively. Spring-damper systems are incorporated in this structure, in order to both limit and filter the simulator's motion response.

Analysing the aerodynamic performance highlighted several characteristics of the Aeolusim. Among them is the tip vortex, it results in an ineffective outboard region of 8 % of the wing (half the span). Decreasing the distance between the wing and the wall decreased this tip vortex. However, this decrease turned out to be so small that it could be neglected.
In addition, the wake created by the pilot and structure causes a significant reduction in airflow velocity at the horizontal and vertical tail. Positioning an aerodynamic fairing behind the pilot increased the effective velocity with 57 % and was therefore introduced in the design. Since the simulator only has to rotate around its three axes, creating lift is not of great importance. On the other hand, creating a rolling moment is, and so a symmetric airfoil was chosen for its simplicity and to ensure that the ailerons are equally effective when deflecting up and down.

An initial assessment of the Aeolusim's motion response concluded that it is able to simulate aircraft-like behaviour, when compared to a Cessna Citation II. Large deflection angles are favourable for the entertainment value of the Aeolusim, while aircraft-like behaviour is an amicable feature for any simulator. The latter case however urged an undesirable decrease in the maximum deflection and has therefore been disregarded in the design. This will lead to maximum deflection of 10, 20 and 9.4 degrees , reached after 2.27, 2.3 and 2.5 seconds for for pitch, roll and yaw, respectively.
An important conclusion that was drawn from the model, is that *low powered* suspended wind-driven simulators are inherently sensitive to a shift in the centre of gravity. It is very unlikely, if not impossible, to design a suspension where the rotation point coincides with the centre of gravity a 100% of the time for all kinds of users. A small offset in the $x-$ or $y-$direction (body axis frame) leads to large and unwanted deflections. Increasing the stiffness of the springs will limit these deflections, though will not solve it and affect the simulator's motion response.Conventional solutions such as trimtabs are not effective for the design at hand due to the small scale and the low airflow velocity.
Maximum control forces were found to be 22.5 N, 21.4 N and 7.03 N for the ailerons, elevator and rudder, respectively. To ensure such control forces could be obtained, the rotation point of the tail surfaces was placed inside the fuselage at 40 and 50 cm in front of the leading edge of the rudder and elevator, respectively. This increased the hinge moment, on which the control forces depend linearly. This, however, was insufficient for the rudder control force and was therefore mechanically increased to 12.75 N by introducing a spring between the stick and the rudder.

Structural characteristics have been analysed using ANSYS Mechanical APDL. The fuselage consists of a truss structure covered with a fabric, where the main wing is made of a combination of aluminium and wood; and the tail wings of wood covered with fabric. This configuration is chosen because a user is expected to lean/sit on the wing but is not expected to be in the vicinity of the tail wings. The latter would require the user to jump over the main wing, which has a main chord of one m. The structural integrity of the complete system was designed such that it is able to cope with all expected loads during its operational life. These include the aerodynamic

forces and the loads caused by user interaction. The minimum safety factor found during stress analysis were 3.87, 2.56 and 1.97 for the wing, fuselage and support structure, respectively. Other load cases such as bumping in to the wing had safety factors reaching values in the 100s, indicating an over-designed structure. This however could not be overcome, since the design was limited by production and cost factors, rather than the applied load.

In the end, the Aeolusim is a technically viable product with the limitations being: its relatively low deflections and sensitivity w.r.t. the centre of gravity. A market analysis proved that there are chances for the simulator to enter the entertainment market by using a launching customer, preferably a scientific museum. However the costs to operate the Aeolusim when compared to substitute products are expected to reduce the number of potential buyers. This in combination with a high investment in research & development results in a dreary outlook on any quick return of investment. Several cases were analysed, only the best case scenario showed a small profit after six years. This makes the Aeolusim an economically unprofitable product: continuation of the development is therefore disadvised.

Recommendations
As previously stated, further development of the Aeolusim is not encouraged. If, however, development is continued some technical recommendations are to be made.

As mentioned earlier, this design phase focused on the Aeolusim's hardware. Software is integration with, for instance, a flight dynamics engine is yet to be designed.

The analysis of the fans required a pressure increase to be known. This pressure increase was in turn estimated using reference material, which introduces uncertainty. To analyse the actual pressure increase, CFD analysis is to be performed. This CFD analysis is also to investigate the interaction between the fans. Each axial fan introduced an individual swirl to the airflow, in turn interacting with another swirl. This interaction is expected to affect the airflow upstream.

Regarding the simulator's aerodynamic performance, some improvements can be made. The flow around the simulator is currently influenced by vortices and wake structures. These arise along the wing and fuselage surfaces and behind the pilot. The flow around the fuselage can be smoothed by using bent beams instead of straight ones. Moreover, the flow at the rudder is quite ineffective. A possibility would be to investigate the use of an H-tail to remove the rudder from the wake of the pilot and increase its respective efficiency. The use of an H-tail does, however, imply difficulties in the design of the structure of the tail, since all control surfaces rotate about a point in front of their leading edge.
In addition, because the wing-tips are located relatively close to the wind tunnel, it is to be investigated what the effects are of the boundary layer of the wind tunnel. The propagation of the boundary layer from the nozzle to the simulation section might influence the lift generated by the ailerons.
In total, a secondary analysis is to be performed using more advanced viscous models. This will in turn increase the accuracy of the outcome. Current results did not allow for these advanced techniques due to the limited computational resources and the author's familiarity with these subjects.

Analogous to the analysis of the aerodynamic properties, the structural analysis could benefit from more computational resources. This will allow for a smaller mesh sizes in the FEA and yield more accurate results. For a complete analysis of the lifting surfaces it is advised to use Fluid Structure Interaction (FSI) analysis. FSI analysis uses CFD to compute the internal stresses due to the passing airflow. This will be of primary interest for the ailerons and tail surfaces, since the aerodynamic loads are the only expected operating loads for these subsystems. The main wing is in turn to be analysed when rivets are incorporated in the model. Analytical models sizing the rivet spacing could not be verified during the current design phase. In addition, proper references could not be found to determine optimum thicknesses for the chosen production methods and bend radii. Since the loads acting on the structure are relatively small, it the production limits that become dominant. Production costs can be optimised by investigating this optimum.

Bibliography

[1] R. van Paassen. *Project Guide Design Synthesis Exercise - Aeolusim.* TU Delft, October 2014.

[2] DSE group 07. Baseline report aeolusim. Technical report, Delft University of Technology, Faculty of Aerospace Engineering, 2014.

[3] DSE group 07. Midterm report aeolusim. Technical report, Delft University of Technology, Faculty of Aerospace Engineering, 2014.

[4] M. Karlson. The development of a technical cost model for composites. Technical report, 2013.

[5] M. T. Pascu. Modern layout and design strategy for axial fans, 2009.

[6] R. I. Lewis. *Turbomachinery performance analysis.* Butterworth-Heinemann, 1996.

[7] M. Pascu and P. Epple. Numerical investigation of the validity of axial blade design. In ASME, editor, *ASME International Mechanical Engineering Congress and Exposition, Proceedings*, volume 8, pages 437–445, 2008.

[8] B. Eckert and E. Schnell. *Axial- und Radialkompressoren Anwendung/Theorie/Berechnung.* Berlin Springer, 2013.

[9] The Commission of the European Communities. Commission regulation (ec) no 640/2009. Official Journal of the European Union, 2009. implementing Directive 2005/32/EC of the European Parliament and of the Council with regard to ecodesign requirements for electric motors.

[10] ANSYS, Inc. *ANSYS Fluid Dynamics Verification Manual*, November 2013.

[11] B. Galbraith. *Aircraft Coefficient Comparisons between Datcom and Published Data.* Holy Cows, Inc, 2011.

[12] K. H. Huebner, D. L. Dewhirst, D. E. Smith, and T. G. Byrom. *The Finite Element Method for Engineers.* Wiley-Interscience, September 2011.

[13] Inc. ANSYS. *Verification Manual for the Mechanical APDL Application.* SAS IP, November 2009.

[14] C. Kassapoglou. Ae2211 lecture notes: lecture 2.

[15] T. H. G. Megson. *Aircraft Structures for Engineering Students.* Elsevier, 2012.

[16] Russell Charles Hibbeler and Peter Schiavone. *Engineering mechanics: statics and dynamics.* Pearson Education India, 2004.

[17] J. A. Mulder et al., 2014. [AE3202 - Flight Dynamics Lecture notes].

[18] R. B. Schultz, L. A. Obergefell, A. Rizer, and C. B. Albery. Whole body center of gravity and moments of inertia study. Technical report, DTIC Online, December 1996.

[19] S. Spronk et al. Flight dynamics report. Technical report, TU Delft, March 2014.

[20] R. de Breuker, 2014. [AE2135-II - Vibrations Lecture notes version 2.01].

[21] Public Domain Aeronautical Software. *The USAF Stability and Control DATCOM*, December 1999.

[22] M. Stevens. Fan performance, 1999.

[23] Algemene Energieraad. *Elektriciteitsplan 1993-2002.* 1992.

[24] A. Cervone, 2014. [AE2111-II Aerospace Design and Systems Engineering Lecture 8], 2014.

[25] ISO/TMB. Iso 31000:2009 risk management–principles and guidelines. *International Organization for Standardization, Geneva, Switzerland*, 2009.

[26] TEA/AECOM. *2013 Theme and Museum Index: Global Attractions attendance Report.* 2013.

[27] International Monetary Fund. *Regional Economic Outlook: Asia and Pacific.* April 2014.

[28] TEA/AECOM. *2012 Theme and Museum Index: Global Attractions attendance Report.* 2012.

[29] TEA/AECOM. *2011 Theme Index: Global Attractions attendance Report.* 2011.

[30] Nederlandse Museum Vereniging. *Agenda 2026.* September 2010.

[31] Museums Association. Market analysis: Future trends. `www.museumsassociation.org/about/8361`, 2014. [Online; accessed 03-January-2015].

[32] Rollercoaster Database. `http://rcdb.com/`, 2014. [Online; accessed 19-November-2014].

[33] S. Santema and J. van de Rijt. *Klanten Winnen.* Kluwer, September 2008.

[34] N. Kotler, P. Kotler, and W. Kotler. *Museum Marketing and Strategy: Designing Missions, Building Audiences, Generating Revenue and Resources*. Jossey-Bass, July 2008.

[35] S. Allen. Designs for learning: Studying science museum exhibits that do more than entertain. *Science Education*, 2004.

[36] F. Wiersema and M. Treacy. *The Discipline of Market Leaders*. Basic Books, January 1997.

[37] NEMO Science Center. 2013 jaarverslag nemo. `https://www.e-nemo.nl/nl/organisatie/over-nemo/feiten-en-cijfers/`, 2013. [Online; accessed 7-January-2015].

[38] Tarieven gewone stroom voor mkb. `https://www.essent.nl/content/zakelijk/tarieven/elektriciteit/tariefoverzicht_flexibel.html`. [Online; accessed 18-November-2014].

[39] ACES Flight Simulator. `http://www.flyaces.com`, 2014. [Online; accessed 18-November-2014].

[40] What is sustainable development? `https://www.iisd.org/sd/`. [Online; accessed 07-December-2014].

[41] S. Edwards et al. The lowell center framework for sustainable products, November 2009.

[42] T. E. Graedel. Aluminium: Properties & sustainability. `http://aluminium.org.au/properties_and_sustainability`, 2011. [Online; accessed 20-January-2015].

[43] Precision Flight Controls, Inc. *CAT III BATD Desktop Flight Training System*, 2014.

[44] Gtx max aatd cockpit flight simulator. `https://www.flypfc.com/?/training-systems/gtx-max/`. [Online; accessed 18-November-2014].

[45] Computer system extreme. `https://www.flypfc.com/index.php?/products/computers/computer-system-ssd`. [Online; accessed 18-November-2014].

[46] Computer system extreme. `https://www.flypfc.com/?/products/computers/computer-system-max`. [Online; accessed 18-November-2014].

A Stability & Control Model

This appendix contains the inputs & outputs used by the Stability & Control model in Table A.1 and a software flow diagram of this model in Figure A.1.

Inputs	Outputs
ρ	$F_{ailerons}$
V	F_{rudder}
$C_{L_{0_w}}$	$F_{elevators}$
$C_{L_{\alpha_w}}$	Control input plots
$C_{L_{0_h}}$	Pitch plot
$C_{L_{\alpha_h}}$	Pitch rate plot
$C_{L_{0_v}}$	Roll plot
$C_{L_{\alpha_v}}$	Roll rate plot
$m_{structure}$	Yaw plot
$I_{xx_{structure}}$	Yaw rate plot
$I_{yy_{structure}}$	
$I_{zz_{structure}}$	
$I_{xz_{structure}}$	
x_{cg}	
y_{cg}	
z_{cg}	
x_{wing}	
z_{wing}	
x_{hor}	
z_{hor}	
x_{vert}	
z_{vert}	
$l_{fuselage}$	
$r_{fuselage}$	
c_w	
b_w	
c_h	
b_h	
c_v	
b_v	
k_p	
c_p	
k_r	
c_r	
k_y	
c_y	
Airfoil wing	
Airfoil hor. tail	
Airfoil vert. tail	

Table A.1: Inputs and outputs of the Stability & Control model

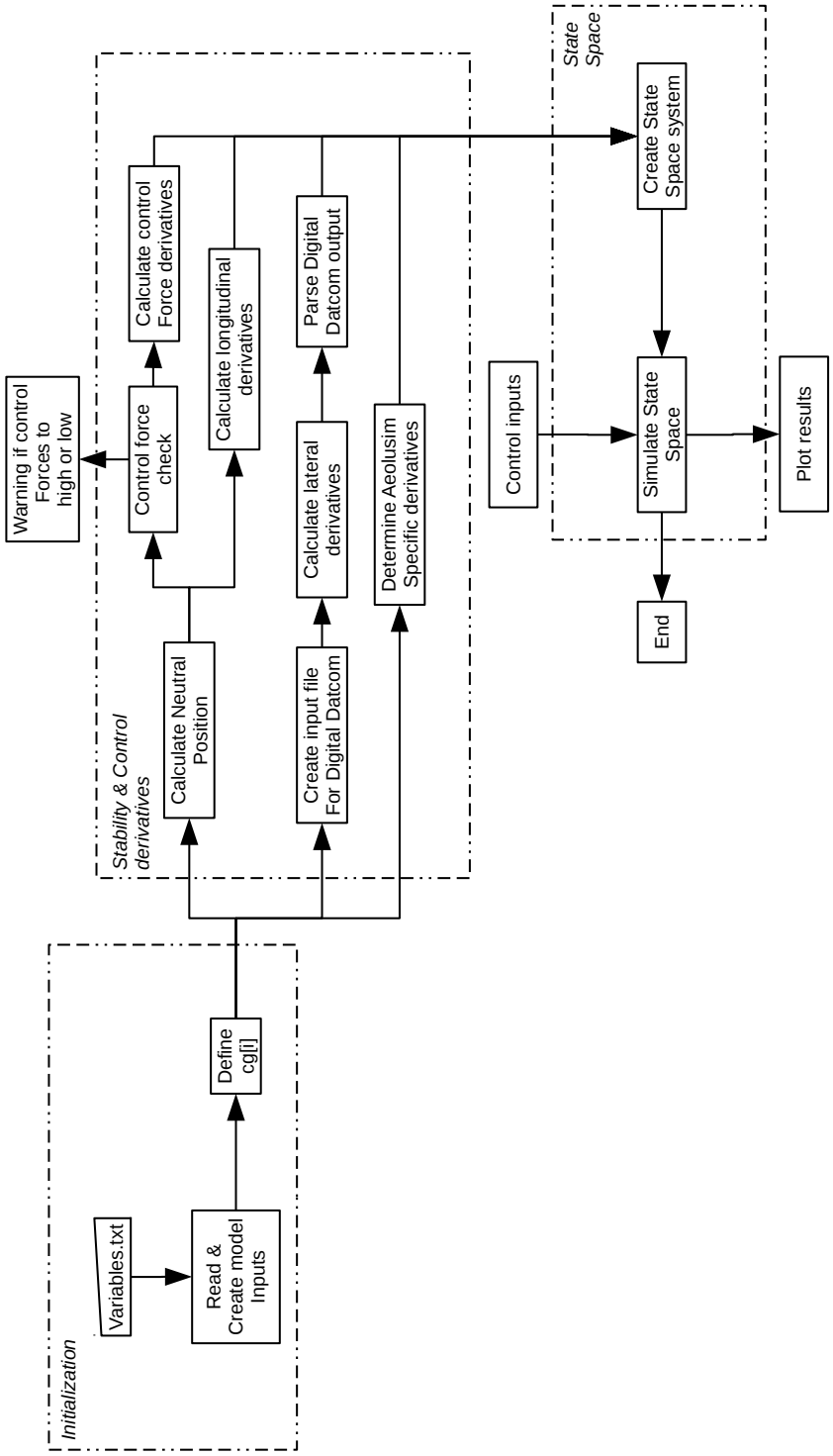

Figure A.1: Stability & Control Model Flowchart

B Cost Breakdown Structure

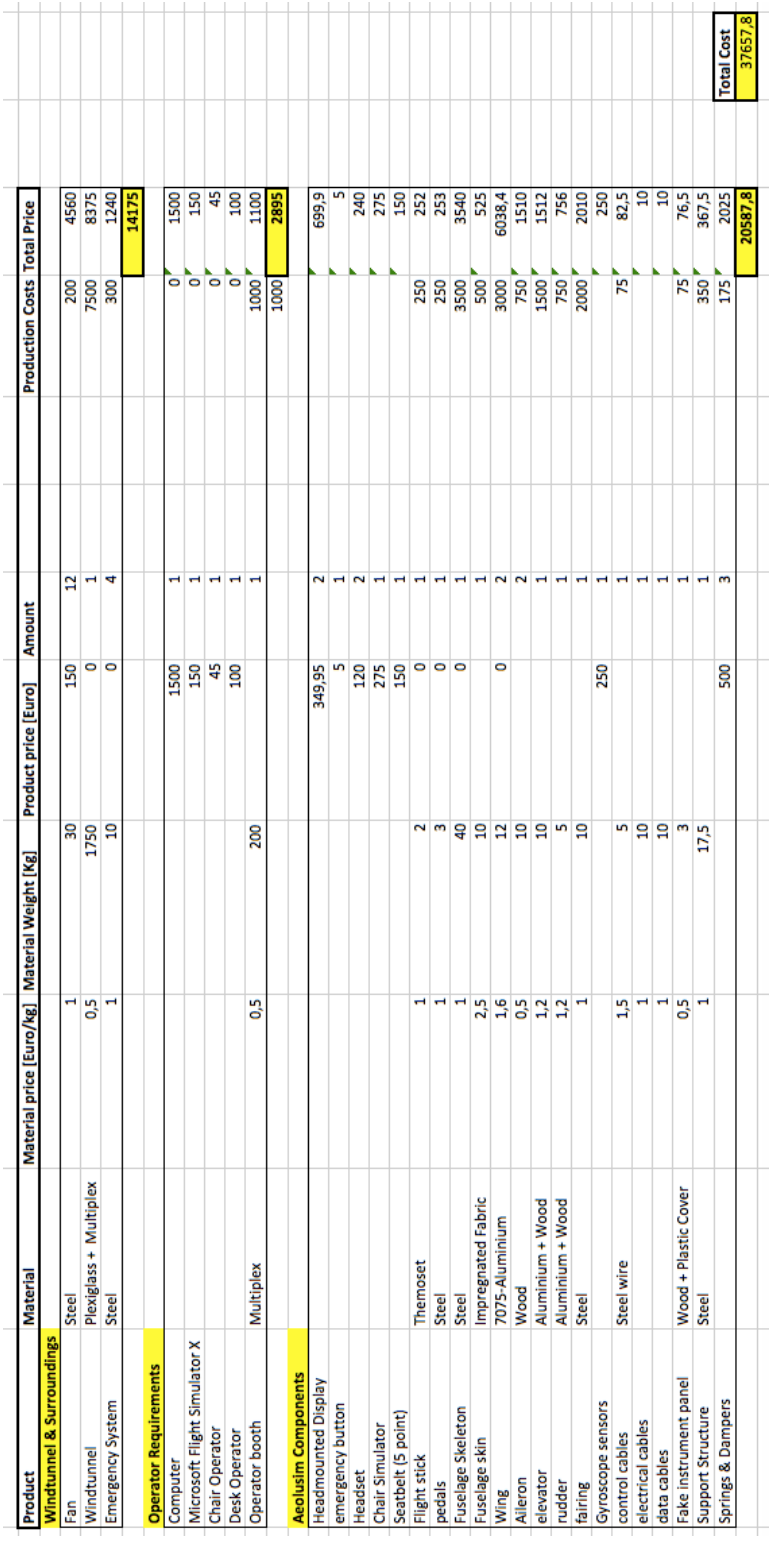

Product	Material	Material price [Euro/kg]	Material Weight [Kg]	Product price [Euro]	Amount		Production Costs	Total Price
Windtunnel & Surroundings								
Fan	Steel	1	30	150	12		200	4560
Windtunnel	Plexiglass + Multiplex	0,5	1750	0	1		7500	8375
Emergency System	Steel	1	10	0	4		300	1240
								14175
Operator Requirements								
Computer				1500	1		0	1500
Microsoft Flight Simulator X				150	1		0	150
Chair Operator				45	1		0	45
Desk Operator				100	1		0	100
Operator booth	Multiplex	0,5	200		1		1000	1100
							1000	**2895**
Aeolusim Components								
Headmounted Display				349,95	2			699,9
emergency button				5	1			5
Headset				120	2			240
Chair Simulator				275	1			275
Seatbelt (5 point)				150	1			150
Flight stick	Themoset	1	2	0	1		250	252
pedals	Steel	1	3	0	1		250	253
Fuselage Skeleton	Steel	1	40	0	1		3500	3540
Fuselage skin	Impregnated Fabric	2,5	10		1		500	525
Wing	7075-Aluminium	1,6	12	0	2		3000	6038,4
Aileron	Wood	0,5	10		2		750	1510
elevator	Aluminium + Wood	1,2	10		1		1500	1512
rudder	Aluminium + Wood	1,2	5		1		750	756
fairing	Steel	1	10		1		2000	2010
Gyroscope sensors				250	1			250
control cables	Steel wire	1,5	5		1		75	82,5
electrical cables		1	10		1			10
data cables		1	10		1			10
Fake instrument panel	Wood + Plastic Cover	0,5	3		1		75	76,5
Support Structure	Steel	1	17,5		1		350	367,5
Springs & Dampers				500	3		175	2025
								20587,8

Total Cost
37657,8

Figure B.1: Cost Breakdown Structure of the Aeolusim

C Risk Events

#	Risk event	Impact	Likelihood	Mitigation strategy
	Design risks			
1	The design will be too complicated to allow it to be taken apart for maintenance: increases maintenance costs	4	3	Limit need for periodic maintenance (safe life standard)
2	The software latency will exceed the 50 ms limit: reduces experience and may cause motion sickness	3	2	Design a stronger computer/use simpler sensor input
3	Processing all data will require too much resources: affect desired output data	3	1	Design a stronger computer/use simpler sensor input
	Manufacturing and assembly risks			
4	Lead time too long for components: increases production and/or maintenance time	3	3	Asses, confirm and obtain assurances from manufacturer
5	Manufacturing delay: increases production and/or maintenance time	4	2	Asses reliability and production capabilities manufacturer before production.
6	Parts not within Tolerances: increases lead time of the specific component	3	3	Obtain quality assurances from manufacturer
7	parts no longer available: sets production on hold	4	3	Design parts such that they can be made by multiple manufacturers/keep list of alternate manufacturers
8	Transportation delay: increases production and/or maintenance time	3	4	Plan transportation time margins
9	Difficulties in hardware integration: Assembly time exceeds scheduled time	5	2	Use standard connectors (electronics) and few complex interfaces
10	Difficulties in software integration: Assembly time exceeds scheduled time	5	2	Provide software debug environment
	Economical risks			
11	Design conflicts with patent: royalties will increase price of the design	3	1	Find out if there are patents which could cause conflicts/redesign system to avoid conflicts
12	Aeolusim cannot be certified (IAAPA/ASTM F-24): reduces number of potential buyers	5	3	File early certification proposal and await feedback
13	Market is too small to make a profit with the targeted sale price (€35000): No breakeven point	5	4	Hire marketing firm to attract potential buyers
14	End-user gets seriously injured or dies using Aeolusim: negative effect on reputation	4	2	Shield moveable parts/design emergency stop and safety harness
15	Operating costs will be more than 50€ per hour: reduces number of potential buyers	3	2	Negotiate bigger budget/reduce design costs
	Operational risks			
16	Severe discomfort to user due simulation out of sync/other problems with spacial awareness	4	4	Perform camera calibration/distortion correction before each run: limit physical movement
17	*cockpit*			
a	- seatbelt malfunction	5	1	Design with high safety factor/regular inspection
b	- joystick malfunction	5	1	Design with high safety factor/emergency stop
c	- Head mounted Display (HMD) malfunction	2	2	Provide backup HMDs
d	- Emergency button malfunction	5	1	Safe life design/regular inspection
e	- Sound system malfunction	5	2	Use commercially available sound system/headset and provide extra component to control cabinet
18	*Control Cabinet*			
a	- Computer malfunction	5	1	Only release updates after stress test, provide remote access to computer from Aeolusim IT dep.
b	- Emergency button malfunction	4	1	Safe life design
c	- lack of extra components (for redundancy, i.e. HMD)	4	1	Regular storage inspection
19	*Airframe*			
a	- Spring subsystem malfunction	5	3	Safe life design/regular inspection
b	- Damper subsystem malfunction	5	3	Safe life design/regular inspection
c	- Lock mechanism fail	5	2	Safe life design/regular inspection
d	- Failure of the load bearing structure	5	1	Safe life design/regular inspection
e	- Control surfaces are jammed	3	3	Perform daily inspection
20	*Wind tunnel/fan*			
a	- Multiple persons in perimeter	4	1	Provide clear view in the control cabinet for operator to verify/clearly state to perform check on operator screen
b	- Fan or engine malfunction	2	4	Regularly inspect the fans and engines
c	- Material build up at blade root: reduces efficiency	2	2	Regularly inspect the fans and engines

D Return on Investment

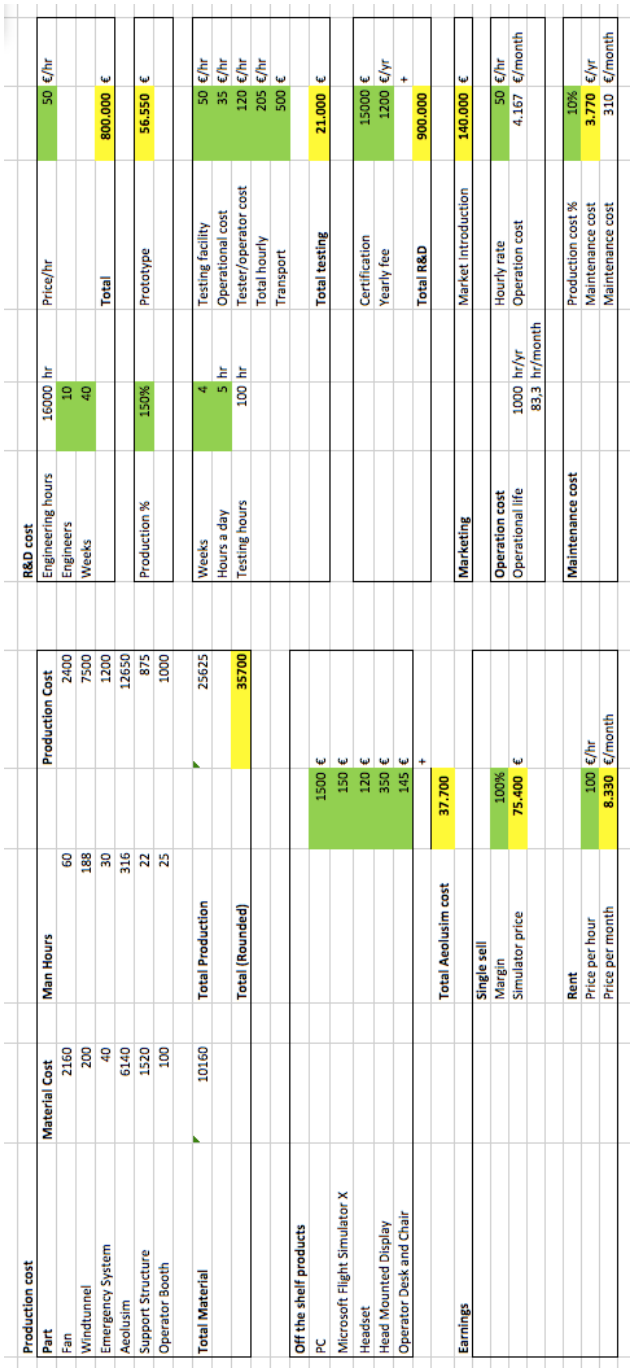

Production cost						R&D cost				
Part	Material Cost	Man Hours		Production Cost		Engineering hours	16000	hr	Price/hr	50 €/hr
Fan	2160	60		2400		Engineers	10			
Windtunnel	200	188		7500		Weeks	40			
Emergency System	40	30		1200					Total	800.000 €
Aeolusim	6140	316		12650						
Support Structure	1520	22		875		Production %	150%		Prototype	56.550 €
Operator Booth	100	25		1000						
						Weeks	4		Testing facility	50 €/hr
Total Material	10160	Total Production		25625		Hours a day	5	hr	Operational cost	35 €/hr
						Testing hours	100	hr	Tester/operator cost	120 €/hr
		Total (Rounded)		35700					Total hourly	205 €/hr
									Transport	500 €
Off the shelf products									Total testing	21.000 €
PC			1500	€						
Microsoft Flight Simulator X			150	€					Certification	15000 €
Headset			120	€					Yearly fee	1200 €/yr
Head Mounted Display			350	€						+
Operator Desk and Chair			145	€					Total R&D	900.000
				+						
		Total Aeolusim cost		37.700		Marketing			Market introduction	140.000 €
Earnings										
		Single sell				Operation cost			Hourly rate	50 €/hr
		Margin		100%		Operational life	1000	hr/yr	Operation cost	4.167 €/month
		Simulator price		75.400	€		83,3	hr/month		
		Rent				Maintenance cost			Production cost %	10%
		Price per hour		100	€/hr				Maintenance cost	3.770 €/yr
		Price per month		8.330	€/month				Maintenance cost	310 €/month

Figure D.1: Costs related to producing, operating and selling the Aeolusim

Figure D.2: Overview of three different scenarios of AEOLUSIM market introduction

E Convergence Ansys Fluent Results

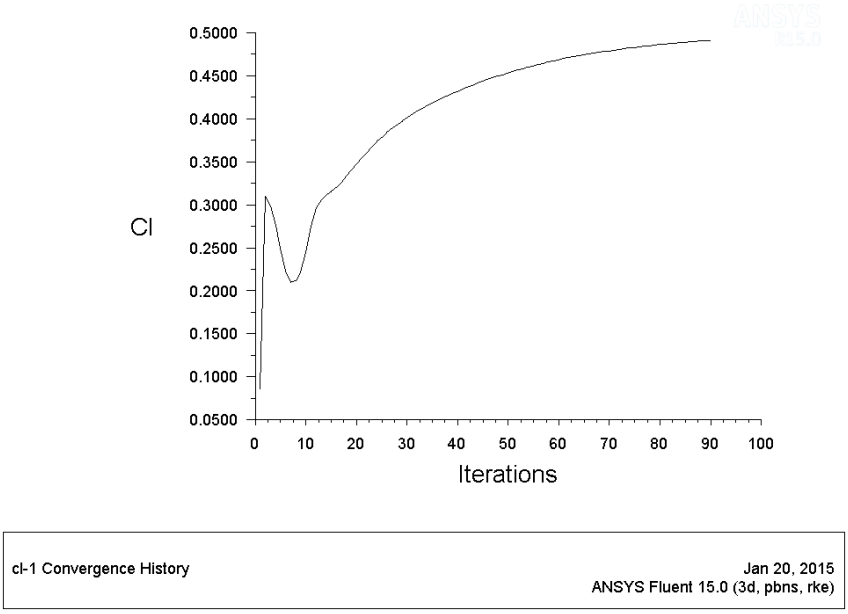

Figure E.1: Lift coefficient convergence of Ansys Fluent analysis for wing at 10 degrees pitch

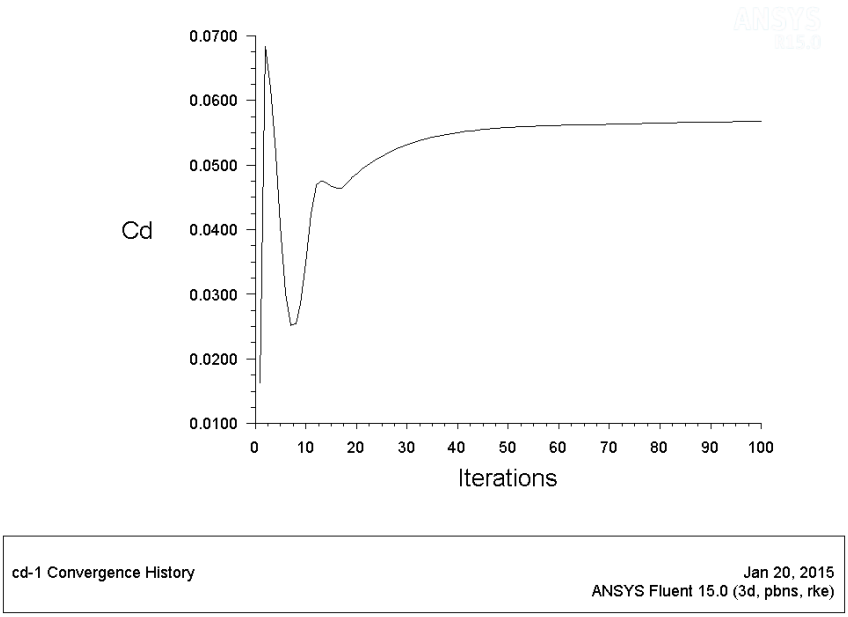

Figure E.2: Drag coefficient convergence of Ansys Fluent analysis for wing at 10 degrees pitch

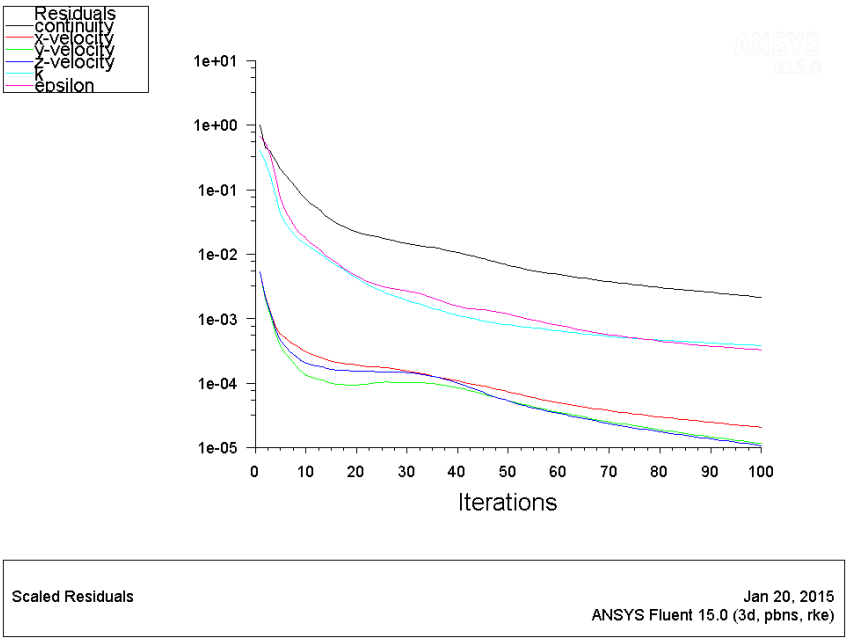

Figure E.3: Scaled residuals as function of amount of iterations in Ansys Fluent analysis for wing at 10 degrees pitch

F Post-DSE Gantt Chart

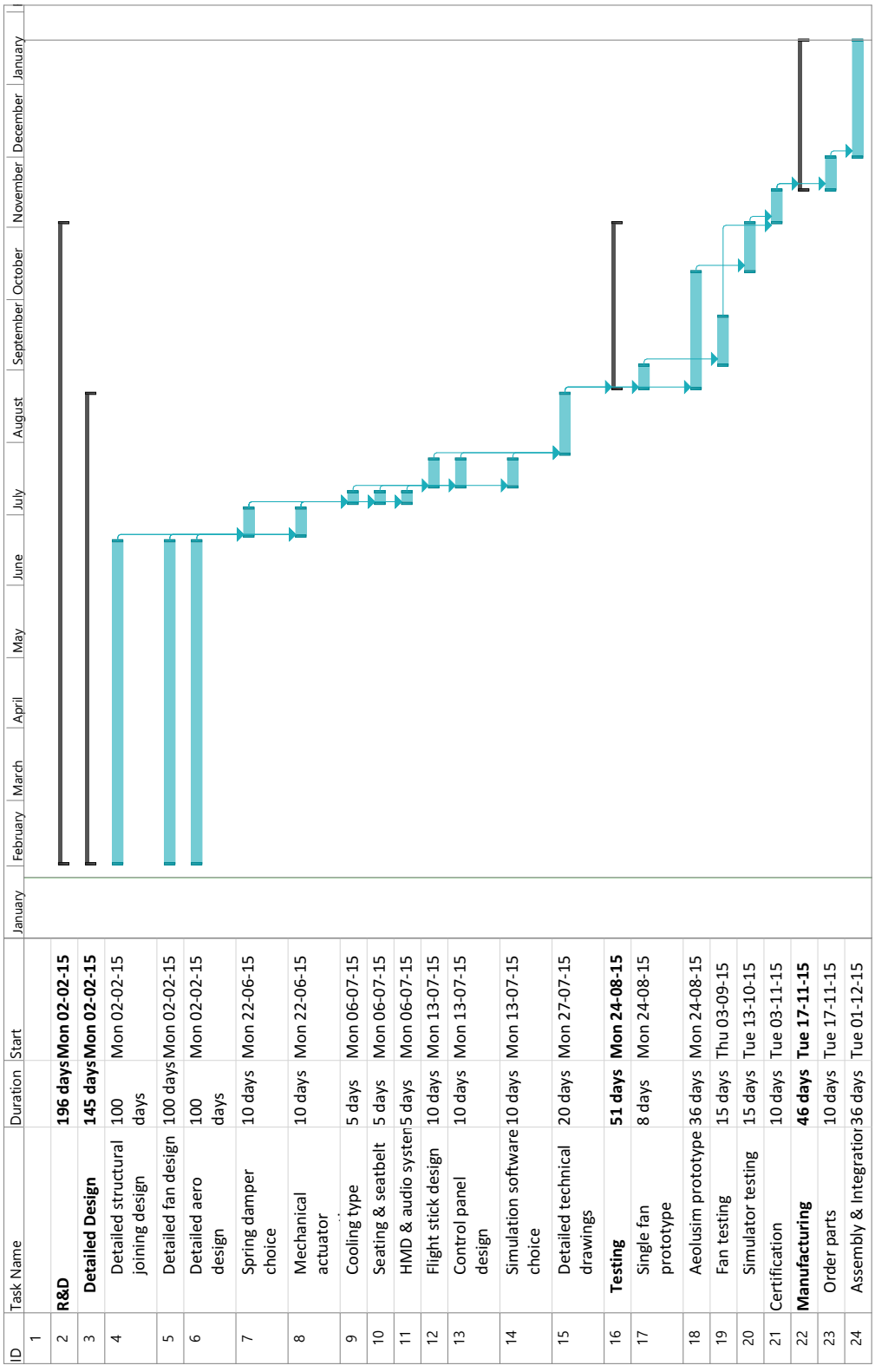

ID	Task Name	Duration	Start
1			
2	**R&D**	**196 days**	**Mon 02-02-15**
3	**Detailed Design**	**145 days**	**Mon 02-02-15**
4	Detailed structural joining design	100 days	Mon 02-02-15
5	Detailed fan design	100 days	Mon 02-02-15
6	Detailed aero design	100 days	Mon 02-02-15
7	Spring damper choice	10 days	Mon 22-06-15
8	Mechanical actuator	10 days	Mon 22-06-15
9	Cooling type	5 days	Mon 06-07-15
10	Seating & seatbelt	5 days	Mon 06-07-15
11	HMD & audio systen	5 days	Mon 06-07-15
12	Flight stick design	10 days	Mon 13-07-15
13	Control panel design	10 days	Mon 13-07-15
14	Simulation software choice	10 days	Mon 13-07-15
15	Detailed technical drawings	20 days	Mon 27-07-15
16	**Testing**	**51 days**	**Mon 24-08-15**
17	Single fan prototype	8 days	Mon 24-08-15
18	Aeolusim prototype	36 days	Mon 24-08-15
19	Fan testing	15 days	Thu 03-09-15
20	Simulator testing	15 days	Tue 13-10-15
21	Certification	10 days	Tue 03-11-15
22	**Manufacturing**	**46 days**	**Tue 17-11-15**
23	Order parts	10 days	Tue 17-11-15
24	Assembly & Integratior	36 days	Tue 01-12-15

Figure F.1: Gantt-Chart planning for Post-DSE activities

G Technical Drawings

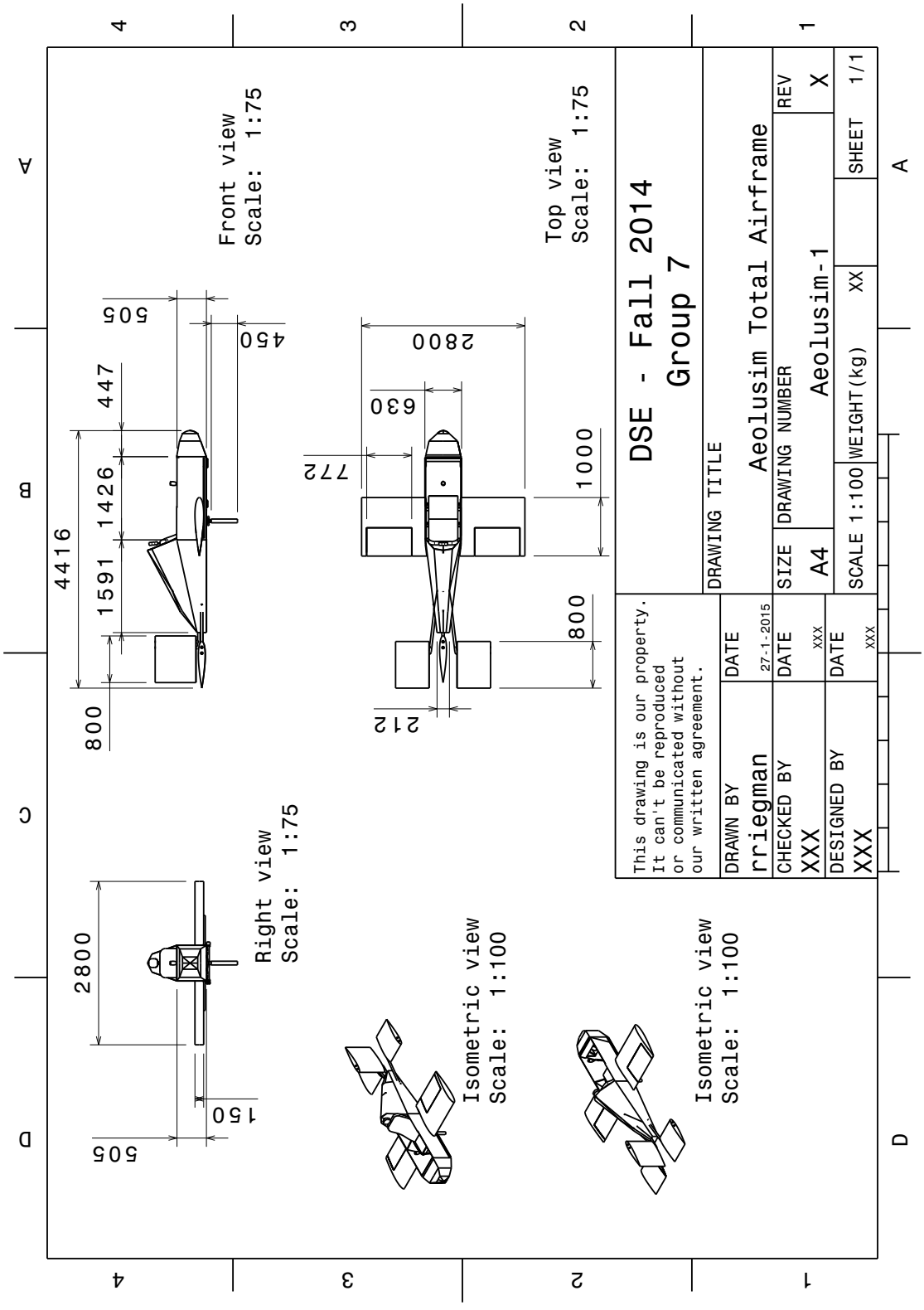

Figure G.1: Total Airframe

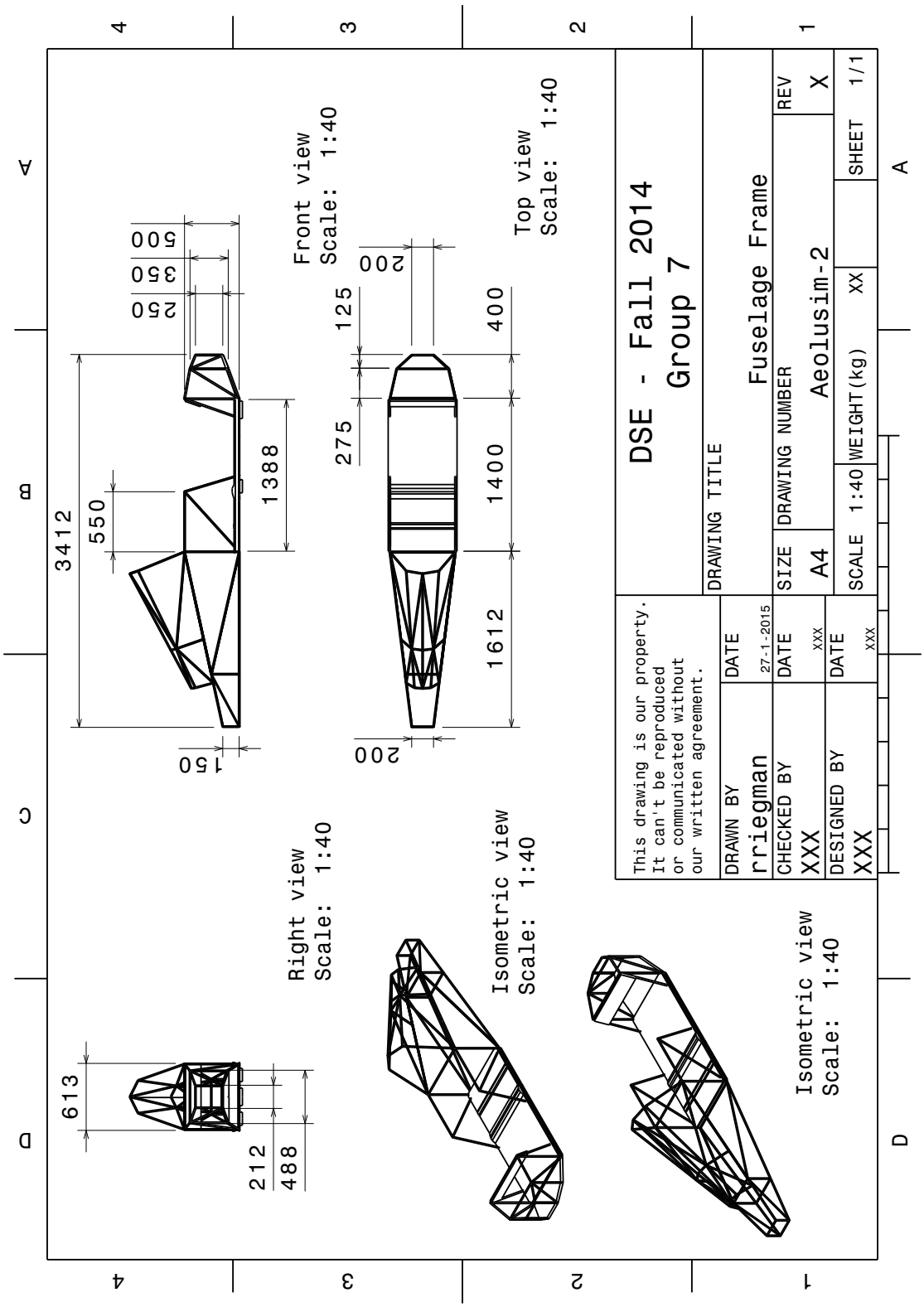

Figure G.2: Fuselage Frame

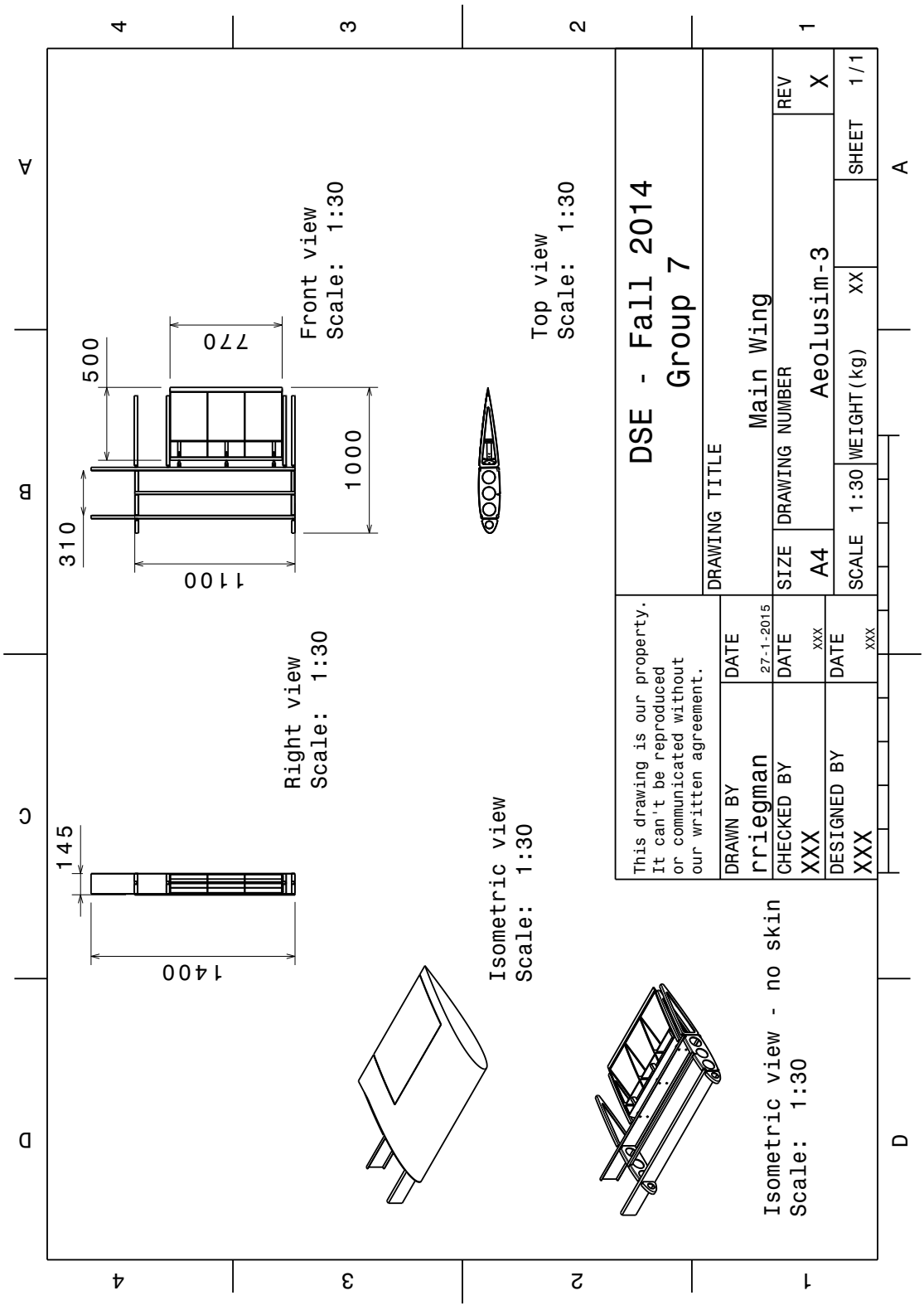

Figure G.3: Main Wing

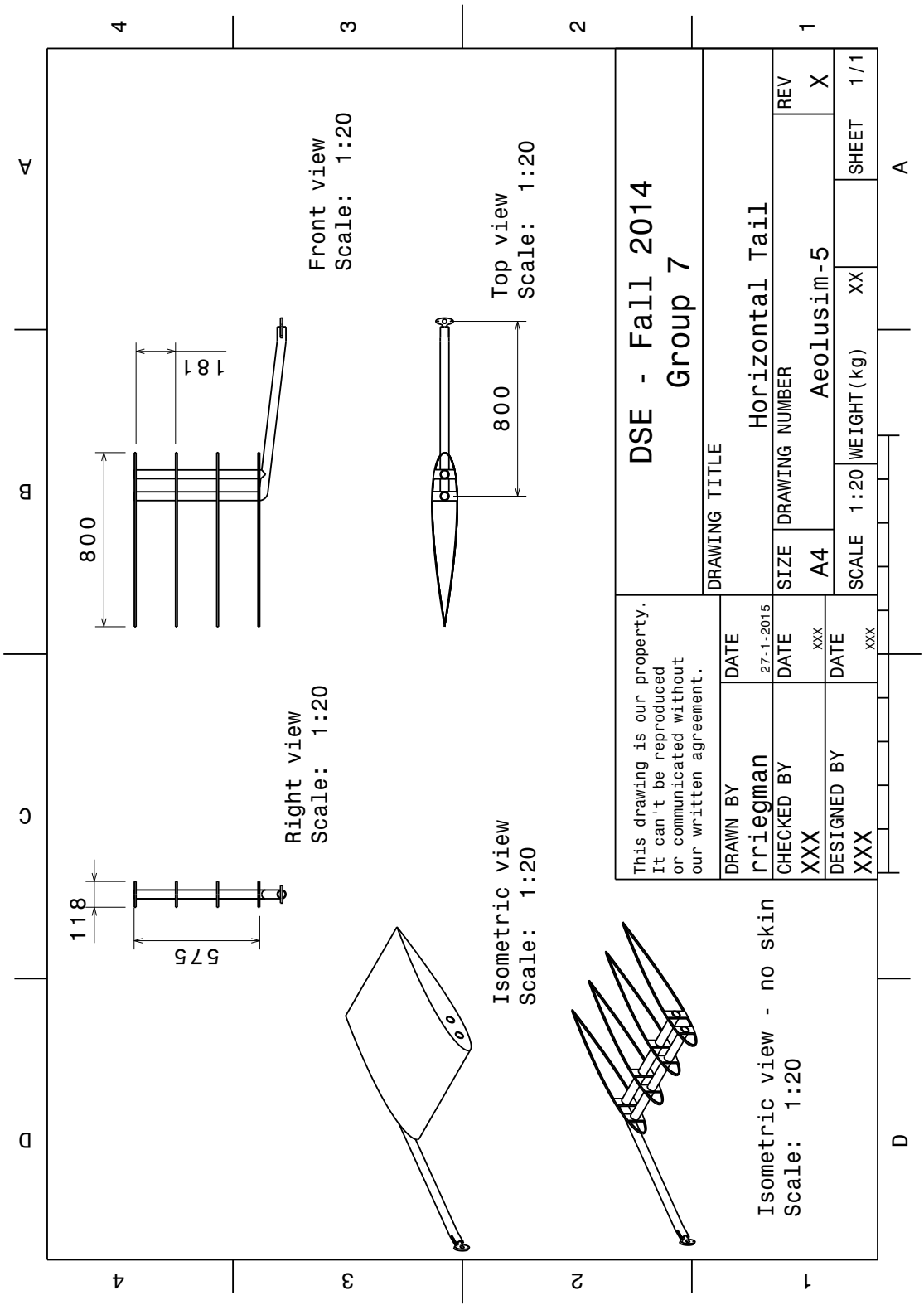

Figure G.4: Horizontal Tail

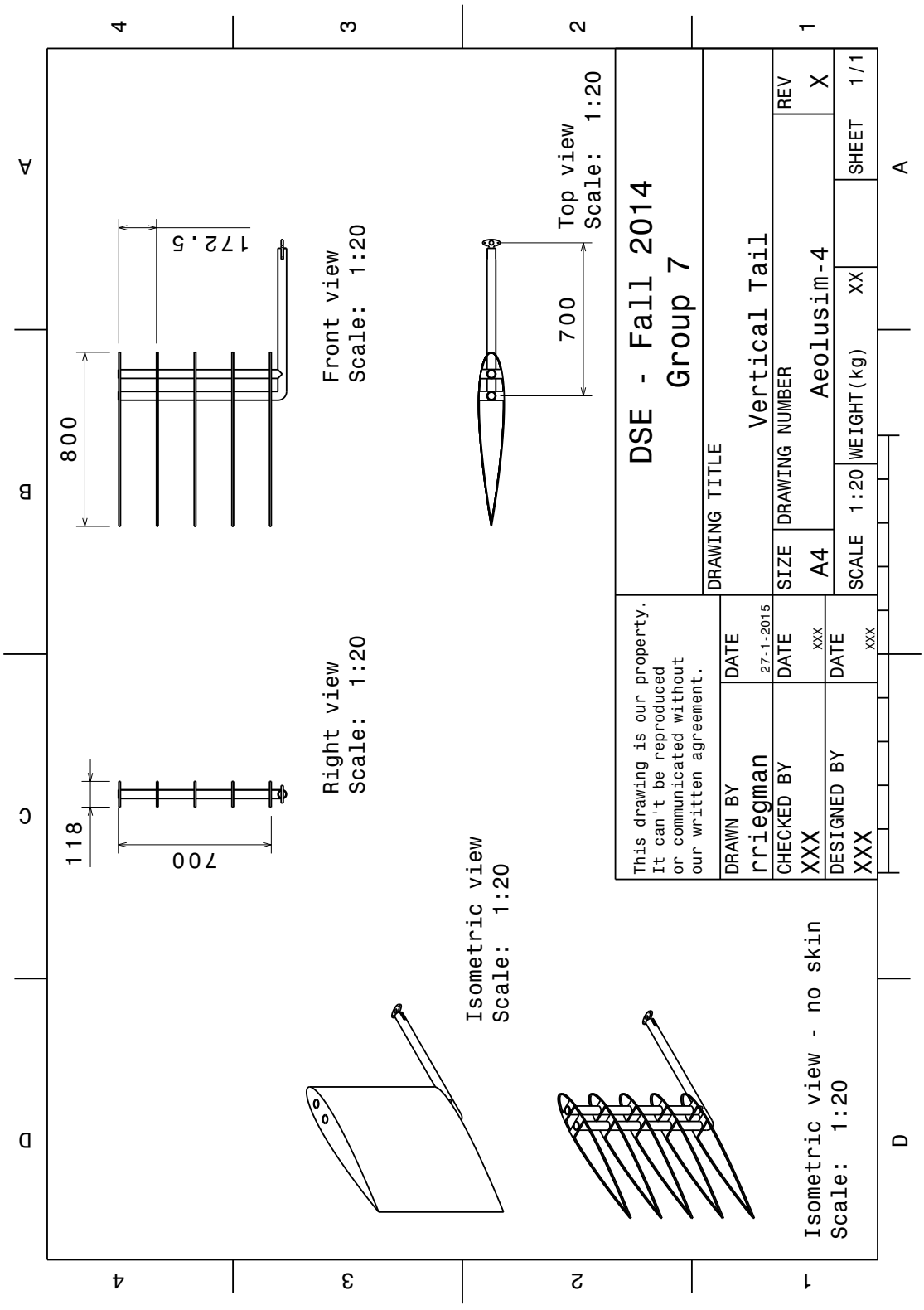

Figure G.5: Vertical Tail

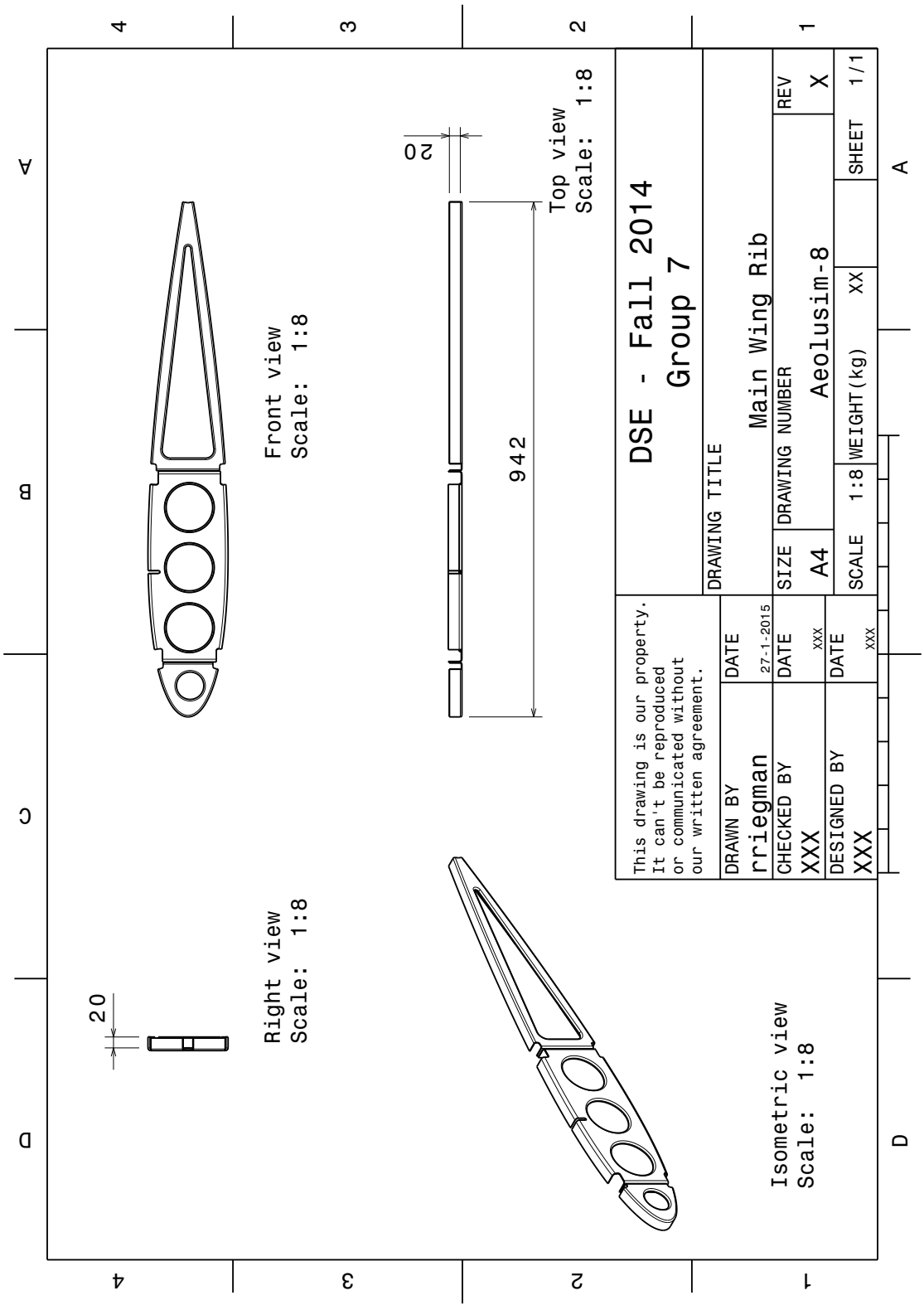

Figure G.6: Rib

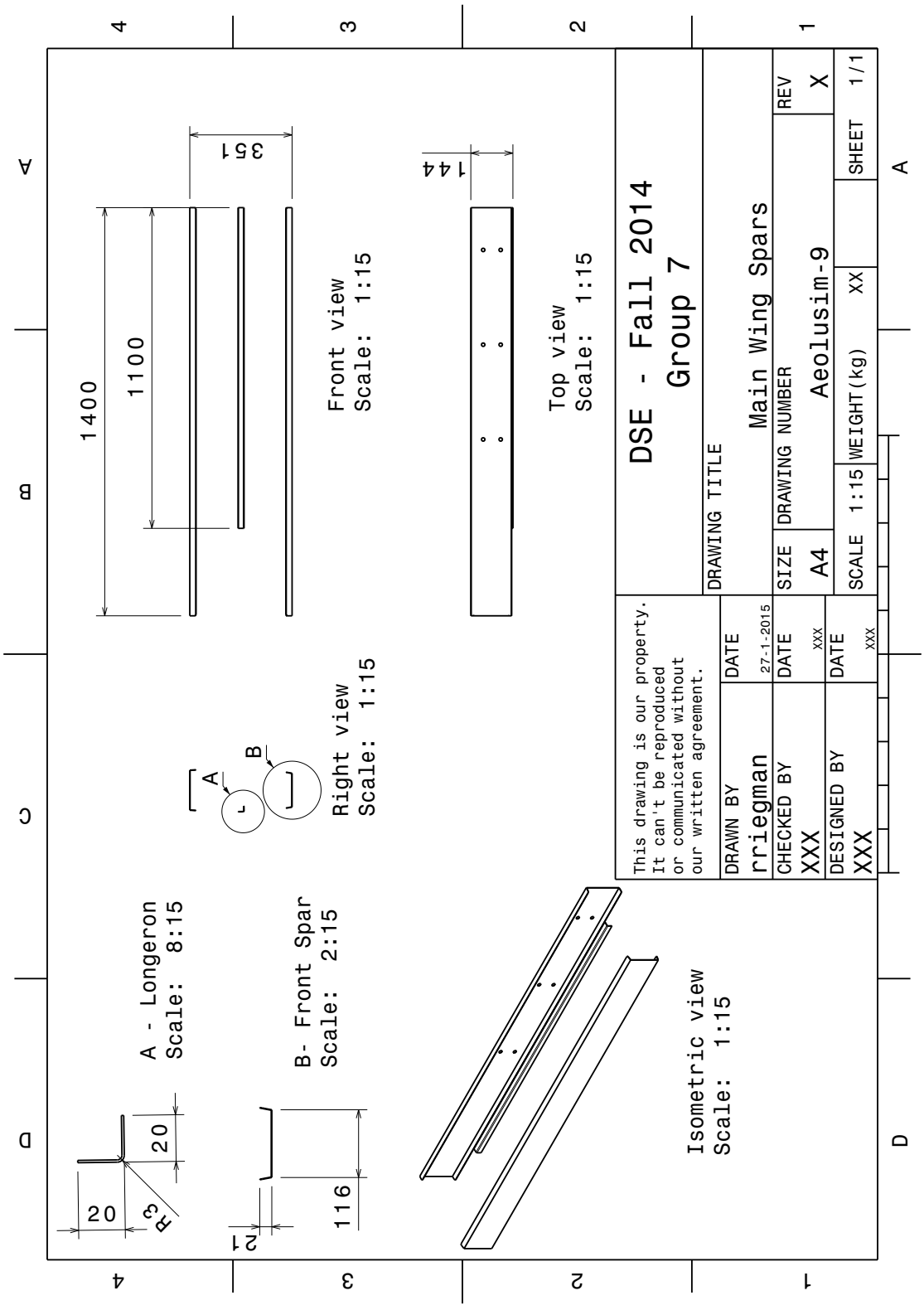

Figure G.7: Spar

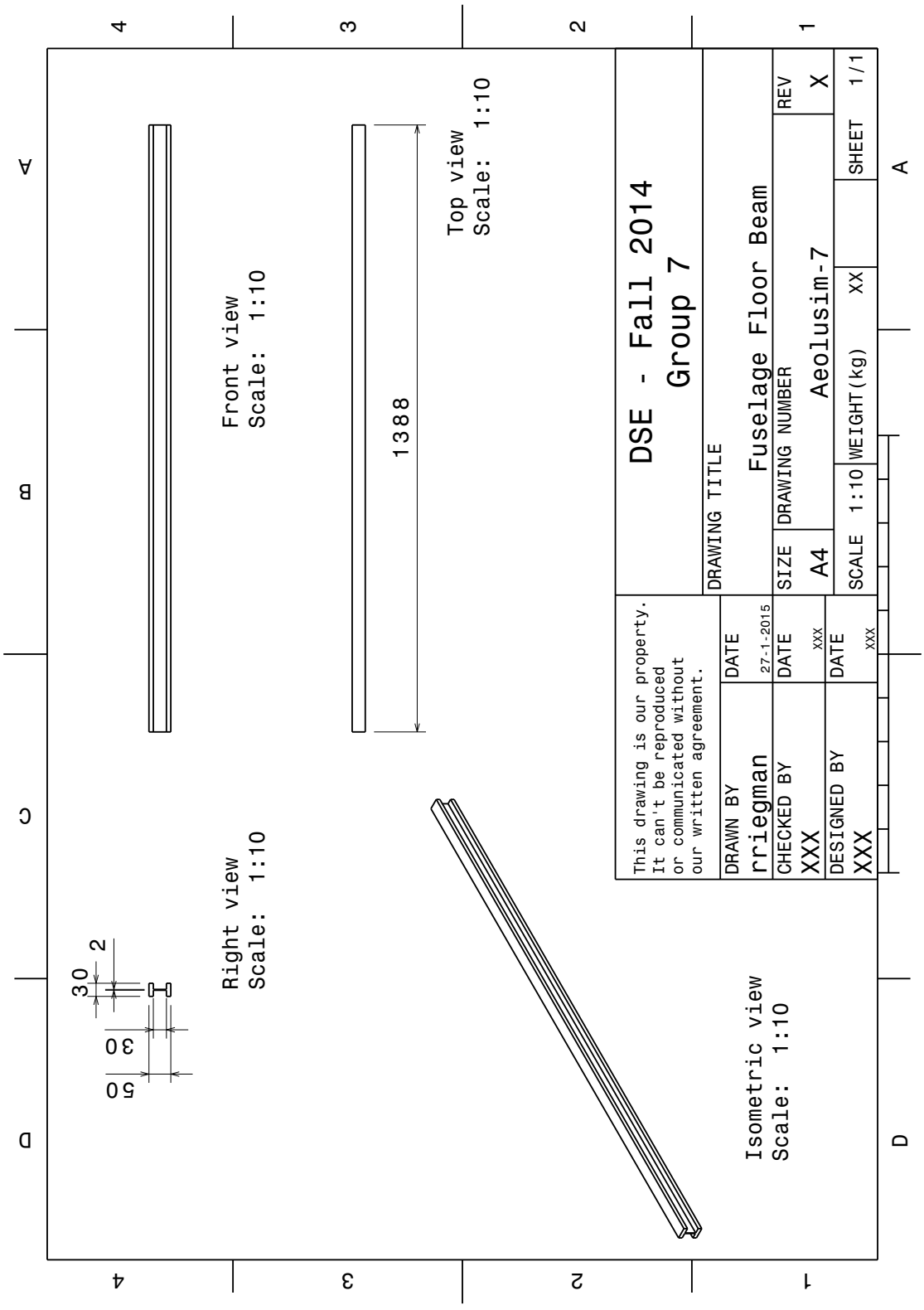

Figure G.8: I-Beam

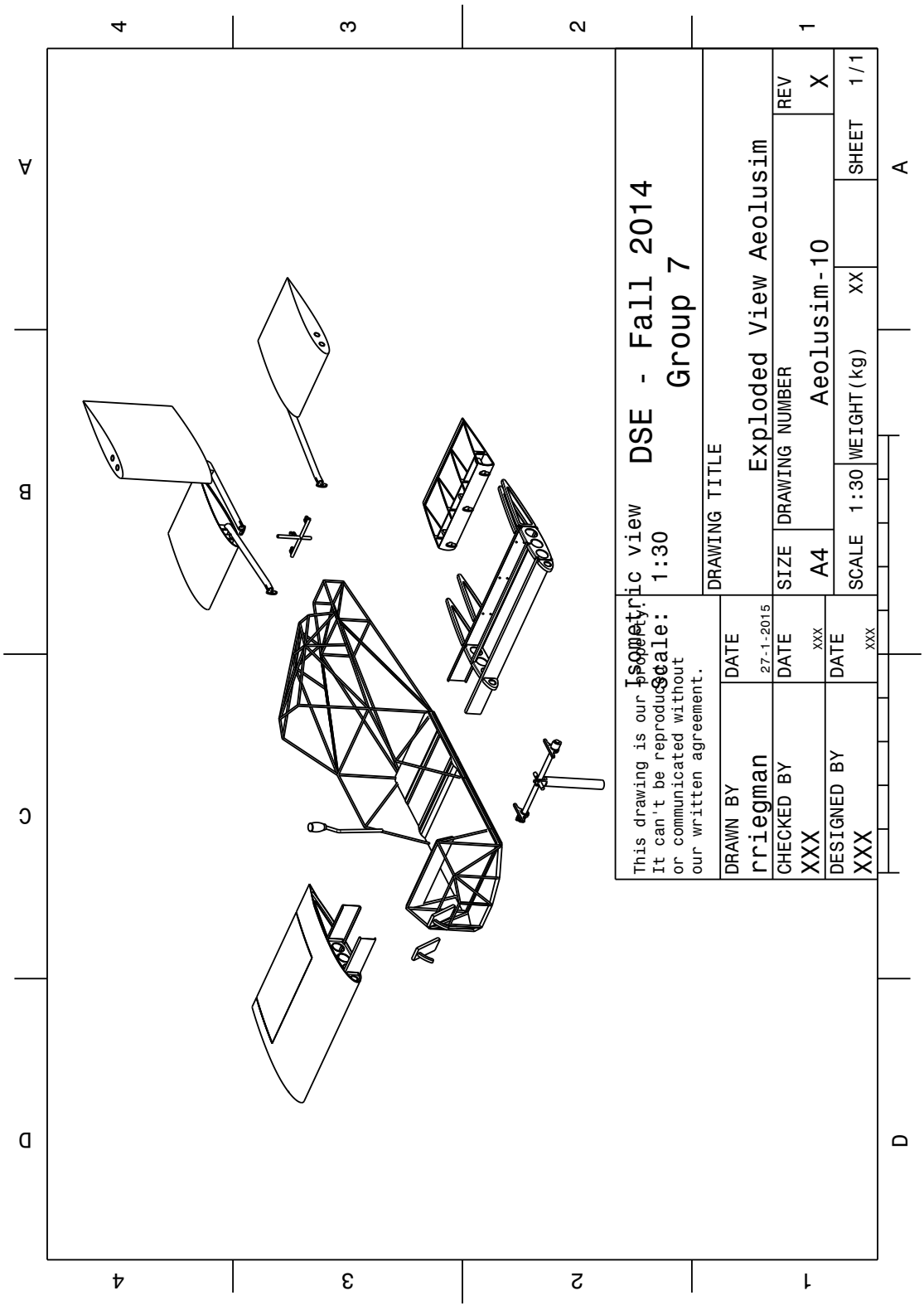

Figure G.9: Exploded View